The initial development of a jet caused by fluid, body and free surface interaction

by

Meurig Thomas Gallagher

A thesis submitted to the
University of Birmingham
for the degree of
Doctor of Philosophy

School of Mathematics
University of Birmingham
January 2015

Abstract

The aim of this thesis is to investigate the problem of a rigid plate, inclined at an angle $\alpha \in \left(0, \frac{1}{2}\pi\right)$ to the horizontal, accelerating uniformly from rest into, or away from, a semi-infinite expanse of inviscid, incompressible fluid. This work generalises that of Needham, Chamberlain and Billingham [24], by considering the case of negative plate accelerations. We use the method of matched asymptotic expansions to investigate the asymptotic structure of the solution to the free surface evolution problem as $t \to 0^+$, paying particular attention to the innermost asymptotic region encompassing the initial interaction between the fluid free surface and the inclined accelerating plate.

Acknowledgements

I would like to thank my supervisor David Needham, for his help, patience, and understanding throughout this process, especially during prolonged periods of my poor health. I would also like to thank the University of Birmingham and the EPSRC for funding my studies and providing me with the space and resources necessary to carry out this work.

I am also very grateful to John Billingham at the University of Nottingham for, amongst other things, providing some very useful code used in this thesis.

Lastly, I would like to thank my family and close friends for their continued support, I would not have been able to complete this without them.

Contents

List of Figures

List of Tables

Chapter 1

The Physical Problem and Equations of Motion

In this chapter we introduce the problem of a rigid plate, inclined at an angle $\alpha \in \left(0, \frac{1}{2}\pi\right)$ to the horizontal, accelerating uniformly from rest into, or away from, a semi-infinite expanse of inviscid, incompressible fluid. A sketch of this problem is illustrated in Figure 1.1. We begin in §1.1 by detailing the background of the problem, including an outline of previous studies into similar problems. In §1.2 we formulate the mathematical problem via the governing hydrodynamic equations along with the associated boundary and initial conditions, and regularity requirements.

1.1 Review

In this thesis we consider the motion of an inviscid incompressible fluid under the action of gravity, and bounded above by a free surface. The sudden change in the uniform motion of the fluid and/or a surface piercing rigid body leads to the localised formation of a jet-like behaviour in the neighbourhood of the contact point between the free surface of the fluid and the rigid body as the non-uniform transition takes place. This jet-like behaviour has significant consequences in practical applications; it can affect the stability

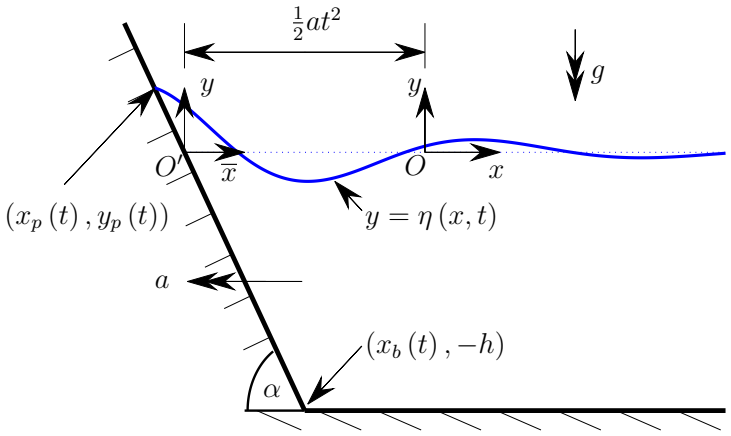

Figure 1.1: Definition sketch.

of a floating and manoeuvring vessel and can cause damage to a rigid body structure, as in the case of flood defences being attacked by waves.

In modelling such jet-like behaviour, there are two approaches that are widely used; investigation of scale-model experiments (see [7], [30]) and the construction of a full numerical solution to the set of governing hydrodynamic equations with corresponding initial and boundary conditions (see [7], [10]). Numerical studies into the behaviour of such jets must be based upon the spatial resolution needed to accurately model the jet-like behaviour. For example, in [14], the jet forming at the initial intersection of the plate and free surface has thickness $O(-t^2 \log t)$ as $t \to 0^+$, with t being the time from jet formation, whilst in [23] the jet forming at the initial intersection of the plate and free surface has thickness $O(t)$. As discussed by Greenhow [6], when the order of magnitude of the thickness of such jets is known *a priori*, then the accuracy and efficiency of numerical calculation of such flows can be improved. However, as discussed in [9], there can be considerable difficulty in establishing an estimate for the order of magnitude of thickness of such jets for a particular problem.

This thesis is a continuation of the work presented in a series of papers by King and

Needham [14], Needham, Billingham and King [23], and finally Needham, Chamberlain and Billingham [24]. In King and Needham [14] the case of a vertical rigid plate, accelerated uniformly into a stationary, semi-infinite, horizontal strip of inviscid incompressible fluid is discussed. The authors found that, in a thin region of size $O\left(-t^2 \log t\right)$ about the intersection point of the plate and the free surface, vertical motion was dominant as it became easier for the fluid to rise towards the low-pressure free surface than to move horizontally by overcoming the fluids' inertia. In Needham, Billingham and King [23], this theme was continued by investigating the situation where the initially stationary vertical plate is impulsively displaced into the horizontal strip of fluid. In this case it was found that a significantly more violent jet formed than in the case of a uniformly accelerated plate, with jet momentum flux of $O\left(t \log^2 t\right)$ as opposed to $O\left(t^3 \log^3 t\right)$ as $t \to 0^+$ in [14]. Subsequently Needham, Chamberlain and Billingham [24] generalised the theory in [14] by investigating the case of a plate inclined at an angle $\alpha \in \left(0, \frac{1}{2}\pi\right) \cup \left(\frac{1}{2}\pi, \pi\right)$ to the horizontal, accelerated uniformly into a semi-infinite, horizontal strip of inviscid incompressible fluid, initially at rest. The details of this paper are omitted here, as they will be discussed throughout this thesis in comparison with the results formulated within.

In addition to the above mentioned series of papers, there have been a number of studies (both experimental and numerical) by other authors. Notable works include the following. Greenhow and Lin [7] performed a series of scale-model experiments involving the impulsive start of a wavemaker, and the high speed entry of a wedge into calm water. For the former they found that the fluid free surface rises up the vertical face of the wavemaker, almost becoming parallel, before a jet is ejected at an angle almost perpendicular to the wavemaker. In the case of high speed wedge entry they found that a jet formed on the surface of the wedge at the intersection of the wedge and the fluid free surface. These jets then separate from the wedge and form the beginning of an ellipse with the fluid free surface. Yang and Chwang [30] investigated the case of a surface piercing,

vertical plate impulsively accelerated into an expanse of, initially stationary, fluid. Their scale-model experiments found that water rises up the plate during the initial stages of plate motion, with good agreements of the numerical solutions found in [29]. Greenhow [6], performed a numerical investigation into the wedge entry problem. He found that a jet of fluid rises up the side of the wedge and may then separate from the wedge surface, which agrees qualitatively with the experiments of [7]. This behaviour is not explained exactly, but it is suggested by the author that there is an introduction of new free surface particles between the original intersection between the surface of the wedge and the tip of the jet, with a modified numerical scheme achieving some success in simulating such flows.

This thesis aims to extend the work of Needham, Chamberlain and Billingham [24] by considering the case of a plate, inclined at an angle $\alpha \in \left(0, \frac{1}{2}\pi\right)$ to the horizontal, accelerating uniformly from rest *away* from a semi-infinite expanse of inviscid, incompressible fluid. We use the method of matched asymptotic expansions (see, for example, [19]) to investigate the asymptotic structure of the solution to our problem as $t \to 0^+$. We find that, for dimensionless accelerations $\sigma < 0$ with $\alpha \in \left(0, \frac{1}{2}\pi\right)$, we can extend the results of [24] to encompass all accelerations which satisfy $\mu = 1 + \sigma \tan\alpha > 0$.

The outline of this thesis is as follows. In §1.2 we consider the motion of an inviscid incompressible fluid under the action of gravity, and bounded above by a free surface. We introduce a coordinate system, which is fixed relative to the inclined accelerating plate, define the fluid velocity potential $\phi(\overline{x}, y, t)$ and free surface displacement $\eta(\overline{x}, t)$ and establish that conservation of mass leads to the Laplace equation, and construct the boundary and initial conditions for the problem that we shall call $[IBVP]$. Following the method of matched asymptotic expansions, Chapter 2 contains the construction of the *outer asymptotic region* in which $(\overline{x}, y) = O(1)$ as $t \to 0^+$. Here the initial conditions require that $\phi, \eta = o(1)$ as $t \to 0^+$ in the outer asymptotic region and, in particular,

the boundary conditions require that $\phi = O(t)$ and $\eta = O(t^2)$ as $t \to 0^+$. We then introduce the outer region asymptotic expansions and show that, on substitution into $[IBVP]$ to obtain $[OBVP]$, the solution to our governing hydrodynamic equations in the outer asymptotic region is independent of dimensionless acceleration σ, *except* in sign and scalar proportionality. We conclude this chapter by showing that the full regularity conditions fail to be satisfied by the outer region asymptotic expansions in a neighbourhood of the initial point of interaction of the plate and the free surface. In order to capture the full regularity in such a neighbourhood, in Chapter 3 we introduce an *inner asymptotic region*, in which $(\overline{x}, y) = o(1)$ as $t \to 0^+$. Here we introduce scaled inner region coordinates $(X, Y) = O(1)$ as $t \to 0^+$, and the inner region asymptotic expansions for ϕ and η. Substitution of the inner region asymptotic expansions into $[IBVP]$ yields a nonlinear harmonic free boundary problem which is solved exactly to leading order in §3.1. Subsequently, in §3.2, we introduce translated inner coordinates $\left(\overline{X}, \overline{Y}\right)$ and scale the velocity potential, free surface displacement, and coordinate system in order to achieve the two linear harmonic boundary value problems termed $[BVP]^{\pm}$, both depending only upon α, with the $+$ sign corresponding to values of $\sigma < 0$ such that $\mu = 1 + \sigma \tan\alpha > 0$, and the $-$ sign corresponding to those $\sigma < 0$ with $\mu < 0$. We are then able to remove the free surface displacement from our problem to obtain two linear harmonic boundary value problems $[PBVP]^{\pm}$, for ψ (which is related to the velocity potential) alone, depending only upon α. It is shown that $[PBVP]^{\pm}$ admits an exact solution when $\alpha = \frac{\pi}{2(n+1)}$ $(n = 1, 2, \dots)$. The details of the finite difference scheme used to solve $[PBVP]^{\pm}$ are contained within §3.3. The results for $[PBVP]^{+}$ are given in §3.4. Subsequently the results for $[PBVP]^{-}$ are shown in §3.5. Here we notice that the angles $\alpha = \alpha_i^*$ $(i = 1, 2, \dots)$ separate pairs of near resonances, with $[PBVP]^{-}$ having a stationary point at the intersection of the free surface and inclined plate at these angles. The remaining case, $\mu = 0$ $(\sigma = -\cot\alpha)$, is analysed in §3.7.4 when $\alpha \in \left(0, \frac{1}{4}\pi\right]$. However the case $\mu = 0$, with $\alpha \in \left(\frac{1}{4}\pi, \frac{1}{2}\pi\right)$, requires the

introduction of an *inner-inner asymptotic region* in which $\left(\overline{X}, \overline{Y}\right) = o(1)$ as $t \to 0^+$, and this is discussed in Chapter 4. The resulting boundary value problem $[RBVP]$ is solved numerically using a boundary integral method (which follows directly the approach given in [24]), the results of which are contained in §4.1.1. The numerical solution motivates the examination of the structure of solutions to $[RBVP]$ close to the contact point of the free surface and the plate, the analysis of which is found in §4.1.2. Finally, in Chapter 5, we consider whether the problem $[IBVP]$ is well-posed with respect to perturbations in initial data in the inner asymptotic region, and further, whether the problem $[IBVP]$ is stable with respect to perturbations in initial data in the inner asymptotic region. This work is split into two sections: §5.1 investigating the case $(\alpha, \mu) \in \left(0, \frac{1}{2}\pi\right) \times \mathbb{R} \backslash \left(\frac{1}{4}\pi, \frac{1}{2}\pi\right) \times \{0\}$, and §5.2.3 which considers the remaining case $(\alpha, \mu) \in \left(\frac{1}{4}\pi, \frac{1}{2}\pi\right) \times \mathcal{G}(\delta)$, with $\mathcal{G}(\delta)$ being a $o(1)$ neighbourhood of $\mu = 0$ ($\sigma = -\cot\alpha$) as $\delta \to 0$.

1.2 Equations of Motion

We consider the case of a semi-infinite expanse of inviscid and incompressible fluid, which is initially at rest and lies above a plane horizontal bed (which is rigid and impermeable) located at $y = -h$, bounded above by a horizontal free surface at $y = 0$, and bounded on the left by an inclined rigid plate at $y = -x\tan\alpha$, with $\alpha \in \left(0, \frac{1}{2}\pi\right)$ being the angle of inclination (exterior to the fluid layer) of the plate with the horizontal. Here (x, y) denotes the Cartesian coordinate system fixed in space, with x pointing horizontally into the fluid layer and y pointing vertically upwards, and $t \geqslant 0$ denotes time. From $t = 0$ the plate translates in the negative x-direction with constant acceleration $a\,(< 0)$. The free surface of the fluid is subsequently located at $y = \eta(x, t)$, with the contact point between the free surface of the fluid and the inclined plate denoted by $(x, y) = (x_p(t), y_p(t))$, with $y_p(t) = \eta(x_p(t), t)$. In addition the intersection point of the inclined plate and the rigid bed is denoted by $(x, y) = (x_b(t), -h)$. The situation is illustrated in Figure 1.1.

Since the fluid is initially at rest it follows from Kelvin's Circulation Theorem (see, for example, [2]), that the fluid motion for $t > 0$ remains irrotational, and so there exists a velocity potential for the flow which we denote by $\phi = \phi(x, y, t)$ (see, for example, [16]). In addition we denote the pressure field of the fluid by $p = p(x, y, t)$ (relative to atmospheric pressure p_a). Dimensionless variables are introduced as follows,

$$x' = \frac{x}{h}, \quad y' = \frac{y}{h}, \quad \eta' = \frac{\eta}{h},$$
$$\phi' = \frac{\phi}{h\sqrt{gh}}, \quad p' = \frac{p}{\rho g h}, \quad t' = t\sqrt{\frac{g}{h}}, \quad \sigma = \frac{a}{g}, \tag{1.2.1}$$

where $'$ denotes dimensionless variables and σ is the dimensionless acceleration of the plate. Here h, g and ρ are the initial height of the free surface, the acceleration due to gravity, and the density of the fluid, respectively. Hereafter we drop the primes for convenience.

For $t > 0$ it is convenient to introduce the coordinates $(\overline{x}, y)$, where $\overline{x} = x - s(t)$, with

$$s(t) = \frac{1}{2}\sigma t^2. \tag{1.2.2}$$

The origin O' of the $(\overline{x}, y)$ Cartesian coordinate system, as shown in Figure 1.1, is now located on the plate. We define the domain occupied by the fluid in the $(\overline{x}, y)$ plane to be given, for $t \geqslant 0$, by

$$\mathcal{D}(t) = \mathcal{D}_1(t) \cup \mathcal{D}_2(t), \tag{1.2.3}$$

with

$$\mathcal{D}_1(t) = \left\{(\overline{x}, y) \in \mathbb{R}^2 : \overline{x}_p(t) < \overline{x} \leqslant \overline{x}_b,\ -\overline{x}\tan\alpha < y < \eta(\overline{x}, t)\right\}, \tag{1.2.4}$$

$$\mathcal{D}_2(t) = \left\{(\overline{x}, y) \in \mathbb{R}^2 : \overline{x} > \overline{x}_b,\ -1 < y < \eta(\overline{x}, t)\right\}; \tag{1.2.5}$$

where $\overline{x}_p(t) = x_p(t) - s(t)$ and $\overline{x}_b = \cot\alpha$, with $y_p(t) = \eta(\overline{x}_p(t), t) = -\overline{x}_p(t)\tan\alpha$ for $t \geqslant 0$.

Conservation of fluid mass within $\mathcal{D}(t)$ $(t > 0)$ requires that the fluid velocity potential is harmonic on $\mathcal{D}(t)$ $(t > 0)$ so that,

$$\nabla^2\phi = 0, \qquad (\overline{x}, y) \in \mathcal{D}(t),\ t > 0, \tag{1.2.6}$$

where $\nabla = \left(\frac{\partial}{\partial\overline{x}}, \frac{\partial}{\partial y}\right)$ is the two-dimensional gradient operator in the $(\overline{x}, y)$ Cartesian coordinate system. At the rigid, impermeable bed, where $y = -1$ with $\overline{x} > \overline{x}_b$, we must have the boundary condition

$$\phi_y = 0,\ \text{on } y = -1, \quad \overline{x} > \overline{x}_b, \quad t > 0. \tag{1.2.7}$$

Similarly, on the impermeable rigid plate, we must have the boundary condition

$$\nabla\phi \cdot \hat{\mathbf{n}} = \sigma t \sin\alpha,\ \text{on } y = -\overline{x}\tan\alpha,\ \overline{x}_p(t) < \overline{x} < \overline{x}_b,\ t > 0, \tag{1.2.8}$$

with the unit vector normal to the plate (pointing into the fluid) given by $\hat{\mathbf{n}} = (\sin\alpha, \cos\alpha)$.

The fluid pressure field is given by the unsteady Bernoulli equation, namely,

$$p + \phi_t - \sigma t\phi_{\overline{x}} + \frac{1}{2}|\nabla\phi|^2 + y = 0, \qquad (\overline{x}, y) \in \mathcal{D}(t),\ t > 0. \tag{1.2.9}$$

We are now able to formulate the two boundary conditions on the fluid free surface. The

dynamic boundary condition requires that the fluid pressure vanishes on the free surface of the fluid, which, via the unsteady Bernoulli equation (1.2.9), requires,

$$\phi_t - \sigma t \phi_{\overline{x}} + \frac{1}{2} |\nabla \phi|^2 + \eta = 0, \text{ on } y = \eta(\overline{x}, t), \ \overline{x} > \overline{x}_p(t), \ t > 0. \tag{1.2.10}$$

The kinematic boundary condition on the fluid free surface requires that the normal velocity of the free surface is equal to the normal fluid velocity at the free surface. This leads to,

$$\eta_t - \sigma t \eta_{\overline{x}} + \phi_{\overline{x}} \eta_{\overline{x}} - \phi_y = 0, \text{ on } y = \eta(\overline{x}, t), \ \overline{x} > \overline{x}_p(t), \ t > 0. \tag{1.2.11}$$

The far-field boundary conditions require that,

$$\eta \to 0, \qquad \text{as } \overline{x} \to \infty, \ t > 0, \tag{1.2.12}$$

$$|\nabla \phi| \to 0, \qquad \text{as } \overline{x} \to \infty, \text{ uniformly for } -1 \leqslant y \leqslant \eta(\overline{x}, t), \ t > 0. \tag{1.2.13}$$

In addition, at the contact point between the fluid free surface and the plate, we require,

$$\eta + \overline{x}_p(t) \tan \alpha = 0 \text{ when } \overline{x} = \overline{x}_p(t), \ t > 0. \tag{1.2.14}$$

Finally, the initial conditions are

$$\phi(\overline{x}, y, 0) = 0, \quad (\overline{x}, y) \in \overline{\mathcal{D}}(0), \tag{1.2.15}$$

$$\eta(\overline{x}, 0) = 0, \quad \overline{x} \geqslant 0. \tag{1.2.16}$$

Thus, to summarize, we now have the following initial boundary value problem for ϕ

and η, namely,

$$\nabla^2\phi = 0, \qquad (\overline{x}, y) \in \mathcal{D}(t),\ t > 0; \tag{1.2.17}$$

$$\nabla\phi \cdot \hat{\mathbf{n}} = \dot{s}(t)\sin\alpha, \qquad y = -\overline{x}\tan\alpha,\ \overline{x}_p(t) < \overline{x} < \overline{x}_b,\ t > 0; \tag{1.2.18}$$

$$\phi_y = 0, \qquad y = -1,\ \overline{x} > \overline{x}_b,\ t > 0; \tag{1.2.19}$$

$$\eta_t + [\phi_{\overline{x}} - \sigma t]\,\eta_{\overline{x}} - \phi_y = 0, \qquad y = \eta(\overline{x}, t),\ \overline{x} > \overline{x}_p(t),\ t > 0; \tag{1.2.20}$$

$$\phi_t - \sigma t\phi_{\overline{x}} + \frac{1}{2}|\nabla\phi|^2 + \eta = 0, \qquad y = \eta(\overline{x}, t),\ \overline{x} > \overline{x}_p(t),\ t > 0. \tag{1.2.21}$$

$$\eta + \overline{x}_p(t)\tan\alpha = 0, \qquad \overline{x} = \overline{x}_p(t),\ t > 0, \tag{1.2.22}$$

$$\eta \to 0, \qquad \text{as } \overline{x} \to \infty,\ t > 0, \tag{1.2.23}$$

$$|\nabla\phi| \to 0, \qquad \text{as } \overline{x} \to \infty, \text{ uniformly for } -1 \leqslant y \leqslant \eta(\overline{x}, t),\ t > 0, \tag{1.2.24}$$

$$\phi(\overline{x}, y, 0) = 0, \qquad (\overline{x}, y) \in \overline{\mathcal{D}}(0), \tag{1.2.25}$$

$$\eta(\overline{x}, 0) = 0, \qquad \overline{x} \geqslant 0. \tag{1.2.26}$$

The fluid pressure field p is obtained explicitly from the unsteady Bernoulli equation (1.2.9). It is convenient to write,

$$p = p_d - y, \qquad (\overline{x}, y) \in \overline{\mathcal{D}}(t), \quad t > 0, \tag{1.2.27}$$

with p_d being the dynamic fluid pressure field, which is given via (1.2.9) as

$$p_d = -\phi_t + \sigma t\phi_{\overline{x}} - \frac{1}{2}|\nabla\phi|^2, \qquad (\overline{x}, y) \in \overline{\mathcal{D}}(t), \quad t > 0. \tag{1.2.28}$$

Finally the fluid velocity field (non-dimensionalised with the velocity scale $\sqrt{gh}$), *relative to the fixed origin* O, is given by

$$\mathbf{q} = \nabla\phi, \qquad (\overline{x}, y) \in \overline{\mathcal{D}}(t), \quad t > 0. \tag{1.2.29}$$

We will study classical solutions to the initial boundary value problem (1.2.17) - (1.2.26), hereafter referred to as $[IBVP]$, which satisfy the following regularity conditions

$$\phi \in C\left(\overline{\mathcal{G}}\right) \cap C^1\left(\mathcal{G} \cup \partial\mathcal{G}\right) \cap C^2\left(\mathcal{G}\right), \tag{1.2.30}$$

$$\eta \in C\left(\overline{\mathcal{H}}\right) \cap C^1\left(\mathcal{H}\right), \tag{1.2.31}$$

with

$$\mathcal{G} = \left\{(\overline{x}, y, t) \in \mathbb{R}^3 : (\overline{x}, y) \in \mathcal{D}\left(t\right), t \in (0, \infty)\right\}, \tag{1.2.32}$$

$$\partial\mathcal{G} = \left\{(\overline{x}, y, t) \in \mathbb{R}^3 : (\overline{x}, y) \in \overline{\mathcal{D}}\left(t\right) \backslash \mathcal{D}\left(t\right), t \in (0, \infty)\right\}, \tag{1.2.33}$$

$$\mathcal{H} = \left\{(\overline{x}, t) \in \mathbb{R}^2 : \overline{x} \in [\overline{x}_p\left(t\right), \infty), t \in (0, \infty)\right\}. \tag{1.2.34}$$

The aim of this thesis is to investigate the asymptotic structure of the solution to $[IBVP]$ as $t \to 0^+$ via the method of matched asymptotic expansions (see, for example, [19]), and, in particular, to extend the theory in [24] to the situation when the plate has negative acceleration, so that $\sigma < 0$, with $\alpha \in \left(0, \frac{1}{2}\pi\right)$. We begin in Chapter 2 by introducing two asymptotic regions, and investigating the behaviour in an outer region in which $(\overline{x}, y) \in \overline{\mathcal{D}}\left(t\right) = O\left(1\right)$ as $t \to 0^+$. The associated inner regions with $(\overline{x}, y) \in \overline{\mathcal{D}}\left(t\right) = o\left(1\right)$ are then discussed in Chapters 3 and 4. Finally, the well-posedness and stability of our problem with respect to perturbations in the innermost asymptotic region is discussed in Chapter 5.

Chapter 2

Outer Region Asymptotic Structure to $[IBVP]$ as $t \to 0^+$ with $\alpha \in \left(0, \frac{1}{2}\pi\right)$

In this chapter we begin the asymptotic development of the solution to $[IBVP]$, as $t \to 0^+$, in an *outer asymptotic region* in which $(\overline{x}, y) \in \overline{\mathcal{D}}(t) \setminus \mathcal{N}(t)$ as $t \to 0^+$, with $\mathcal{N}(t)$ being a $o(1)$ neighbourhood of $(\overline{x}, y) = (0, 0)$ as $t \to 0^+$. Here the gauge function $\delta(t)$ will be determined in the course of the analysis. A definition sketch of the outer asymptotic region is shown in Figure 2.1. The initial conditions (1.2.25) and (1.2.26) require that ϕ, $\eta = o(1)$ as $t \to 0^+$ in the outer asymptotic region. In particular, boundary conditions (1.2.18) and (1.2.20) require that $\phi = O(t)$ and $\eta = O(t^2)$ as $t \to 0^+$ in the outer asymptotic region. Therefore, we introduce the outer region asymptotic expansions in the form,

$$\phi(\overline{x}, y, t) = t\sigma \sin\alpha \overline{\phi}(\overline{x}, y) + O\left(t^2\right), \tag{2.0.1}$$

$$\eta(\overline{x}, t) = t^2 \overline{\eta}(\overline{x}) + O\left(t^3\right), \tag{2.0.2}$$

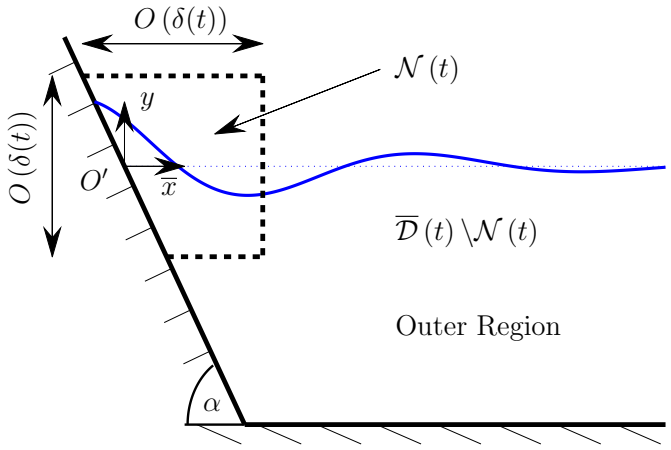

Figure 2.1: Definition sketch of the outer asymptotic region

as $t \to 0^+$ in the outer asymptotic region, with the factor $\sigma \sin\alpha$ in (2.0.1) included for algebraic convenience at a later stage. Substituting expansions (2.0.1) and (2.0.2) into $[IBVP]$ (with the exception of condition (1.2.22), since the application point $(\overline{x}, y) = (\overline{x}_p(t), y_p(t)) \to (0,0)$ as $t \to 0^+$ lies outside the outer asymptotic region), we obtain the leading order problem in the outer region, for $\overline{\phi}$, namely

$$\nabla^2\overline{\phi} = 0, \quad (\overline{x}, y) \in \mathcal{D}(0); \tag{2.0.3}$$

$$\nabla\overline{\phi}\cdot\hat{\mathbf{n}} = 1, \quad y = -\overline{x}\tan\alpha,\ 0 < \overline{x} < \cot\alpha; \tag{2.0.4}$$

$$\overline{\phi}_y = 0, \quad y = -1,\ \overline{x} > \cot\alpha; \tag{2.0.5}$$

$$\overline{\phi} = 0, \quad y = 0,\ \overline{x} > 0; \tag{2.0.6}$$

$$\left|\nabla\overline{\phi}\right| \to 0 \quad \text{as } \overline{x} \to \infty, \text{ uniformly for } -1 \leqslant y \leqslant 0; \tag{2.0.7}$$

with $\overline{\eta}$ given, via (1.2.20), as

$$\overline{\eta}(\overline{x}) = \frac{1}{2}\sigma\sin\alpha\ \overline{\phi}_y(\overline{x}, 0), \quad \overline{x} \geqslant 0. \tag{2.0.8}$$

Hence $\overline{\phi}$ is the solution to the linear harmonic boundary value problem (2.0.3) - (2.0.7) henceforth referred to as $[OBVP]$ (which is independent of the dimensionless acceleration σ), and is defined on the fixed, semi-infinite polygonal domain $\overline{\mathcal{D}}(0)$. We require, via (1.2.30), that the solution to $[OBVP]$ must have regularity given by

$$\begin{aligned} &\overline{\phi} \in C\left(\overline{\mathcal{D}}(0)\right) \cap C^1\left(\overline{\mathcal{D}}(0) \setminus \{(0,0)\}\right) \cap C^2\left(\mathcal{D}(0)\right), \\ &\left|\nabla\overline{\phi}\right| \text{ has, at worst, an integrable singularity at } (\overline{x}, y) = (0,0). \end{aligned} \tag{2.0.9}$$

Although the possibility of allowing $\left|\nabla\overline{\phi}\right|$ to have an integrable singularity at $(\overline{x}, y) = (0,0)$ violates the full regularity conditions (1.2.30) on ϕ, and (1.2.31) on η (via (2.0.8)), it is necessary to ensure the existence of a solution to $[OBVP]$. The existence and uniqueness of a solution to $[OBVP]$ that has regularity required by (2.0.9) is guaranteed by the use of the Schwarz-Christoffel Conformal Mapping Theorem [5], together with Green's Theorem [27]. This approach provides a constructional method for determining the solution to $[OBVP]$. However, it is much more illuminative to use direct eigenfunction expansions (see, for example, [15]) to represent the solution to $[OBVP]$. With the regularity condition (2.0.9) it follows that there exist real constants A_n, B_n and C_n, $n = 0, 1, 2, \ldots$, such that

$$\overline{\phi}(r,\theta) = \frac{r\sin\theta}{\cos\alpha} + \sum_{n=0}^{\infty} A_n r^{\left(n+\frac{1}{2}\right)\frac{\pi}{\alpha}} \sin\left(\left(n+\frac{1}{2}\right)\frac{\pi}{\alpha}\theta\right), \tag{2.0.10}$$

for $0 \leqslant r < \operatorname{cosec}\alpha$, $-\alpha \leqslant \theta \leqslant 0$, where $\overline{x} = r\cos\theta$ and $y = r\sin\theta$, whilst

$$\overline{\phi}(\rho,\psi) = \frac{\rho\cos\psi}{\sin\alpha} + \sum_{n=0}^{\infty} B_n \rho^{n\pi/(\pi-\alpha)} \cos\left(\frac{n\pi\psi}{\pi-\alpha}\right), \tag{2.0.11}$$

for $0 \leqslant \rho < 1$, $0 \leqslant \psi \leqslant \pi - \alpha$, where $\overline{x} - \cot\alpha = \rho\cos\psi$, and $y + 1 = \rho\sin\psi$, and finally

$$\overline{\phi}(\overline{x}, y) = \sum_{n=0}^{\infty} C_n e^{-\left(n+\frac{1}{2}\right)\pi\overline{x}} \sin\left(\left(n+\frac{1}{2}\right)\pi y\right), \tag{2.0.12}$$

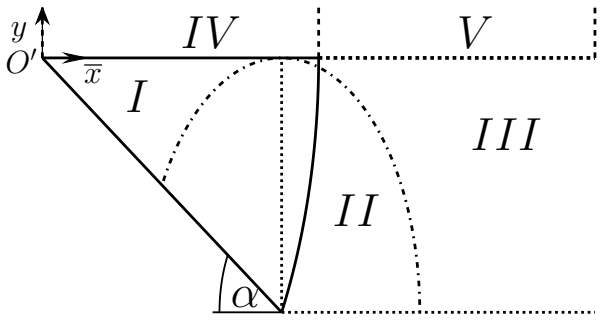

Figure 2.2: Sketch showing domains of validity for I (2.0.10), II (2.0.11), III (2.0.12), IV (2.0.13) and V (2.0.14)

for $\overline{x} > \cot\alpha$, $-1 \leqslant y \leqslant 0$. Equation (2.0.8) together with (2.0.10) and (2.0.12) now give that

$$\overline{\eta}\,(\overline{x}) = \frac{1}{2}\sigma\tan\alpha + \frac{1}{2}\sigma\sin\alpha\sum_{n=0}^{\infty}\left(n+\frac{1}{2}\right)\frac{\pi}{\alpha}A_n\overline{x}^{\left(n+\frac{1}{2}\right)\frac{\pi}{\alpha}-1}, \tag{2.0.13}$$

for $0 \leqslant \overline{x} < \text{cosec}\,\alpha$, and

$$\overline{\eta}\,(\overline{x}) = \frac{1}{2}\sigma\sin\alpha\sum_{n=0}^{\infty}\left(n+\frac{1}{2}\right)\pi C_n e^{-\left(n+\frac{1}{2}\right)\pi\overline{x}}, \tag{2.0.14}$$

for $\overline{x} \geqslant \text{cosec}\,\alpha$.

As in [24] we use the expressions (2.0.10), (2.0.11) and (2.0.12) to obtain numerical approximations for $\overline{\phi}$ and hence $\overline{\eta}$ (via (2.0.13) and (2.0.14). These numerical approximations are calculated by truncating each of the infinite series' and equating these partial sums at a number of points in the intersection of domains of validity (a definition sketch of the intersection of domains can be seen in Figure 2.2). The system of linear equations obtained by equating these partial sums is then solved to obtain the constants A_n, B_n and C_n for $n = 0, 1, \ldots, N$. A value of $N = 8$ was found to give a sufficient level of convergence for the numerical results. The coefficient A_0, appearing in (2.0.10) and (2.0.13) (which depends upon α), is of particular interest at a later stage. An analytical expression for

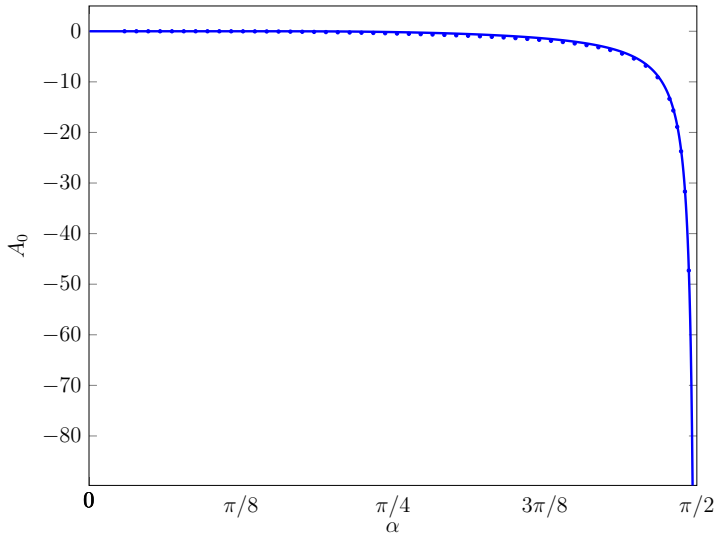

Figure 2.3: Coefficient $A_0(\alpha)$ against α. A solid line shows the analytical expression (2.0.15), while numerical approximations are shown as dots

A_0, derived in [24], is given by

$$A_0(\alpha) = \frac{1}{\left(\alpha - \frac{1}{2}\pi\right)\sin\alpha}\left\{\frac{2\alpha\Gamma\left(\frac{1}{2}+\frac{\alpha}{\pi}\right)}{\sqrt{\pi}\Gamma\left(\frac{\alpha}{\pi}\right)}\right\}^{\frac{\pi}{2\alpha}} \qquad \text{for } \alpha \in \left(0, \frac{1}{2}\pi\right), \tag{2.0.15}$$

from which we obtain,

$$A_0(\alpha) \sim -\frac{2}{\pi\alpha}e^{\frac{\pi}{\alpha}\log\left(\sqrt{\frac{2}{\pi}}\alpha\right)} \quad \text{as } \alpha \to 0^+, \quad A_0(\alpha) \sim \left(\alpha - \frac{\pi}{2}\right)^{-1} \quad \text{as } \alpha \to \left(\frac{1}{2}\pi\right)^-. \tag{2.0.16}$$

A graph of the numerically calculated values of A_0, together with analytical values given by (2.0.15), is shown in Figure 2.3. The agreement is excellent, giving confidence in the numerical solution to $[OBVP]$. Equation (1.2.28), together with the outer region asymptotic expansion for ϕ in (2.0.1), require that the dynamic fluid pressure field in the outer asymptotic region must have the outer region asymptotic expansion

$$p_d(\overline{x}, y, t) = \overline{p}(\overline{x}, y) + O(t), \tag{2.0.17}$$

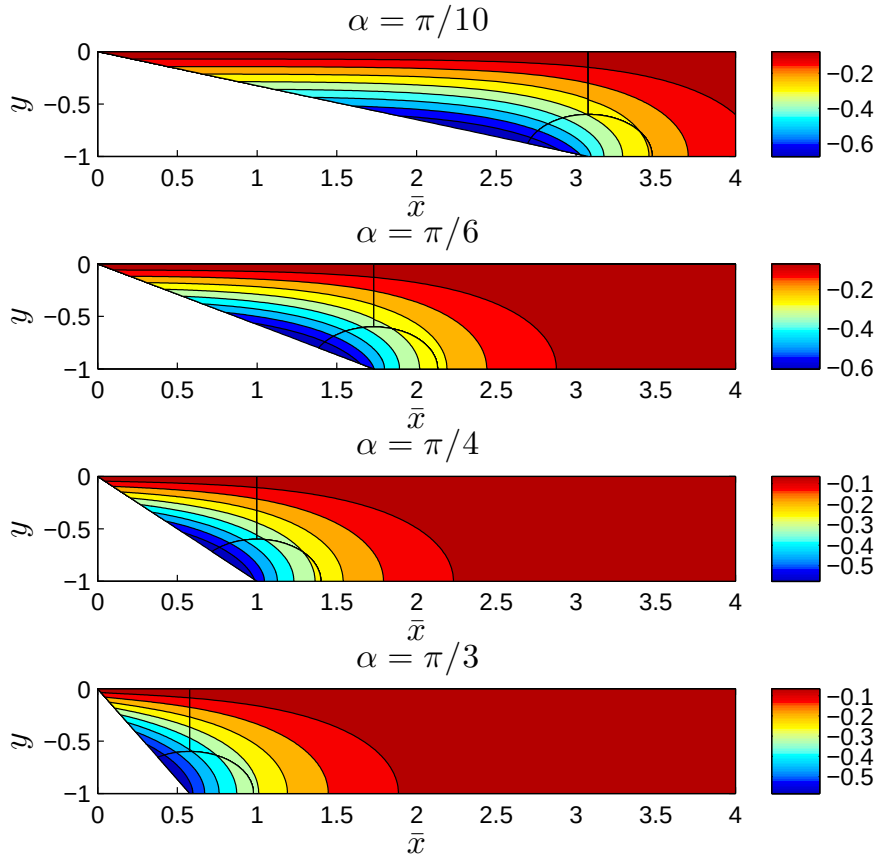

Figure 2.4: Contours of $\overline{\phi}$ for a selection of angles α. Lines separate regions where (2.0.10), (2.0.11) and (2.0.12) are used

as $t \to 0^+$ in the outer asymptotic region, where

$$\overline{p}\left(\overline{x}, y\right) = -\sigma \sin\alpha \overline{\phi}\left(\overline{x}, y\right), \quad \left(\overline{x}, y\right) \in \overline{\mathcal{D}}\left(0\right). \tag{2.0.18}$$

Thus, in the outer asymptotic region, the level curves of $\overline{\phi}$ correspond, via (2.0.18), to the leading order isobars of the dynamic pressure field. Finally, we obtain the outer region asymptotic expansion for the fluid velocity field, via (1.2.29) and (2.0.1), as

$$\mathbf{q}\left(\overline{x}, y, t\right) = t\sigma \sin\alpha \nabla\overline{\phi}\left(\overline{x}, y\right) + O\left(t^2\right), \tag{2.0.19}$$

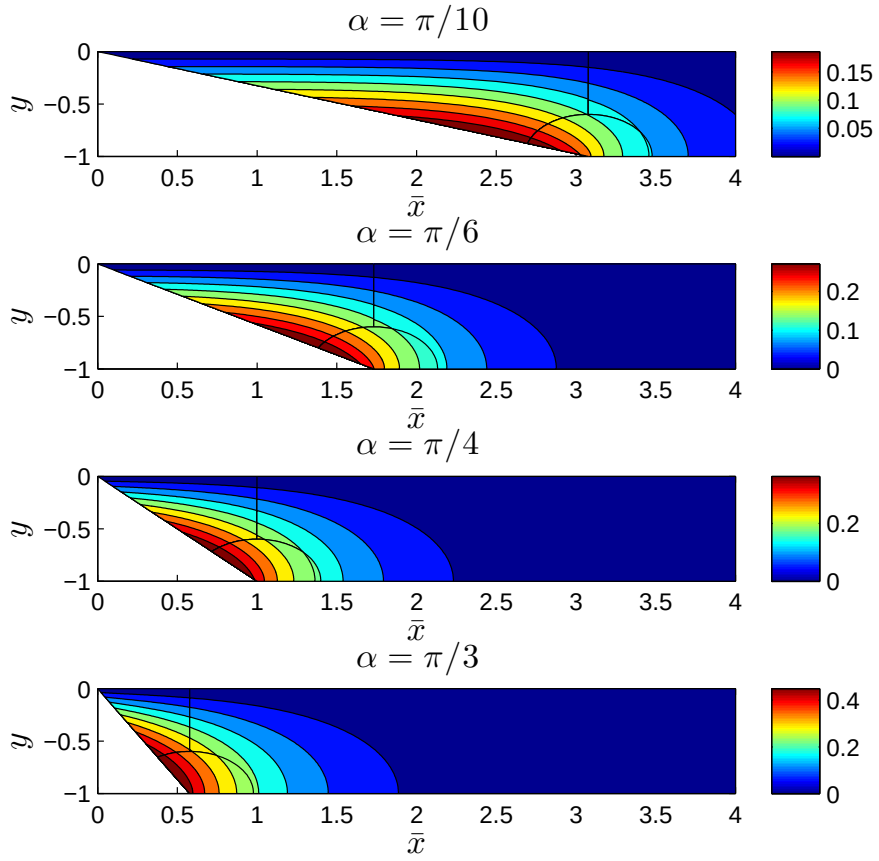

Figure 2.5: Contours of $\overline{p}/\sigma$ for a selection of angles α. Lines separate regions where (2.0.10), (2.0.11) and (2.0.12) are used

as $t \to 0^+$ in the outer asymptotic region. Thus, at leading order in the outer asymptotic region, the fluid flow has streamlines which are orthogonal to the level curves of $\overline{\phi}$.

We now illustrate a selection of numerical results for $[OBVP]$, selecting the angles $\alpha = \frac{\pi}{10}, \frac{\pi}{6}, \frac{\pi}{4}$, and $\frac{\pi}{3}$. At each of these angles we plot the level curves of $\overline{\phi}$ in Figure 2.4, $\overline{p}/\sigma$ in Figure 2.5, and the level curves orthogonal to those of $\overline{\phi}$ (*the streamlines*) in Figure 2.6. We also plot $\overline{\eta}/\sigma$ against $\overline{x} \geqslant 0$ at each of these angles in Figure 2.7 and note that all of these graphs are independent of σ, except in sign and scalar proportionality.

When $\sigma > 0$, it is is clear from Figure 2.5 that, for each α considered, there is a build-

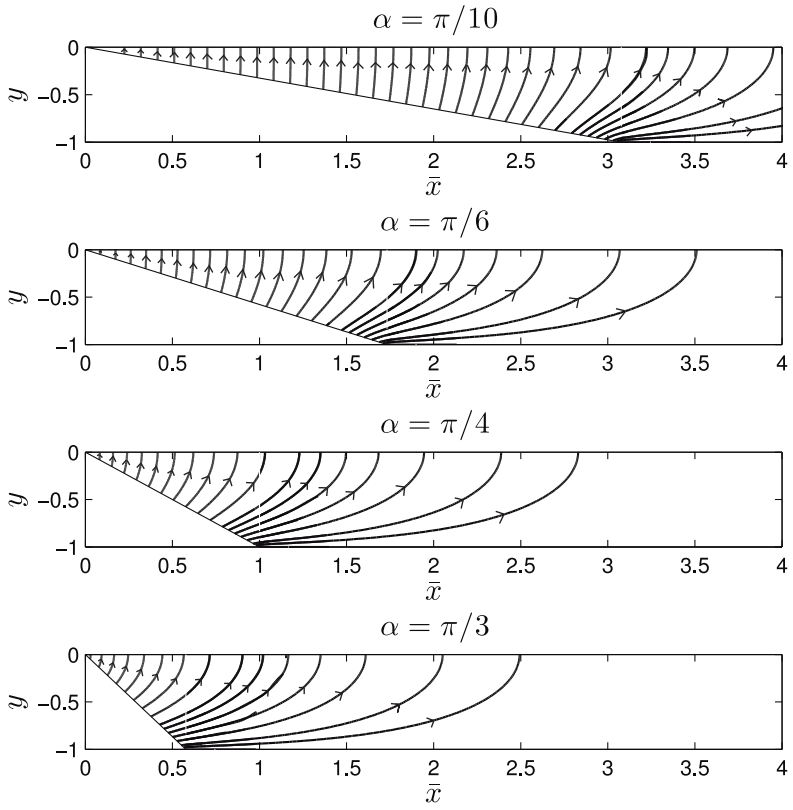

Figure 2.6: Orthogonal contours of $\overline{\phi}$, which represent streamlines, for a selection of angles α, with the arrows indicating the direction of $\nabla\overline{\phi}$

up of dynamic pressure close to the base of the inclined plate. This is typical of all angles investigated, and it is this that leads to the formation of a jet in the inner asymptotic region, as discussed in [24]. When $\sigma < 0$, we see that, for each α plotted, there is a region of low pressure close to the base of the plate. The effect of this on the free surface, close to the intersection point of the plate and the free surface will be discussed in Chapter 3.

We see from (2.0.10), (2.0.11), (2.0.13), and (2.0.14), that the leading order terms in the outer region asymptotic expansions (2.0.1) and (2.0.2) satisfy the required regularity (1.2.30) and (1.2.31), *except* in a neighbourhood of the initial location of the intersection point of the free surface and the plate, at $(\overline{x}, y) = (0, 0) \in \overline{\mathcal{D}}\,(0)$. Close to $(\overline{x}, y) = (0, 0)$

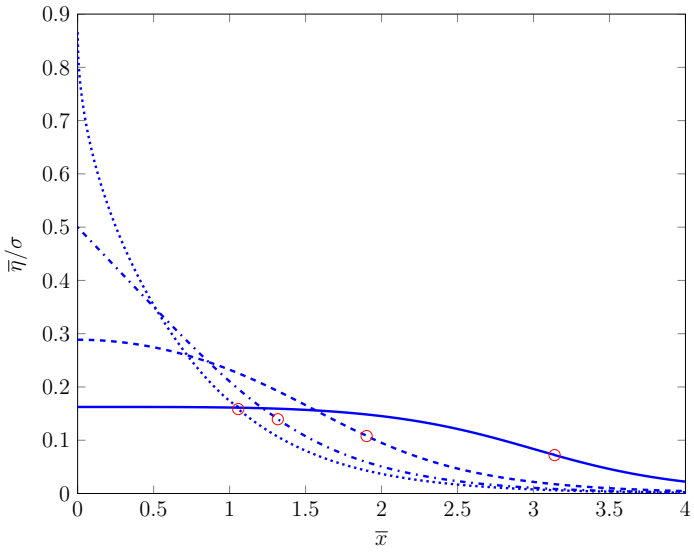

Figure 2.7: The free surface elevation $\overline{\eta}/\sigma$ at the angles $\alpha = \frac{1}{3}\pi$, $\frac{1}{4}\pi$, $\frac{1}{6}\pi$ and $\alpha = \frac{1}{10}\pi$ represented by dotted, dash-dotted, dashed and solid lines respectively. Red circles highlight the transitions from (2.0.13) to (2.0.14)

we have, from (2.0.10) and (2.0.13), that

$$\overline{\phi}\,(r,\theta) = \frac{r\sin\theta}{\cos\alpha} + A_0 r^{\pi/2\alpha}\sin\frac{\pi\theta}{2\alpha} + O\left(r^{3\pi/2\alpha}\right), \tag{2.0.20}$$

as $r \to 0^+$, with $-\alpha \leqslant \theta \leqslant 0$, and

$$\overline{\eta}\,(\overline{x}) = \frac{1}{2}\sigma\tan\alpha + A_0\frac{\pi\sigma\sin\alpha}{4\alpha}\overline{x}^{\frac{\pi}{2\alpha}-1} + O\left(\overline{x}^{\frac{3\pi}{2\alpha}-1}\right), \tag{2.0.21}$$

as $\overline{x} \to 0^+$. It follows from (2.0.19) and (2.0.20) that

$$\left|\nabla\overline{\phi}\,(r,\theta)\right| = \sec\alpha + O\left(r^{\frac{\pi}{2\alpha}-1}\right), \tag{2.0.22}$$

as $r \to 0$, with $-\alpha \leqslant \theta \leqslant 0$. Equation (2.0.21) reveals a weak singularity in $\overline{\eta}'\,(\overline{x})$ as $\overline{x} \to 0^+$. Further investigation reveals that this singular behaviour as $\overline{x} \to 0^+$ is compounded in higher-order terms in the outer region asymptotic expansions for $\overline{\eta}$ in

(2.0.2), and also, as $r \to 0$, in the outer region asymptotic expansion for ϕ in (2.0.1), and so the regularity conditions (1.2.30) and (1.2.31) fail to be satisfied by the outer region asymptotic expansions (2.0.1) and (2.0.2) in a neighbourhood of the initial point of intersection of the plate and free surface, where $(\overline{x}, y) = o(1)$ as $t \to 0^+$. Therefore we introduce an *inner asymptotic region*, in which $(\overline{x}, y) = o(1)$ as $t \to 0^+$, in order to capture the full regularity in the neighbourhood of the intersection point of the plate and the free surface. The inner asymptotic region is now considered in detail in the next chapter.

Chapter 3

Inner Region Asymptotic Structure to $[IBVP]$ as $t \to 0^+$ with $\alpha \in \left(0, \frac{1}{2}\pi\right)$

In this chapter we introduce the inner asymptotic region associated with $[IBVP]$ when $(\overline{x}, y) = o(1)$ as $t \to 0^+$. Specifically, following Chapter 2, we write $(\overline{x}, y) = O(\delta(t))$ with $\delta(t) = o(1)$ as $t \to 0^+$. It then follows from (2.0.2) and (2.0.21) that $\eta = O(t^2)$ as $t \to 0^+$ in the inner asymptotic region, and so, to capture the free surface in the inner asymptotic region, we must take $\delta(t) = O(t^2)$ as $t \to 0^+$; therefore, without loss of generality, we set $\delta(t) = t^2$. An examination of (2.0.1) and (2.0.20) then requires that $\phi = O(t^3)$ as $t \to 0^+$ in the inner asymptotic region, whilst (2.0.17), (2.0.18) and (2.0.19) require that $p_d = O(t^2)$ and $\mathbf{q} = O(t)$ as $t \to 0^+$ in the inner asymptotic region. Finally, the intersection point of the free surface and the plate must be captured in the inner asymptotic region, and so $\overline{x}_p(t) = O(t^2)$ as $t \to 0^+$. A sketch of the location of the inner asymptotic region is illustrated in Figure 3.1.

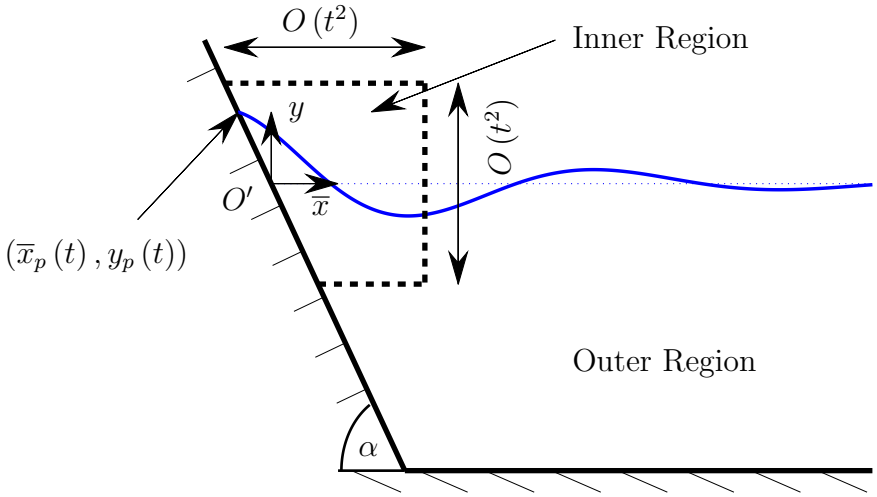

Figure 3.1: A sketch of the location of the inner asymptotic region

3.1 Inner Region Problems

Formally we introduce scaled inner region coordinates (X, Y) by

$$\overline{x} = t^2 X, \quad y = t^2 Y, \tag{3.1.1}$$

with $(X, Y) = O(1)$ as $t \to 0^+$ in the inner asymptotic region. The location of the plate in the inner asymptotic region is given by $Y = -X \tan\alpha$, whilst the plate and free surface intersection point is denoted by $(X, Y) = (X_p(t), Y_p(t))$, with,

$$\overline{x}_p(t) = t^2 X_p(t), \quad y_p(t) = t^2 Y_p(t), \tag{3.1.2}$$

and $(X_p(t), Y_p(t)) = O(1)$ as $t \to 0^+$ in the inner asymptotic region. We now write the free surface and velocity potential in the inner asymptotic region as

$$\eta(X,t) = t^2 \eta_I(X,t), \quad X \geqslant X_p(t), \ t \geqslant 0; \tag{3.1.3}$$

$$\phi(X,Y,t) = t^3 \phi_I(X,Y,t), \quad X \geqslant X_p(t), \ -X\tan\alpha \leqslant Y \leqslant \eta_I(X,t), \ t \geqslant 0; \tag{3.1.4}$$

with $\eta_I(X,t), \phi_I(X,Y,t) = O(1)$ as $t \to 0^+$. The inner region asymptotic expansions are then introduced as,

$$\eta_I(X,t) = \eta_0(X) + t^{\frac{\pi}{\alpha}-2}\tilde{\eta}(X) + o\left(t^{\frac{\pi}{\alpha}-2}\right), \tag{3.1.5}$$

$$\phi_I(X,Y,t) = \phi_0(X,Y) + t^{\frac{\pi}{\alpha}-2}\tilde{\phi}(X,Y) + o\left(t^{\frac{\pi}{\alpha}-2}\right), \tag{3.1.6}$$

as $t \to 0^+$ with $(X,Y) = O(1)$ in the inner asymptotic region. Finally, it follows from (3.1.1), (3.1.2), (3.1.3) and (3.1.5) that we expand $X_p(t)$ in the form

$$X_p(t) = X_0 + t^{\frac{\pi}{\alpha}-2}X_1 + o\left(t^{\frac{\pi}{\alpha}-2}\right), \tag{3.1.7}$$

as $t \to 0^+$, with

$$Y_p(t) = -X_p(t)\tan\alpha. \tag{3.1.8}$$

The free surface in the inner asymptotic region is located at

$$Y = \eta_I(X,t), \quad X > X_p(t), \ t \geqslant 0, \tag{3.1.9}$$

whilst the spatial domain in the inner asymptotic region is

$$\mathcal{D}_I(t) = \{(X,Y) : X > X_p(t), -X\tan\alpha < Y < \eta_I(X,t)\}, \tag{3.1.10}$$

for $t \geqslant 0$, with closure $\overline{\mathcal{D}}_I(t)$. A sketch of the inner asymptotic region geometry is given in Figure 3.2.

We now write $[IBVP]$ in terms of the inner asymptotic region coordinates (X,Y),

and the inner asymptotic region variables ϕ_I and η_I, to obtain,

$$\overline{\nabla}^2\phi_I = 0, \qquad (X,Y) \in \mathcal{D}_I(t),\ t>0; \quad (3.1.11)$$

$$\overline{\nabla}\phi_I \cdot \hat{\mathbf{n}} = \sigma \sin\alpha, \qquad X > X_p(t),\ Y = -X\tan\alpha,\ t>0; \quad (3.1.12)$$

$$t\eta_{I,t} + 2\eta_I + [\phi_{I,X} - \sigma - 2X]\,\eta_{I,X} - \phi_{I,Y} = 0,$$

$$X > X_p(t),\ Y = \eta_I(X,t),\ t>0; \quad (3.1.13)$$

$$t\phi_{I,t} + 3\phi_I - (2X+\sigma)\,\phi_{I,X} - 2Y\phi_{I,Y} + \frac{1}{2}\left|\overline{\nabla}\phi_I\right|^2 + \eta_I = 0,$$

$$X > X_p(t),\ Y = \eta_I(X,t),\ t>0; \quad (3.1.14)$$

$$\eta_I(X_p(t),t) = -X_p(t)\tan\alpha, \qquad t>0; \quad (3.1.15)$$

with $\overline{\nabla} = (\partial/\partial X, \partial/\partial Y)$. On substituting from (3.1.5), (3.1.6) and (3.1.7) into (3.1.11) - (3.1.15) we obtain, at leading order, the following nonlinear harmonic free boundary problem[1] for $\phi_0(X,Y)$, $\eta_0(X)$, and X_0, namely

$$\overline{\nabla}^2\phi_0 = 0, \qquad X > X_0,\ -X\tan\alpha < Y < \eta_0(X); \quad (3.1.16)$$

$$\overline{\nabla}\phi_0 \cdot \hat{\mathbf{n}} = \sigma\sin\alpha, \qquad X > X_0,\ Y = -X\tan\alpha; \quad (3.1.17)$$

$$2\eta_0 + [\phi_{0,X} - \sigma - 2X]\,\eta_{0,X} - \phi_{0,Y} = 0, \qquad X > X_0,\ Y = \eta_0(X); \quad (3.1.18)$$

$$3\phi_0 - (2X+\sigma)\,\phi_{0,X} - 2Y\phi_{0,Y} + \frac{1}{2}\left|\overline{\nabla}\phi_0\right|^2 + \eta_0 = 0, \qquad X > X_0,\ Y = \eta_0(X); \quad (3.1.19)$$

$$\eta_0(X_0) = -X_0\tan\alpha. \quad (3.1.20)$$

The problem (3.1.16) - (3.1.20) must be completed by asymptotic matching conditions between the inner asymptotic region and outer asymptotic region. Following Van Dyke's Matching Principle (see, for example, [19]), we obtain

[1] See Appendix A.1 for derivation

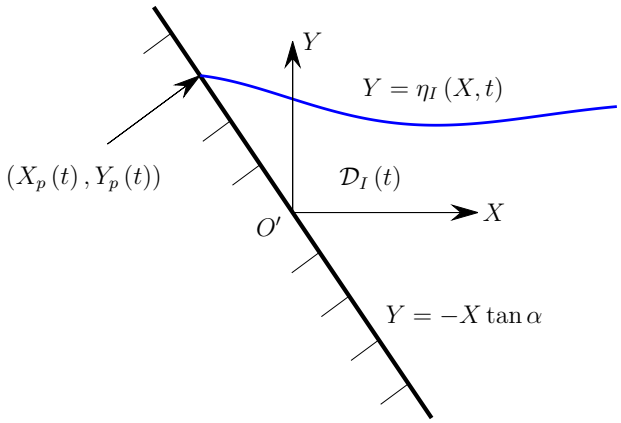

Figure 3.2: The inner asymptotic region geometry

$$\phi_0(R,\theta) \sim \sigma\tan\alpha\ R\sin\theta \quad \text{as} \quad R\to\infty,\ -\alpha<\theta<0, \tag{3.1.21}$$

$$\eta_0(X) \to \frac{1}{2}\sigma\tan\alpha \qquad \text{as} \quad X\to\infty, \tag{3.1.22}$$

where R and θ are polar coordinates given by $X = R\cos\theta$, $Y = R\sin\theta$. It is readily established that the exact solution to the leading order problem (3.1.16) - (3.1.22) is given by

$$\eta_0(X) = \frac{1}{2}\sigma\tan\alpha, \quad X \geqslant X_0, \tag{3.1.23}$$

$$\phi_0(X,Y) = \sigma\tan\alpha\left[Y - \frac{1}{3}\left(\frac{1}{2}+\sigma\tan\alpha\right)\right],$$

$$X \geqslant X_0,\ -X\tan\alpha \leqslant Y \leqslant \frac{1}{2}\sigma\tan\alpha, \tag{3.1.24}$$

with

$$X_0 = -\frac{1}{2}\sigma. \tag{3.1.25}$$

This is represented in the inner asymptotic region in Figure 3.3a. We now formulate the problem at $O\left(t^{\frac{\pi}{\alpha}-2}\right)$, where it is convenient to shift the origin in the inner asymptotic region coordinates. Following Figure 3.3b, we introduce the translated inner region coordinates $\left(\overline{X},\overline{Y}\right)$ according to,

$$X=-\frac{1}{2}\sigma+\overline{X},\quad Y=\frac{1}{2}\sigma\tan\alpha+\overline{Y}, \tag{3.1.26}$$

and then write

$$\tilde{\phi}=A_0\left(\alpha\right)\sigma\sin\alpha\ \hat{\phi}, \tag{3.1.27}$$

$$\tilde{\eta}=A_0\left(\alpha\right)\sigma\sin\alpha\ \hat{\eta}, \tag{3.1.28}$$

with $A_0\left(\alpha\right)$ given in (2.0.15), and the $A_0\left(\alpha\right)\sigma\sin\alpha$ scaling chosen for algebraic convenience. We can now write the problem[2] at $O\left(t^{\frac{\pi}{\alpha}-2}\right)$, for $\hat{\phi}$, $\hat{\eta}$ and X_1, as

$$\hat{\overline{\nabla}}^2\hat{\phi}=0,\qquad \overline{X}>0,\ -\overline{X}\tan\alpha<\overline{Y}<0; \tag{3.1.29}$$

$$\hat{\overline{\nabla}}\hat{\phi}\cdot\hat{\mathbf{n}}=0,\qquad \overline{X}>0,\ \overline{Y}=-\overline{X}\tan\alpha; \tag{3.1.30}$$

$$\frac{\pi}{\alpha}\hat{\eta}-2\overline{X}\hat{\eta}_{\overline{X}}-\hat{\phi}_{\overline{Y}}=0,\qquad \overline{X}>0,\ \overline{Y}=0; \tag{3.1.31}$$

$$\left(1+\frac{\pi}{\alpha}\right)\hat{\phi}-2\overline{X}\hat{\phi}_{\overline{X}}+\left(1+\sigma\tan\alpha\right)\hat{\eta}=0,\qquad \overline{X}>0,\ \overline{Y}=0; \tag{3.1.32}$$

$$\hat{\phi}\left(\overline{R},\theta\right)=-\overline{R}^{\frac{\pi}{2\alpha}}\cos\frac{\pi}{2\alpha}\left(\theta+\alpha\right)+o\left(\overline{R}^{\frac{\pi}{2\alpha}}\right)\qquad \text{as } \overline{R}\to\infty,\ -\alpha<\theta<0; \tag{3.1.33}$$

$$\hat{\eta}\left(\overline{X}\right)=\frac{\pi}{4\alpha}\overline{X}^{\frac{\pi}{2\alpha}-1}+o\left(\overline{X}^{\frac{\pi}{2\alpha}-1}\right)\qquad \text{as } \overline{X}\to\infty. \tag{3.1.34}$$

Here $\hat{\overline{\nabla}}=\left(\partial/\partial\overline{X},\partial/\partial\overline{Y}\right)$, the final conditions (3.1.33) and (3.1.34) are the matching conditions with the outer asymptotic region, and we have introduced polar coordinates

[2]See Appendix A.1 for derivation

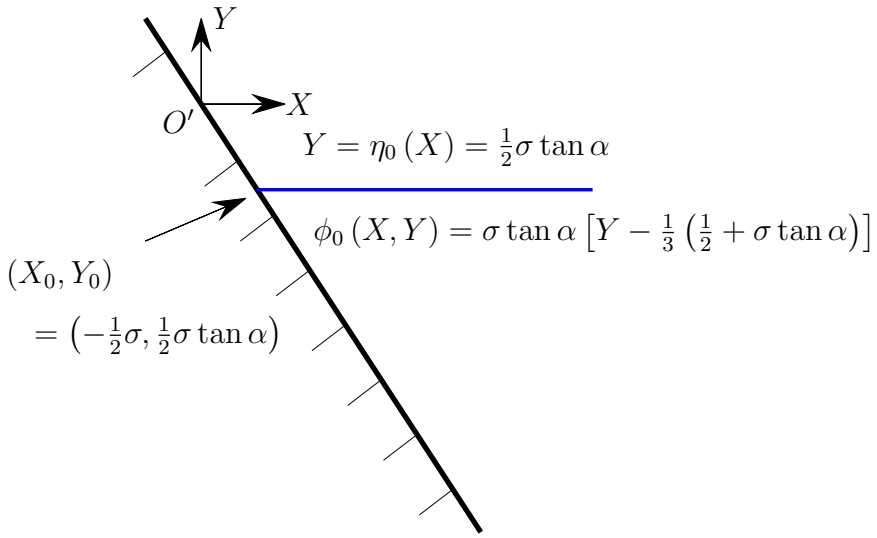

(a) Solution of $[IBVP]$ at leading order in the inner asymptotic region

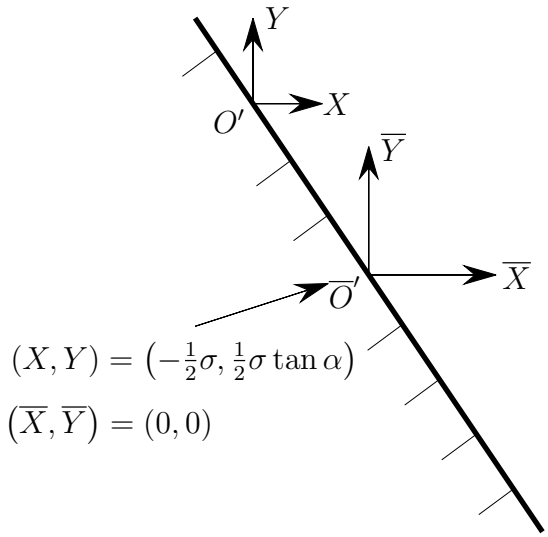

(b) Coordinate shift in the inner asymptotic region

Figure 3.3: Sketches in the inner asymptotic region

$\left(\overline{R},\theta\right)$, given by $\overline{X}=\overline{R}\cos\theta$, $\overline{Y}=\overline{R}\sin\theta$. Finally we have

$$X_1=-A_0\left(\alpha\right)\sigma\cos\alpha\ \hat{\eta}\left(0\right). \tag{3.1.35}$$

We notice that in the boundary value problem (3.1.29) - (3.1.35), the dimensionless acceleration σ appears only in the dynamic boundary condition (3.1.32) in the form $(1+\sigma\tan\alpha)$. Thus, we set $\mu=1+\sigma\tan\alpha$ and, *in the case that* $\mu\neq 0$, we introduce the following scalings[3]

$$\hat{\phi}=|\mu|^{\frac{\pi}{2\alpha}}\psi,\quad \hat{\eta}=|\mu|^{\frac{\pi}{2\alpha}-1}\xi,\quad \overline{X}=|\mu|\,\widehat{X},\quad \overline{Y}=|\mu|\,\widehat{Y}. \tag{3.1.36}$$

The corresponding boundary value problem for $\psi\left(\widehat{X},\widehat{Y}\right)$ and $\xi\left(\widehat{X}\right)$ is now independent of μ, and is given by

$$\widehat{\nabla}^2\psi=0,\quad \widehat{X}>0,\ -\widehat{X}\tan\alpha<\widehat{Y}<0, \tag{3.1.37}$$

$$\widehat{\nabla}\psi\cdot\hat{\mathbf{n}}=0,\quad \widehat{X}>0,\ \widehat{Y}=-\widehat{X}\tan\alpha, \tag{3.1.38}$$

$$\frac{\pi}{\alpha}\xi-2\widehat{X}\xi_{\widehat{X}}-\psi_{\widehat{Y}}=0,\quad \widehat{X}>0,\ \widehat{Y}=0, \tag{3.1.39}$$

$$\left(1+\frac{\pi}{\alpha}\right)\psi-2\widehat{X}\psi_{\widehat{X}}\pm\xi=0,\quad \widehat{X}>0,\ \widehat{Y}=0, \tag{3.1.40}$$

$$\psi\left(\widehat{R},\theta\right)=-\widehat{R}^{\frac{\pi}{2\alpha}}\cos\frac{\pi}{2\alpha}\left(\theta+\alpha\right)+o\left(\widehat{R}^{\frac{\pi}{2\alpha}}\right),\quad \text{as } \widehat{R}\to\infty,\ -\alpha<\theta<0, \tag{3.1.41}$$

$$\xi\left(\widehat{X}\right)=\frac{\pi}{4\alpha}\widehat{X}^{\frac{\pi}{2\alpha}-1}+o\left(\widehat{X}^{\frac{\pi}{2\alpha}-1}\right),\quad \text{as } \widehat{X}\to\infty, \tag{3.1.42}$$

after which,

$$X_1=-A_0\left(\alpha\right)\sigma\cos\alpha\,|\mu|^{\frac{\pi}{2\alpha}-1}\,\xi\left(0\right). \tag{3.1.43}$$

Here $\widehat{\nabla}=\left(\partial/\partial\widehat{X},\partial/\partial\widehat{Y}\right)$, and $\left(\widehat{R},\theta\right)$ are polar coordinates given by $\widehat{X}=\widehat{R}\cos\theta$ and $\widehat{Y}=\widehat{R}\sin\theta$. In this boundary value problem, the + sign is taken in (3.1.40) when $\mu>0$,

[3]See Appendix A.2 for the derivation of these scalings

and the $-$ sign is taken in (3.1.40) when $\mu < 0$. We refer to these two linear harmonic boundary value problems as $[BVP]^+$ and $[BVP]^-$ respectively. We note that α is now the only parameter remaining in each of $[BVP]^+$ and $[BVP]^-$.

3.2 Analysis of $[BVP]^{\pm}$

The full regularity conditions (1.2.30) and (1.2.31) on $[IBVP]$ require the following regularity conditions on each of $[BVP]^{\pm}$, namely,

$$\psi \in \mathcal{C}^1\left(\overline{\mathcal{T}}\right) \cap \mathcal{C}^2\left(\mathcal{T}\right), \qquad \xi \in \mathcal{C}^1\left([0,\infty)\right), \tag{3.2.1}$$

with

$$\mathcal{T} = \left\{\left(\widehat{R},\theta\right) : \widehat{R} > 0,\ -\alpha < \theta < 0\right\}. \tag{3.2.2}$$

Before considering the solution of $[BVP]^{\pm}$ in detail, we first examine the structure of solutions to $[BVP]^{\pm}$ as $\widehat{X}, \widehat{R} \to 0$ and, subsequently, as $\widehat{X}, \widehat{R} \to \infty$. We observe that, from (3.1.40), we have, explicitly,

$$\xi\left(\widehat{X}\right) = \pm\left(2\widehat{X}\psi_{\widehat{X}} - \left(1+\frac{\pi}{\alpha}\right)\psi\right), \quad \widehat{X} > 0,\ \widehat{Y} = 0, \tag{3.2.3}$$

and thus we can eliminate ξ from $[BVP]^{\pm}$ to obtain $[PBVP]^{\pm}$ for ψ alone, as,

$$\psi_{\widehat{R}\widehat{R}} + \frac{1}{\widehat{R}}\psi_{\widehat{R}} + \frac{1}{\widehat{R}^2}\psi_{\theta\theta} = 0, \quad \widehat{R} > 0, \quad -\alpha < \theta < 0, \tag{3.2.4}$$

$$\psi_\theta = 0, \quad \theta = -\alpha, \quad \widehat{R} > 0, \tag{3.2.5}$$

$$\frac{1}{\widehat{R}}\psi_\theta = \pm\left(-\frac{\pi}{\alpha}\left(1+\frac{\pi}{\alpha}\right)\psi + 2\left(1+\frac{2\pi}{\alpha}\right)\widehat{R}\psi_{\widehat{R}} - 4\widehat{R}\left(\widehat{R}\psi_{\widehat{R}}\right)_{\widehat{R}}\right),$$
$$\theta = 0, \quad \widehat{R} > 0, \tag{3.2.6}$$

with the far-field condition,

$$\psi\left(\widehat{R},\theta\right) = -\widehat{R}^{\frac{\pi}{2\alpha}}\cos\frac{\pi}{2\alpha}\left(\theta+\alpha\right) + o\left(\widehat{R}^{\frac{\pi}{2\alpha}}\right) \quad \text{as } \widehat{R}\to\infty \text{ for } -\alpha<\theta<0, \tag{3.2.7}$$

and regularity condition (3.2.1). To begin, it is readily established that any pair of functions $\psi=\Psi$ and $\xi=\zeta$ which satisfy (3.2.3) - (3.2.7) must have the asymptotic form, for some real constants a_n, b_n, $(n=0,1,2,\dots)$,

$$\begin{aligned}\Psi\left(\widehat{R},\theta\right) \sim \sum_{n=1}^{\infty} a_n\psi_{-n}\left(\widehat{R},\theta\right)\widehat{R}^{-\frac{n\pi}{\alpha}}\cos\frac{n\pi}{\alpha}\left(\theta+\alpha\right)\\ + a_0\psi_0^0\left(\widehat{R},\theta\right) + b_0\left(\psi_0^1\left(\widehat{R},\theta\right)\log\widehat{R} + \psi_0^2\left(\widehat{R},\theta\right)\right)\\ + \sum_{n=1}^{\infty} b_n\psi_n\left(\widehat{R},\theta\right)\widehat{R}^{\frac{n\pi}{\alpha}}\cos\frac{n\pi}{\alpha}\left(\theta+\alpha\right),\end{aligned} \tag{3.2.8}$$

as $\widehat{R}\to 0$, uniformly for $-\alpha\leqslant\theta\leqslant 0$, after which

$$\begin{aligned}\zeta\left(\widehat{X}\right) \sim \pm\Bigg\{\sum_{n=1}^{\infty} a_n\left(-1\right)^{n+1}\Big[\left(\left(2n+1\right)\frac{\pi}{\alpha}+1\right)\psi_{-n}\left(\widehat{X},0\right)\widehat{X}^{-\frac{n\pi}{\alpha}}\\ -2\psi_{-n,\widehat{X}}\left(\widehat{X},0\right)\widehat{X}^{1-\frac{n\pi}{\alpha}}\Big] + a_0\Big[-\left(1+\frac{\pi}{\alpha}\right)\psi_0^0\left(\widehat{X},0\right) + 2\widehat{X}\psi_{0,\widehat{X}}^0\left(\widehat{X},0\right)\Big]\\ + b_0\Big[2\psi_0^1\left(\widehat{X},0\right) - \left(1+\frac{\pi}{\alpha}\right)\psi_0^2\left(\widehat{X},0\right) + \widehat{X}\psi_{0,\widehat{X}}^2\left(\widehat{X},0\right)\\ - \left(1+\frac{\pi}{\alpha}\right)\psi_0^1\left(\widehat{X},0\right)\log\widehat{X} + \psi_{0,\widehat{X}}^1\widehat{X}\log\widehat{X}\Big]\\ + \sum_{n=1}^{\infty} b_n\left(-1\right)^n\Big[\left(\left(2n-1\right)\frac{\pi}{\alpha}-1\right)\psi_n\left(\widehat{X},0\right)\widehat{X}^{\frac{n\pi}{\alpha}}\\ +2\psi_{n,\widehat{X}}\left(\widehat{X},0\right)\widehat{X}^{1+\frac{n\pi}{\alpha}}\Big]\Bigg\},\end{aligned} \tag{3.2.9}$$

as $\widehat{X}\to 0$. Here $\psi_{\pm n}\left(\widehat{R},\theta\right)$ $(n=1,2,\dots)$, $\psi_0^0\left(\widehat{R},\theta\right)$, $\psi_0^1\left(\widehat{R},\theta\right)$, $\psi_0^2\left(\widehat{R},\theta\right)$ are regular as $\widehat{R}\to 0$, with $-\alpha\leqslant\theta\leqslant 0$, are determined uniquely term by term in integral powers of

$\widehat{R}$ as $\widehat{R} \to 0$, and satisfy

$$\begin{cases} \psi_{\pm n}\left(\widehat{R},\theta\right), \psi_0^0\left(\widehat{R},\theta\right), \psi_0^1\left(\widehat{R},\theta\right) \to 1, \\ \psi_0^2\left(\widehat{R},\theta\right) \to 0, \end{cases} \tag{3.2.10}$$

as $\widehat{R} \to 0$, uniformly for $-\alpha \leqslant \theta \leqslant 0$. Specifically,

$$\psi_0^0\left(\widehat{R},\theta\right) = 1 + \widehat{R}\widehat{F}\left(\theta\right) + O\left(\widehat{R}^2\right), \tag{3.2.11}$$

as $\widehat{R} \to 0$ for $-\alpha \leqslant \theta \leqslant 0$, where,

$$\widehat{F}\left(\theta\right) = \pm \frac{\pi\left(1+\frac{\pi}{\alpha}\right)}{\alpha \sin\alpha} \cos\left(\theta+\alpha\right), \quad -\alpha \leqslant \theta \leqslant 0, \tag{3.2.12}$$

for $[PBVP]^+$ and $[PBVP]^-$ respectively. We conclude from the regularity condition (3.2.1) and the asymptotic form (3.2.8) that any solution to $[PBVP]^{\pm}$ must have,

$$\psi\left(\widehat{R},\theta\right) \sim a_0\psi_0^0\left(\widehat{R},\theta\right) + \sum_{n=1}^{\infty} b_n\psi_n\left(\widehat{R},\theta\right)\widehat{R}^{\frac{n\pi}{\alpha}} \cos\frac{n\pi}{\alpha}\left(\theta+\alpha\right), \tag{3.2.13}$$

as $\widehat{R} \to 0$, uniformly for $-\alpha \leqslant \theta \leqslant 0$, and some globally determined real constants, a_0, b_n $(n = 1, 2, \dots)$ not all zero, and, via (3.2.1) and (3.2.9),

$$\begin{aligned} \xi\left(\widehat{X}\right) \sim \pm a_0 &\left[-\left(1+\frac{\pi}{\alpha}\right)\psi_0^0\left(\widehat{X},0\right) + 2\widehat{X}\psi_{0,\widehat{X}}^0\left(\widehat{X},0\right)\right] \\ &+ \sum_{n=1}^{\infty} b_n\left(-1\right)^n\left\{\left[\left(2n-1\right)\frac{\pi}{\alpha}-1\right]\psi_n\left(\widehat{X},0\right)\widehat{X}^{\frac{n\pi}{\alpha}} + 2\widehat{X}^{\frac{n\pi}{\alpha}+1}\psi_{n,\widehat{X}}\right\}, \end{aligned} \tag{3.2.14}$$

as $\widehat{X} \to 0$. Similarly we can establish the asymptotic form,

$$\Psi\left(\widehat{R},\theta\right) \sim \sum_{n=1}^{\infty} a_n^{\infty}\psi_n^{\infty}\left(\widehat{R},\theta\right)\widehat{R}^{\left(n+\frac{1}{2}\right)\frac{\pi}{\alpha}}\cos\left(n+\frac{1}{2}\right)\frac{\pi}{\alpha}\left(\theta+\alpha\right)$$
$$+ a_0^{\infty}\psi_0^{\infty}\left(\widehat{R},\theta\right)\widehat{R}^{\frac{\pi}{2\alpha}}\cos\frac{\pi}{2\alpha}\left(\theta+\alpha\right)$$
$$+ \sum_{n=1}^{\infty} b_n^{\infty}\psi_{-n}^{\infty}\left(\widehat{R},\theta\right)\widehat{R}^{-\left(n-\frac{1}{2}\right)\frac{\pi}{\alpha}}\cos\left(n-\frac{1}{2}\right)\frac{\pi}{\alpha}\left(\theta+\alpha\right), \qquad (3.2.15)$$

as $\widehat{R} \to \infty$, uniformly for $-\alpha \leqslant \theta \leqslant 0$, for some real constants a_0^{∞} and a_n^{∞}, b_n^{∞} $(n = 1, 2, \dots)$, after which

$$\zeta\left(\widehat{X}\right) \sim \sum_{n=1}^{\infty} \hat{a}_n^{\infty}\xi_n^{\infty}\left(\widehat{X}\right)\widehat{X}^{\left(n+\frac{1}{2}\right)\frac{\pi}{\alpha}-1} + \hat{a}_0^{\infty}\xi_0^{\infty}\left(\widehat{X}\right)\widehat{X}^{\frac{\pi}{2\alpha}-1}$$
$$+ \sum_{n=1}^{\infty} \hat{b}_n^{\infty}\xi_{-n}^{\infty}\left(\widehat{X}\right)\widehat{X}^{-\left(n-\frac{1}{2}\right)\frac{\pi}{\alpha}-1}, \qquad (3.2.16)$$

as $\widehat{X} \to \infty$, for some real constants $\hat{a}_0^{\infty}$ and $\hat{a}_n^{\infty}$, $\hat{b}_N^{\infty}$ $(n = 1, 2, \dots)$. Here $\psi_{\pm n}^{\infty}\left(\widehat{R},\theta\right)$ are regular as $\widehat{R} \to \infty$ with $-\alpha \leqslant \theta \leqslant 0$, and are determined uniquely term by term in powers of $\widehat{R}^{-1}$ as $\widehat{R} \to \infty$, and satisfy

$$\psi_{\pm n}^{\infty}\left(\widehat{R},\theta\right) \to 1, \qquad \text{as } \widehat{R} \to \infty, \text{ uniformly for } -\alpha \leqslant \theta \leqslant 0. \qquad (3.2.17)$$

Similarly $\xi_{\pm n}^{\infty}\left(\widehat{X}\right)$ are regular as $\widehat{X} \to \infty$, and are determined uniquely term by term in powers of $\widehat{X}^{-1}$, and satisfy

$$\xi_{\pm n}^{\infty}\left(\widehat{X}\right) \to 1, \qquad \text{as } \widehat{X} \to \infty. \qquad (3.2.18)$$

Specifically, we have,

$$\psi_0^{\infty}\left(\widehat{R},\theta\right) = 1 + \frac{1}{\widehat{R}}P_1\left(\theta\right) + \frac{1}{\widehat{R}^2}P_2\left(\theta\right) + O\left(\frac{1}{\widehat{R}^3}\right), \qquad (3.2.19)$$

as $\widehat{R} \to \infty$, uniformly for $-\alpha \leqslant \theta \leqslant 0$. Here

$$p_1(\theta) = \mp \frac{\pi}{12\alpha \sin\alpha} \frac{\cos\left(\frac{\pi}{2\alpha} - 1\right)(\theta + \alpha)}{\cos\frac{\pi}{2\alpha}(\theta + \alpha)}, \tag{3.2.20}$$

$$p_2(\theta) = -\frac{\pi\left(\frac{\pi}{2\alpha} - 1\right)\cos\alpha}{240\alpha \sin\alpha \sin 2\alpha} \frac{\cos\left(\frac{\pi}{2\alpha} - 2\right)(\theta + \alpha)}{\cos\frac{\pi}{2\alpha}(\theta + \alpha)}, \tag{3.2.21}$$

for $-\alpha \leqslant \theta \leqslant 0$, after which

$$\xi_0^\infty\left(\widehat{X}\right) = 1 + \frac{1}{\widehat{X}} Q_1 + \frac{1}{\widehat{X}^2} Q_2 + O\left(\frac{1}{\widehat{X}^3}\right), \tag{3.2.22}$$

as $\widehat{X} \to \infty$. Here

$$Q_1 = -\frac{\left(\frac{\pi}{2\alpha} - 1\right)}{12\alpha \tan\alpha}, \tag{3.2.23}$$

$$Q_2 = \frac{\left(\frac{\pi}{2\alpha} - 1\right)\left(\frac{\pi}{2\alpha} - 2\right)}{360\alpha \tan\alpha \tan 2\alpha}. \tag{3.2.24}$$

We may now conclude from (3.2.15) and (3.2.16), that any solution to $[PBVP]^{\pm}$ must have,

$$\begin{aligned}\psi\left(\widehat{R}, \theta\right) \sim & -\psi_0^\infty\left(\widehat{R}, \theta\right) \widehat{R}^{\frac{\pi}{2\alpha}} \cos\frac{\pi}{2\alpha}(\theta + \alpha) \\ & + \sum_{n=1}^{\infty} b_n^\infty \psi_{-n}^\infty\left(\widehat{R}, \theta\right) \widehat{R}^{-\left(n - \frac{1}{2}\right)\frac{\pi}{\alpha}} \cos\left(n - \frac{1}{2}\right)\frac{\pi}{\alpha}(\theta + \alpha),\end{aligned} \tag{3.2.25}$$

as $\widehat{R} \to \infty$, uniformly for $-\alpha \leqslant \theta \leqslant 0$, and some globally determined real constants b_n^∞ $(n = 1, 2, \dots)$, with

$$\xi\left(\widehat{X}\right) \sim \frac{\pi}{4\alpha} \xi_0^\infty\left(\widehat{X}\right) \widehat{X}^{\frac{\pi}{2\alpha} - 1} + \sum_{n=1}^{\infty} \hat{b}_n^\infty \xi_{-1}^\infty \widehat{X}^{-\left(n - \frac{1}{2}\right)\frac{\pi}{\alpha} - 1}, \tag{3.2.26}$$

as $\widehat{X} \to \infty$, and some globally determined real constants $\hat{b}_n^{\infty}$ $(n = 1, 2, \dots)$. Thus both of $[PBVP]^+$ and $[PBVP]^-$ will admit a solution with regularity (3.2.1) as $\widehat{X}, \widehat{R} \to 0$. Following [24], we observe that both $[PBVP]^{\pm}$ admit exact solutions for the angles $\alpha = \alpha_n \in \left(0, \frac{1}{4}\pi\right]$, where

$$\alpha_n = \frac{\pi}{2\,(n+1)}, \qquad n = 1, 2, \dots . \tag{3.2.27}$$

For $[PBVP]^+$, we have the exact solution at $\alpha = \alpha_n$, $(n = 1, 2, \dots)$ given by,

$$\psi\left(\widehat{R}, \theta\right) = \sum_{p=0}^{n+1} \overline{a}_p \widehat{R}^p \cos p\,(\theta + \alpha_n), \quad \widehat{R} \geqslant 0,\ -\alpha_n \leqslant \theta \leqslant 0; \tag{3.2.28}$$

with, via (3.2.3),

$$\xi\left(\widehat{X}\right) = \sum_{p=0}^{n} \overline{a}_p \left[2p - (2n+3)\right] \cos\left(p\alpha_n\right) \widehat{X}^p, \qquad \widehat{X} \geqslant 0; \tag{3.2.29}$$

and where,

$$\overline{a}_p = \frac{-\left(\frac{1}{2}\right)!\,(n+1)! \prod_{k=p+1}^{n+1} \sin\left(k\alpha_n\right)}{4^{n+1-p} p!\,(n+1-p)!\left(n + \frac{3}{2} - p\right)! \prod_{k=p}^{n} \cos\left(k\alpha_n\right)}, \tag{3.2.30}$$

for $p = 0, 1, 2, \dots, n$, with $a_{n+1} = -1$. In this case, the near-field constant, a_0 in (3.2.13), for $[PBVP]^+$, is given by

$$a_0 = \frac{-\left(\frac{1}{2}\right)! \prod_{k=1}^{n+1} \sin\left(k\alpha_n\right)}{4^{n+1}\left(n + \frac{3}{2}\right)! \prod_{k=0}^{n} \cos\left(k\alpha_n\right)}. \tag{3.2.31}$$

For $[PBVP]^-$ we have the exact solution at $\alpha = \alpha_n$ $(n = 1, 2, \dots)$ given by,

$$\psi\left(\widehat{R}, \theta\right) = \sum_{p=0}^{n+1} (-1)^{n+1-p}\, \overline{a}_p \widehat{R}^p \cos p\,(\theta + \alpha_n), \quad \widehat{R} \geqslant 0,\ -\alpha_n \leqslant \theta \leqslant 0; \tag{3.2.32}$$

with, via (3.2.3),

$$\xi\left(\widehat{X}\right)=\sum_{p=0}^{n}(-1)^{n-p}\,\overline{a}_p\,[2p-(2n+3)]\cos\left(p\alpha_n\right)\widehat{X}^p,\qquad \widehat{X}\geqslant 0; \tag{3.2.33}$$

and the near-field constant for $[PBVP]^-$, a_0 in (3.2.13), is given by,

$$a_0=\frac{(-1)^n\left(\frac{1}{2}\right)!\prod_{k=1}^{n+1}\sin\left(k\alpha_n\right)}{4^{n+1}\left(n+\frac{3}{2}\right)!\prod_{k=0}^{n}\cos\left(k\alpha_n\right)}. \tag{3.2.34}$$

The simplest case occurs for $n=1$ when $\alpha=\alpha_1=\frac{1}{4}\pi$, with, from (3.2.28), (3.2.29), and (3.2.30), for $[PBVP]^+$ we have,

$$\psi\left(\widehat{R},\theta\right)=-\frac{1}{60}-\frac{\sqrt{2}}{3}\widehat{R}\cos\left(\theta+\frac{\pi}{4}\right)-\widehat{R}^2\cos 2\left(\theta+\frac{\pi}{4}\right),$$
$$\widehat{R}\geqslant 0,\ -\frac{\pi}{4}\leqslant\theta\leqslant 0, \tag{3.2.35}$$

$$\xi\left(\widehat{X}\right)=\frac{1}{12}+\widehat{X},\qquad \widehat{X}\geqslant 0, \tag{3.2.36}$$

whilst, from (3.2.30), (3.2.32), and (3.2.33), for $[PBVP]^-$ we have,

$$\psi\left(\widehat{R},\theta\right)=-\frac{1}{60}+\frac{\sqrt{2}}{3}\widehat{R}\cos\left(\theta+\frac{\pi}{4}\right)-\widehat{R}^2\cos 2\left(\theta+\frac{\pi}{4}\right),$$
$$\widehat{R}\geqslant 0,\ -\frac{\pi}{4}\leqslant\theta\leqslant 0, \tag{3.2.37}$$

$$\xi\left(\widehat{X}\right)=-\frac{1}{12}+\widehat{X},\qquad \widehat{X}\geqslant 0. \tag{3.2.38}$$

In this case, the near field constant is given by

$$a_0=-\frac{1}{60}, \tag{3.2.39}$$

for both $[PBVP]^+$ and $[PBVP]^-$.

We now consider the numerical solution of both $[PBVP]^+$ and $[PBVP]^-$ in detail.

3.3 Numerical Method

In this section we outline the numerical method used to provide a numerical solution to $[PBVP]^{\pm}$. This is based upon a finite difference approach, with the associated linear algebraic equations solved using MATLAB® [21].

We first discretise the wedge domain for $[PBVP]^{\pm}$ using a five-point stencil in polar coordinates as illustrated in Figure 3.4. The grid is composed of two regions, within which we employ a uniform grid-spacing (I and II in Figure 3.4a) with azimuthal grid spacing $\Delta\theta$ and radial grid spacings of $\Delta\widehat{R}_1$ and $\Delta\widehat{R}_2$ respectively. These two regions are connected across the arc at $\widehat{R} = \widehat{R}^*$, as shown in Figure 3.4a. Such schemes are discussed in [18].

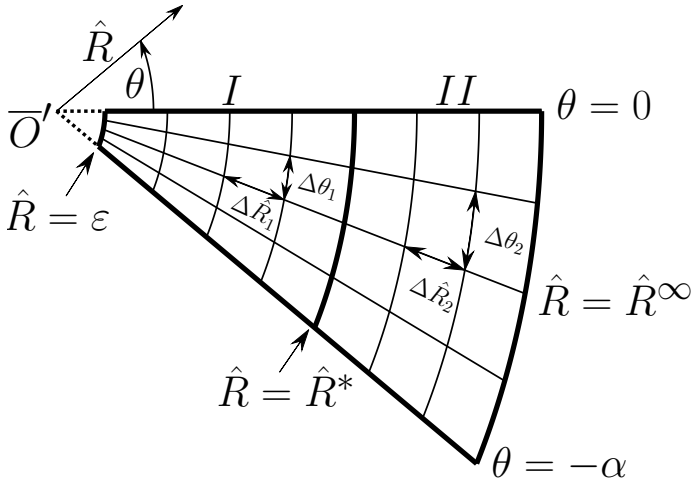

(a) The discretised wedge

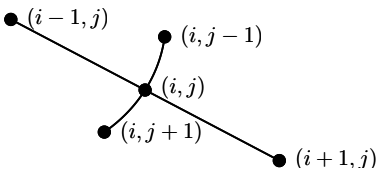

(b) The five-point stencil in polar coordinates

Figure 3.4: Discretisation of the wedge with a non-uniform grid

3.3.1 The Grid

The grid, as shown in Figure 3.4a, is discretised as follows:

(a) Azimuthally:

We write,

$$\theta = \theta_j = -\left(j-1\right)\Delta\theta, \qquad j = 1, 2, \ldots, J+1, \tag{3.3.1}$$

with $\Delta\theta = \frac{\alpha}{J}$, and $J \in \mathbb{N}$ to be chosen.

(b) Radially:

We write,

$$\widehat{R} = \widehat{R}_i = i\Delta\widehat{R}_1, \qquad i = 1, 2, \ldots, n \qquad \text{in } I, \tag{3.3.2}$$

$$\widehat{R} = \widehat{R}_i = \widehat{R}^* + (i-n)\,\Delta\widehat{R}_2, \qquad i = n+1, n+2, \ldots, N+1 \qquad \text{in } II, \tag{3.3.3}$$

with

$$\Delta\widehat{R}_1 = \frac{\widehat{R}^*}{n}, \qquad \text{and} \qquad \Delta\widehat{R}_2 = \frac{\left(\widehat{R}^\infty - \widehat{R}^*\right)}{(N+1-n)}, \tag{3.3.4}$$

where $n, N \in \mathbb{N}$ (with $N > n$), $\widehat{R}^*$ and $\widehat{R}^\infty$ are to be chosen.

In what follows we impose the far-field boundary condition (3.2.25) in $[PBVP]^{\pm}$ at $\widehat{R} = \widehat{R}^\infty \left(\gg 1\right)$. In addition we impose a near-field boundary condition at $\widehat{R} = \varepsilon \left(\ll 1\right)$, the details of which are found in Appendix A.3, which expresses the regularity requirement (3.2.1) in $[PBVP]^{\pm}$ as $\widehat{R} \to 0$.

3.3.2 Finite Difference Approximations

With the notation $\psi_{i,j} = \psi\left(\widehat{R}_i, \theta_j\right)$ we use the centred finite difference scheme with a five-point stencil (see Figure 3.4b) to approximate the derivatives in $[PBVP]^{\pm}$, giving

the following discretisations,

$$\left.\frac{\partial\psi}{\partial\theta}\right|_{i,j} = \frac{\psi_{i,j-1}-\psi_{i,j+1}}{2\Delta\theta}, \qquad \left.\frac{\partial\psi}{\partial\widehat{R}}\right|_{i,j} = \frac{\psi_{i+1,j}-\psi_{i-1,j}}{\delta},$$
$$\left.\frac{\partial^2\psi}{\partial\widehat{R}^2}\right|_{i,j} = \frac{2}{\delta}\left(\frac{\psi_{i+1,j}-\psi_{i,j}}{\Delta\widehat{R}_l} - \frac{\psi_{i,j}-\psi_{i-1,j}}{\Delta\widehat{R}_k}\right), \quad \left.\frac{\partial^2\psi}{\partial\theta^2}\right|_{i,j} = \frac{\psi_{i,j-1}-2\psi_{i,j}+\psi_{i,j+1}}{\Delta\theta^2}, \quad (3.3.5)$$

where

$$\delta = \Delta\widehat{R}_k + \Delta\widehat{R}_l \qquad \text{and} \qquad k,l = \begin{cases} (1,1)\,, & i = 1,2,\ldots,n-1, \\ (1,2) & i = n, \\ (2,2) & i = n+1, n+2, \ldots, N+1. \end{cases} \quad (3.3.6)$$

3.3.3 Linear Algebraic Equations for $\psi_{i,j}$ $(i = 1,2,\ldots,N+1;$ $j = 1,2,\ldots,J+1)$

As detailed in Appendix A.4, we use the aforementioned finite difference approximations for partial derivatives (3.3.5) in order to generate $N\,(J+1)$ linear algebraic equations to be solved for the unknowns $\psi_{i,j}$ $(i = 1,2,\ldots,N;\ j = 1,2,\ldots,J+1)$. We order these unknowns by grouping along a ray, then incrementing θ to cover the whole domain. It is convenient to introduce notation in the following way. First, we introduce the $N\,(J+1)\times 1$ vector $\mathbf{v}$ by

$$\mathbf{v} = \begin{bmatrix} \overline{\psi}_1 \\ \overline{\psi}_2 \\ \vdots \\ \overline{\psi}_J \\ \overline{\psi}_{J+1} \end{bmatrix} \quad \text{with} \quad \overline{\psi}_j = \begin{bmatrix} \psi_{1,j} \\ \psi_{2,j} \\ \vdots \\ \psi_{N-1,j} \\ \psi_{N,j} \end{bmatrix} \quad (3.3.7)$$

After discretisation of the equations and boundary conditions in $[PBVP]^{\pm}$, together with a suitable regularity condition at $\widehat{R}_1$ (see Appendix A.3 for details), we obtain the large, sparse, linear algebraic system

$$A\mathbf{v} = \mathbf{b}. \tag{3.3.8}$$

Here A is a large, sparse, block tridiagonal matrix of dimension $N(J+1) \times N(J+1)$ and $\mathbf{b}$ is a $N(J+1) \times 1$ vector. In particular $\mathbf{b}$ is given by

$$\mathbf{b} = \begin{bmatrix} \overline{\mathbf{b}}_1 \\ \overline{\mathbf{b}}_2 \\ \vdots \\ \overline{\mathbf{b}}_J \\ \overline{\mathbf{b}}_{J+1} \end{bmatrix}, \tag{3.3.9}$$

with

$$\overline{\mathbf{b}}_i(j) = 0, \qquad i = 1, 2, \ldots, J+1, \ j = 1, 2, \ldots, N-1, \tag{3.3.10}$$

$$\overline{\mathbf{b}}_i(N) = \begin{cases} \left(c_N^e + c_N^n c_N^{fe}\right) \psi_1^{\infty}, & i = 1, \\ c_n^e \psi_{i/N}^{\infty}, & i = 2, 3, \ldots, J+1, \end{cases} \tag{3.3.11}$$

and A is given by

$$A = \begin{bmatrix} C + C_f & C_s + C_n & & & 0 \\ C_n & C & C_s & & \\ & \ddots & \ddots & \ddots & \\ & & C_n & C & C_s \\ 0 & & & C_n + C_s & C \end{bmatrix}, \tag{3.3.12}$$

with C, C_f tridiagonal and C_n, C_s diagonal matrices all of dimension $N \times N$, given by

$$C_n = diag\left(c_1^n + \frac{\delta}{2\Delta\theta\widehat{R}_1 \tan(\theta_j + \alpha)} c_1^w, c_2^n, \ldots, c_{N_1}^n, c_N^n\right),$$
$$C_s = diag\left(c_1^s - \frac{\delta}{2\Delta\theta\widehat{R}_1 \tan(\theta_j + \alpha)} c_1^w, c_2^s, \ldots, c_{N_1}^s, c_N^s\right),$$

$$C = \begin{bmatrix} c_1^o & c_1^e + c_1^w & & & 0 \\ c_2^w & c_2^o & c_2^e & & \\ & \ddots & \ddots & \ddots & \\ & & c_{N-1}^w & c_{N-1}^o & c_{N-1}^e \\ 0 & & & c_N^w & c_N^o \end{bmatrix}, \tag{3.3.13}$$

$$C_f = \begin{bmatrix} \frac{1}{1-\frac{\delta}{2\Delta\theta\widehat{R}_1 \tan\alpha} c_1^{fw}} c_1^{fo} & \frac{1}{1-\frac{\delta}{2\Delta\theta\widehat{R}_1 \tan\alpha} c_1^{fw}} \left(c_1^{fe} + c_1^{fw}\right) & & 0 \\ c_2^n c_2^{fw} & c_2^n c_2^{fo} & c_2^n c_2^{fe} & \\ \ddots & \ddots & \ddots & \\ & c_{N-1}^n c_{N-1}^{fw} & c_{N-1}^n c_{N-1}^{fo} & c_{N-1}^n c_{N-1}^{fe} \\ 0 & & c_N^n c_N^{fw} & c_N^n c_N^{fo} \end{bmatrix}, \tag{3.3.14}$$

where $c_i^n, c_i^s, c_i^e, c_i^w, c_i^o$ are the coefficients of the five-point stencil, derived in Appendix A.4,

and are given by

$$c_i^w = \widehat{R}_i^2 \delta^* \left(\frac{2}{\delta \Delta \widehat{R}_k} - \frac{1}{\delta \widehat{R}_i} \right), \tag{3.3.15}$$

$$c_i^o = -2\widehat{R}_i^2 \delta^* \left(\frac{1}{\Delta\theta^2 \widehat{R}_i^2} + \frac{1}{\delta^*} \right), \tag{3.3.16}$$

$$c_i^e = \widehat{R}_i^2 \delta^* \left(\frac{2}{\delta \Delta \widehat{R}_l} + \frac{1}{\delta \widehat{R}_i} \right), \tag{3.3.17}$$

$$c_i^n = c_i^s = \frac{\delta^*}{\Delta\theta^2}, \tag{3.3.18}$$

for $i = 1, 2, \ldots, N$ with $\delta^* = \Delta \widehat{R}_k \Delta \widehat{R}_l$, and c_i^{fo}, c_i^{fe}, c_i^{fw}, also derived in Appendix A.4, given by

$$c_i^{fw} = -2\widehat{R}_i \Delta\theta \left[\frac{8\widehat{R}_i^2}{\delta \Delta \widehat{R}_k} - 2\widehat{R}_i \frac{1}{\delta} \left(1 - 2\frac{\pi}{\alpha} \right) \right], \tag{3.3.19}$$

$$c_i^{fo} = -2\widehat{R}_i \Delta\theta \left[\frac{\pi}{\alpha} \left(1 + \frac{\pi}{\alpha} \right) - \frac{2}{\delta} \left(\frac{4\widehat{R}_i^2}{\Delta \widehat{R}_l} + \frac{4\widehat{R}_i^2}{\Delta \widehat{R}_k} \right) \right], \tag{3.3.20}$$

$$c_i^{fe} = -2\widehat{R}_i \Delta\theta \left[\frac{8\widehat{R}_i^2}{\delta \Delta \widehat{R}_l} + 2\widehat{R}_i \frac{1}{\delta} \left(1 - 2\frac{\pi}{\alpha} \right) \right], \tag{3.3.21}$$

for $[PBVP]^+$ $(i = 1, 2, \ldots, N)$, and finally

$$c_i^{fw} = 2\widehat{R}_i \Delta\theta \left[\frac{8\widehat{R}_i^2}{\delta \Delta \widehat{R}_k} - 2\widehat{R}_i \frac{1}{\delta} \left(1 - 2\frac{\pi}{\alpha} \right) \right], \tag{3.3.22}$$

$$c_i^{fo} = 2\widehat{R}_i \Delta\theta \left[\frac{\pi}{\alpha} \left(1 + \frac{\pi}{\alpha} \right) - \frac{2}{\delta} \left(\frac{4\widehat{R}_i^2}{\Delta \widehat{R}_l} + \frac{4\widehat{R}_i^2}{\Delta \widehat{R}_k} \right) \right], \tag{3.3.23}$$

$$c_i^{fe} = 2\widehat{R}_i \Delta\theta \left[\frac{8\widehat{R}_i^2}{\delta \Delta \widehat{R}_l} + 2\widehat{R}_i \frac{1}{\delta} \left(1 - 2\frac{\pi}{\alpha} \right) \right], \tag{3.3.24}$$

for $[PBVP]^-$ $(i = 1, 2, \ldots, N)$. The large sparse system (3.3.8) is now solved using MATLAB's mldivide algorithm.

3.4 Numerical Results for $[PBVP]^+$

In this section we examine results obtained by solving $[PBVP]^+$ numerically, as discussed in §3.3. When solving $[PBVP]^+$ numerically, we first set the numerical parameters as discussed in §3.3.1. We begin by setting $\widehat{R}^\infty = 2.5$. This value could be optimised, but it has proven to be sufficient for achieving the far-field form for ψ (3.2.19) and ξ (3.2.22). This choice of $\widehat{R}^\infty$ is useful in that it allows comparison with the results in [24], and it is also small enough to allow us to take $\Delta\widehat{R}_1 = \Delta\widehat{R}_2$, leaving us free to choose $\widehat{R}^*$ to be any suitable value in the range $\varepsilon < \widehat{R}^* < \widehat{R}^\infty$. For simplicity we let $\widehat{R}^* = 1$. We also choose $\varepsilon = 10^{-4}$, as a sufficiently small value to satisfy regularity required by (3.2.1), via the near-field condition (A.3.2).

Table 3.1: Convergence of the numerical solution to $[PBVP]^+$ to the far-field asymptotic forms (3.2.19) and (3.2.22) for decreasing $\Delta\widehat{R}_1$, $\alpha = \frac{1}{4}\pi$ and $J + 1 = 30$. In this case $\Delta\widehat{R}_1 = \Delta\widehat{R}_2$. This table shows the percentage error between numerically calculated solutions and the far-field asymptotic forms. Time t (given in seconds) is the calculation time for a typical run

$\Delta\widehat{R}_1$	ξ_{error} (%)	ψ_{error} (%)	t (seconds)
5×10^{-2}	9.59×10^{-4}	1.49×10^{-5}	0.0618
1×10^{-2}	1.92×10^{-4}	5.88×10^{-7}	0.0812
5×10^{-3}	9.63×10^{-5}	1.47×10^{-7}	0.115
1×10^{-3}	1.93×10^{-5}	5.86×10^{-9}	0.577
5×10^{-4}	9.63×10^{-6}	1.46×10^{-9}	1.54
1×10^{-4}	1.93×10^{-6}	5.89×10^{-11}	24.4
5×10^{-5}	9.62×10^{-7}	1.49×10^{-11}	91.5
1×10^{-5}	1.86×10^{-7}	1.32×10^{-12}	2280

In Table 3.1 we show the percentage error between numerically calculated solutions to $[PBVP]^+$ and the far-field asymptotic forms, (3.2.19) and (3.2.22) for ψ and ξ respectively, for decreasing values of $\Delta\widehat{R}_1$. We can see from Table 3.1 that as we decrease the step-size $\Delta\widehat{R}_1$ by a factor of 10, the percentage error between our numerically calculated solution to $[PBVP]^+$ and the far-field asymptotic forms (3.2.19) and (3.2.22) also drops by a factor of

Table 3.2: Convergence of the numerical solution to $[PBVP]^+$ to the far-field asymptotic forms (3.2.19) and (3.2.22) for decreasing $\Delta\theta$, $\alpha = \frac{1}{4}\pi$ and $\Delta\widehat{R}_1 = \Delta\widehat{R}_2 = 10^{-3}$. In this case $\Delta\widehat{R}_1 = \Delta\widehat{R}_2$. This table shows the percentage error between numerically calculated solutions and the far-field asymptotic forms. Time t (given in seconds) is the calculation time for a typical run. All values rounded to 3 s.f.

$J+1$	$\Delta\theta$	ξ_{error} (%)	ψ_{error} (%)	t (seconds)
8	1×10^{-1}	2.54×10^{-4}	7.71×10^{-8}	0.171
16	5×10^{-2}	6.33×10^{-5}	1.93×10^{-8}	0.305
79	1×10^{-2}	2.59×10^{-6}	7.89×10^{-10}	1.44
157	5×10^{-3}	6.57×10^{-7}	2.00×10^{-10}	3.95
785	1×10^{-3}	2.63×10^{-8}	7.84×10^{-12}	49.3
1571	5×10^{-4}	6.55×10^{-9}	1.87×10^{-12}	161
7854	1×10^{-4}	2.63×10^{-101}	2.74×10^{-13}	4470

10. However this comes with a run time penalty; it is clear that as we increase the number of points, the computation time increases considerably. Based on these figures, a radial grid-spacing of $\Delta\widehat{R}_1 = 10^{-3}$ was chosen, giving small percentage errors whilst keeping the time costs of numerically solving $[PBVP]^+$ at a reasonable level. Similarly, in Table 3.2 we show the percentage error between numerically calculated solutions to $[PBVP]^+$ and the far-field asymptotic forms, (3.2.19) and (3.2.22) for ψ and ξ respectively, for decreasing values of $\Delta\theta$. We see that as we decrease $\Delta\theta$ the percentage error drops ten times as quickly as for $\Delta\widehat{R}_1$, and, as before, the run time cost increases with decreasing $\Delta\theta$. We chose a value of $\Delta\theta = 10^{-2}$ as sufficient here.

To begin, we choose angles $\alpha = \frac{1}{4}\pi$ and $\alpha = \frac{1}{6}\pi$, numerically solve $[PBVP]^+$ using the scheme detailed in §3.3 for each angle, and plot the level curves of ψ in $\widehat{R} \geqslant 0$, $-\alpha \leqslant \theta \leqslant 0$, (Figure 3.5), the vector field $\widehat{\nabla}\psi$ in $\widehat{R} \geqslant 0$, $-\alpha \leqslant \theta \leqslant 0$, (Figure 3.6) and ξ in $\widehat{X} \geqslant 0$ (Figure 3.7).

The exact solution to $[PBVP]^+$ for ψ, and corresponding exact solution for ξ, (equations (3.2.28) and (3.2.29)), are plotted in Figures 3.8, and 3.9 for both $\alpha = \frac{1}{4}\pi$ and $\alpha = \frac{1}{6}\pi$. Comparisons show excellent agreement between these exact solutions and the numerically calculated solutions. Choosing two more angles, namely $\alpha = \frac{3}{8}\pi$ and $\alpha = \frac{1}{8}\pi$,

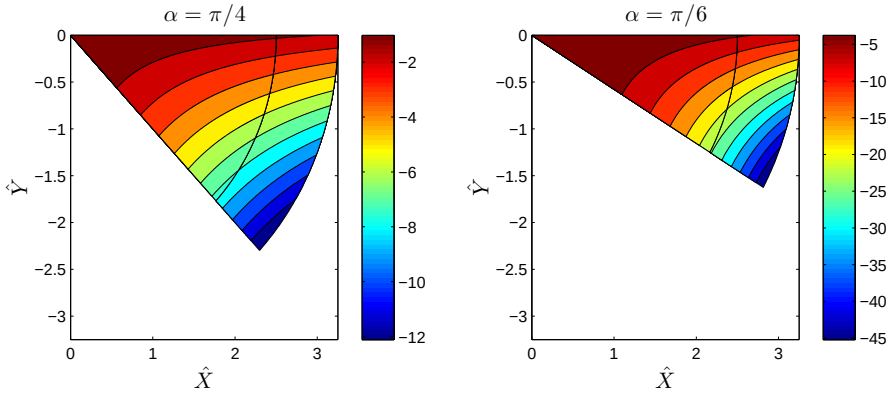

Figure 3.5: Contours of ψ for the numerical solution of $[PBVP]^+$ with $\alpha = \frac{1}{4}\pi$ and $\alpha = \frac{1}{6}\pi$. In each plot a black line shows $\widehat{R}^{\infty} = 2.5$, after which the far-field asymptotic form (3.2.19) is plotted

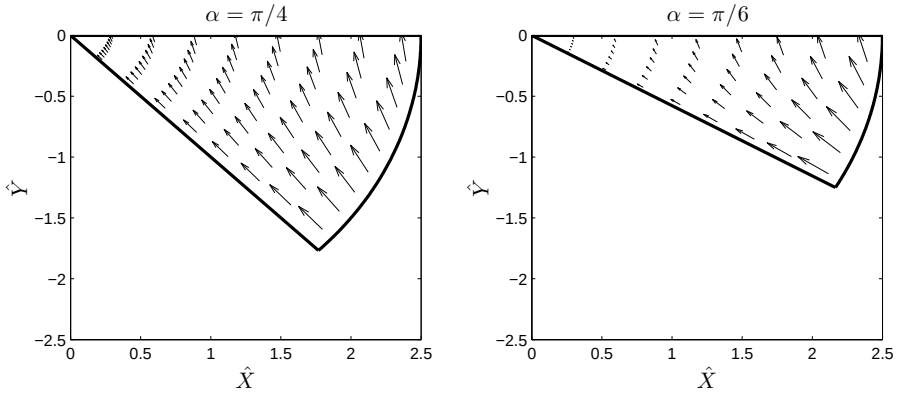

Figure 3.6: The vector field $\widehat{\nabla}\psi$ for the numerical solution of $[PBVP]^+$ with $\alpha = \frac{1}{4}\pi$ and $\alpha = \frac{1}{6}\pi$

we plot the level curves of ψ in $\widehat{R} \geqslant 0$, $-\alpha \leqslant \theta \leqslant 0$, (Figure 3.10), the vector field $\widehat{\nabla}\psi$ in $\widehat{R} \geqslant 0$, $-\alpha \leqslant \theta \leqslant 0$, (Figure 3.11) and ξ in $\widehat{X} \geqslant 0$ (Figure 3.12) as before.

Figure 3.13 plots the numerically determined near-field constant $a_0(\alpha)$, as given in (3.2.13), for $[PBVP]^+$ against $\alpha \in \left(0, \frac{1}{2}\pi\right)$, where the exact values for $\alpha = \alpha_n$ in (3.2.31), are shown as circles. The numerical evidence shows that $a_0(\alpha) < 0$ for all $\alpha \in \left(0, \frac{1}{2}\pi\right)$, with $a_0(\alpha) \to 0$ as $\alpha \to 0^+$, that $a_0(\alpha)$ is monotonically decreasing as α increases, and that $a_0(\alpha) \to -\frac{1}{6}$ as $\alpha \to \frac{1}{2}\pi^-$. We have excellent agreement between the numerically calculated values and the exact solution (3.2.31). We will denote the numerical solution to $[PBVP]^+$ by $\psi = \psi_{\alpha}^{+}\left(\widehat{R}, \theta\right)$, with corresponding solution for ξ, given via (3.2.3),

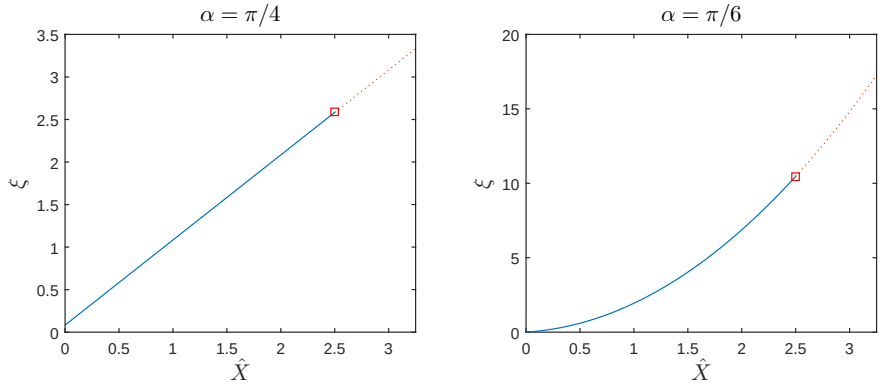

Figure 3.7: Graphs of ξ for the numerical solution of $[PBVP]^+$ with $\alpha = \frac{1}{4}\pi$ and $\alpha = \frac{1}{6}\pi$. In each graph a square shows $\widehat{R}^{\infty} = 2.5$, after which the far-field asymptotic form (3.2.22) is plotted

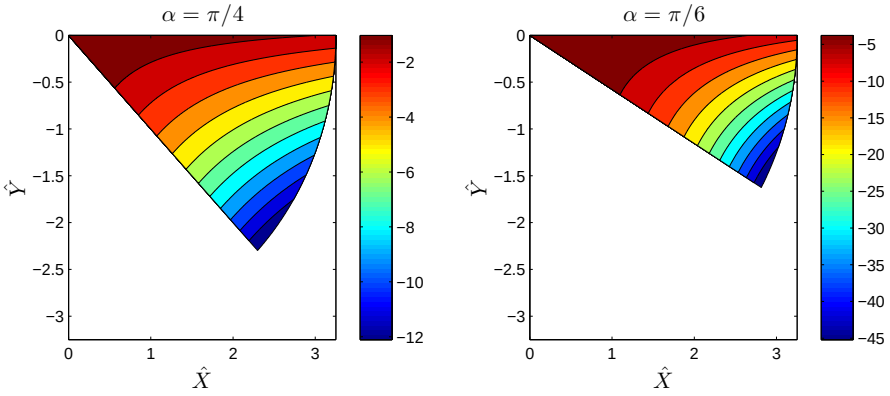

Figure 3.8: Contours of ψ for the exact solution (3.2.28) of $[PBVP]^+$ with $\alpha = \frac{1}{4}\pi$ and $\alpha = \frac{1}{6}\pi$

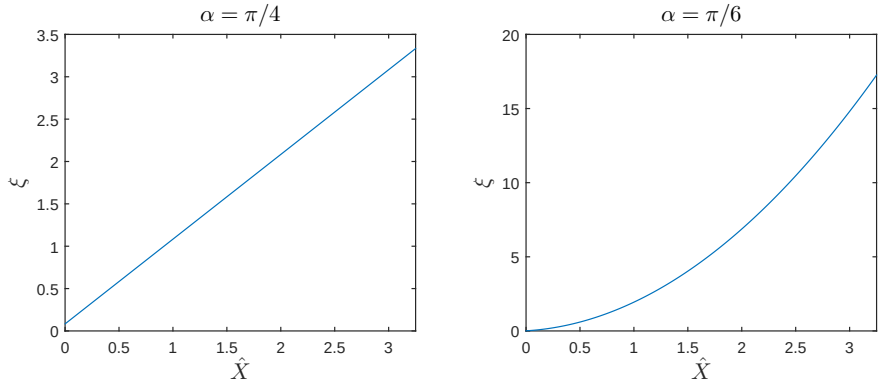

Figure 3.9: Graphs of ξ for the exact solution (3.2.29) of $[PBVP]^+$ with $\alpha = \frac{1}{4}\pi$ and $\alpha = \frac{1}{6}\pi$

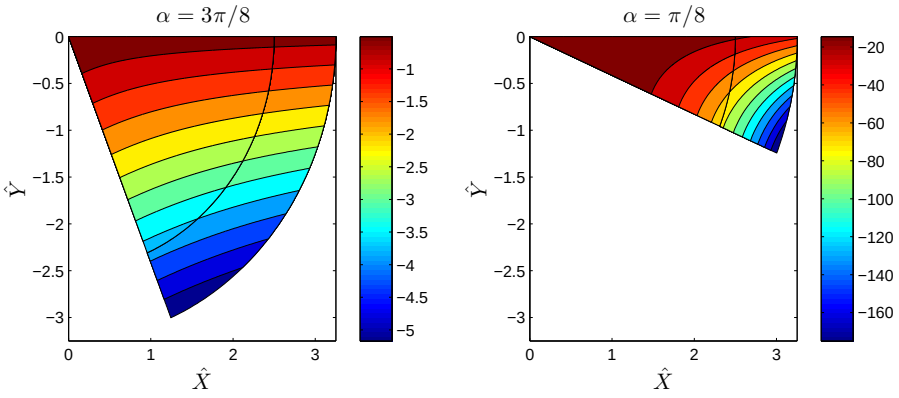

Figure 3.10: Contours of ψ for the numerical solution of $[PBVP]^+$ with $\alpha = \frac{3}{8}\pi$ and $\alpha = \frac{1}{8}\pi$. In each plot a black line shows $\widehat{R}^\infty = 2.5$, after which the far-field asymptotic form (3.2.19) is plotted

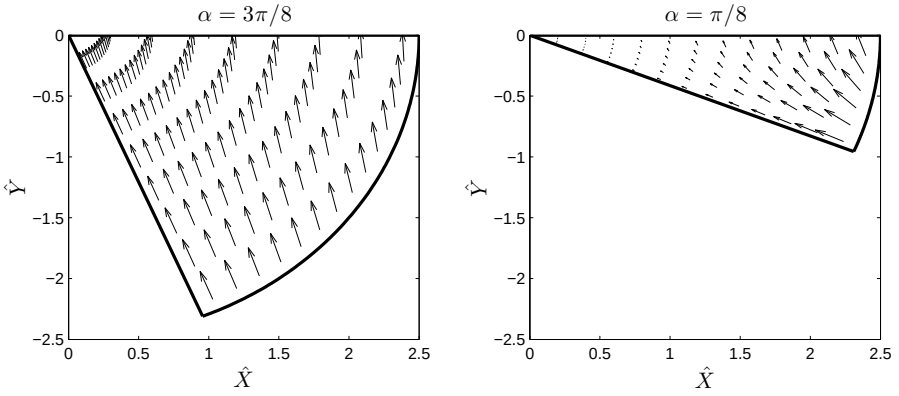

Figure 3.11: The vector field $\widehat{\nabla}\psi$ for the numerical solution of $[PBVP]^+$ with $\alpha = \frac{3}{8}\pi$ and $\alpha = \frac{1}{8}\pi$

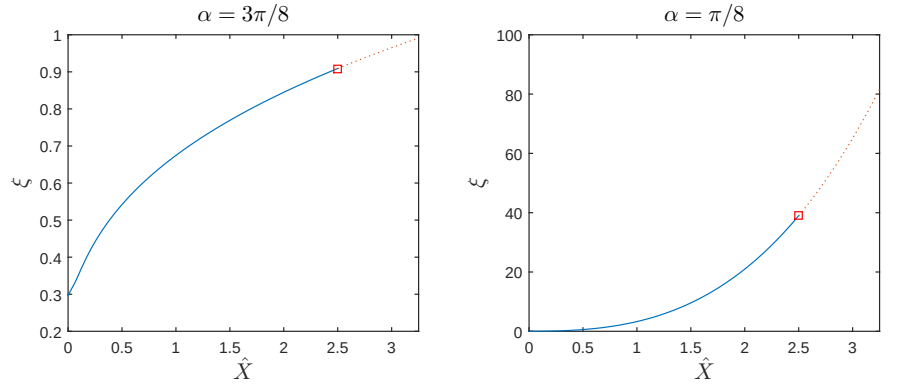

Figure 3.12: Graphs of ξ for the numerical solution of $[PBVP]^+$ with $\alpha = \frac{3}{8}\pi$ and $\alpha = \frac{1}{8}\pi$. In each graph a square shows $\widehat{R}^\infty = 2.5$, after which the far-field asymptotic form (3.2.22) is plotted

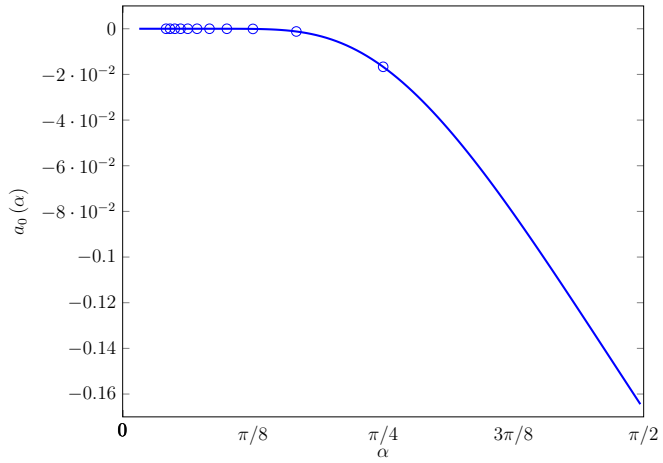

Figure 3.13: Numerical approximation to the near-field constant $a_0(\alpha)$ for $[PBVP]^+$ plotted against α. Exact solutions for $\alpha = \alpha_n$ $(n = 1, 2, \ldots, 10)$ (3.2.31) are shown as circles

which we denote by $\xi = \xi_\alpha^+\left(\widehat{X}\right)$, and numerical evidence shows that $\xi_\alpha^+\left(\widehat{X}\right)$ is monotone increasing in $\widehat{X} > 0$. It follows from (3.2.11) - (3.2.14) that,

$$\psi_\alpha^+\left(\widehat{R},\theta\right) = a_0(\alpha)\left(1 + \frac{\pi\left(1+\frac{\pi}{\alpha}\right)}{\alpha\sin\alpha}\widehat{R}\cos(\theta+\alpha) + O\left(\widehat{R}^2\right)\right),$$

$$\text{as } \widehat{R}\to 0,\ -\alpha\leqslant\theta\leqslant 0, \qquad (3.4.1)$$

$$\xi_\alpha^+\left(\widehat{X}\right) = -\left(1+\frac{\pi}{\alpha}\right)a_0(\alpha)\left(1 - \frac{\pi\left(1-\frac{\pi}{\alpha}\right)}{\alpha\tan\alpha}\widehat{X} + O\left(\widehat{X}^2\right)\right),\ \text{as } \widehat{X}\to 0, \qquad (3.4.2)$$

with $a_0(\alpha)$ as given in Figure 3.13.

Figure 3.14 plots $\xi(0)$ and $\xi_{\widehat{X}}(0)$ against α. We see that as $\alpha\to 0^+$, $\xi(0)\to 0^+$ and $\xi_{\widehat{X}}(0)\to 0^+$, whilst as $\alpha\to\frac{1}{2}\pi^-$, $\xi(0)\to\frac{1}{2}$ and $\xi_{\widehat{X}}(0)\to 0^+$. We notice that $\xi_{\widehat{X}}(0)$ has a maximum value close to $\alpha = \frac{1}{4}\pi$. As before, the angles which have exact solutions are shown as circles, with excellent agreement between exact and numerical values.

In Figure 3.15 $|\widehat{\nabla}\psi(0,0)|$ is plotted against $\alpha\in\left(0,\frac{1}{2}\pi\right)$. We see that as $\alpha\to 0^+$, $|\widehat{\nabla}\psi(0,0)|\to 0^+$, with $|\widehat{\nabla}\psi(0,0)|$ monotonically increasing, and that $|\widehat{\nabla}\psi(0,0)|\to 1^-$ as $\alpha\to\frac{1}{2}\pi^-$.

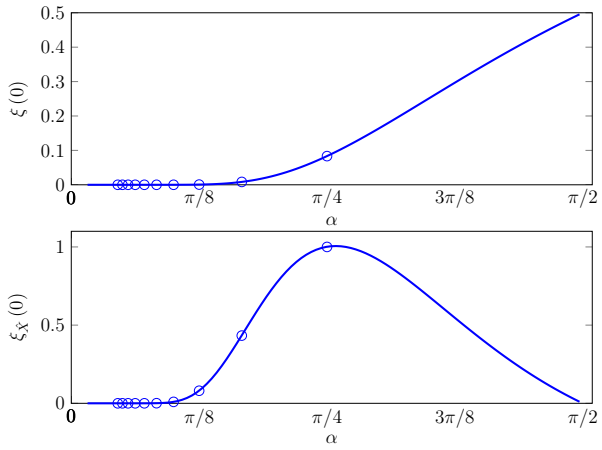

Figure 3.14: Numerical approximation to $\xi(0)$ and $\xi_{\widehat{X}}(0)$ for $[PBVP]^+$ plotted against α. Exact values for $\alpha = \alpha_n$ $(n = 1, 2, \ldots, 10)$ (via (3.2.29)) are shown as circles

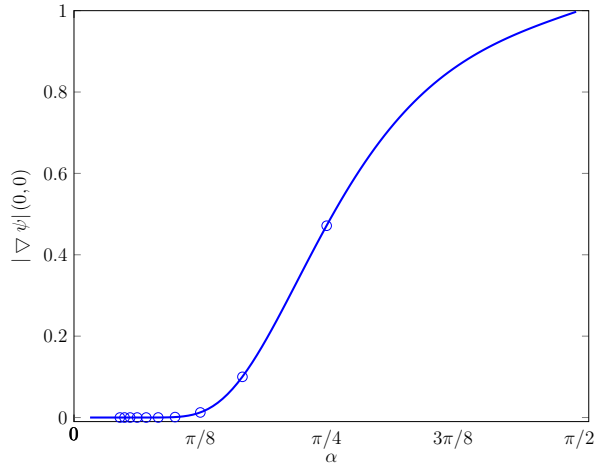

Figure 3.15: Numerical approximation to $|\widehat{\nabla}\psi(0,0)|$ for $[PBVP]^+$ plotted against α. Exact values for $\alpha = \alpha_n$ $(n = 1, 2, \ldots, 10)$ (via (3.2.28)) are shown as circles

3.5 Numerical Results for $[PBVP]^-$

In this section we examine the results obtained by solving $[PBVP]^-$ numerically, as discussed in §3.3. The numerical solution reveals a delicate structure around points $\alpha = \alpha_n^*$ $(n = 1, 2, \dots)$ with α_n^* located at

$$\begin{cases} \frac{1}{4}\pi < \alpha_1^* < \frac{1}{2}\pi, \\ \\ \frac{\pi}{2(n+1)} < \alpha_n^* < \frac{\pi}{2n}, \quad n = 2, 3, \dots. \end{cases} \tag{3.5.1}$$

Following the approach used to solve $[PBVP]^+$, we first set the numerical parameters as discussed in §3.3.1. For angles $\alpha = \alpha_n$ $(n = 1, 2, \dots)$ where we have exact solutions, we choose $\widehat{R}^\infty = 10$, which must then be increased as we approach $\alpha = \alpha_n^*$ $(n = 1, 2, \dots)$. We set $\Delta\widehat{R}_2 = c\Delta\widehat{R}_1$, with $c > 0$ to be chosen later. As we increase $\widehat{R}^\infty$ we increase the multiplier c, in order to keep the run time required to solve $[PBVP]^-$ acceptably small. As for the solution to $[PBVP]^+$, we choose $\widehat{R}^* = 1$ and $\varepsilon = 10^{-4}$.

Table 3.3: Convergence of the numerical solution to $[PBVP]^-$ to the far-field asymptotic forms (3.2.19) and (3.2.22) for decreasing $\Delta\widehat{R}_1$, $\alpha = \frac{1}{4}\pi$, $c = 1$ and $J + 1 = 30$. In this case $\Delta\widehat{R}_1 = \Delta\widehat{R}_2$. This table shows the percentage error between numerically calculated solutions and the far-field asymptotic forms. Time t (given in seconds) is the calculation time for a typical run.

$\Delta\widehat{R}_1$	ξ_{error} (%)	ψ_{error} (%)	t (seconds)
1×10^{-1}	49.4	9.89	0.0864
5×10^{-2}	16.2	5.00	0.0912
1×10^{-2}	0.808	1.01	0.145
5×10^{-3}	0.422	0.505	0.241
1×10^{-3}	0.410	0.101	1.46
5×10^{-4}	0.428	0.0506	3.66
1×10^{-4}	0.445	0.0101	58.3
5×10^{-5}	0.447	0.00506	221

In Table 3.3 we show the percentage error between numerically calculated solutions to $[PBVP]^-$ and the far-field asymptotic forms, (3.2.19) and (3.2.22) for ψ and ξ respectively,

Table 3.4: Convergence of the numerical solution to $[PBVP]^-$ to the far-field asymptotic forms (3.2.19) and (3.2.22) for decreasing $\Delta\theta$, $\alpha = \frac{1}{4}\pi$ and $\Delta\widehat{R}_1 = 10^{-3}$. In this case $\Delta\widehat{R}_1 = \Delta\widehat{R}_2$. This table shows the percentage error between numerically calculated solutions and the far-field asymptotic forms. Time t (given in seconds) is the calculation time for a typical run. All values rounded to 3 s.f.

$J+1$	$\Delta\theta$	ξ_{error} (%)	ψ_{error} (%)	t (seconds)
8	1×10^{-1}	4.18	0.101	0.224
16	5×10^{-2}	1.35	0.101	0.382
79	1×10^{-2}	0.271	0.101	1.75
157	5×10^{-3}	0.0239	0.101	4.80
785	1×10^{-3}	0.0409	0.101	55.0
1571	5×10^{-4}	0.415	0.101	188

for decreasing values of $\Delta\widehat{R}_1$. We can see from Table 3.3 that as we decrease the step-size $\Delta\widehat{R}_1$ by a factor of 10, the percentage error between our numerically calculated solution to $[PBVP]^-$ and the far-field asymptotic forms (3.2.19) and (3.2.22) also drops by a factor of 10, albeit with a run time cost associated as before. However there are two main differences between the errors in solving $[PBVP]^+$ and $[PBVP]^-$. The first is that the percentage errors are several orders of magnitude higher when solving $[PBVP]^-$ than $[PBVP]^+$, although they are still acceptably small. The second difference is that once $\Delta\widehat{R}_1$ gets small enough, the error in calculating ξ begins to increase. We believe this is due to rounding errors in the numerical solution of (3.2.3) for ξ, and for this reason we choose a value of $\Delta\widehat{R}_1 = 10^{-3}$ for our computations. Similarly, in Table 3.4 we show the percentage error between numerically calculated solutions to $[PBVP]^-$ and the far-field asymptotic forms, (3.2.19) and (3.2.22) for ψ and ξ respectively, for decreasing values of $\Delta\theta$. We see that as we decrease $\Delta\theta$ the error in calculating ψ does not appear to change, and, as before we see the same pattern in the error in the calculation of ξ. We choose $\Delta\theta = 5 \times 10^{-3}$ to give acceptably small errors while keeping run time costs down.

As with the solution to $[PBVP]^+$, we begin by choosing angles $\alpha = \frac{1}{4}\pi$ and $\alpha = \frac{1}{6}\pi$, numerically solve $[PBVP]^-$ using the scheme detailed in §3.3 for each angle, and plot the

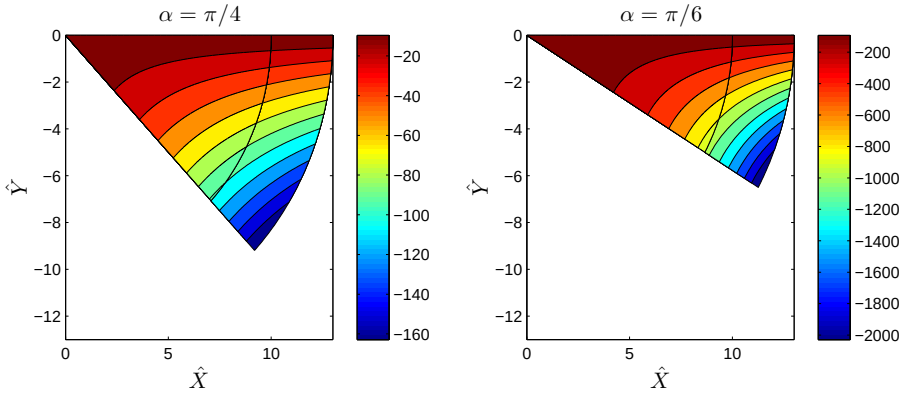

Figure 3.16: Contours of ψ for the numerical solution of $[PBVP]^-$ with $\alpha = \frac{1}{4}\pi$ and $\alpha = \frac{1}{6}\pi$. In each plot a line shows $\widehat{R}^{\infty} = 10$, after which the far-field asymptotic form (3.2.19) is plotted

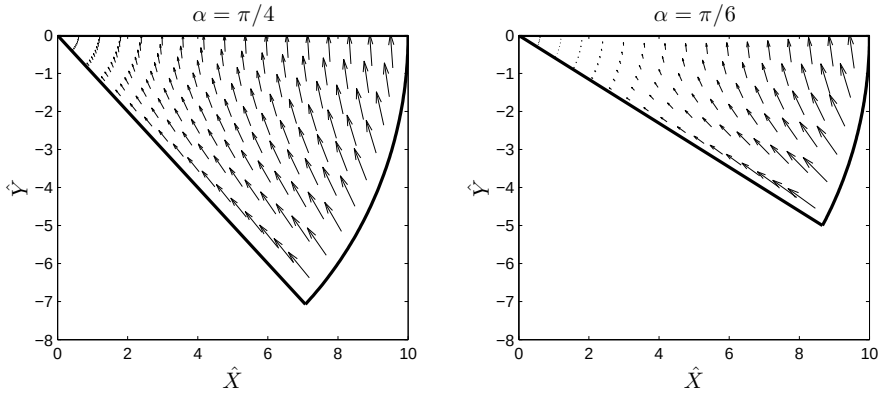

Figure 3.17: The vector field $\widehat{\nabla}\psi$ for the numerical solution for $[PBVP]^-$ with $\alpha = \frac{1}{4}\pi$ and $\alpha = \frac{1}{6}\pi$

level curves of ψ in $\widehat{R} \geqslant 0$, $-\alpha \leqslant \theta \leqslant 0$, (Figure 3.16), the vector field $\widehat{\nabla}\psi$ in $\widehat{R} \geqslant 0$, $-\alpha \leqslant \theta \leqslant 0$, (Figure 3.17) and ξ in $\widehat{X} \geqslant 0$ (Figure 3.18). It is of interest to examine the structure of the level curves of ψ and the vector field $\widehat{\nabla}\psi$, in both cases $\alpha = \frac{1}{4}\pi$ and $\alpha = \frac{1}{6}\pi$, closer to the tip of the wedge. These are shown in Figures 3.19 and 3.20. For $\alpha = \frac{1}{4}\pi$, Figure 3.19a reveals a stationary point (saddle) for ψ on the boundary $\theta = -\frac{1}{4}\pi$ when $\widehat{R} \approx 0.24$. This leads to a reversal in $\widehat{\nabla}\psi$ on $\theta = -\frac{1}{4}\pi$ when the stationary point is crossed, and a consequent weak reversal in $\widehat{\nabla}\psi \cdot \mathbf{j}$ on $\theta = 0$, as can be seen in Figure 3.20a. For $\alpha = \frac{1}{6}\pi$, Figure 3.19b reveals that there are now two stationary points (both saddles) for ψ on the boundary $\theta = -\frac{1}{6}\pi$, when $\widehat{R} \approx 0.054$ and $\widehat{R} \approx 0.61$. Consequently,

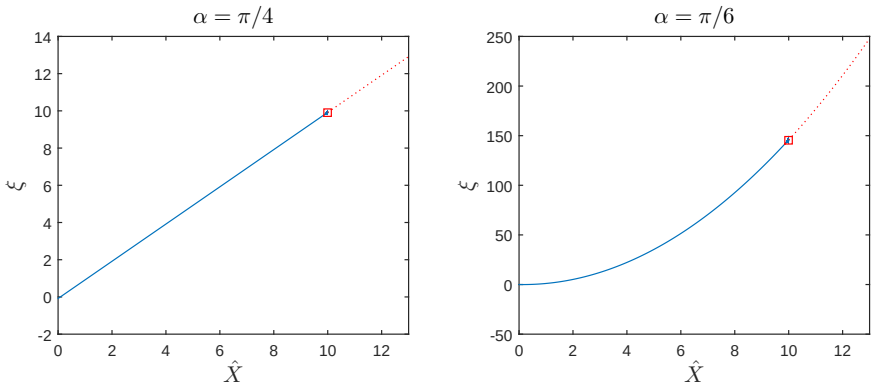

Figure 3.18: Graphs of ξ for the numerical solution of $[PBVP]^-$ with $\alpha = \frac{1}{4}\pi$ and $\alpha = \frac{1}{6}\pi$. In each plot a square shows $\widehat{R}^\infty = 10$, after which the far-field asymptotic form (3.2.22) is plotted

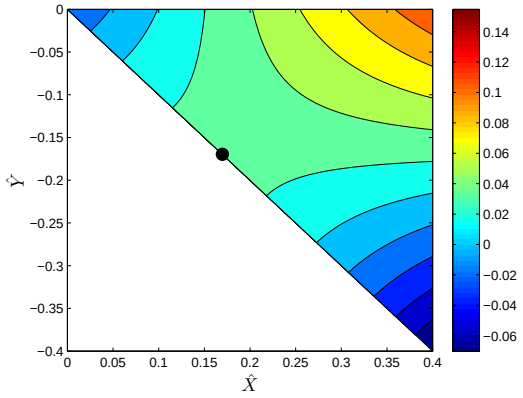

(a) $\alpha = \frac{1}{4}\pi$

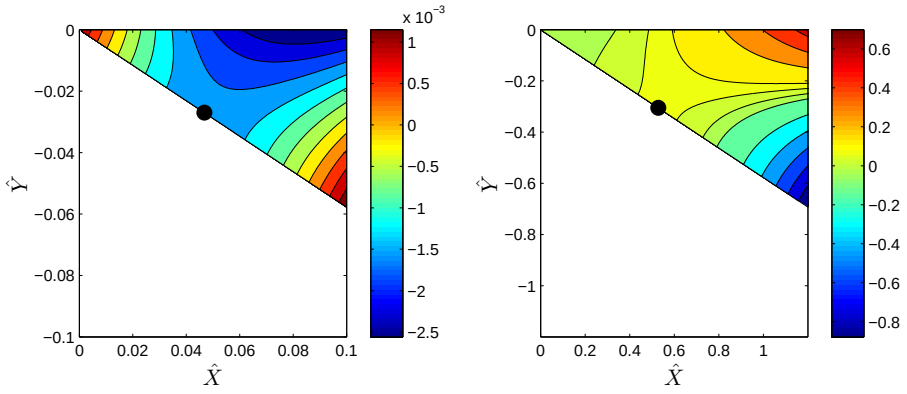

(b) $\alpha = \frac{1}{6}\pi$

Figure 3.19: Contours of ψ for the numerical solution of $[PBVP]^-$ close to the tip of the wedge with $\alpha = \frac{1}{4}\pi$ and $\alpha = \frac{1}{6}\pi$. The stationary points are marked with a dot

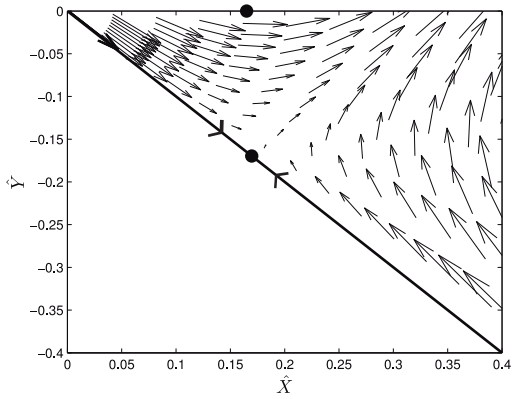

(a) $\alpha = \frac{1}{4}\pi$

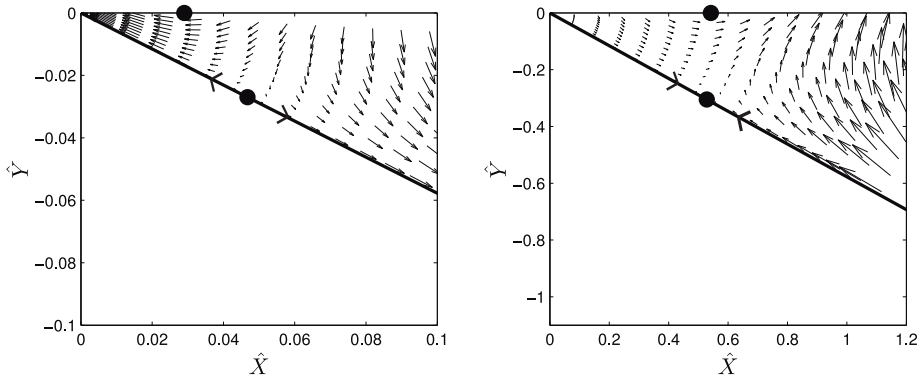

(b) $\alpha = \frac{1}{6}\pi$

Figure 3.20: The vector field $\widehat{\nabla}\psi$ for the numerical solution of $[PBVP]^-$ close to the tip of the wedge with $\alpha = \frac{1}{4}\pi$ and $\alpha = \frac{1}{6}\pi$. The reversal points are marked with a dot

there are now two reversals in $\widehat{\nabla}\psi$ on $\theta = -\frac{1}{6}\pi$, and two associated weak reversals in $\widehat{\nabla}\psi \cdot \mathbf{j}$ on $\theta = 0$, as can be seen in Figure 3.20b. An investigation of each of the angles $\alpha = \alpha_n$ $(n = 1, 2, \dots)$ where exact solutions are available (given in (3.2.32) and (3.2.33)) reveals that when $\alpha = \alpha_n$ $(n = 1, 2, \dots)$, then ψ has exactly n stationary points (each saddle points) on $\theta = -\alpha_n$, and consequently, there are n reversals in $\widehat{\nabla}\psi$ on $\theta = -\alpha_n$, and n associated weak reversals in $\widehat{\nabla}\psi \cdot \mathbf{j}$ on $\theta = 0$. Significantly, each of these reversals leads to a zero of $\xi\left(\widehat{X}\right)$ in $\widehat{X} > 0$. Thus, when $\alpha = \alpha_n$ $(n = 1, 2, \dots)$, $\xi\left(\widehat{X}\right)$ has exactly n zeros in $\widehat{X} > 0$, and $\xi(0)$ has sign $(-1)^n$, with $\xi\left(\widehat{X}\right) \to \infty$ as $\widehat{X} \to \infty$. Since $\xi\left(\widehat{X}\right)$ is a polynomial of degree n, then this establishes that $\xi\left(\widehat{X}\right)$ has exactly $(n-1)$ turning

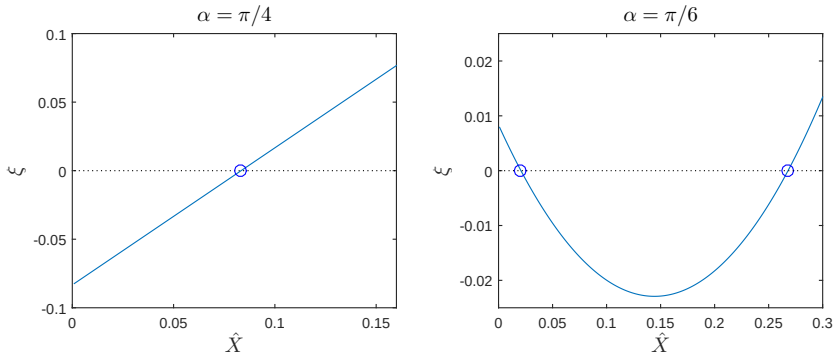

Figure 3.21: Graphs of ξ close to the tip of the wedge for the numerical solution of [PBVP]$^-$ with $\alpha = \pi/4$ and $\alpha = \pi/6$. In each plot circles highlight the location of zeros of ξ

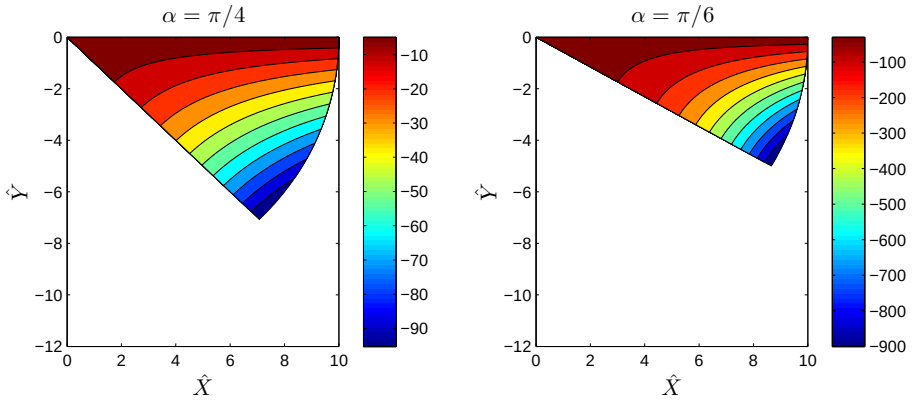

Figure 3.22: Contours of ψ for the exact solution (3.2.32) of $[PBVP]^-$ with $\alpha = \frac{1}{4}\pi$ and $\alpha = \frac{1}{6}\pi$

points in $\widehat{X} > 0$. This is illustrated in Figure 3.21 which graphs $\xi\left(\widehat{X}\right)$ for $\alpha = \frac{1}{4}\pi$ and $\alpha = \frac{1}{6}\pi$, close to $\widehat{X} = 0$. We will return to the implications of these observations at a later stage.

The exact solutions to $[PBVP]^-$ ((3.2.32) and (3.2.33)), when $\alpha = \frac{1}{4}\pi$ and $\alpha = \frac{1}{6}\pi$ are plotted in Figures 3.22, and 3.23. Comparison between Figures 3.16, and 3.18, and Figures 3.22, and 3.23 shows excellent agreement.

The case when $\alpha = \frac{1}{8}\pi$ is illustrated in Figures 3.24 - 3.26. As may be anticipated, Figure 3.24b reveals three stationary points (all saddles) for ψ on the boundary $\theta = -\frac{1}{8}\pi$, when $\widehat{R} \approx 0.0218$, $\widehat{R} \approx 0.123$ and $\widehat{R} \approx 1.16$ respectively, with associated reversals in $\widehat{\nabla}\psi$

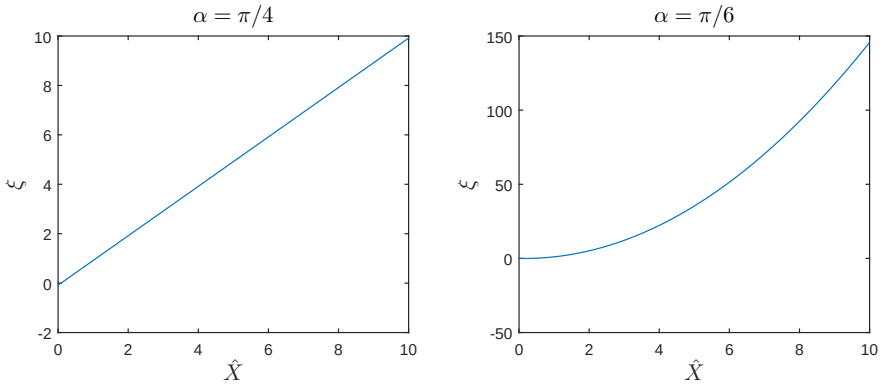

Figure 3.23: Graphs of ξ for the exact solution (3.2.33) of $[PBVP]^-$ with $\alpha = \frac{1}{4}\pi$ and $\alpha = \frac{1}{6}\pi$

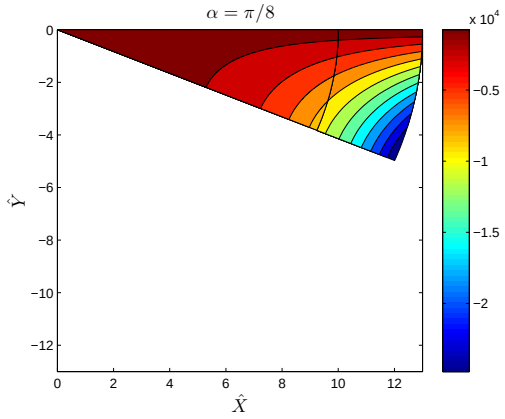

(a) $\alpha = \frac{1}{8}\pi$

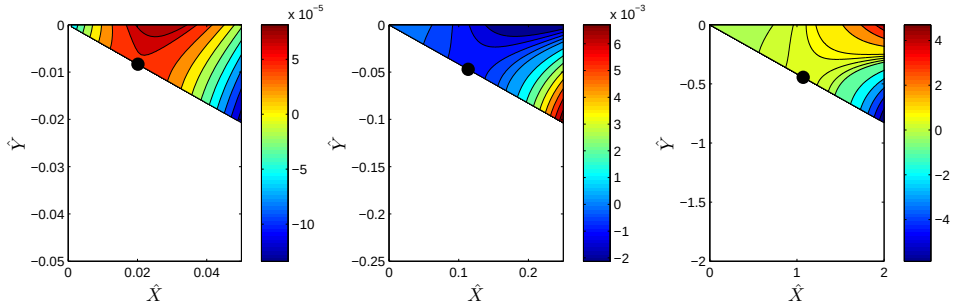

(b) Refinements close to the tip of the wedge for $\alpha = \frac{1}{8}\pi$

Figure 3.24: Contours of ψ for the numerical solution of $[PBVP]^-$ with $\alpha = \frac{1}{8}\pi$. In Figure 3.24a a line shows $\widehat{R}^{\infty} = 10$, after which the far-field asymptotic form (3.2.19) is plotted. In Figure 3.24b the stationary points are marked with a dot

on $\theta = -\frac{1}{8}\pi$, and in $\widehat{\nabla}\psi \cdot \mathbf{j}$ on $\theta = 0$, as can be seen in Figure 3.25b. The graph of $\xi\left(\widehat{X}\right)$ in $\widehat{X} > 0$, Figure 3.26, now has three zeros and two turning points.

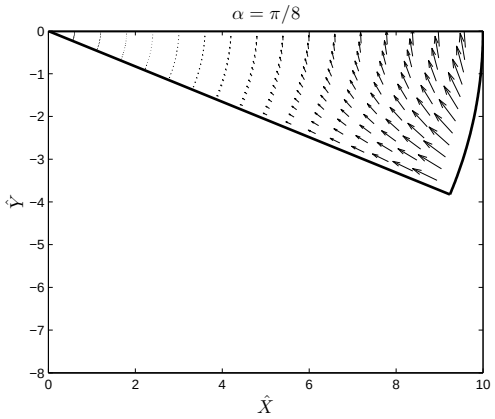

(a) $\alpha = \frac{1}{8}\pi$

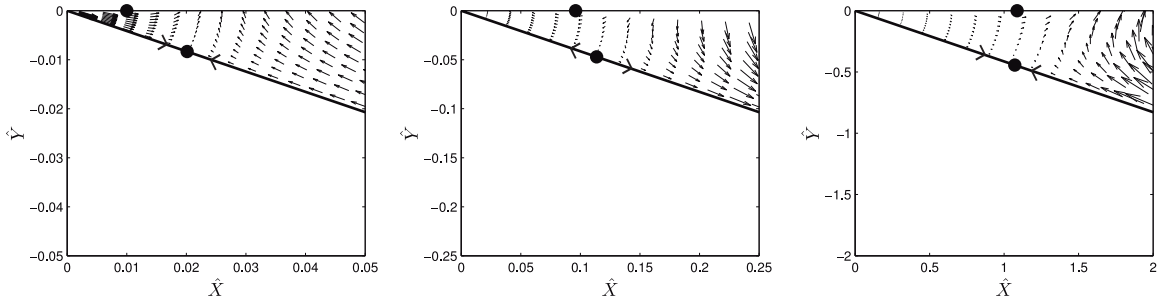

(b) Refinements close to the tip of the wedge for $\alpha = \frac{1}{8}\pi$

Figure 3.25: The vector field $\widehat{\nabla}\psi$ for the numerical solution $[PBVP]^-$ close to the tip of the wedge with $\alpha = \frac{1}{8}\pi$. In Figure 3.25b the reversal points are marked with a dot

The near-field constant $a_0(\alpha)$, as given in (3.2.13) for $[PBVP]^-$, is now investigated for $\alpha \in \left(0, \frac{1}{2}\pi\right)$. A careful numerical study shows, in the case of $[PBVP]^-$, that $a_0(\alpha)$ has a delicate structure, which supports our observations earlier for the cases when $\alpha = \alpha_n$ $(n = 1, 2, \dots)$ and the exact polynomial solution is available. Numerical agreement with the cases $\alpha = \alpha_n$ $(n = 1, 2, \dots)$ is excellent, and gives us confidence in the determination of $a_0(\alpha)$ for $\alpha \in \left(0, \frac{1}{2}\pi\right)$. The structure of the graph of $a_0(\alpha)$ for $\alpha \in \left(0, \frac{1}{2}\pi\right)$ is as follows:

1. $a_0(\alpha)$ has a sequence of pairs of near resonances, between which $a_0(\alpha)$ rapidly changes sign, vanishing at a sequence of points $\alpha = \alpha_n^*$ $(n = 1, 2, \dots)$, which are decreasing in n and approach zero as $n \to \infty$. Moreover $\alpha = \alpha_n^*$ $(n = 1, 2, \dots)$

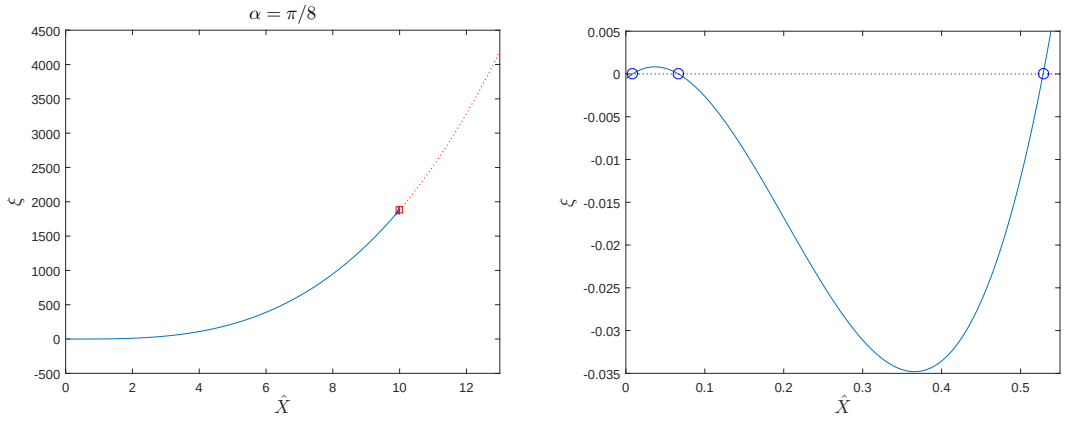

(a) $\alpha = \frac{1}{8}\pi$

(b) Refinements close to the tip of the wedge for $\alpha = \frac{1}{8}\pi$

Figure 3.26: Graphs of ξ for the numerical solution of $[PBVP]^-$ with $\alpha = \frac{1}{8}\pi$, with refinements close to $\widehat{X} = 0$. A square shows $\widehat{R}^\infty = 10$, after which the far-field asymptotic form (3.2.22) is plotted. Circles highlight the location of the zeros of ξ

interlace with $\alpha = \alpha_n$ $(n = 1, 2, \dots)$ so that,

$$\frac{\pi}{2\,(n+1)} = \alpha_n < \alpha_n^* < \alpha_{n-1} = \frac{\pi}{2n}, \qquad n = 2, 3, \dots, \tag{3.5.2}$$

with $\alpha_1^* \approx 1.41$. Numerical calculations of α_n^* for $n = 1, 2, \dots, 10$ are shown in Table 3.5.

Table 3.5: Numerical calculations of α_n^* for $n = 1, 2, \dots, 10$

n	1	2	3	4	5	6	7	8	9	10
α_n^*	1.41	0.739	0.493	0.378	0.303	0.251	0.214	0.186	0.163	0.146

2. Between the near resonance pairs $a_0\,(\alpha)$ is positive and monotone decreasing for $\alpha \in \left(\alpha_1^*, \frac{1}{2}\pi\right)$. Subsequently, $a_0\,(\alpha)$ is positive, with a single minimum point when $\alpha \in \left(\alpha_{2n+1}^*, \alpha_{2n}^*\right)$ $(n = 1, 2, \dots)$, whilst $a_0\,(\alpha)$ is negative, with a single maximum point when $\alpha \in \left(\alpha_{2n}^*, \alpha_{2n-1}^*\right)$ $(n = 1, 2, \dots)$.

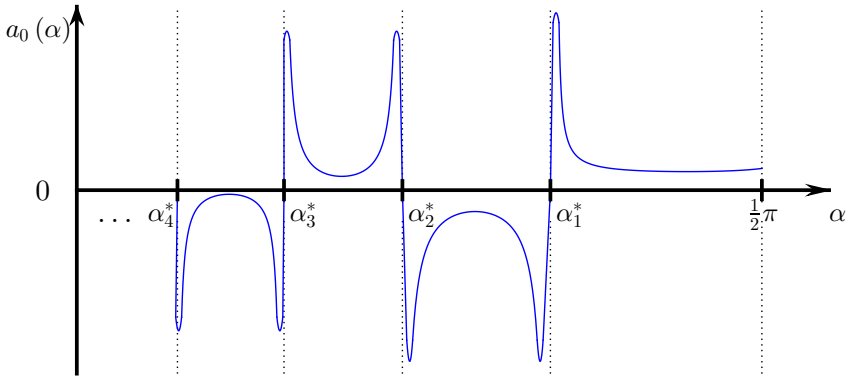

Figure 3.27: A qualitative sketch of the structure of $a_0(\alpha)$ for $\alpha \in \left(0, \frac{1}{2}\pi\right)$

A qualitative sketch of $a_0(\alpha)$ for $\alpha \in \left(0, \frac{1}{2}\pi\right)$ is illustrated in Figure 3.27. Numerical calculation shows that the consecutive stationary values of $a_0(\alpha)$, between consecutive near resonance pairs, approach zero as $\alpha \to 0^+$, whilst $a_0(\alpha)$ approaches a finite positive value as $\alpha \to \frac{1}{2}\pi^-$. In addition, as each α_n^* $(n = 1, 2, \ldots)$ is crossed, with *decreasing* α, the number of stationary points (saddles) of ψ on $\theta = -\alpha$ increases by one, whilst the number of zeros and turning points of $\xi\left(\widehat{X}\right)$ in $\widehat{X} \geqslant 0$ increases by one. At $\alpha = \alpha_n^*$, ψ has a stationary point (saddle) at the tip of the wedge. For $\alpha \in (\alpha_2^*, \alpha_1^*)$, $\xi\left(\widehat{X}\right)$ has two turning points when $\alpha \in (\alpha_c^*, \alpha_1^*)$ and becomes monotone when $\alpha \in (\alpha_2^*, \alpha_c^*]$. Numerical solution indicates that α_c^* lies in the range $1.36 < \alpha_c^* < 1.41$. This structure is detailed in Table 3.6.

For $\alpha \in \left(\alpha_1^*, \frac{1}{2}\pi\right)$, ψ has no stationary points, and $\xi\left(\widehat{X}\right)$ has no zeros but has a single minimum point in $\widehat{X} > 0$. The numerical solution of $[PBVP]^-$, for angles close to $\alpha = \alpha_n^*$ $(n = 1, 2, \ldots)$, required increasingly large values of $\widehat{R}_\infty$ to achieve suitable accuracy in the far-field boundary condition. Numerical approximation to $a_0(\alpha)$, with refinements close to $\alpha = \alpha_n^*$ $(n = 1, 2, 3, 4)$, are shown in Figure 3.28, together with graphs of $\xi(0)$ and $\xi_{\widehat{X}}(0)$ in Figure 3.29. Finally $|\widehat{\nabla}\psi(0,0)|$ is shown in Figure 3.31.

Denoting the solution to $[PVBP]^-$ as $\psi = \psi_\alpha^-\left(\widehat{R}, \theta\right)$ and $\xi = \xi_\alpha^-\left(\widehat{X}\right)$, the behaviour

Table 3.6: The number of zeros and turning points in $\xi\left(\widehat{X}\right)$ on $\widehat{X}>0$, and the number of stationary points (saddles) of ψ on $\theta=-\alpha$, for $\alpha\in\left(\alpha_{n+1}^{*},\alpha_{n}^{*}\right)$ $(n=1,2,\ldots,6)$

$\alpha\in\left(\alpha_{n+1}^{*},\alpha_{n}^{*}\right)$	†	$n=1$	$n=2$	$n=3$	$n=4$	$n=5$	$n=6$
Number of zeros of $\xi\left(\widehat{X}\right)$	0	1	2	3	4	5	6
Number of turning points of $\xi\left(\widehat{X}\right)$	1	††	1	2	3	4	5
Number of stationary points of ψ on $\theta=-\alpha$	0	1	2	3	4	5	6

$$\dagger:\alpha\in\left(\alpha_{1}^{*},\frac{1}{2}\pi\right),$$

$$\dagger\dagger:\begin{cases}2 & \alpha\in\left(\alpha_{c}^{*},\alpha_{1}^{*}\right),\\ 0 & \alpha\in\left(\alpha_{2}^{*},\alpha_{c}^{*}\right].\end{cases}$$

close to the tip of the wedge is as follows:

1. $\underline{\alpha\in\left(0,\frac{1}{2}\pi\right)\setminus\left\{\alpha_{n}^{*}:n=1,2,\ldots\right\}}$

   It follows from (3.2.8) - (3.2.14) that,

$$\psi_{\alpha}^{-}\left(\widehat{R},\theta\right)=a_{0}\left(\alpha\right)\left(1-\frac{\pi\left(1+\frac{\pi}{\alpha}\right)}{\alpha\sin\alpha}\widehat{R}\cos\left(\theta+\alpha\right)+O\left(\widehat{R}^{2}\right)\right)$$

$$\text{as }\widehat{R}\to0,\ -\alpha\leqslant\theta\leqslant0, \tag{3.5.3}$$

$$\xi_{\alpha}^{-}\left(\widehat{X}\right)=\left(1+\frac{\pi}{\alpha}\right)a_{0}\left(\alpha\right)\left(1+\frac{\pi\left(1-\frac{\pi}{\alpha}\right)}{\alpha\tan\alpha}\widehat{X}+O\left(\widehat{X}^{2}\right)\right)\text{ as }\widehat{X}\to0, \tag{3.5.4}$$

   with $a_{0}\left(\alpha\right)$ as given in Figure 3.28.

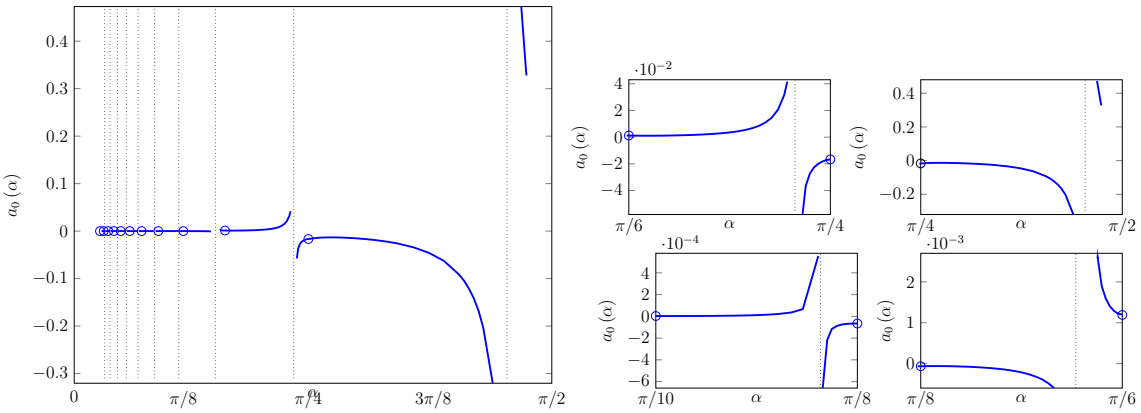

Figure 3.28: Numerical approximation to the constant $a_0(\alpha)$ for $[PBVP]^-$ plotted against α, with refinements close to $\alpha = \alpha_n^*$, $(n = 1, 2, 3, 4)$. Exact solutions for $\alpha = \alpha_n$ $(n = 1, 2, \ldots, 10)$ (3.2.34) are shown as circles

2. $\underline{\alpha \in \{\alpha_n^* : n = 1, 2, \ldots\}}$

It follows from (3.2.8) - (3.2.14) that,

$$\psi^-_{\alpha_n^*}\left(\widehat{R}, \theta\right) = b_1(\alpha_n^*)\left(\widehat{R}^{\frac{\pi}{\alpha_n^*}} \cos\frac{\pi}{\alpha_n^*}(\theta + \alpha_n^*) + O\left(\widehat{R}^{1+\frac{\pi}{\alpha_n^*}}\right)\right)$$

$$\text{as } \widehat{R} \to 0, \ -\alpha_n^* \leqslant \theta \leqslant 0, \qquad (3.5.5)$$

$$\xi^-_{\alpha_n^*}\left(\widehat{X}\right) = b_1(\alpha_n^*)\left(1 - \frac{\pi}{\alpha_n^*}\right)\widehat{X}^{\frac{\pi}{\alpha_n^*}}\left(1 + O\left(\widehat{X}\right)\right) \qquad \text{as } \widehat{X} \to 0, \qquad (3.5.6)$$

with $b_1(\alpha_n^*)$ $(n = 1, 2, \ldots)$ being a globally determined real constant.

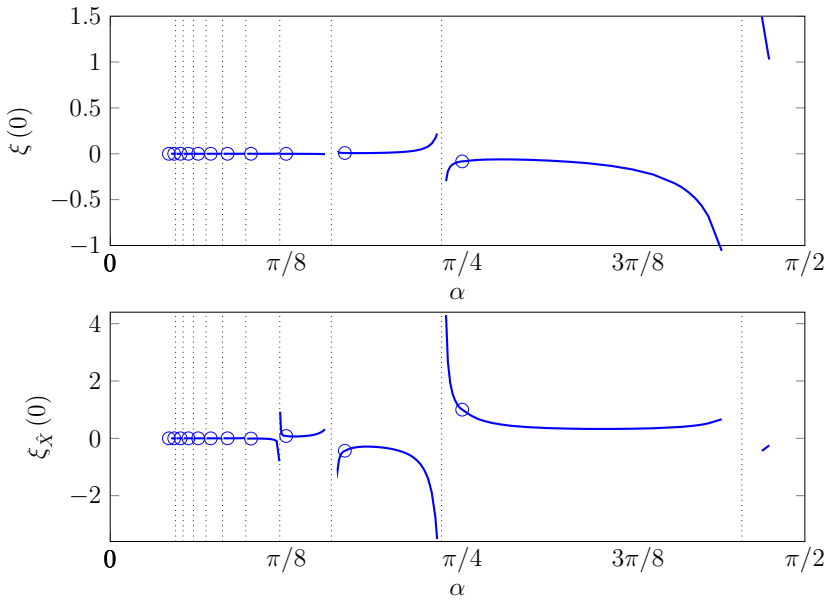

Figure 3.29: Numerical approximation to $\xi(0)$ and $\xi_{\widehat{X}}(0)$ for $[PBVP]^-$ plotted against α. Exact values for $\alpha = \alpha_n$ $(n = 1, 2, \ldots, 10)$ (via (3.2.33)) are shown as circles

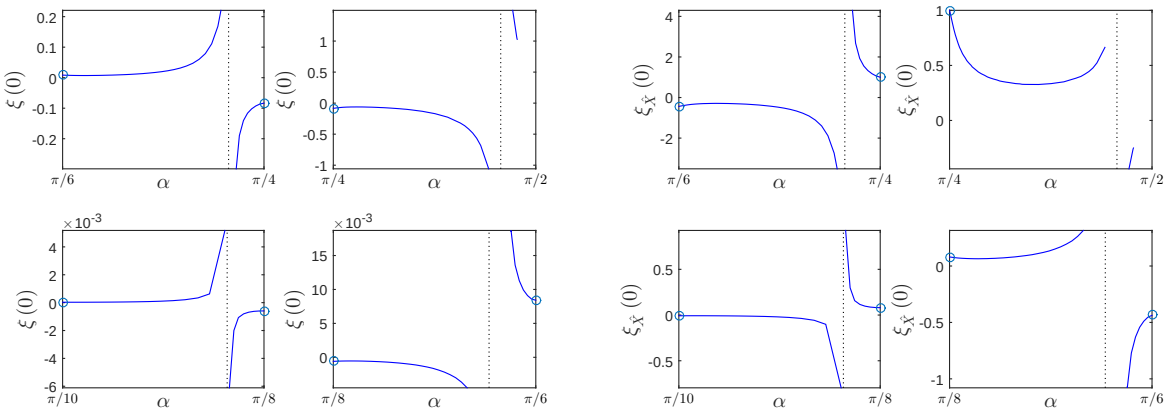

Figure 3.30: Refinements close to $\alpha = \alpha_n^*$ $(n = 1, 2, 3, 4)$, for the numerical approximation to $\xi(0)$ and $\xi_{\widehat{X}}(0)$ for $[PBVP]^-$ plotted against α. Exact values for $\alpha = \alpha_n$ $(n = 1, 2, 3, 4)$ (via (3.2.33)) are shown as circles

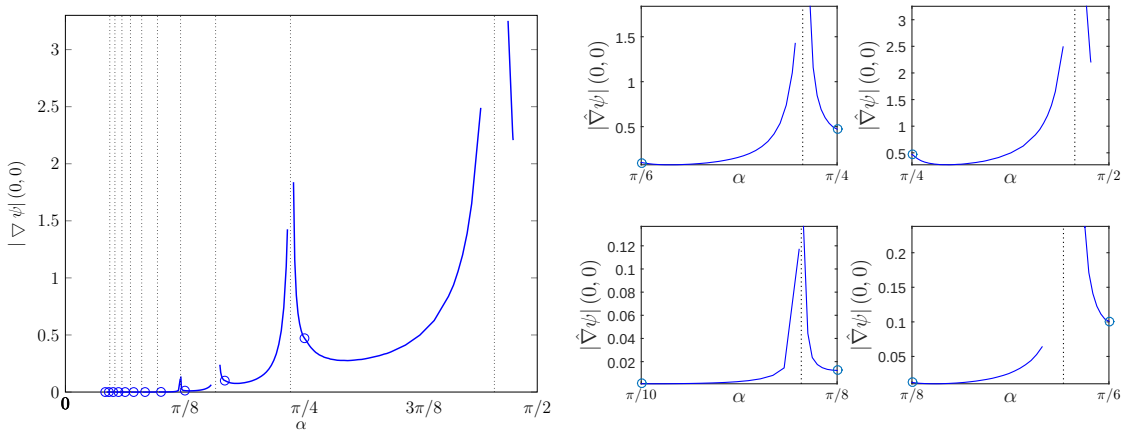

Figure 3.31: Numerical approximation to $|\widehat{\nabla}\psi\,(0,0)\,|$ for $[PBVP]^-$ plotted against α, with refinements close to $\alpha = \alpha_n^*$ $(n = 1, 2, 3, 4)$. Exact values for $\alpha = \alpha_n$ $(n = 1, 2, \ldots, 10)$ (via (3.2.32)) are shown as circles

3.6 Summary of the Solution Structure to the Boundary Value Problem (3.1.29) - (3.1.34)

We are now able to summarize the results of the previous three subsections in relation to the boundary value problem (3.1.29) - (3.1.34). We interpret these results in terms of the parameters $\alpha \in \left(0, \frac{1}{2}\pi\right)$ and $\mu \in \mathbb{R}$ (with $\mu = 1 + \sigma \tan\alpha$). We have:

1. $\underline{\mu > 0,\ \alpha \in \left(0, \frac{1}{2}\pi\right)}$

   A solution exists to the boundary value problem (3.1.29) - (3.1.34) with the required regularity (3.2.1) at $\left(\overline{X}, \overline{Y}\right) = (0, 0)$, given by

$$\widehat{\phi}\left(\overline{R}, \theta\right) = \mu^{\frac{\pi}{2\alpha}} \psi_\alpha^+ \left(\frac{\overline{R}}{\mu}, \theta\right), \ \overline{R} \geqslant 0, \ -\alpha \leqslant \theta \leqslant 0; \tag{3.6.1}$$

$$\widehat{\eta}\left(\overline{X}\right) = \mu^{\frac{\pi}{2\alpha}-1} \xi_\alpha^+ \left(\frac{\overline{X}}{\mu}\right), \quad \overline{X} \geqslant 0; \tag{3.6.2}$$

   with ψ_α^+ and ξ_α^+ as given in (3.4.1) and (3.4.2) respectively.

2. $\underline{\mu < 0,\ \alpha \in \left(0, \frac{1}{2}\pi\right) \setminus \{\alpha_n^* : n = 1, 2, \dots\}}$

A solution exists to the boundary value problem (3.1.29) - (3.1.34) with the required regularity (3.2.1) at $\left(\overline{X}, \overline{Y}\right) = (0, 0)$, given by,

$$\widehat{\phi}\left(\overline{R}, \theta\right) = (-\mu)^{\frac{\pi}{2\alpha}}\, \psi_\alpha^-\left(\frac{\overline{R}}{(-\mu)}, \theta\right),\ \overline{R} \geqslant 0,\ -\alpha \leqslant \theta \leqslant 0; \tag{3.6.3}$$

$$\widehat{\eta}\left(\overline{X}\right) = (-\mu)^{\frac{\pi}{2\alpha}-1}\, \xi_\alpha^-\left(\frac{\overline{X}}{(-\mu)}\right),\ \overline{X} \geqslant 0; \tag{3.6.4}$$

with ψ_α^- and ξ_α^- as given in (3.5.3) and (3.5.4) respectively.

3. $\underline{\mu < 0,\ \alpha \in \{\alpha_n^* : n = 1, 2, \dots\}}$

A solution exists to the boundary value problem (3.1.29) - (3.1.34) with the required regularity (3.2.1) at $\left(\overline{X}, \overline{Y}\right) = (0, 0)$, given by,

$$\widehat{\phi}\left(\overline{R}, \theta\right) = (-\mu)^{\frac{\pi}{2\alpha_n^*}}\, \psi_{\alpha_n^*}^-\left(\frac{\overline{R}}{(-\mu)}, \theta\right),\ \overline{R} \geqslant 0,\ -\alpha_n^* \leqslant \theta \leqslant 0; \tag{3.6.5}$$

$$\widehat{\eta}\left(\overline{X}\right) = (-\mu)^{\frac{\pi}{2\alpha_n^*}-1}\, \xi_{\alpha_n^*}^-\left(\frac{\overline{X}}{(-\mu)}\right),\ \overline{X} \geqslant 0; \tag{3.6.6}$$

with $\psi_{\alpha_n^*}^-$ and $\xi_{\alpha_n^*}^-$ as given in (3.5.5) and (3.5.6) respectively.

4. $\underline{\mu = 0,\ \alpha \in \left(0, \frac{1}{2}\pi\right)}$

This case has not been treated as yet. However, it is readily established (and anticipated by the coordinate scalings within (1) - (3) above) that, in this degenerate case, the solution to the boundary value problem (3.1.29) - (3.1.34), which has least singular behaviour at $\left(\overline{X}, \overline{Y}\right) = (0, 0)$, is simply given by the far-field forms; that is,

$$\widehat{\phi}\left(\overline{R}, \theta\right) = -\overline{R}^{\frac{\pi}{2\alpha}} \cos\frac{\pi}{2\alpha}\left(\theta + \alpha\right),\ \overline{R} \geqslant 0,\ -\alpha \leqslant \theta \leqslant 0; \tag{3.6.7}$$

$$\widehat{\eta}\left(\overline{X}\right) = \frac{\pi}{4\alpha}\overline{X}^{\frac{\pi}{2\alpha}-1},\ \overline{X} \geqslant 0. \tag{3.6.8}$$

3.7 Reconstructing the Inner Region Asymptotic Expansions

In this section we reconstruct the inner region asymptotic expansions for the fluid velocity potential ϕ, free surface elevation η, dynamic fluid pressure field p_d and fluid velocity field $\mathbf{q}$ in terms of the inner region coordinates $\overline{X}$, $\overline{Y}$, and then consider the behaviour close to the intersection point of the fluid free surface and the inclined accelerating plate. We consider the four cases $\mu > 0$ with $\alpha \in \left(0, \frac{1}{2}\pi\right)$, $\mu < 0$ with $\alpha \in \left(0, \frac{1}{2}\pi\right) \setminus \{\alpha_n^* : n = 1, 2, \dots\}$, $\mu < 0$ with $\alpha \in \{\alpha_n^* : n = 1, 2, \dots\}$, and $\mu = 0$ with $\alpha \in \left(0, \frac{1}{2}\pi\right)$ separately.

3.7.1 Case 1: $\mu > 0$ with $\alpha \in \left(0, \frac{1}{2}\pi\right)$

It follows from (3.1.7), (3.1.8), (3.1.25), (3.1.26), (3.1.35), and (3.1.36), that the intersection point of the plate and the fluid free surface is located at $\left(\overline{X}, \overline{Y}\right) = \left(\overline{X}_p(t), \overline{Y}_p(t)\right)$ $= \left(X_p(t) + \frac{1}{2}\sigma, Y_p(t) - \frac{1}{2}\sigma\tan\alpha\right)$, with

$$\overline{X}_p(t) = -t^{\frac{\pi}{\alpha}-2} A_0(\alpha)(\mu - 1)\cot\alpha \ \cos\alpha \ \mu^{\frac{\pi}{2\alpha}-1}\xi_\alpha^+(0) + o\left(t^{\frac{\pi}{\alpha}-2}\right), \tag{3.7.1}$$

$$\overline{Y}_p(t) = t^{\frac{\pi}{\alpha}-2} A_0(\alpha)(\mu - 1)\cos\alpha \ \mu^{\frac{\pi}{2\alpha}-1}\xi_\alpha^+(0) + o\left(t^{\frac{\pi}{\alpha}-2}\right), \tag{3.7.2}$$

as $t \to 0^+$. We then have, via (3.1.3), (3.1.5), (3.1.23), (3.1.26), (3.1.28), and (3.1.36), that

$$\eta_I\left(\overline{X}, t\right) = \frac{1}{2}(\mu - 1) + t^{\frac{\pi}{\alpha}-2} A_0(\alpha)(\mu - 1)\cos\alpha \ \mu^{\frac{\pi}{2\alpha}-1}\xi_\alpha^+\left(\frac{\overline{X}}{\mu}\right) + o\left(t^{\frac{\pi}{\alpha}-2}\right), \tag{3.7.3}$$

for $\overline{X} \geqslant \overline{X}_p(t)$, as $t \to 0^+$. We recall that, in the inner asymptotic region, the fluid free surface is located at $Y = \eta_I(X, t)$, so that in the shifted coordinates $\left(\overline{X}, \overline{Y}\right)$, the free surface is located at

$$\overline{Y} = \eta_I\left(\overline{X}, t\right) - \frac{1}{2}(\mu - 1), \tag{3.7.4}$$

for $\overline{X} \geqslant \overline{X}_p(t)$. Then, from (3.7.3), the free surface in the inner asymptotic region is located at

$$\overline{Y} = \overline{Y}_I\left(\overline{X}, t\right) = t^{\frac{\pi}{\alpha}-2} A_0(\alpha)(\mu-1)\cos\alpha\ \mu^{\frac{\pi}{2\alpha}-1}\xi_\alpha^+\left(\frac{\overline{X}}{\mu}\right) + o\left(t^{\frac{\pi}{\alpha}-2}\right), \tag{3.7.5}$$

for $\overline{X} \geqslant \overline{X}_p(t)$, as $t \to 0^+$. We next have, via (3.1.4), (3.1.6), (3.1.24), (3.1.26), (3.1.27), and (3.1.36), that

$$\begin{aligned}\phi_I\left(\overline{X}, \overline{Y}, t\right) = (\mu-1)\left[\overline{Y} - \frac{1}{6}(2-\mu)\right] \\ + t^{\frac{\pi}{\alpha}-2} A_0(\alpha)(\mu-1)\cos\alpha\ \mu^{\frac{\pi}{2\alpha}}\psi_\alpha^+\left(\frac{\overline{X}}{\mu}, \frac{\overline{Y}}{\mu}\right) + o\left(t^{\frac{\pi}{\alpha}-2}\right),\end{aligned} \tag{3.7.6}$$

for $\overline{X} \geqslant \overline{X}_p(t)$, $-\overline{X}\tan\alpha \leqslant \overline{Y} \leqslant \overline{Y}_I\left(\overline{X}, t\right)$ as $t \to 0^+$. An examination of (1.2.28) and (3.1.4) requires that we write in the the inner asymptotic region

$$p_d\left(\overline{X}, \overline{Y}, t\right) = t^2 p_I\left(\overline{X}, \overline{Y}, t\right), \quad \overline{X} \geqslant \overline{X}_p(t),\ -\overline{X}\tan\alpha \leqslant \overline{Y} \leqslant \overline{Y}_I\left(\overline{X}, t\right),\ t \geqslant 0, \tag{3.7.7}$$

after which we have, via (1.2.28), (3.1.4), and (3.7.6), the inner region asymptotic expansion for the dynamic fluid pressure field as,

$$\begin{aligned}p_I\left(\overline{X}, \overline{Y}, t\right) = \frac{1}{2}(\mu-1)\left(1-2\overline{Y}\right) + t^{\frac{\pi}{\alpha}-2} A_0(\alpha)(\mu-1)\cos\alpha\ \mu^{\frac{\pi}{2\alpha}}\left(2\overline{X}\psi_{\alpha,\overline{X}}^+\left(\frac{\overline{X}}{\mu}, \frac{\overline{Y}}{\mu}\right)\right. \\ \left. + 2\overline{Y}\psi_{\alpha,\overline{Y}}^+\left(\frac{\overline{X}}{\mu}, \frac{\overline{Y}}{\mu}\right) - \left(1+\frac{\pi}{\alpha}\right)\psi_\alpha^+\left(\frac{\overline{X}}{\mu}, \frac{\overline{Y}}{\mu}\right)\right) + o\left(t^{\frac{\pi}{\alpha}-2}\right),\end{aligned} \tag{3.7.8}$$

as $t \to 0^+$ with $\overline{X} \geqslant \overline{X}_p(t)$, $-\overline{X}\tan\alpha \leqslant \overline{Y} \leqslant \overline{Y}_I\left(\overline{X}, t\right)$. Finally, in the inner asymptotic region, the fluid velocity field is given, via (1.2.29), (3.1.4), and (3.7.6), as,

$$\mathbf{q}\left(\overline{X}, \overline{Y}, t\right) = t(\mu-1)\,\mathbf{j} + t^{\frac{\pi}{\alpha}-1} A_0(\alpha)(\mu-1)\cos\alpha\ \mu^{\frac{\pi}{2\alpha}}\left(\psi^+_{\alpha,\overline{X}}\left(\frac{\overline{X}}{\mu}, \frac{\overline{Y}}{\mu}\right)\mathbf{i} + \psi^+_{\alpha,\overline{Y}}\left(\frac{\overline{X}}{\mu}, \frac{\overline{Y}}{\mu}\right)\mathbf{j}\right) + o\left(t^{\frac{\pi}{\alpha}-2}\right), \tag{3.7.9}$$

as $t \to 0^+$ with $\overline{X} \geqslant \overline{X}_p(t)$, $-\overline{X}\tan\alpha \leqslant \overline{Y} \leqslant \overline{Y}_I\left(\overline{X}, t\right)$. We now consider the structure of the inner region asymptotic expansions close to the intersection point of the inclined plate and the fluid free surface when $\left(\overline{X}, \overline{Y}\right) = O\left(\mu^{\frac{\pi}{2\alpha}-1} t^{\frac{\pi}{\alpha}-2}\right)$ as $t \to 0^+$. We have, via (3.4.1), (3.4.2), (3.6.1), and (3.6.2), together with (3.7.1) - (3.7.9), that

$$\overline{X}_p(t) = t^{\frac{\pi}{\alpha}-2}\left(1+\frac{\pi}{\alpha}\right) A_0(\alpha)\, a_0(\alpha)(\mu-1)\cot\alpha\cos\alpha\ \mu^{\frac{\pi}{2\alpha}-1} + o\left(t^{\frac{\pi}{\alpha}-2}\right), \tag{3.7.10}$$

$$\overline{Y}_p(t) = -t^{\frac{\pi}{\alpha}-2}\left(1+\frac{\pi}{\alpha}\right) A_0(\alpha)\, a_0(\alpha)(\mu-1)\cos\alpha\ \mu^{\frac{\pi}{2\alpha}-1} + o\left(t^{\frac{\pi}{\alpha}-2}\right), \tag{3.7.11}$$

$$\phi_I\left(\overline{R}, \theta, t\right) = (\mu-1)\left[\overline{R}\sin\theta - \frac{1}{6}(2-\mu)\right] + t^{\frac{\pi}{\alpha}-2} A_0(\alpha)\, a_0(\alpha)(\mu-1)\cos\alpha\ \mu^{\frac{\pi}{2\alpha}}\left(1 + \frac{\pi\left(1+\frac{\pi}{\alpha}\right)}{\mu\alpha\sin\alpha}\overline{R}\cos(\theta+\alpha) + O\left(\overline{R}^2\right)\right) + o\left(t^{\frac{\pi}{\alpha}-2}\right),$$

$$\text{for } 0 < \overline{R} \ll \min(1,\mu),\ -\alpha \leqslant \theta \leqslant 0, \tag{3.7.12}$$

$$\eta_I\left(\overline{X}, t\right) = \frac{1}{2}(\mu-1) - t^{\frac{\pi}{\alpha}-2}\left(1+\frac{\pi}{\alpha}\right) A_0(\alpha)\, a_0(\alpha)(\mu-1)\cos\alpha\ \mu^{\frac{\pi}{2\alpha}-1}\left(1 - \frac{\pi\left(1-\frac{\pi}{\alpha}\right)}{\mu\alpha\tan\alpha}\overline{X} + O\left(\overline{X}^2\right)\right) + o\left(t^{\frac{\pi}{\alpha}-2}\right),$$

$$\text{for } 0 < \overline{X} \ll \min(1,\mu), \tag{3.7.13}$$

$$p_I\left(\overline{R}, \theta, t\right) = \frac{1}{2}(\mu-1)\left(1 - 2\overline{R}\sin\theta\right) - t^{\frac{\pi}{\alpha}-2}\left(1+\frac{\pi}{\alpha}\right) A_0(\alpha)\, a_0(\alpha)(\mu-1)\cos\alpha\ \mu^{\frac{\pi}{2\alpha}}\left(1 - \frac{\pi\left(1-\frac{\pi}{\alpha}\right)}{\mu\alpha\sin\alpha}\overline{R}\cos(\theta+\alpha) + O\left(\overline{R}^2\right)\right) + o\left(t^{\frac{\pi}{\alpha}-2}\right),$$

$$\text{for } 0 < \overline{R} \ll \min(1,\mu),\ -\alpha \leqslant \theta \leqslant 0, \tag{3.7.14}$$

$$\mathbf{q}\left(\overline{R},\theta,t\right)=t\left(\mu-1\right)\mathbf{j}+t^{\frac{\pi}{\alpha}-1}\frac{\pi}{\alpha}\left(1+\frac{\pi}{\alpha}\right)A_0\left(\alpha\right)a_0\left(\alpha\right)\left(\mu-1\right)\cos\alpha\;\mu^{\frac{\pi}{2\alpha}-1}\left(\cot\alpha\mathbf{i}\right.$$
$$\left.-\mathbf{j}\right)\left(1+O\left(\overline{R}\right)\right)+o\left(t^{\frac{\pi}{\alpha}-2}\right),$$
$$\text{for } 0<\overline{R}\ll\min\left(1,\mu\right),\ -\alpha\leqslant\theta\leqslant 0, \tag{3.7.15}$$

as $t\rightarrow 0^{+}$ in the inner asymptotic region, with $A_0\left(\alpha\right)$ and $a_0\left(\alpha\right)$ as given in Figures 2.3 and 3.13 respectively. We observe from (3.7.12) - (3.7.15) that, in this case, each of the inner region asymptotic expansions remain uniform up to the contact point, where $\left(\overline{X},\overline{Y}\right)=O\left(\mu^{\frac{\pi}{2\alpha}-1}t^{\frac{\pi}{\alpha}-2}\right)$. Thus the asymptotic structure as $t\rightarrow 0^{+}$, of the solution to $[IBVP]$, is complete in this case. It is worth noting at this stage that, in this case, the expansions close to the contact point, (3.7.12) - (3.7.15), require $\left(\overline{X},\overline{Y}\right)=O\left(\mu^{\frac{\pi}{2\alpha}-1}t^{\frac{\pi}{\alpha}-2}\right)$ and $0<\overline{X},\ \overline{Y}\ll\min\left(1,\mu\right)$. This requires the following qualification on the asymptotic structure of $[IBVP]$ as $t\rightarrow 0^{+}$ in this case, namely,

$$0\leqslant t\ll\min\left(1,\lambda_1\left(\mu\right),\lambda_2\left(\mu\right)\right), \tag{3.7.16}$$

where

$$\lambda_1\left(\mu\right)=\mu^{\frac{\left(1-\frac{\pi}{2\alpha}\right)}{\left(\frac{\pi}{\alpha}-2\right)}}, \tag{3.7.17}$$
$$\lambda_2\left(\mu\right)=\mu^{\frac{\left(2-\frac{\pi}{2\alpha}\right)}{\left(\frac{\pi}{\alpha}-2\right)}}, \tag{3.7.18}$$

in $\mu>0$.

We can now draw the following conclusions concerning the free surface, the fluid velocity field and the dynamic pressure field in the inner asymptotic region:

(a) The contact point is located at

$$\left(\overline{x},y\right)=\frac{1}{2}\left(\mu-1\right)t^{2}\left(-\cot\alpha,1\right)+O\left(t^{\frac{\pi}{\alpha}}\right), \tag{3.7.19}$$

as $t \to 0^+$ (see (3.1.2), (3.1.7), (3.1.8), and (3.1.25)).

(b) The free surface slope at the contact point is given by,

$$\begin{aligned}\eta_{\overline{x}}\left(\overline{X}_p(t), t\right) &= \eta_{I,\overline{X}}\left(\overline{X}_p(t), t\right) \\ &= t^{\frac{\pi}{\alpha}-2}\frac{\pi}{\alpha}\left(1-\frac{\pi^2}{\alpha^2}\right)A_0(\alpha)\,a_0(\alpha)\,(\mu-1)\cot\alpha\ \cos\alpha\ \mu^{\frac{\pi}{2\alpha}-2} \\ &\quad + o\left(t^{\frac{\pi}{\alpha}-2}\right), \end{aligned} \tag{3.7.20}$$

as $t \to 0^+$ (see (3.4.2) and (3.7.3)). We see that the free surface slope is positive when $(\alpha, \mu) \in \left(0, \frac{1}{2}\pi\right) \times (0, 1)$ and negative when $(\alpha, \mu) \in \left(0, \frac{1}{2}\pi\right) \times (1, \infty)$. A contour plot of $\eta_{\overline{x}}\left(\overline{X}_p(t), t\right) t^{2-\frac{\pi}{\alpha}}$, as $t \to 0^+$, in the (α, μ) plane (with $(\alpha, \mu) \in \left(0, \frac{1}{2}\pi\right) \times (0, \infty)$) is shown in Figure 3.32.

(c) The free surface $\eta\left(\overline{X}, t\right)$ is given by

$$\eta\left(\overline{X}, t\right) = \frac{1}{2}(\mu-1)\,t^2 + t^{\frac{\pi}{\alpha}}A_0(\alpha)\,(\mu-1)\,\mu^{\frac{\pi}{2\alpha}-1}\cos\alpha\ \xi_\alpha^+\left(\frac{\overline{X}}{\mu}\right) + o\left(t^{\frac{\pi}{\alpha}}\right), \tag{3.7.21}$$

as $t \to 0^+$ for $\overline{X} \geqslant \overline{X}_p(t)$ (see (3.1.3), and (3.7.3)). It follows from (3.7.21) that $\eta\left(\overline{X}, t\right)$ is monotone increasing in $\overline{X} \geqslant \overline{X}_p(t)$ when $(\alpha, \mu) \in \left(0, \frac{1}{2}\pi\right) \times (0, 1)$, whilst $\eta\left(\overline{X}, t\right)$ is monotone decreasing in $\overline{X} \geqslant \overline{X}_p(t)$ when $(\alpha, \mu) \in \left(0, \frac{1}{2}\pi\right) \times (1, \infty)$.

When $\mu > 1$ ($\sigma > 0$) examination of (3.7.7) and (3.7.14) reveals that, to leading order in the inner asymptotic region, the acceleration of the inclined plate induces a constant dynamic pressure gradient of $t^2(\mu-1)\,\mathbf{j}$, which drives a vertical jet close to the intersection point of the free surface and the plate of height $\frac{1}{2}t^2(\mu-1)$. When $0 < \mu < 1$ ($-\cot\alpha < \sigma < 0$) we see from (3.7.7) and (3.7.14) that, to leading order in the inner asymptotic region, the acceleration of the inclined plate induces a constant negative dynamic pressure gradient of $t^2(\mu-1)\,\mathbf{j}$, which causes the free surface, close to the inter-

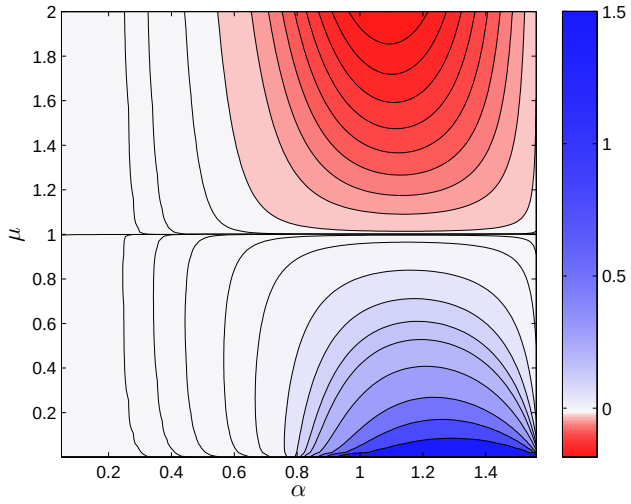

Figure 3.32: Contour plot of $t^{2-\frac{\pi}{\alpha}}\eta_{\overline{x}}\left(\overline{X}_p(t), t\right)$ as $t \to 0^+$ on the (α, μ) plane, in the case $\mu > 0$

section point of the free surface and the plate, to collapse to a height of $\frac{1}{2}t^2(\mu - 1)$.

3.7.2 Case 2: $\mu < 0$ with $\alpha \in \left(0, \frac{1}{2}\pi\right) \setminus \{\alpha_n^* : n = 1, 2, \dots\}$

It follows from (3.1.7), (3.1.8), (3.1.25), (3.1.26), (3.1.35), and (3.1.36), that the intersection point of the plate and the free surface is located at $\left(\overline{X}, \overline{Y}\right) = \left(\overline{X}_p(t), \overline{Y}_p(t)\right) = \left(X_p(t) + \frac{1}{2}\sigma, Y_p(t) - \frac{1}{2}\sigma\tan\alpha\right)$, with

$$\overline{X}_p(t) = -t^{\frac{\pi}{\alpha}-2}A_0(\alpha)(\mu-1)\cot\alpha\ \cos\alpha\ (-\mu)^{\frac{\pi}{2\alpha}-1}\xi_\alpha^-(0) + o\left(t^{\frac{\pi}{\alpha}-2}\right), \tag{3.7.22}$$

$$\overline{Y}_p(t) = t^{\frac{\pi}{\alpha}-2}A_0(\alpha)(\mu-1)\cos\alpha\ (-\mu)^{\frac{\pi}{2\alpha}-1}\xi_\alpha^-(0) + o\left(t^{\frac{\pi}{\alpha}-2}\right), \tag{3.7.23}$$

as $t \to 0^+$. We then have, via (3.1.3), (3.1.5), (3.1.23), (3.1.26), (3.1.28), and (3.1.36), that

$$\eta_I\left(\overline{X}, t\right) = \frac{1}{2}(\mu-1) + t^{\frac{\pi}{\alpha}-2}A_0(\alpha)(\mu-1)\cos\alpha\ (-\mu)^{\frac{\pi}{2\alpha}-1}\xi_\alpha^-\left(\frac{\overline{X}}{(-\mu)}\right) + o\left(t^{\frac{\pi}{\alpha}-2}\right), \tag{3.7.24}$$

for $\overline{X} \geqslant \overline{X}_p(t)$, as $t \to 0^+$. We now have, from (3.7.4) and (3.7.24), that in the shifted coordinates $\left(\overline{X}, \overline{Y}\right)$, the free surface in the inner asymptotic region is located at

$$\overline{Y} = \overline{Y}_I\left(\overline{X}, t\right) = t^{\frac{\pi}{\alpha}-2} A_0(\alpha)(\mu-1)\cos\alpha \ (-\mu)^{\frac{\pi}{2\alpha}-1} \xi_\alpha^- \left(\frac{\overline{X}}{(-\mu)}\right) + o\left(t^{\frac{\pi}{\alpha}-2}\right), \quad (3.7.25)$$

for $\overline{X} \geqslant \overline{X}_p(t)$, as $t \to 0^+$. We next have, via (3.1.4), (3.1.6), (3.1.24), (3.1.26), (3.1.27), and (3.1.36), that

$$\begin{aligned}\phi_I\left(\overline{X}, \overline{Y}, t\right) &= (\mu-1)\left[\overline{Y} - \frac{1}{6}(2-\mu)\right] \\ &\quad + t^{\frac{\pi}{\alpha}-2} A_0(\alpha)(\mu-1)\cos\alpha \ (-\mu)^{\frac{\pi}{2\alpha}} \psi_\alpha^- \left(\frac{\overline{X}}{(-\mu)}, \frac{\overline{Y}}{(-\mu)}\right) + o\left(t^{\frac{\pi}{\alpha}-2}\right), \quad (3.7.26)\end{aligned}$$

for $\overline{X} \geqslant \overline{X}_p(t)$, $-\overline{X}\tan\alpha \leqslant \overline{Y} \leqslant \overline{Y}_I\left(\overline{X}, t\right)$ as $t \to 0^+$. The inner region asymptotic expansion for the dynamic fluid pressure field is given, via (1.2.28), (3.1.4), (3.7.7), and (3.7.26), as

$$\begin{aligned}p_I\left(\overline{X}, \overline{Y}, t\right) &= \frac{1}{2}(\mu-1)\left(1-2\overline{Y}\right) \\ &\quad + t^{\frac{\pi}{\alpha}-2} A_0(\alpha)(\mu-1)\cos\alpha \ (-\mu)^{\frac{\pi}{2\alpha}} \left(2\overline{X}\psi^-_{\alpha,\overline{X}}\left(\frac{\overline{X}}{(-\mu)}, \frac{\overline{Y}}{(-\mu)}\right)\right. \\ &\quad + 2\overline{Y}\psi^-_{\alpha,\overline{Y}}\left(\frac{\overline{X}}{(-\mu)}, \frac{\overline{Y}}{(-\mu)}\right) \\ &\quad \left. - \left(1+\frac{\pi}{\alpha}\right)\psi_\alpha^-\left(\frac{\overline{X}}{(-\mu)}, \frac{\overline{Y}}{(-\mu)}\right)\right) + o\left(t^{\frac{\pi}{\alpha}-2}\right), \quad (3.7.27)\end{aligned}$$

as $t \to 0^+$ with $\overline{X} \geqslant \overline{X}_p(t)$, $-\overline{X}\tan\alpha \leqslant \overline{Y} \leqslant \overline{Y}_I\left(\overline{X}, t\right)$. Finally, in the inner asymptotic region, the fluid velocity field is given, via (1.2.29), (3.1.4), and (3.7.26), as

$$\begin{aligned}\mathbf{q}\left(\overline{X}, \overline{Y}, t\right) &= t(\mu-1)\,\mathbf{j} + t^{\frac{\pi}{\alpha}-1} A_0(\alpha)(\mu-1)\cos\alpha \ (-\mu)^{\frac{\pi}{2\alpha}} \left(\psi^-_{\alpha,\overline{X}}\left(\frac{\overline{X}}{(-\mu)}, \frac{\overline{Y}}{(-\mu)}\right)\mathbf{i}\right. \\ &\quad \left. + \psi^-_{\alpha,\overline{Y}}\left(\frac{\overline{X}}{(-\mu)}, \frac{\overline{Y}}{(-\mu)}\right)\mathbf{j}\right) + o\left(t^{\frac{\pi}{\alpha}-2}\right), \quad (3.7.28)\end{aligned}$$

as $t \to 0^+$ with $\overline{X} \geqslant \overline{X}_p(t)$, $-\overline{X}\tan\alpha \leqslant \overline{Y} \leqslant \overline{Y}_I\left(\overline{X}, t\right)$. We now consider the structure of the inner region asymptotic expansions close to the intersection point of the inclined plate and the fluid free surface when $\left(\overline{X}, \overline{Y}\right) = O\left((-\mu)^{\frac{\pi}{2\alpha}-1} t^{\frac{\pi}{\alpha}-2}\right)$ as $t \to 0^+$. We have, via (3.5.3), (3.5.4), (3.6.3), and (3.6.4), together with (3.7.22) - (3.7.28), that

$$\overline{X}_p(t) = -t^{\frac{\pi}{\alpha}-2}\left(1+\frac{\pi}{\alpha}\right) A_0(\alpha)\, a_0(\alpha)\,(\mu-1)\cot\alpha\cos\alpha\,(-\mu)^{\frac{\pi}{2\alpha}-1} + o\left(t^{\frac{\pi}{\alpha}-2}\right), \tag{3.7.29}$$

$$\overline{Y}_p(t) = t^{\frac{\pi}{\alpha}-2}\left(1+\frac{\pi}{\alpha}\right) A_0(\alpha)\, a_0(\alpha)\,(\mu-1)\cos\alpha\;\;(-\mu)^{\frac{\pi}{2\alpha}-1} + o\left(t^{\frac{\pi}{\alpha}-2}\right), \tag{3.7.30}$$

$$\begin{aligned}
\phi_I\left(\overline{R}, \theta, t\right) &= (\mu-1)\left[\overline{R}\sin\theta - \frac{1}{6}(2-\mu)\right] \\
&\quad + t^{\frac{\pi}{\alpha}-2} A_0(\alpha)\, a_0(\alpha)\,(\mu-1)\cos\alpha\;\;(-\mu)^{\frac{\pi}{2\alpha}}\left(1\right. \\
&\qquad \left. + \frac{\pi\left(1+\frac{\pi}{\alpha}\right)}{\mu\alpha\sin\alpha}\overline{R}\cos(\theta+\alpha) + O\left(\overline{R}^2\right)\right) + o\left(t^{\frac{\pi}{\alpha}-2}\right), \\
&\qquad \text{for } 0 < \overline{R} \ll \min(1, -\mu),\;\; -\alpha \leqslant \theta \leqslant 0,
\end{aligned} \tag{3.7.31}$$

$$\begin{aligned}
\eta_I\left(\overline{X}, t\right) &= \frac{1}{2}(\mu-1) \\
&\quad + t^{\frac{\pi}{\alpha}-2}\left(1+\frac{\pi}{\alpha}\right) A_0(\alpha)\, a_0(\alpha)\,(\mu-1)\cos\alpha\;\;(-\mu)^{\frac{\pi}{2\alpha}-1}\left(1\right. \\
&\qquad \left. - \frac{\pi\left(1-\frac{\pi}{\alpha}\right)}{\mu\alpha\tan\alpha}\overline{X} + O\left(\overline{X}^2\right)\right) + o\left(t^{\frac{\pi}{\alpha}-2}\right), \\
&\qquad \text{for } 0 < \overline{X} \ll \min(1, -\mu),
\end{aligned} \tag{3.7.32}$$

$$\begin{aligned}
p_I\left(\overline{R}, \theta, t\right) &= \frac{1}{2}(\mu-1)\left(1 - 2\overline{R}\sin\theta\right) \\
&\quad - t^{\frac{\pi}{\alpha}-2}\left(1+\frac{\pi}{\alpha}\right) A_0(\alpha)\, a_0(\alpha)\,(\mu-1)\cos\alpha\;\;(-\mu)^{\frac{\pi}{2\alpha}}\left(1\right. \\
&\qquad \left. - \frac{\pi\left(1-\frac{\pi}{\alpha}\right)}{\mu\alpha\sin\alpha}\overline{R}\cos(\theta+\alpha) + O\left(\overline{R}^2\right)\right) + o\left(t^{\frac{\pi}{\alpha}-2}\right), \\
&\qquad \text{for } 0 < \overline{R} \ll \min(1, -\mu),\;\; -\alpha \leqslant \theta \leqslant 0,
\end{aligned} \tag{3.7.33}$$

$$\mathbf{q}\left(\overline{R},\theta,t\right)=t\left(\mu-1\right)\mathbf{j}+t^{\frac{\pi}{\alpha}-1}\frac{\pi}{\alpha}\left(1+\frac{\pi}{\alpha}\right)A_0\left(\alpha\right)a_0\left(\alpha\right)\left(\mu-1\right)\cos\alpha\ \ (-\mu)^{\frac{\pi}{2\alpha}-1}\left(\cot\alpha\mathbf{i}\right.$$
$$\left.-\mathbf{j}\right)\left(1+O\left(\overline{R}\right)\right)+o\left(t^{\frac{\pi}{\alpha}-1}\right),$$
$$\text{for } 0<\overline{R}\ll\min\left(1,-\mu\right),\ -\alpha\leqslant\theta\leqslant 0, \tag{3.7.34}$$

as $t\to 0^+$ in the inner asymptotic region, with $A_0\left(\alpha\right)$ and $a_0\left(\alpha\right)$ as given in Figures 2.3 and 3.28 respectively. We observe from (3.7.31) - (3.7.34) that in this case, each of the inner region asymptotic expansions remain uniform up to the contact point, where $\left(\overline{X},\overline{Y}\right)=O\left((-\mu)^{\frac{\pi}{2\alpha}-1}t^{\frac{\pi}{\alpha}-2}\right)$. Thus the asymptotic structure, as $t\to 0^+$, of the solution to $[IBVP]$, is complete in this case. It is worth noting at this stage that in this case the expansions close to the contact point, (3.7.31) - (3.7.34), require $\left(\overline{X},\overline{Y}\right)=O\left((-\mu)^{\frac{\pi}{2\alpha}-1}t^{\frac{\pi}{\alpha}-2}\right)$ and $0<\overline{X},\overline{Y}\ll\min\left(1,-\mu\right)$. This requires the following qualification on the asymptotic structure of $[IBVP]$ as $t\to 0^+$ in this case, namely,

$$0\leqslant t\ll\min\left(1,\lambda_1\left(\mu\right),\lambda_2\left(\mu\right)\right), \tag{3.7.35}$$

where

$$\lambda_1\left(\mu\right)=(-\mu)^{\frac{\left(1-\frac{\pi}{2\alpha}\right)}{\left(\frac{\pi}{\alpha}-2\right)}}, \tag{3.7.36}$$
$$\lambda_2\left(\mu\right)=(-\mu)^{\frac{\left(2-\frac{\pi}{2\alpha}\right)}{\left(\frac{\pi}{\alpha}-2\right)}}, \tag{3.7.37}$$

in $\mu<0$.

Also, we have, in particular,

(a) The contact point is located at

$$\left(\overline{x},y\right)=\frac{1}{2}\left(\mu-1\right)t^2\left(-\cot\alpha,1\right)+O\left(t^{\frac{\pi}{\alpha}}\right), \tag{3.7.38}$$

as $t \to 0^+$ (see (3.1.2), (3.1.7), (3.1.8), and (3.1.25)).

(b) The free surface slope at the contact point is given by,

$$\begin{aligned}\eta_{\overline{x}}\left(\overline{X}_p(t), t\right) &= \eta_{I,\overline{X}}\left(\overline{X}_p(t), t\right), \\ &= t^{\frac{\pi}{\alpha}-2}\frac{\pi}{\alpha}\left(1-\frac{\pi^2}{\alpha^2}\right)A_0(\alpha)\,a_0(\alpha)\,(\mu-1)\cot\alpha\ \cos\alpha\ (-\mu)^{\frac{\pi}{2\alpha}-2} \\ &\quad + o\left(t^{\frac{\pi}{\alpha}-2}\right),\end{aligned} \tag{3.7.39}$$

as $t \to 0^+$ (see (3.5.4) and (3.7.24)). We see that the free surface slope is *positive* when $(\alpha, \mu) \in \left(\alpha^*_{2n}, \alpha^*_{2n-1}\right) \times (-\infty, 0)$ $(n = 1, 2, \dots)$ and *negative* when $(\alpha, \mu) \in \left(\alpha^*_{2n+1}, \alpha^*_{2n}\right) \times (-\infty, 0)$ $(n = 1, 2, \dots)$ and $(\alpha, \mu) \in \left(\alpha^*_1, \frac{1}{2}\pi\right) \times (-\infty, 0)$. A contour plot of $\eta_{\overline{x}}\left(\overline{X}_p(t), t\right) t^{2-\frac{\pi}{\alpha}}$, as $t \to 0^+$, in the (α, μ) plane (with $(\alpha, \mu) \in \left(0, \frac{1}{2}\pi\right) \times (-\infty, 0)$) is shown in Figure 3.33.

(c) The free surface $\eta\left(\overline{X}, t\right)$ is given by

$$\eta\left(\overline{X}, t\right) = t^2\frac{1}{2}(\mu-1) + t^{\frac{\pi}{\alpha}}A_0(\alpha)\,(\mu-1)\cos\alpha\ (-\mu)^{\frac{\pi}{2\alpha}-1}\,\xi^-_\alpha\left(\frac{\overline{X}}{(-\mu)}\right) + o\left(t^{\frac{\pi}{\alpha}}\right), \tag{3.7.40}$$

as $t \to 0^+$ for $\overline{X} \geqslant \overline{X}_p(t)$ (see (3.1.3), and (3.7.24)). It follows from (3.7.40) that $\eta\left(\overline{X}, t\right)$ is initially decreasing with a single turning point for $\alpha \in \left(\alpha^*_1, \frac{1}{2}\pi\right)$. For $\alpha \in (\alpha^*_c, \alpha^*_1)$, $\eta\left(\overline{X}, t\right)$ is initially increasing, with two turning points. For $\alpha \in (\alpha^*_2, \alpha^*_c]$, $\eta\left(\overline{X}, t\right)$ is monotone increasing. For $\alpha \in \left(\alpha^*_{2n+1}, \alpha^*_{2n}\right)$ $(n = 1, 2, \dots)$ $\eta\left(\overline{X}, t\right)$ is initially decreasing and has $(2n-1)$ turning points. Finally, for $\alpha \in \left(\alpha^*_{2n}, \alpha^*_{2n-1}\right)$ $(n = 2, 3, \dots)$ $\eta\left(\overline{X}, t\right)$ is initially increasing, and has $(2n-2)$ turning points.

When $\mu < 0$ $(\sigma < -\cot\alpha)$ with $\alpha \in \left(0, \frac{1}{2}\pi\right) \setminus \{\alpha^*_n : n = 1, 2, \dots\}$, examination of (3.7.7) and (3.7.33) reveals that, to leading order in the inner asymptotic region, the

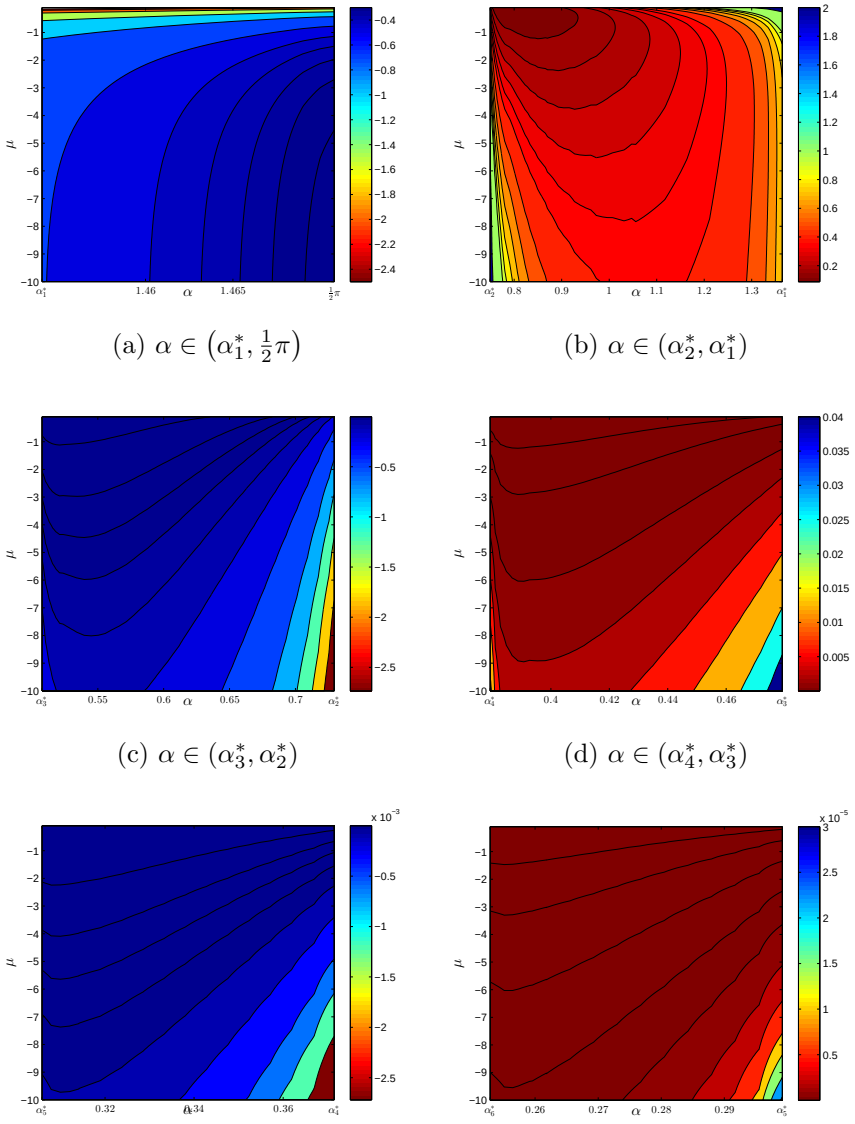

(a) $\alpha \in \left(\alpha_1^*, \frac{1}{2}\pi\right)$

(b) $\alpha \in (\alpha_2^*, \alpha_1^*)$

(c) $\alpha \in (\alpha_3^*, \alpha_2^*)$

(d) $\alpha \in (\alpha_4^*, \alpha_3^*)$

(e) $\alpha \in (\alpha_5^*, \alpha_4^*)$

(f) $\alpha \in (\alpha_6^*, \alpha_5^*)$

Figure 3.33: Contour plots of $t^{2-\frac{\pi}{\alpha}}\eta_{\overline{x}}\left(\overline{X}_p\left(t\right), t\right)$ as $t \to 0^+$ on the (α, μ) plane in the case $\mu < 0$ with $\alpha \in \left(\alpha_1^*, \frac{1}{2}\pi\right)$ and $\alpha \in \left(\alpha_{n+1}^*, \alpha_n^*\right)$ $(n = 1, 2, \ldots, 5)$

acceleration of the inclined plate induces a constant negative dynamic pressure gradient of $t^2(\mu-1)\mathbf{j}$, which causes the free surface, close to the intersection point of the free surface and the plate, to collapse to a height of $\frac{1}{2}t^2(\mu-1)$.

3.7.3 Case 3: $\mu < 0$ with $\alpha \in \{\alpha_n^* : n = 1, 2, \dots\}$

It follows from (3.1.7), (3.1.8), (3.1.25), (3.1.26), (3.1.35), and (3.1.36), that the intersection point of the plate and the free surface is located at $\left(\overline{X}, \overline{Y}\right) = \left(\overline{X}_p(t), \overline{Y}_p(t)\right) = \left(X_p(t) + \frac{1}{2}\sigma, Y_p(t) - \frac{1}{2}\sigma\tan\alpha_n^*\right)$, with

$$\overline{X}_p(t) = -t^{\frac{\pi}{\alpha}-2}A_0(\alpha_n^*)(\mu-1)\cot\alpha_n^* \cos\alpha_n^* (-\mu)^{\frac{\pi}{2\alpha_n^*}-1}\xi^-_{\alpha_n^*}(0) + o\left(t^{\frac{\pi}{\alpha}-2}\right), \tag{3.7.41}$$

$$\overline{Y}_p(t) = t^{\frac{\pi}{\alpha}-2}A_0(\alpha_n^*)(\mu-1)\cos\alpha_n^* (-\mu)^{\frac{\pi}{2\alpha_n^*}-1}\xi^-_{\alpha_n^*}(0) + o\left(t^{\frac{\pi}{\alpha}-2}\right), \tag{3.7.42}$$

as $t \to 0^+$. We then have, via (3.1.3), (3.1.5), (3.1.23), (3.1.26), (3.1.28), and (3.1.36), that

$$\eta_I\left(\overline{X}, t\right) = \frac{1}{2}(\mu-1) + t^{\frac{\pi}{\alpha_n^*}-2}A_0(\alpha_n^*)(\mu-1)\cos\alpha_n^* (-\mu)^{\frac{\pi}{2\alpha_n^*}-1}\xi^-_{\alpha_n^*}\left(\frac{\overline{X}}{(-\mu)}\right) + o\left(t^{\frac{\pi}{\alpha_n^*}-2}\right), \tag{3.7.43}$$

for $\overline{X} \geqslant \overline{X}_p(t)$, as $t \to 0^+$. We now have, from (3.7.4) and (3.7.43), that in the shifted coordinates $\left(\overline{X}, \overline{Y}\right)$, the free surface in the inner asymptotic region is located at

$$\begin{aligned}\overline{Y} &= \overline{Y}_I\left(\overline{X}, t\right), \\ &= t^{\frac{\pi}{\alpha_n^*}-2}A_0(\alpha_n^*)(\mu-1)\cos\alpha_n^* (-\mu)^{\frac{\pi}{2\alpha_n^*}-1}\xi^-_{\alpha_n^*}\left(\frac{\overline{X}}{(-\mu)}\right) + o\left(t^{\frac{\pi}{\alpha_n^*}-2}\right),\end{aligned} \tag{3.7.44}$$

for $\overline{X} \geqslant \overline{X}_p(t)$, as $t \to 0^+$. We next have, via (3.1.4), (3.1.6), (3.1.24), (3.1.26), (3.1.27), and (3.1.36), that

$$\phi_I\left(\overline{X},\overline{Y},t\right) = (\mu-1)\left[\overline{Y} - \frac{1}{6}(2-\mu)\right] + t^{\frac{\pi}{\alpha_n^*}-2} A_0(\alpha_n^*)(\mu-1)\cos\alpha_n^* \ (-\mu)^{\frac{\pi}{2\alpha_n^*}} \psi^-_{\alpha_n^*}\left(\frac{\overline{X}}{(-\mu)},\frac{\overline{Y}}{(-\mu)}\right) + o\left(t^{\frac{\pi}{\alpha_n^*}-2}\right), \tag{3.7.45}$$

for $\overline{X} \geqslant \overline{X}_p(t)$, $-\overline{X}\tan\alpha_n^* \leqslant \overline{Y} \leqslant \overline{Y}_I\left(\overline{X},t\right)$ as $t \to 0^+$. The inner region asymptotic expansion for the dynamic fluid pressure field is given, via (1.2.28), (3.1.4), (3.7.7), and (3.7.45), as

$$\begin{aligned} p_I\left(\overline{X},\overline{Y},t\right) = {} & \frac{1}{2}(\mu-1)\left(1-2\overline{Y}\right) \\ & + t^{\frac{\pi}{\alpha_n^*}-2} A_0(\alpha_n^*)(\mu-1)\cos\alpha_n^* \ (-\mu)^{\frac{\pi}{2\alpha_n^*}} \left(2\overline{X}\psi^-_{\alpha_n^*,\overline{X}}\left(\frac{\overline{X}}{(-\mu)},\frac{\overline{Y}}{(-\mu)}\right)\right. \\ & \quad + 2\overline{Y}\psi^-_{\alpha_n^*,\overline{Y}}\left(\frac{\overline{X}}{(-\mu)},\frac{\overline{Y}}{(-\mu)}\right) \\ & \quad \left. - \left(1+\frac{\pi}{\alpha_n^*}\right)\psi^-_{\alpha_n^*}\left(\frac{\overline{X}}{(-\mu)},\frac{\overline{Y}}{(-\mu)}\right)\right) + o\left(t^{\frac{\pi}{\alpha_n^*}-2}\right), \end{aligned} \tag{3.7.46}$$

as $t \to 0^+$ with $\overline{X} \geqslant \overline{X}_p(t)$, $-\overline{X}\tan\alpha_n^* \leqslant \overline{Y} \leqslant \overline{Y}_I\left(\overline{X},t\right)$. Finally, in the inner asymptotic region, the fluid velocity field is given, via (1.2.29), (3.1.4), and (3.7.45), as

$$\begin{aligned} \mathbf{q}\left(\overline{X},\overline{Y},t\right) = {} & t(\mu-1)\mathbf{j} + t^{\frac{\pi}{\alpha_n^*}-1} A_0(\alpha_n^*)(\mu-1)\cos\alpha_n^* \ (-\mu)^{\frac{\pi}{2\alpha_n^*}} \left(\psi^-_{\alpha_n^*,\overline{X}}\left(\frac{\overline{X}}{(-\mu)},\frac{\overline{Y}}{(-\mu)}\right)\mathbf{i}\right. \\ & \left. + \psi^-_{\alpha_n^*,\overline{Y}}\left(\frac{\overline{X}}{(-\mu)},\frac{\overline{Y}}{(-\mu)}\right)\mathbf{j}\right) + o\left(t^{\frac{\pi}{\alpha_n^*}-2}\right), \end{aligned} \tag{3.7.47}$$

as $t \to 0^+$ with $\overline{X} \geqslant \overline{X}_p(t)$, $-\overline{X}\tan\alpha_n^* \leqslant \overline{Y} \leqslant \overline{Y}_I\left(\overline{X},t\right)$. We now consider the structure of the inner region asymptotic expansions close to the intersection point of the inclined plate and the fluid free surface when $\left(\overline{X},\overline{Y}\right) = O\left((-\mu)^{\frac{\pi}{2\alpha_n^*}-1} t^{\frac{\pi}{\alpha_n^*}-2}\right)$ as $t \to 0^+$. We have,

via (3.5.5), (3.5.6), (3.6.5), and (3.6.6), together with (3.7.41) - (3.7.47), that

$$\overline{X}_p(t) = o\left(t^{\frac{\pi}{\alpha_n^*}-2}\right), \tag{3.7.48}$$

$$\overline{Y}_p(t) = o\left(t^{\frac{\pi}{\alpha_n^*}-2}\right), \tag{3.7.49}$$

$$\begin{aligned}\phi_I\left(\overline{R},\theta,t\right) &= (\mu-1)\left[\overline{R}\sin\theta - \frac{1}{6}(2-\mu)\right] \\ &\quad + t^{\frac{\pi}{\alpha}-2}A_0(\alpha_n^*)\,b_1(\alpha_n^*)\,(\mu-1)\cos\alpha_n^*\ (-\mu)^{-\frac{\pi}{2\alpha_n^*}}\left(\overline{R}^{\frac{\pi}{\alpha_n^*}}\cos\frac{\pi}{\alpha_n^*}(\theta+\alpha_n^*)\right. \\ &\quad \left. + O\left(\overline{R}^{\frac{\pi}{\alpha_n^*}+1}\right)\right) + o\left(t^{\frac{\pi}{\alpha}-2}\right), \\ &\quad \text{for } 0<\overline{R}\ll\min(1,-\mu),\ -\alpha_n^*\leqslant\theta\leqslant 0,\end{aligned} \tag{3.7.50}$$

$$\begin{aligned}\eta_I\left(\overline{X},t\right) &= \frac{1}{2}(\mu-1) \\ &\quad + t^{\frac{\pi}{\alpha_n^*}-2}A_0(\alpha_n^*)\,b_1(\alpha_n^*)\,(\mu-1)\cos\alpha_n^*\ (-\mu)^{-\frac{\pi}{2\alpha_n^*}-1}\,\overline{X}^{\frac{\pi}{\alpha_n^*}}\left(1+O\left(\overline{X}\right)\right) \\ &\quad + o\left(t^{\frac{\pi}{\alpha}-2}\right), \\ &\quad \text{for } 0<\overline{X}\ll\min(1,-\mu),\end{aligned} \tag{3.7.51}$$

$$\begin{aligned}p_I\left(\overline{R},\theta,t\right) &= \frac{1}{2}(\mu-1)\left(1-2\overline{R}\sin\theta\right) \\ &\quad + t^{\frac{\pi}{\alpha_n^*}-2}\left(\frac{\pi}{\alpha_n^*}-1\right)A_0(\alpha_n^*)\,b_1(\alpha_n^*)\,(\mu-1)\cos\alpha_n^*\ (-\mu)^{-\frac{\pi}{2\alpha_n^*}}\left(\right. \\ &\quad \left.\overline{R}^{\frac{\pi}{\alpha_n^*}}\cos\frac{\pi}{\alpha_n^*}(\theta+\alpha)+O\left(\overline{R}^{\frac{\pi}{\alpha_n^*}+1}\right)\right)+o\left(t^{\frac{\pi}{\alpha}-2}\right), \\ &\quad \text{for } 0<\overline{R}\ll\min(1,-\mu),\ -\alpha_n^*\leqslant\theta\leqslant 0,\end{aligned} \tag{3.7.52}$$

$$\begin{aligned}\mathbf{q}\left(\overline{R},\theta,t\right) &= t(\mu-1)\,\mathbf{j} + t^{\frac{\pi}{\alpha_n^*}-1}\frac{\pi}{\alpha_n^*}A_0(\alpha_n^*)\,b_1(\alpha_n^*)\,(\mu-1)\cos\alpha_n^*\ (-\mu)^{-\frac{\pi}{2\alpha_n^*}}(\cos\alpha_n^*\mathbf{i} \\ &\quad - \sin\alpha_n^*\mathbf{j})\left(\overline{R}^{\frac{\pi}{\alpha_n^*}-1}+O\left(\overline{R}^{\frac{\pi}{\alpha_n^*}}\right)\right)+o\left(t^{\frac{\pi}{\alpha_n^*}-1}\right), \\ &\quad \text{for } 0<\overline{R}\ll\min(1,-\mu),\ -\alpha_n^*\leqslant\theta\leqslant 0,\end{aligned} \tag{3.7.53}$$

as $t\to 0^+$ in the inner asymptotic region, with $A_0(\alpha)$ as given in Figure 2.3, and $b_1(\alpha_n^*)$ a globally determined real constant. We observe from (3.7.50) - (3.7.53) that, in this case, each of the inner region asymptotic expansions remain uniform up to the contact

point, where $\left(\overline{X},\overline{Y}\right)=O\left((-\mu)^{\frac{\pi}{2\alpha_n^*}-1}t^{\frac{\pi}{\alpha_n^*}-2}\right)$. Thus the asymptotic structure, as $t\to 0^+$, of the solution to $[IBVP]$ is complete in this case. It is worth noting at this stage that, in this case, the expansions close to the contact point require $\left(\overline{X},\overline{Y}\right)=o\left(t^{\frac{\pi}{\alpha_n^*}-2}\right)$ and $0<\overline{X},\ \overline{Y}\ll\min\left(1,-\mu\right)$. This requires the following qualification on the asymptotic structure of $[IBVP]$ as $t\to 0^+$ in this case, namely,

$$0\leqslant t\ll\min\left(1,\lambda_1\left(\mu\right)\right), \tag{3.7.54}$$

where

$$\lambda_1\left(\mu\right)=(-\mu)^{\frac{1}{\frac{\pi}{\alpha_n^*}-2}}, \tag{3.7.55}$$

in $\mu<0$.

Also, we have, in particular,

(a) The contact point is located at

$$\left(\overline{x},y\right)=\frac{1}{2}\left(\mu-1\right)t^2\left(-\cot\alpha_n^*,1\right)+O\left(t^{\frac{\pi}{\alpha_n^*}}\right), \tag{3.7.56}$$

as $t\to 0^+$ (see (3.1.2), (3.1.7), (3.1.8), and (3.1.25)).

(b) The free surface slope at the contact point is given by,

$$\eta_{\overline{x}}\left(\overline{X}_p\left(t\right),t\right)=\eta_{I,\overline{X}}\left(\overline{X}_p\left(t\right),t\right)=o\left(t^{\frac{\pi}{\alpha_n^*}-2}\right), \tag{3.7.57}$$

as $t\to 0^+$ (see (3.5.4) and (3.7.43)).

(c) The free surface $\eta\left(\overline{X},t\right)$ is given by

$$\eta\left(\overline{X},t\right)=t^2\frac{1}{2}\left(\mu-1\right)+t^{\frac{\pi}{\alpha_n^*}}A_0\left(\alpha_n^*\right)\left(\mu-1\right)\cos\alpha_n^*\ \left(-\mu\right)^{\frac{\pi}{2\alpha_n^*}-1}\xi_{\alpha_n^*}^{-}\left(\frac{\overline{X}}{(-\mu)}\right)$$
$$+\,o\left(t^{\frac{\pi}{\alpha_n^*}}\right), \tag{3.7.58}$$

as $t\to 0^+$ for $\overline{X}\geqslant\overline{X}_p\left(t\right)$ (see (3.1.3), and (3.7.43)).

When $\mu<0$ $(\sigma<-\cot\alpha_n^*)$ with $\alpha\in\{\alpha_n^*:n=1,2,\dots\}$, examination of (3.7.7) and (3.7.52) reveals that, to leading order in the inner asymptotic region, the acceleration of the inclined plate induces a constant negative dynamic pressure gradient of $t^2\left(\mu-1\right)\mathbf{j}$, which causes the free surface, close to the intersection point of the free surface and the plate, to collapse to a height of $\frac{1}{2}t^2\left(\mu-1\right)$.

3.7.4 Case 4: $\mu=0$ with $\alpha\in\left(0,\frac{1}{2}\pi\right)$

This case has not been treated as yet. However, as discussed in §3.6, it is readily established that in this degenerate case, the solution to the boundary value problem (3.1.29) - (3.1.34), which has least singular behaviour at $\left(\overline{X},\overline{Y}\right)=(0,0)$, is simply given by the far-field forms. In this case we have, via (3.6.7) and (3.6.8), that

$$\overline{X}_p\left(t\right)=o\left(t^{\frac{\pi}{\alpha}-2}\right), \tag{3.7.59}$$

$$\overline{Y}_p\left(t\right)=o\left(t^{\frac{\pi}{\alpha}-2}\right), \tag{3.7.60}$$

$$\phi_I\left(\overline{R},\theta,t\right)=-\left(\overline{R}\sin\theta-\frac{1}{3}\right)+t^{\frac{\pi}{\alpha}-2}A_0\left(\alpha\right)\cos\alpha\ \overline{R}^{\frac{\pi}{2\alpha}}\cos\frac{\pi}{2\alpha}\left(\theta+\alpha\right)+o\left(t^{\frac{\pi}{\alpha}-2}\right),$$
$$\text{for } \overline{R}>0,\ -\alpha\leqslant\theta\leqslant 0, \tag{3.7.61}$$

$$\eta_I\left(\overline{X},t\right)=\overline{Y}_I\left(\overline{X},t\right)-\frac{1}{2}=-\frac{1}{2}-t^{\frac{\pi}{\alpha}-2}A_0\left(\alpha\right)\cos\alpha\ \frac{\pi}{4\alpha}\overline{X}^{\frac{\pi}{2\alpha}-1}+o\left(t^{\frac{\pi}{\alpha}-2}\right),$$
$$\text{for } \overline{X}>0, \tag{3.7.62}$$

$$p_I\left(\overline{R},\theta,t\right) = -\frac{1}{2}\left(1-2\overline{R}\sin\theta\right) - t^{\frac{\pi}{\alpha}-2}A_0\left(\alpha\right)\cos\alpha\ \overline{R}^{\frac{\pi}{2\alpha}}\cos\frac{\pi}{2\alpha}\left(\theta+\alpha\right) + o\left(t^{\frac{\pi}{\alpha}-2}\right),$$
$$\text{for } \overline{R}>0,\ -\alpha\leqslant\theta\leqslant 0, \tag{3.7.63}$$

$$\mathbf{q}\left(\overline{R},\theta,t\right) = -t\mathbf{j} - t^{\frac{\pi}{\alpha}-1}\frac{\pi}{2\alpha}A_0\left(\alpha\right)\cos\alpha\ \overline{R}^{\frac{\pi}{2\alpha}-1}\left(\sin\left(1-\frac{\pi}{2\alpha}\right)\theta\mathbf{i}\right.$$
$$\left.-\cos\left(1-\frac{\pi}{2\alpha}\right)\theta\mathbf{j}\right)\left(1+O\left(\overline{R}\right)\right) + o\left(t^{\frac{\pi}{\alpha}+1}\right),$$
$$\text{for } \overline{R}>0,\ -\alpha\leqslant\theta\leqslant 0, \tag{3.7.64}$$

as $t\to 0^+$ in the inner asymptotic region. In this case we observe, from (3.7.61) - (3.7.64), that each of the inner region asymptotic expansions remain uniform up to the contact point, when $\left(\overline{X},\overline{Y}\right) = o\left(t^{\frac{\pi}{\alpha}-2}\right)$ *provided* $0<\alpha\leqslant\frac{1}{4}\pi$. However, *for* $\frac{1}{4}\pi<\alpha<\frac{1}{2}\pi$, a weak nonuniformity in derivatives $\left(\eta_{I,\overline{X}},\hat{\hat{\nabla}}\phi_I\right)$ persists close to the contact point and, in particular, when $\overline{X},\,\overline{Y} = O\left(t^{\frac{\left(\frac{\pi}{\alpha}-2\right)}{2\left(1-\frac{\pi}{4\alpha}\right)}}\right)$ as $t\to 0^+$. In this case an inner-inner asymptotic region will be required when $\overline{X},\,\overline{Y} = O\left(t^{\frac{\left(\frac{\pi}{\alpha}-2\right)}{2\left(1-\frac{\pi}{4\alpha}\right)}}\right)$ as $t\to 0^+$ in order to correctly capture the behaviour of the free surface at the contact point.

When $0<\alpha\leqslant\frac{1}{4}\pi$, we can draw the following conclusions concerning the free surface, the fluid velocity field, and the dynamic pressure field in the inner asymptotic region:

(a) The contact point is located at

$$\left(\overline{x},y\right) = -\frac{1}{2}t^2\left(-\cot\alpha,1\right) + o\left(t^{\frac{\pi}{\alpha}}\right), \tag{3.7.65}$$

as $t\to 0^+$.

(b) The free surface slope at the contact point is given by

$$\eta_{\overline{x}}\left(\overline{X}_p\left(t\right),t\right) = \eta_{I,\overline{X}}\left(\overline{X}_p\left(t\right),t\right) = \begin{cases} o\left(t^{\frac{\pi}{\alpha}-2}\right), & 0<\alpha<\frac{1}{4}\pi, \\ -\frac{A_0\left(\frac{1}{4}\pi\right)}{\sqrt{2}}t^2 + o\left(t^2\right), & \alpha=\frac{1}{4}\pi, \end{cases} \tag{3.7.66}$$

as $t \to 0^+$.

(c) The free surface $\eta\left(\overline{X}, t\right)$ is given by

$$\eta\left(\overline{X}, t\right) = -\frac{1}{2}t^2 - t^{\frac{\pi}{\alpha}} A_0(\alpha) \cos\alpha \ \frac{\pi}{4\alpha} \overline{X}^{\frac{\pi}{2\alpha}-1} + o\left(t^{\frac{\pi}{\alpha}}\right), \tag{3.7.67}$$

as $t \to 0^+$ for $\overline{X} \geqslant \overline{X}_p(t)$ (see (3.1.3), and (3.7.62)).

When $\frac{1}{4}\pi < \alpha < \frac{1}{2}\pi$, we consider the inner-inner asymptotic region, where $\overline{X}, \overline{Y} = O\left(t^{\frac{(\frac{\pi}{\alpha}-2)}{2(1-\frac{\pi}{4\alpha})}}\right)$ as $t \to 0^+$, in the next chapter.

Chapter 4

Inner-Inner Region Asymptotic Structure to $[IBVP]$ as $t \to 0^+$

In this chapter we introduce the inner-inner asymptotic region associated with $[IBVP]$ when $\left(\overline{X}, \overline{Y}\right) = o(1)$ as $t \to 0^+$, for $\mu = 0$ with $\alpha \in \left(\frac{1}{4}\pi, \frac{1}{2}\pi\right)$. Specifically, following Chapter 3, we write $\left(\overline{X}, \overline{Y}\right) = O(\Delta(t))$ with $\Delta(t) = o(1)$ as $t \to 0^+$ in the inner-inner asymptotic region. It then follows from (3.7.62) that $\overline{Y}_I = \frac{1}{2} + \eta_I = O\left(t^{\frac{\pi}{\alpha}-2}\Delta(t)^{\frac{\pi}{2\alpha}-1}\right)$ as $t \to 0^+$ in the inner-inner asymptotic region. The free surface must be captured in the inner-inner asymptotic region. This requires

$$\Delta(t) = O\left(t^{\Gamma}\right), \quad \text{with} \quad \Gamma = \frac{\left(\frac{\pi}{\alpha} - 2\right)}{2\left(1 - \frac{\pi}{4\alpha}\right)}, \tag{4.0.1}$$

as $t \to 0^+$. A sketch of the location of the inner-inner asymptotic region is illustrated in Figure 4.1.

4.1 Inner-Inner Region Asymptotic Structure for $\mu = 0$ with $\alpha \in \left(\frac{1}{4}\pi, \frac{1}{2}\pi\right)$

Formally we introduce scaled inner-inner asymptotic region coordinates $(\tilde{x}, \tilde{y})$ by

$$\overline{X} = t^{\Gamma}\tilde{x}, \quad \overline{Y} = t^{\Gamma}\tilde{y}, \tag{4.1.1}$$

with $(\tilde{x}, \tilde{y}) = O(1)$ as $t \to 0^+$ in the inner-inner asymptotic region. The location of the plate in the inner-inner asymptotic region is given by $\tilde{y} = -\tilde{x}\tan\alpha$, whilst the plate and the free surface intersection point is denoted by $(\tilde{x}, \tilde{y}) = (\tilde{x}_p(t), \tilde{y}_p(t))$, with,

$$\overline{X}_p(t) = t^{\Gamma}\tilde{x}_p(t), \quad \overline{Y}_p(t) = t^{\Gamma}\tilde{y}_p(t), \tag{4.1.2}$$

and $(\tilde{x}_p(t), \tilde{y}_p(t)) = O(1)$ as $t \to 0^+$ in the inner-inner asymptotic region. An examination of (3.7.61) and (3.7.62) reveals that $\eta_I = -\frac{1}{2} + O\left(t^{\Gamma}\right)$ and $\phi_I = \frac{1}{3} - t^{\Gamma}\tilde{y} + O\left(t^{2\Gamma}\right)$ as $t \to 0^+$ in the inner-inner asymptotic region. We now write the free surface and velocity potential in the inner-inner asymptotic region as

$$\eta_I(\tilde{x}, t) = -\frac{1}{2} + t^{\Gamma}\eta_{II}(\tilde{x}, t), \qquad \tilde{x} \geqslant \tilde{x}_p(t),\ t \geqslant 0; \tag{4.1.3}$$

$$\phi_I(\tilde{x}, \tilde{y}, t) = \frac{1}{3} - t^{\Gamma}\tilde{y} + t^{2\Gamma}\phi_{II}(\tilde{x}, \tilde{y}, t), \qquad \tilde{x} \geqslant \tilde{x}_p(t),\ -\tilde{x}\tan\alpha \leqslant \tilde{y} \leqslant \eta_{II}(\tilde{x}, t),\ t \geqslant 0; \tag{4.1.4}$$

with $\eta_{II}(\tilde{x},t)$, $\phi_{II}(\tilde{x},\tilde{y},t) = O(1)$ as $t \to 0^+$. The inner-inner region asymptotic expansions are then introduced as,

$$\eta_{II}(\tilde{x},t) = \tilde{\eta}_0(\tilde{x}) + o(1), \tag{4.1.5}$$

$$\phi_{II}(\tilde{x},\tilde{y},t) = \tilde{\phi}_0(\tilde{x},\tilde{y}) + o(1), \tag{4.1.6}$$

as $t \to 0^+$ with $(\tilde{x},\tilde{y}) = O(1)$ in the inner-inner asymptotic region. Finally, it follows from (4.1.1) - (4.1.3), and (4.1.5) that we expand $\tilde{x}_p(t)$ in the form

$$\tilde{x}_p(t) = \tilde{x}_0 + o(1), \tag{4.1.7}$$

as $t \to 0^+$, with

$$\tilde{y}_p(t) = -\tilde{x}_p(t)\tan\alpha. \tag{4.1.8}$$

The free surface in the inner-inner asymptotic region is located at

$$\tilde{y} = \eta_{II}(\tilde{x},t), \quad \tilde{x} > \tilde{x}_p(t),\ t \geqslant 0, \tag{4.1.9}$$

whilst the spatial domain in the inner-inner asymptotic region is

$$\mathcal{D}_{II}(t) = \{(\tilde{x},\tilde{y}) : \tilde{x} > \tilde{x}_p(t),\ -\tilde{x}\tan\alpha < \tilde{y} < \eta_{II}(\tilde{x},t)\}, \tag{4.1.10}$$

for $t \geqslant 0$, with closure $\overline{\mathcal{D}}_{II}(t)$. A sketch of the inner-inner asymptotic region geometry is given in Figure 4.2.

We now write $[IBVP]$ in terms of the inner-inner asymptotic region coordinates $(\tilde{x},\tilde{y})$,

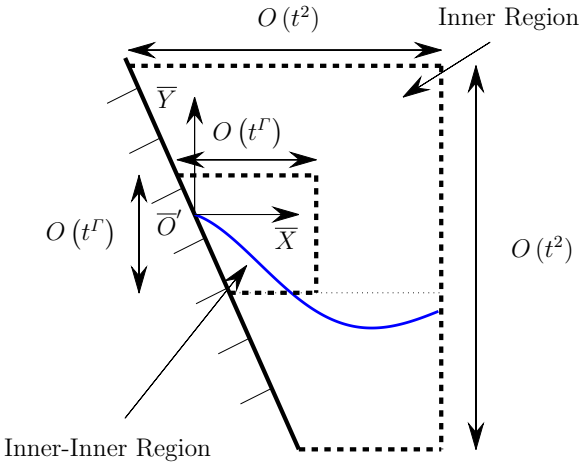

Figure 4.1: A sketch of the location of the inner-inner asymptotic region for $\mu = 0$, with $\alpha \in \left(\frac{1}{4}\pi, \frac{1}{2}\pi\right)$

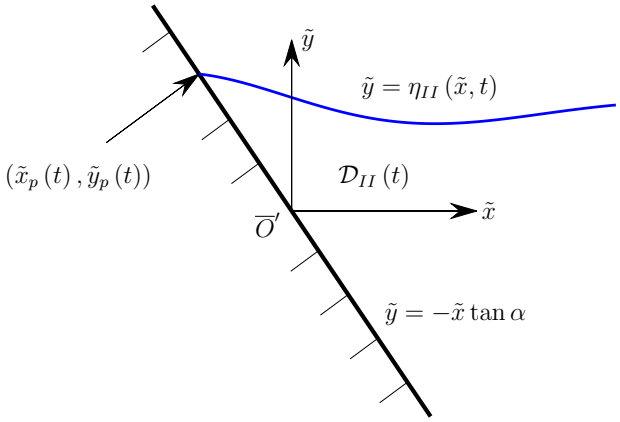

Figure 4.2: The inner-inner asymptotic region geometry for $\mu = 0$, with $\alpha \in \left(\frac{1}{4}\pi, \frac{1}{2}\pi\right)$

and the inner-inner asymptotic region variables ϕ_{II} and η_{II}, to obtain,

$$\widetilde{\nabla}^2\phi_{II}\left(\tilde{x},\tilde{y}\right)=0, \qquad \left(\tilde{x},\tilde{y}\right)\in\mathcal{D}_{II}\left(t\right),\ t>0; \tag{4.1.11}$$

$$\widetilde{\nabla}\phi_{II}\cdot\hat{\mathbf{n}}=0, \qquad \tilde{x}>\tilde{x}_p\left(t\right),\ \tilde{y}=-\tilde{x}\tan\alpha,\ t>0; \tag{4.1.12}$$

$$\left(\Gamma+2\right)\eta_{II}+\left[\phi_{II,\tilde{x}}-\left(\Gamma+2\right)\tilde{x}\right]\eta_{II,\tilde{x}}-\phi_{II,\tilde{y}}+t\eta_{II,t}=0,$$
$$\tilde{x}>\tilde{x}_p\left(t\right),\ \tilde{y}=\eta_{II}\left(\tilde{x},t\right),\ t>0; \tag{4.1.13}$$

$$\left(2\Gamma+3\right)\phi_{II}-\left(\Gamma+2\right)\left(\tilde{x}\phi_{II,\tilde{x}}+\tilde{y}\phi_{II,\tilde{y}}\right)+\frac{1}{2}\phi_{II,\tilde{x}}^2+\frac{1}{2}\phi_{II,\tilde{y}}^2+t\phi_{II,t}=0,$$
$$\tilde{x}>\tilde{x}_p\left(t\right),\ \tilde{y}=\eta_{II}\left(\tilde{x},t\right),\ t>0; \tag{4.1.14}$$

$$\eta_{II}\left(\tilde{x}_p\left(t\right),t\right)=-\tilde{x}_p\left(t\right)\tan\alpha, \qquad t>0; \tag{4.1.15}$$

with $\widetilde{\nabla}=\left(\partial/\partial\tilde{x},\partial/\partial\tilde{y}\right)$. On substituting from (4.1.5) - (4.1.7) into (4.1.11) - (4.1.15) we obtain, at leading order, the following nonlinear harmonic free boundary problem for $\tilde{\phi}_0\left(\tilde{x},\tilde{y}\right)$, $\tilde{\eta}_0\left(\tilde{x}\right)$, and $\tilde{x}_0$, namely

$$\widetilde{\nabla}^2\tilde{\phi}_0=0, \qquad \tilde{x}>\tilde{x}_0,\ -\tilde{x}\tan\alpha<\tilde{y}<\tilde{\eta}_0\left(\tilde{x}\right); \tag{4.1.16}$$

$$\widetilde{\nabla}\tilde{\phi}_0\cdot\hat{\mathbf{n}}=0, \qquad \tilde{x}>\tilde{x}_0,\ \tilde{y}=-\tilde{x}\tan\alpha; \tag{4.1.17}$$

$$\gamma\tilde{\eta}_0+\left[\tilde{\phi}_{0,\tilde{x}}-\gamma\tilde{x}\right]\tilde{\eta}_{0,\tilde{x}}-\tilde{\phi}_{0,\tilde{y}}=0, \qquad \tilde{x}>\tilde{x}_0,\ \tilde{y}=\tilde{\eta}_0\left(\tilde{x}\right); \tag{4.1.18}$$

$$\left(2\gamma-1\right)\tilde{\phi}_0-\gamma\left(\tilde{x}\tilde{\phi}_{0,\tilde{x}}+\tilde{y}\tilde{\phi}_{0,\tilde{y}}\right)+\frac{1}{2}\tilde{\phi}_{0,\tilde{x}}^2+\frac{1}{2}\tilde{\phi}_{0,\tilde{y}}^2=0, \qquad \tilde{x}>\tilde{x}_0,\ \tilde{y}=\tilde{\eta}_0\left(\tilde{x}\right); \tag{4.1.19}$$

$$\tilde{\eta}_0\left(\tilde{x}_0\right)=-\tilde{x}_0\tan\alpha; \tag{4.1.20}$$

with

$$\gamma=\Gamma+2=\frac{1}{1-\frac{\pi}{4\alpha}}. \tag{4.1.21}$$

The problem (4.1.16) - (4.1.20) must be completed by asymptotic matching conditions between the inner-inner asymptotic region and the inner asymptotic region. Following

Van Dyke's Matching Principle (see, for example, [19]), we obtain,

$$\tilde{\phi}_0(\tilde{r},\theta) = A_0(\alpha)\cos\alpha\ \tilde{r}^{\frac{\pi}{2\alpha}}\cos\frac{\pi}{2\alpha}(\theta+\alpha) + o\left(\tilde{r}^{\frac{\pi}{2\alpha}}\right) \quad \text{as } \tilde{r}\to\infty,\ -\alpha<\theta<0, \tag{4.1.22}$$

$$\tilde{\eta}_0(\tilde{x}) = -A_0(\alpha)\cos\alpha\ \frac{\pi}{4\alpha}\tilde{x}^{\frac{\pi}{2\alpha}-1} + o\left(\tilde{x}^{\frac{\pi}{2\alpha}-1}\right) \qquad \text{as } \tilde{x}\to\infty, \tag{4.1.23}$$

where $\tilde{r}$ and θ are polar coordinates given by $\tilde{x}=\tilde{r}\cos\theta$, $\tilde{y}=\tilde{r}\sin\theta$. To remove $A_0(\alpha)$ from the problem, we introduce the following scalings,

$$\tilde{\phi}_0 = \kappa^2\widehat{\psi}, \qquad \tilde{\eta}_0 = \kappa\widehat{\xi},$$
$$\tilde{x}=\kappa\hat{x}, \quad \tilde{y}=\kappa\hat{y}, \quad \tilde{r}=\kappa\hat{r}, \quad \tilde{x}_0=\kappa\hat{x}_0, \tag{4.1.24}$$

with, recalling that $A_0(\alpha)<0$ for $\alpha\in\left(\frac{1}{4}\pi,\frac{1}{2}\pi\right)$,

$$\kappa = \left(-A_0(\alpha)\cos\alpha\right)^{\frac{1}{2}\gamma}, \tag{4.1.25}$$

illustrated in Figure 4.3. The corresponding boundary problem for $\widehat{\psi}$ and $\widehat{\xi}$ is dependent only upon α and is given by

$$\widehat{\nabla}^2\widehat{\psi} = 0, \qquad \hat{x}>\hat{x}_0,\ -\hat{x}\tan\alpha<\hat{y}<\widehat{\xi}(\hat{x}); \tag{4.1.26}$$

$$\widehat{\nabla}\widehat{\psi}\cdot\hat{\mathbf{n}} = 0, \qquad \hat{x}>\hat{x}_0,\ \hat{y}=-\hat{x}\tan\alpha; \tag{4.1.27}$$

$$\gamma\widehat{\xi} + \left[\widehat{\psi}_{\hat{x}} - \gamma\hat{x}\right]\widehat{\xi}_{\hat{x}} - \widehat{\psi}_{\hat{y}} = 0, \qquad \hat{x}>\hat{x}_0,\ \hat{y}=\widehat{\xi}(\hat{x}); \tag{4.1.28}$$

$$(2\gamma-1)\widehat{\psi} - \gamma\left(\hat{x}\widehat{\psi}_{\hat{x}} + \hat{y}\widehat{\psi}_{\hat{y}}\right) + \frac{1}{2}\widehat{\psi}_{\hat{x}}^2 + \frac{1}{2}\widehat{\psi}_{\hat{y}}^2 = 0, \qquad \hat{x}>\hat{x}_0,\ \hat{y}=\widehat{\xi}(\hat{x}); \tag{4.1.29}$$

$$\widehat{\xi}(\hat{x}_0) = -\hat{x}_0\tan\alpha; \tag{4.1.30}$$

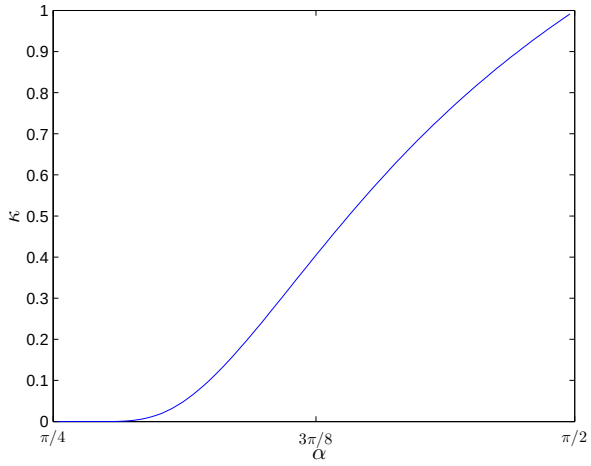

Figure 4.3: Graph of $\kappa(\alpha)$ against α calculated exactly via (2.0.15) and (4.1.25)

$$\widehat{\xi}(\hat{x}) = \frac{\pi}{4\alpha}\hat{x}^{\frac{\pi}{2\alpha}-1} + o\left(\hat{x}^{\frac{\pi}{2\alpha}-1}\right) \qquad \text{as} \quad \hat{x} \to \infty; \tag{4.1.31}$$

$$\widehat{\psi}(\hat{r},\theta) = -\hat{r}^{\frac{\pi}{2\alpha}}\cos\frac{\pi}{2\alpha}(\theta+\alpha) + o\left(\hat{r}^{\frac{\pi}{2\alpha}}\right) \qquad \text{as} \quad \hat{r} \to \infty,\ -\alpha < \theta < 0; \tag{4.1.32}$$

where $\widehat{\nabla}$ is now defined by $\widehat{\nabla} = (\partial/\partial\hat{x}, \partial/\partial\hat{y})$, and $(\hat{r},\theta)$ are polar coordinates given by $\hat{x} = \hat{r}\cos\theta$, $\hat{y} = \hat{r}\sin\theta$. This boundary value problem is similar to that studied by Needham et al [24] for $\alpha \in \left(\frac{1}{2}\pi, \pi\right)$. We will now outline the method used to construct numerical solutions to this boundary value problem. We begin by defining the position of the free boundary parametrically in terms of arc length s, with $s = 0$ at the contact point of the plate and the free boundary and s increasing as we move away from the plate along the free boundary, giving

$$\hat{x} = \hat{x}(s), \quad \hat{y} = \hat{y}(s), \quad \widehat{\xi} = \widehat{\xi}(s), \quad \text{for } s \geqslant 0, \tag{4.1.33}$$

along the free boundary $\hat{y} = \widehat{\xi}(\hat{x})$ for $\hat{x} \geqslant \hat{x}_0$. The free boundary conditions (4.1.28) and

(4.1.29) become

$$\widehat{\nabla}\widehat{\psi}\cdot\hat{\mathbf{n}}=\gamma\left(\hat{x}'\hat{y}-\hat{x}\hat{y}'\right), \qquad \text{on} \quad (\hat{x},\hat{y})=\left(\hat{x}\left(s\right),\hat{y}\left(s\right)\right) \quad \text{with} \quad s>0. \tag{4.1.34}$$

$$\frac{1}{2}\Phi'^{2}-\gamma\left(\hat{x}\hat{x}'+\hat{y}\hat{y}'\right)\Phi'+\left(2\gamma-1\right)\Phi-\frac{1}{2}\gamma^{2}\left(\hat{x}'\hat{y}-\hat{x}\hat{y}'\right)^{2}=0,$$

$$\text{on} \quad (\hat{x},\hat{y})=\left(\hat{x}\left(s\right),\hat{y}\left(s\right)\right) \quad \text{with} \quad s>0. \tag{4.1.35}$$

Here $'$ denotes d/ds, $\hat{\mathbf{n}}=\left(-\hat{y}'\left(s\right),\hat{x}'\left(s\right)\right)$ is the unit normal on the free boundary pointing out of the fluid and $\Phi=\widehat{\psi}\left(\hat{x}\left(s\right),\hat{y}\left(s\right)\right)$. Additionally, we also have the arc-length condition given by

$$\hat{x}'^{2}+\hat{y}'^{2}=1, \qquad s>0. \tag{4.1.36}$$

It is convenient at this stage to introduce a rotated (x,y)[1] coordinate system oriented so that the y-axis lies parallel to (and points up) the plate, with the x-axis pointing into the fluid. A sketch of the rotated coordinate system is given in Figure 4.4. The associated coordinate transformation is

$$x=\hat{x}\sin\alpha+\hat{y}\cos\alpha, \qquad y=-\hat{x}\cos\alpha+\hat{y}\sin\alpha, \tag{4.1.37}$$

with the free boundary now located at $y=\tilde{\xi}\left(x\right)$ $(x\geqslant 0)$ and, in parametric form, at $(x,y)=\left(X\left(s\right),Y\left(s\right)\right)$ $(s\geqslant 0)$, and the plate located at $x=0$ $(-\infty<y<\infty)$. The boundary value problem (4.1.26) - (4.1.29) may now be written (invoking symmetry in the y-axis, via (4.1.27), as,

$$\widehat{\nabla}^{2}\widehat{\psi}=0, \qquad -\infty<x<\infty,\ -\infty<y<Y\left(s\right),\ \left(s\in\mathbb{R}\right); \tag{4.1.38}$$

$$\hat{\mathbf{n}}\cdot\widehat{\nabla}\widehat{\psi}=\gamma\left(YX'-XY'\right), \qquad x=X\left(s\right),\ y=Y\left(s\right),\ \left(s\in\mathbb{R}\right); \tag{4.1.39}$$

[1]This notation should not be confused with the original coordinate system used in Chapter 1

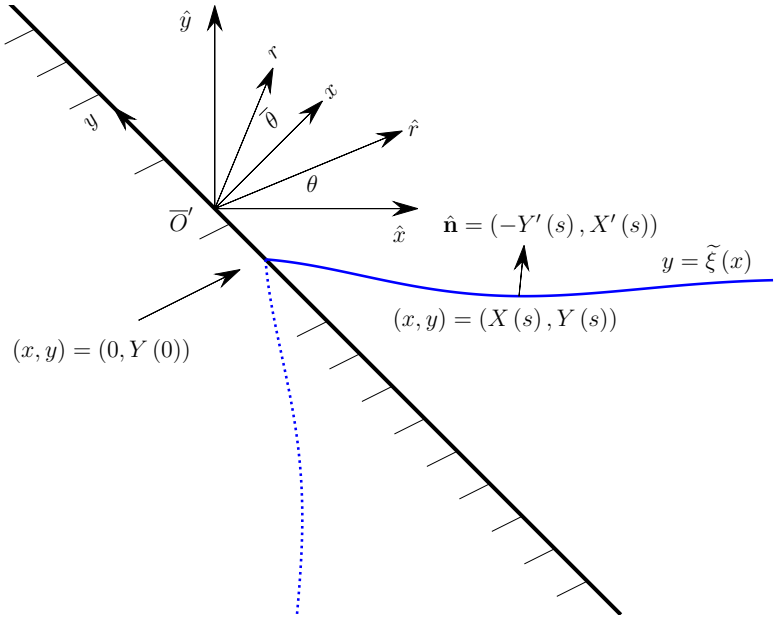

Figure 4.4: The inner-inner asymptotic region rotated coordinate system for $\mu = 0$, with $\alpha \in \left(\frac{1}{4}\pi, \frac{1}{2}\pi\right)$

$$\frac{1}{2}\Phi'^2 - \gamma\left(XX' + YY'\right)\Phi' + (2\gamma - 1)\Phi - \frac{1}{2}\gamma^2\left(X'Y - XY'\right)^2 = 0,$$
$$x = X(s),\ y = Y(s),\ (s \in \mathbb{R}); \quad (4.1.40)$$

$$X'^2 + Y'^2 = 1, \qquad x = X(s),\ y = Y(s),\ (s \in \mathbb{R}); \quad (4.1.41)$$

$$X(s) = s + o(s) \qquad \text{as } |s| \to \infty; \quad (4.1.42)$$

$$Y(s) = -\cot\alpha\,|X(s)| + \frac{\pi}{4\alpha(\sin\alpha)^{\frac{\pi}{2\alpha}}}|X(s)|^{\frac{\pi}{2\alpha}-1} + o\left(|X(s)|^{\frac{\pi}{2\alpha}-1}\right)$$
$$\text{as } |s| \to \infty; \quad (4.1.43)$$

$$\widehat{\psi}\left(r, \overline{\theta}\right) = -r^{\frac{\pi}{2\alpha}}\cos\frac{\pi}{2\alpha}\left(\overline{\theta} + \frac{1}{2}\pi\right) + o\left(r^{\frac{\pi}{2\alpha}}\right)$$
$$\text{as} \quad r \to \infty,\ -\alpha - \frac{1}{2}\pi < \overline{\theta} < \alpha - \frac{1}{2}\pi; \quad (4.1.44)$$

where $\hat{\mathbf{n}} = \left(-Y'(s), X'(s)\right)$, and $\left(r, \overline{\theta}\right)^2$ are polar coordinates given by $x = r\cos\overline{\theta}$, $y = r\sin\overline{\theta}$. The boundary value problem (4.1.38) - (4.1.44), henceforth referred to as $[RBVP]$, can now be solved numerically using a boundary integral method, which follows

[2]These should not be confused with the outer region polar coordinates used in Chapter 2

directly the approach given in [24], and so further details are not reproduced here.

4.1.1 Numerical Results for $[RBVP]$

Numerical solutions to $[RBVP]$, rotated back so as to be presented in terms of $(\hat{x}, \hat{y})$, are plotted in Figures 4.5 - 4.11. The numerical solution demonstrates that the free surface $\hat{y} = \widehat{\xi}(\hat{x})$ is monotone increasing in $\hat{x} \geqslant \hat{x}_0$, for all angles $\alpha \in \left(\frac{1}{4}\pi, \frac{1}{2}\pi\right)$, with the gradient of the free surface at the contact point $\widehat{\xi}_{\hat{x}}(\hat{x}_0)$ decreasing with increasing $\alpha \in \left(\frac{1}{4}\pi, \frac{1}{2}\pi\right)$, and approaching zero as $\alpha \to \frac{1}{2}\pi$. In Figure 4.5 we demonstrate the good agreement of the numerical solution with the far-field asymptotic form in $[RBVP]$ (4.1.31). In Figure 4.6 we present the free surface $\widehat{\xi}(\hat{x})$ against $\hat{x}$ for the numerical solution of $[RBVP]$, for a selection of angles $\alpha \in \left(\frac{1}{4}\pi, \frac{1}{2}\pi\right)$. Figure 4.8 plots $\left|\widehat{\xi}(\hat{x}_0)\right|$ cosec α, the distance from the origin of the $(\hat{x}, \hat{y})$ coordinate system to the contact point of the free surface and the plate, against $\alpha \in \left(\frac{1}{4}\pi, \frac{1}{2}\pi\right)$, whilst Figure 4.7 shows the numerical approximations to $\hat{x}_0$, $\widehat{\xi}(\hat{x}_0)$, with correspondingly $\tilde{x}_0$ and $\tilde{\eta}_0(\tilde{x}_0)$ shown in Figures 4.9 and 4.10 respectively. In Figure 4.7c $\widehat{\xi}_{\hat{x}}(\hat{x}_0)$ is plotted against $\alpha \in \left(\frac{1}{4}\pi, \frac{1}{2}\pi\right)$. Finally Figure 4.11 shows the behaviour of the free surface $\tilde{\xi}(x) - \tilde{\xi}(0)$ against x, presented in the rotated (x, y) coordinate system, very close to the plate for a typical angle $\alpha = 1.56$.

We see in Figure 4.7b that $\widehat{\xi}(\hat{x}_0)$ has a minimum at $\alpha \approx 1.22$, where $\widehat{\xi}(\hat{x}_0) \approx 0.392$, and that $\widehat{\xi}(\hat{x}_0) \to \frac{1}{2}$ as $\alpha \to \frac{1}{2}\pi^-$, which agrees with the findings of Needham et al [24]. We notice that the free surface meets the plate with a constant angle of $\frac{1}{2}\pi$, for all $\alpha \in \left(\frac{1}{4}\pi, \frac{1}{2}\pi\right)$, a condition which we investigate in detail in §4.1.2. It follows from this that the gradient of the free surface at the contact point must be given by

$$\widehat{\xi}_{\hat{x}}(\hat{x}_0) = \tan\left(\frac{1}{2}\pi - \alpha\right). \tag{4.1.45}$$

In Figure 4.7c we plot the numerical approximation to the gradient of the free surface $\widehat{\xi}_{\hat{x}}(\hat{x}_0)$ at the contact point, against $\alpha \in \left(\frac{1}{4}\pi, \frac{1}{2}\pi\right)$, and compare this with $\tan\left(\frac{1}{2}\pi - \alpha\right)$.

We notice the introduction of some noise into our solutions as $\alpha \to \frac{1}{4}\pi$, this is due to the difficulty in obtaining converging solutions as $\alpha \to \frac{1}{4}\pi$. Finally, as shown in Figure 4.11, the numerical solution indicates that $\widehat{\xi}(\hat{x})$ oscillates very rapidly very close to the contact point $\hat{x} = \hat{x}_0$. The amplitude of the oscillations is very small, decreasing to zero at the contact point, whilst the frequency of the oscillations increases, becoming unbounded as the contact point is approached. This structure is verified in the following section.

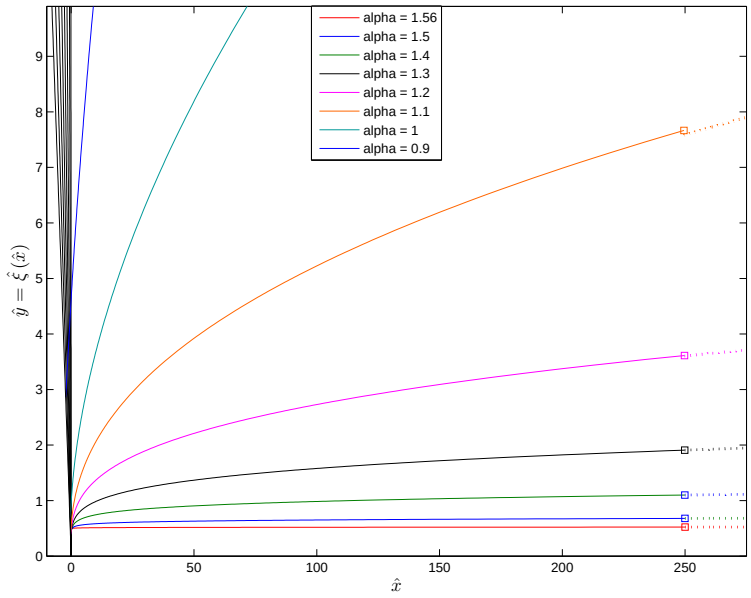

Figure 4.5: Graph of $\widehat{\xi}(\hat{x})$ against $\hat{x}$, showing agreement with the far-field asymptotic form (4.1.31), for the numerical solution of $[RBVP]$ with $\alpha = \left(0.9, \frac{1}{2}\pi\right)$. For each angle a square shows $s = 250$, after which the far-field asymptotic form (4.1.31) is plotted

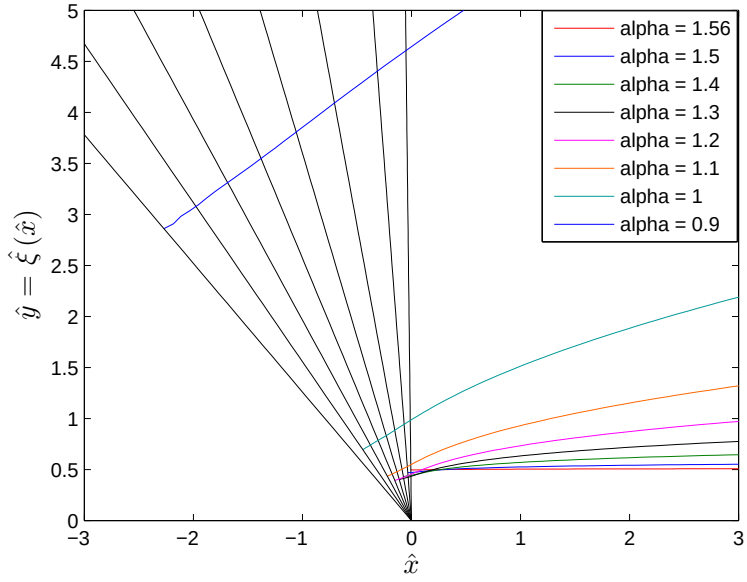

(a) $\alpha \in \left(0.9, \frac{1}{2}\pi\right)$

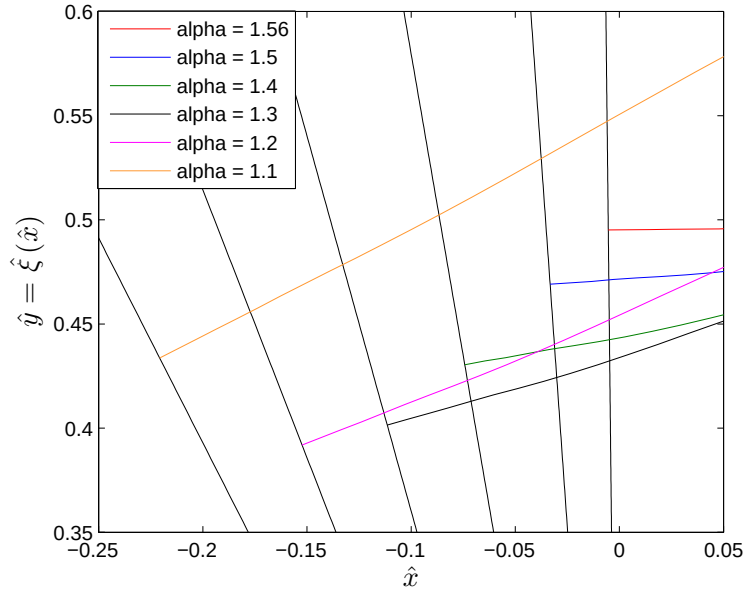

(b) $\alpha > 1.1$

Figure 4.6: Graphs of $\widehat{\xi}(\hat{x})$ against $\hat{x}$ for the numerical solution of $[RBVP]$. Figure 4.6a plots solutions with $\alpha \in \left(0.9, \frac{1}{2}\pi\right)$, while Figure 4.6b plots solutions with $\alpha \in \left(1.1, \frac{1}{2}\pi\right)$ for clarity. For each angle a black line shows the location of the plate

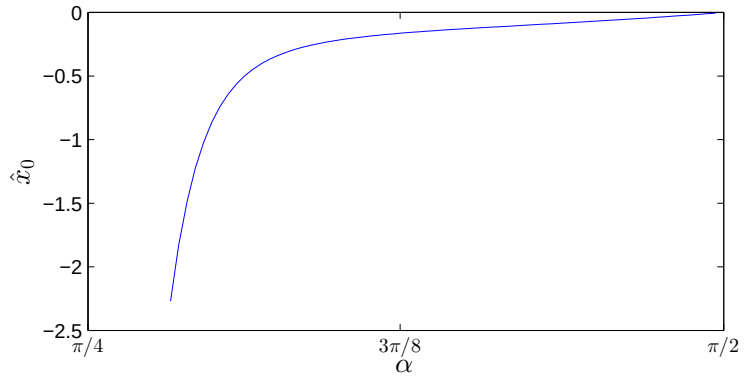

(a) $\hat{x}_0$ against α

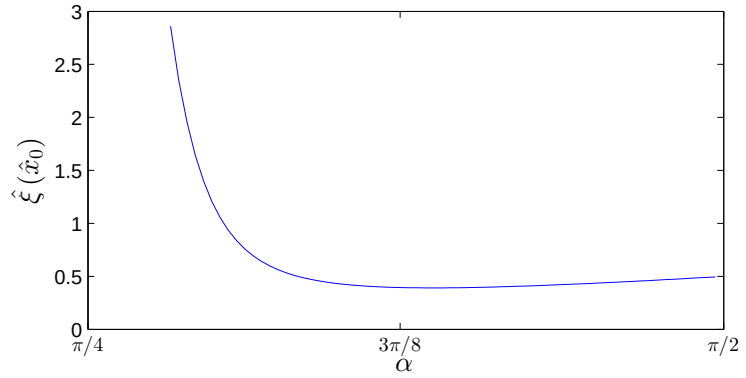

(b) $\widehat{\xi}(\hat{x}_0)$ against α

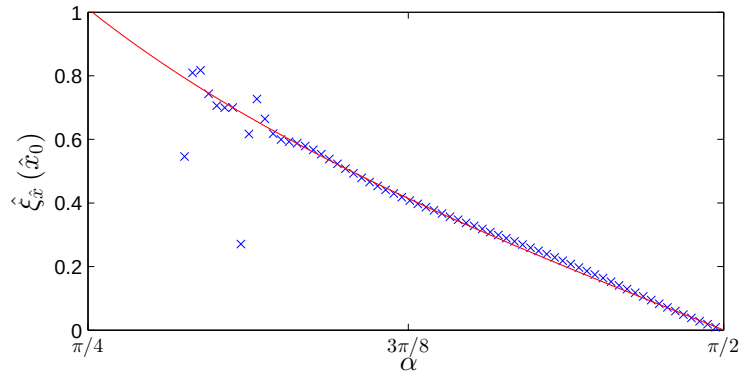

(c) $\widehat{\xi}_{\hat{x}}(\hat{x}_0)$ against α

Figure 4.7: Numerical approximations to $\hat{x}_0(\alpha)$, $\widehat{\xi}(\hat{x}_0(\alpha))$ and $\widehat{\xi}_{\hat{x}}(\hat{x}_0(\alpha))$ for $[RBVP]$ plotted against $\alpha \in \left(\frac{1}{4}\pi, \frac{1}{2}\pi\right)$. In Figure 4.7c the line $\widehat{\xi}_{\hat{x}}(\hat{x}_0(\alpha)) = \tan\left(\frac{1}{2}\pi - \alpha\right)$ is plotted in red

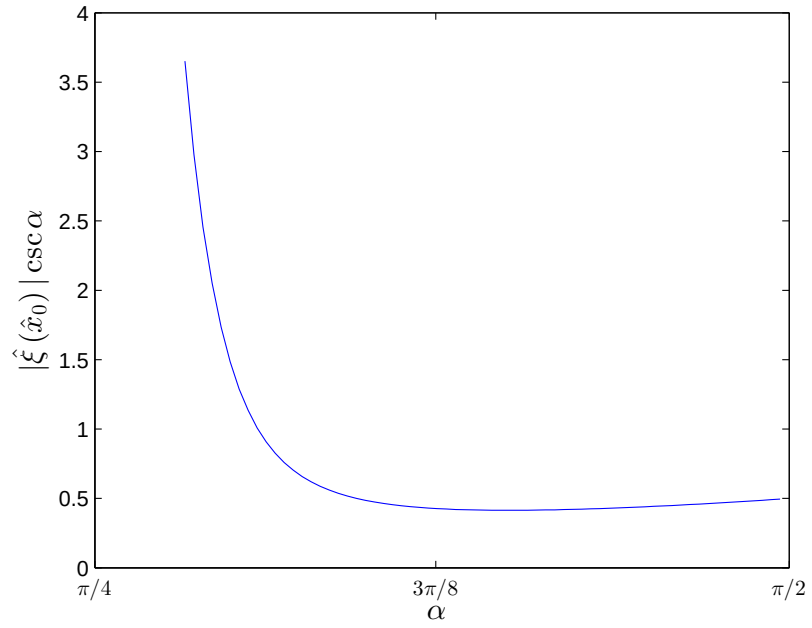

Figure 4.8: Graph showing the distance in the $(\hat{x}, \hat{y})$ coordinate system from the origin of the $(\hat{x}, \hat{y})$ coordinate system to the contact point of the free surface and the plate against $\alpha \in \left(\frac{1}{4}\pi, \frac{1}{2}\pi\right)$, as determined by the numerical solution of $[RBVP]$

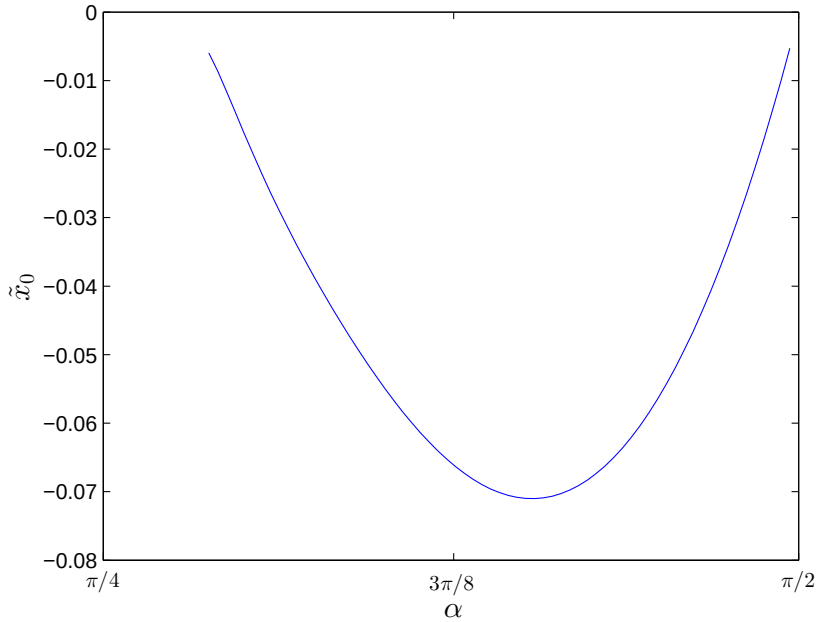

Figure 4.9: Graph of $\tilde{x}_0(\alpha)$ against α calculated numerically

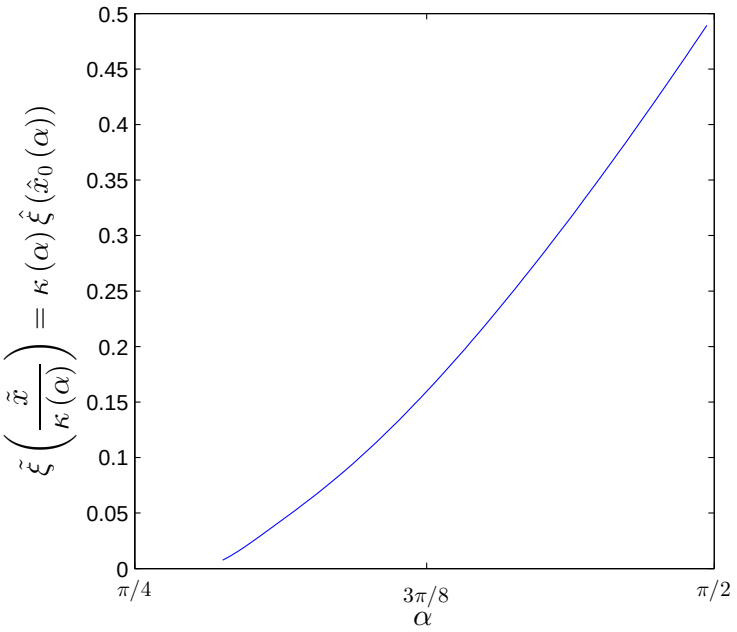

Figure 4.10: Graph of $\tilde{\eta}_0(\tilde{x}_0(\alpha)) = -\tilde{x}_0(\alpha)\tan\alpha$ against α calculated numerically

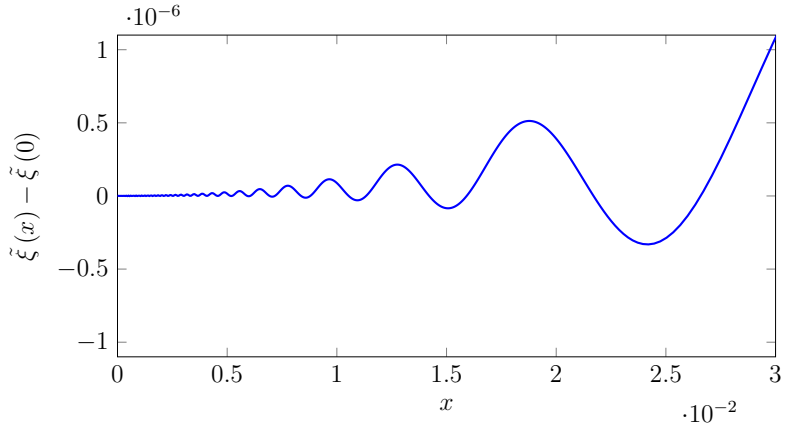

Figure 4.11: Graph of $\tilde{\xi}(x) - \tilde{\xi}(0)$ against x for the numerical solution of $[RBVP]$ close to the plate for a typical angle $\alpha = 1.56$, with coordinates rotated so that the plate is located at $x = 0$

4.1.2 Analysis of $[RBVP]$ as $x \to 0$, Close to the Contact Point of the Free Surface and the Plate

Motivated by the numerical solution in Section 4.1.1, we examine the structure of solutions to $[RBVP]$ close to the contact point of the free surface and the plate, as $(\hat{x}, \hat{y}) \to \left(\hat{x}_0, \widehat{\xi}(\hat{x}_0)\right)$. It is convenient to work in the rotated coordinate system (x, y), and the corresponding limit is then $(x, y) \to \left(0, \tilde{\xi}(0)\right)$. In terms of the rotated coordinates (x, y) $[RBVP]$ is given by

$$\nabla^2 \widehat{\psi} = 0, \qquad x > 0,\ -\infty < y < \tilde{\xi}(x); \tag{4.1.46}$$

$$\widehat{\psi}_x = 0, \qquad x = 0,\ \infty < y < \tilde{\xi}(0); \tag{4.1.47}$$

$$\gamma\tilde{\xi} + \left[\widehat{\psi}_x - \gamma x\right]\tilde{\xi}_x - \widehat{\psi}_y = 0, \qquad x > 0,\ y = \tilde{\xi}(x); \tag{4.1.48}$$

$$(2\gamma - 1)\,\widehat{\psi} - \gamma\left(x\widehat{\psi}_x + \tilde{\xi}\widehat{\psi}_y\right) + \frac{1}{2}\widehat{\psi}_x^2 + \frac{1}{2}\widehat{\psi}_y^2 = 0, \qquad x > 0,\ y = \tilde{\xi}(x). \tag{4.1.49}$$

The free surface in the inner-inner asymptotic region is located at $y = \tilde{\xi}(x)$, $x \geqslant 0$, and the contact point is given by $(x, y) = \left(0, \tilde{\xi}_0\right)$, with $\tilde{\xi}_0 = \tilde{\xi}(0)$. As $(x, y) \to \left(0, \tilde{\xi}_0\right)$, (4.1.46) - (4.1.49) admit the asymptotic forms

$$\tilde{\xi}(x) \sim \tilde{\xi}_0 \qquad \text{as} \quad x \to 0, \tag{4.1.50}$$

$$\widehat{\psi}(x, \overline{y}) \sim \gamma\tilde{\xi}_0^2\left(\frac{(2 - 3\gamma)}{2(2\gamma - 1)} + 1\right) + \gamma\tilde{\xi}_0\overline{y} \qquad \text{as} \quad (x, \overline{y}) \to (0, 0), \tag{4.1.51}$$

where we have written $\overline{y} = y - \tilde{\xi}_0$, and $\tilde{\xi}_0$ remains a globally determined constant, which has been determined by the numerical solution in Section 4.1.1, and is illustrated in Figure 4.12. We observe that $\tilde{\xi}_0 > 0$ for each $\alpha \in \left(\frac{1}{4}\pi, \frac{1}{2}\pi\right)$.

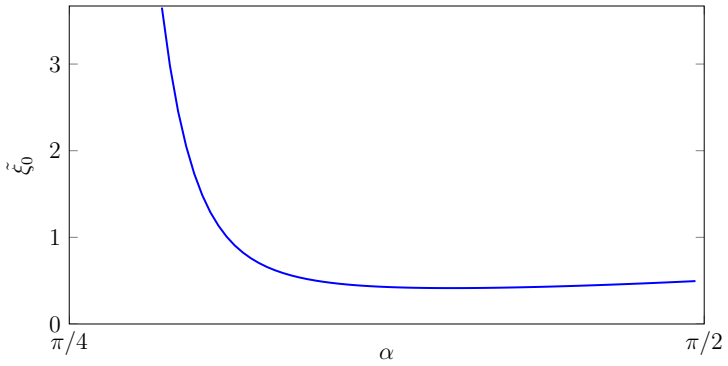

Figure 4.12: Graph of $\tilde{\xi}_0$ for the numerical solution of $[RBVP]$ plotted against $\alpha \in \left(\frac{1}{4}\pi, \frac{1}{2}\pi\right)$

We now consider the correction terms to $\tilde{\xi}(x)$ and $\widehat{\psi}(x,\overline{y})$ as $(x,\overline{y}) \to (0,0)$. We write

$$\tilde{\xi}(x) = \tilde{\xi}_0 + \tilde{\xi}_1(x), \tag{4.1.52}$$

$$\widehat{\psi}(x,\overline{y}) = \gamma\tilde{\xi}_0^2\left(\frac{(2-3\gamma)}{2(2\gamma-1)} + 1\right) + \gamma\tilde{\xi}_0\overline{y} + \widehat{\psi}_2(x,\overline{y}), \tag{4.1.53}$$

with $\tilde{\xi}_1(x) = o(1)$ and $\widehat{\psi}_2(x,\overline{y}) = o(x,\overline{y})$ as $(x,\overline{y}) \to (0,0)$. Substitution of (4.1.52) and (4.1.53) into (4.1.46) - (4.1.49), leads to the linear harmonic problem for $\widehat{\psi}_2(x,\overline{y})$, namely,

$$\overline{\nabla}^2\widehat{\psi}_2 = 0, \qquad x > 0,\ \overline{y} < 0, \tag{4.1.54}$$

$$\widehat{\psi}_{2,x} = 0, \qquad x = 0,\ \overline{y} < 0, \tag{4.1.55}$$

$$(\gamma-1)\tilde{\xi}_0\widehat{\psi}_{2,\overline{y}} + (2\gamma-1)\left[\widehat{\psi}_2 - x\widehat{\psi}_{2,x}\right] + \gamma x^2\widehat{\psi}_{2,xx} = 0, \qquad \overline{y} = 0,\ x > 0, \tag{4.1.56}$$

with $\widehat{\psi}_2(x,\overline{y}) = o(x,\overline{y})$ as $(x,\overline{y}) \to (0,0)$. Thereafter $\tilde{\xi}_1(x)$ is given by

$$\tilde{\xi}_1(x) = -\frac{1}{\gamma(\gamma-1)\tilde{\xi}_0}\left[(2\gamma-1)\widehat{\psi}_2(x,0) - \gamma x\widehat{\psi}_{2,x}(x,0)\right], \qquad x \geqslant 0, \tag{4.1.57}$$

with $\tilde{\xi}_1(x) = o(1)$ as $x \to 0$. To analyse the harmonic problem (4.1.54) - (4.1.56) it is

convenient to introduce the complex variable $z = x + i\overline{y}$, after which we write

$$\widehat{\psi}_2(x, \overline{y}) = Re(f(z)), \qquad z \in \overline{\mathcal{D}}, \tag{4.1.58}$$

with $\mathcal{D}$ being the quadrant $x > 0$, $\overline{y} < 0$, and $f : \overline{\mathcal{D}} \to \mathbb{C}$ being analytic in $\mathcal{D}$ and continuous in $\overline{\mathcal{D}}$, which guarantees that $\widehat{\psi}_2(x, \overline{y})$ is harmonic in $\mathcal{D}$. Condition (4.1.55) then requires that

$$Re(f'(i\overline{y})) = 0, \qquad \overline{y} < 0, \tag{4.1.59}$$

and, condition (4.1.56) is satisfied when,

$$Re\left[\gamma x^2 f''(x) + \left[i(\gamma - 1)\tilde{\xi}_0 - (2\gamma - 1)x\right] f'(x) + (2\gamma - 1) f(x)\right] = 0, \ x > 0, \tag{4.1.60}$$

which is a second order linear ordinary differential equation for $f(x)$ with $x > 0$, and has an irregular singular point at $x = 0$. We require a solution to (4.1.60) with $f(x) = o(1)$ and $f'(x)$ bounded as $x \to 0$. The WKB-type structure (see, for example, [15]) of (4.1.60) as $x \to 0$ leads us to look for a solution in the form

$$f(x) = \exp(g(x)), \qquad x > 0, \tag{4.1.61}$$

with,

$$g(x) = k_0 x^{-1} + k_1 \log x + o(1) \quad \text{as} \quad x \to 0, \tag{4.1.62}$$

with k_0, $k_1 \in \mathbb{C}$ being constants. Substitution of (4.1.61) and (4.1.62), into (4.1.60), gives

$$k_0 = i\left(1 - \frac{1}{\gamma}\right)\tilde{\xi}_0, \qquad k_1 = 4 - \frac{1}{\gamma}. \tag{4.1.63}$$

Thus $f(x)$ satisfies the regularity conditions as $x \to 0$ (since $\gamma > 2$ for $\alpha \in \left(\frac{1}{4}\pi, \frac{1}{2}\pi\right)$). We thus take,

$$f(z) = A \exp\left\{ i \left(1 - \frac{1}{\gamma}\right) \tilde{\xi}_0 \frac{1}{z} + \left(4 - \frac{1}{\gamma}\right) \log z + o(1) \right\}, \quad z \in \overline{\mathcal{D}}, \tag{4.1.64}$$

as $|z| \to 0$ with $A \in \mathbb{C}$ an arbitrary constant. It remains to apply condition (4.1.59). This is satisfied in taking $\arg(A) = \frac{1}{2}\pi\left(4 - \frac{1}{\gamma}\right)$, after which we have

$$f(z) = B \exp\left\{ i \left(1 - \frac{1}{\gamma}\right) \tilde{\xi}_0 \frac{1}{z} + \left(4 - \frac{1}{\gamma}\right) \log z + \frac{1}{2}\pi\left(4 - \frac{1}{\gamma}\right) + o(1) \right\}, \quad z \in \overline{\mathcal{D}} \tag{4.1.65}$$

as $|z| \to 0$, with $B \in \mathbb{R}$ a globally determined constant. Substitution of (4.1.65) into (4.1.58) then gives

$$\begin{aligned} \widehat{\psi}_2\left(\overline{r}, \overline{\theta}\right) \sim B \overline{r}^{4-\frac{1}{\gamma}} \exp\left\{ \left(1 - \frac{1}{\gamma}\right) \tilde{\xi}_0 \overline{r}^{-1} \sin\overline{\theta} \right\} \cos\left[\left(1 - \frac{1}{\gamma}\right) \tilde{\xi}_0 \overline{r}^{-1} \cos\overline{\theta} \right. \\ \left. + \left(4 - \frac{1}{\gamma}\right)\left(\overline{\theta} + \frac{1}{2}\pi\right) \right], \end{aligned} \tag{4.1.66}$$

as $\overline{r} \to 0$, uniformly for $\overline{\theta} \in \left[-\frac{1}{2}\pi, 0\right]$, with $\overline{r} = |z|$ and $\overline{\theta} = \arg(z)$. We observe that $\widehat{\psi}_2\left(\overline{r}, \overline{\theta}\right) = o(1)$ as $\overline{r} \to 0$, uniformly for $\overline{\theta} \in \left[-\frac{1}{2}\pi, 0\right]$, as required (since $\tilde{\xi}_0 > 0$ and $\left(1 - \frac{1}{\gamma}\right) > 0$ for $\alpha \in \left(\frac{1}{4}\pi, \frac{1}{2}\pi\right)$). Also, since $\left(2 - \frac{1}{\gamma}\right) > 0$ for $\alpha \in \left(\frac{1}{4}\pi, \frac{1}{2}\pi\right)$, then $\overline{\nabla}\widehat{\psi}_2\left(\overline{r}, \overline{\theta}\right) \to 0$ as $\overline{r} \to 0$, uniformly for $\overline{\theta} \in \left[-\frac{1}{2}\pi, 0\right]$. Finally, substitution of (4.1.66) into (4.1.57), gives

$$\tilde{\xi}_1(x) \sim B \frac{1}{\gamma} x^{3-\frac{1}{\gamma}} \sin\left[\left(1 - \frac{1}{\gamma}\right) \tilde{\xi}_0 \frac{1}{x} + \frac{1}{2}\pi\left(4 - \frac{1}{\gamma}\right) \right], \tag{4.1.67}$$

as $x \to 0$, and thus

$$\tilde{\xi}_x = \tilde{\xi}_{1,x} \sim -B \frac{(\gamma - 1)}{\gamma^2} \tilde{\xi}_0 x^{1-\frac{1}{\gamma}} \cos\left[\left(1 - \frac{1}{\gamma}\right) \tilde{\xi}_0 \frac{1}{x} + \frac{1}{2}\pi\left(4 - \frac{1}{\gamma}\right) \right], \tag{4.1.68}$$

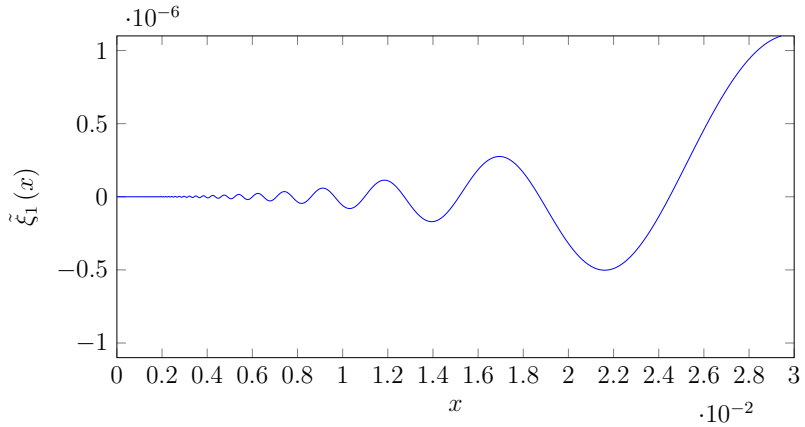

Figure 4.13: The correction term to the free surface $\tilde{\xi}_1(x)$ (4.1.67) plotted against x close to the contact point of the free surface and the plate, with $\alpha = 1.56$ and $B = 0.08$ for comparison with Figure 4.11

as $x \to 0$. We note that, since $\left(1 - \frac{1}{\gamma}\right) > 0$ for $\alpha \in \left(\frac{1}{4}\pi, \frac{1}{2}\pi\right)$, then $\tilde{\xi}_1(x) = o(1)$ and $\tilde{\xi}_{1,x}(x) \to 0$ as $x \to 0$. In particular, we have, via (4.1.68), that $\tilde{\xi}_x(x) \to 0$ as $x \to 0$, and so the contact angle between the free surface and the plate is $\frac{1}{2}\pi$ for all $\alpha \in \left(\frac{1}{4}\pi, \frac{1}{2}\pi\right)$, which is in agreement with the numerically calculated solutions in Figure 4.6. Finally Figure 4.13 plots the free surface correction term $\tilde{\xi}_1(x)$ against x close to the plate, with $\alpha = 1.56$ and $B = 0.08$, for comparison with the numerical solution shown in Figure 4.11. We see very good agreement between the asymptotic form of $\tilde{\xi}_1(x)$ and the numerically calculated form of $\tilde{\xi}(x) - \tilde{\xi}(0)$, confirming the structure of the free surface close to the contact point of the free surface and the plate.

4.1.3 Reconstructing the Inner-Inner Region Asymptotic Expansions

In this section we reconstruct the inner-inner region asymptotic expansions for the fluid velocity potential ϕ, free surface elevation η, dynamic fluid pressure field p_d and fluid velocity field $\mathbf{q}$ in terms of the inner-inner region variables $\tilde{x}, \tilde{y}$, and then consider the behaviour close to the intersection point of the fluid free surface and the inclined accelerating

plate.

It follows from (4.1.7), (4.1.8), (4.1.24) and (4.1.25), that the intersection point of the plate and the fluid free surface is located at $(\tilde{x},\tilde{y})=(\tilde{x}_p(t),\tilde{y}_p(t))$, with

$$\tilde{x}_p(t)=(-A_0(\alpha)\cos\alpha)^{\frac{1}{2}\gamma}\hat{x}_0(\alpha)+o(1), \tag{4.1.69}$$

$$\tilde{y}_p(t)=-(-A_0(\alpha)\cos\alpha)^{\frac{1}{2}\gamma}\tan\alpha\ \hat{x}_0(\alpha)+o(1), \tag{4.1.70}$$

as $t\to 0^+$. We then have, via (4.1.3), (4.1.5), (4.1.24) and (4.1.25), that the free surface in the inner-inner asymptotic region is located at

$$\tilde{y}(\tilde{x},t)=\eta_{II}(\tilde{x},t)=(-A_0(\alpha)\cos\alpha)^{\frac{1}{2}\gamma}\widehat{\xi}\left(\frac{\tilde{x}}{\kappa(\alpha)}\right)+o(1), \tag{4.1.71}$$

for $\tilde{x}\geqslant\tilde{x}_p(t)$, as $t\to 0^+$. We next have, via (4.1.4), (4.1.6), (4.1.24) and (4.1.25), that

$$\phi_{II}(\tilde{x},\tilde{y},t)=(-A_0(\alpha)\cos\alpha)^{\gamma}\widehat{\psi}\left(\frac{\tilde{x}}{\kappa(\alpha)},\frac{\tilde{y}}{\kappa(\alpha)}\right)+o(1), \tag{4.1.72}$$

for $\tilde{x}\geqslant\tilde{x}_p(t)$, $-\tilde{x}\tan\alpha\leqslant\tilde{y}\leqslant\eta_{II}(\tilde{x},t)$ as $t\to 0^+$. An examination of (1.2.28), (3.1.4) and (4.1.4), requires that we write in the inner-inner asymptotic region

$$p_d(\tilde{x},\tilde{y},t)=-\frac{1}{2}t^2+t^{\gamma}\tilde{y}+t^{2\gamma-2}p_{II}(\tilde{x},\tilde{y},t),$$
$$\tilde{x}\geqslant\tilde{x}_p(t),\ -\tilde{x}\tan\alpha\leqslant\tilde{y}\leqslant\eta_{II}(\tilde{x},t),\ t\geqslant 0, \tag{4.1.73}$$

after which we have, via (1.2.28) and (4.1.72), the inner-inner asymptotic expansions for

the dynamic fluid pressure field as,

$$p_{II}(\tilde{x},\tilde{y},t) = (-A_0(\alpha)\cos\alpha)^{\gamma}\left[(1-2\gamma)\,\widehat{\psi}\left(\frac{\tilde{x}}{\kappa(\alpha)},\frac{\tilde{y}}{\kappa(\alpha)}\right)\right.$$
$$+\gamma\left(\tilde{x}\widehat{\psi}_{\tilde{x}}\left(\frac{\tilde{x}}{\kappa(\alpha)},\frac{\tilde{y}}{\kappa(\alpha)}\right)+\tilde{y}\widehat{\psi}_{\tilde{y}}\left(\frac{\tilde{x}}{\kappa(\alpha)},\frac{\tilde{y}}{\kappa(\alpha)}\right)\right)$$
$$\left.-\frac{1}{2}\left(\widehat{\psi}^2_{\tilde{x}}\left(\frac{\tilde{x}}{\kappa(\alpha)},\frac{\tilde{y}}{\kappa(\alpha)}\right)+\widehat{\psi}^2_{\tilde{y}}\left(\frac{\tilde{x}}{\kappa(\alpha)},\frac{\tilde{y}}{\kappa(\alpha)}\right)\right)\right]+o(1), \quad (4.1.74)$$

as $t\to 0^+$, with $\tilde{x}\geqslant\tilde{x}_p(t)$, $-\tilde{x}\tan\alpha\leqslant\tilde{y}\leqslant\eta_{II}(\tilde{x},t)$. Finally, in the inner-inner asymptotic region, the fluid velocity field is given, via (1.2.29), (3.1.4), (4.1.4), and (4.1.72), as,

$$\mathbf{q}(\tilde{x},\tilde{y},t) = -t\mathbf{j}+t^{\gamma-1}(-A_0(\alpha)\cos\alpha)^{\gamma}\left(\widehat{\psi}_{\tilde{x}}\left(\frac{\tilde{x}}{\kappa(\alpha)},\frac{\tilde{y}}{\kappa(\alpha)}\right)\mathbf{i}\right.$$
$$\left.+\widehat{\psi}_{\tilde{y}}\left(\frac{\tilde{x}}{\kappa(\alpha)},\frac{\tilde{y}}{\kappa(\alpha)}\right)\mathbf{j}\right)+o\left(t^{2\gamma-1}\right), \quad (4.1.75)$$

as $t\to 0^+$ with $\tilde{x}\geqslant\tilde{x}_p(t)$, $-\tilde{x}\tan\alpha\leqslant\tilde{y}\leqslant\eta_{II}(\tilde{x},t)$.

We can now draw the following conclusions concerning the free surface, the fluid velocity field, and the dynamic pressure field in the inner-inner asymptotic region:

(a) The contact point is located at

$$(\overline{x},y) = -\frac{1}{2}t^2(-\cot\alpha,1)$$
$$-t^{\gamma}(-A_0(\alpha)\cos\alpha)^{\frac{1}{2}\gamma}\tan\alpha\;\hat{x}_0(\alpha)(-\cot\alpha,1)+o(t^{\gamma}), \quad (4.1.76)$$

as $t\to 0^+$ (see (4.1.2), (4.1.7), (4.1.8), (4.1.24), and (4.1.25)).

(b) The free surface slope at the contact point is given by, following (4.1.45),

$$\begin{aligned}\eta_{\overline{x}}\left(\tilde{x}_p\left(t\right),t\right) &= \eta_{II,\tilde{x}}\left(\tilde{x}_p\left(t\right),t\right),\\ &= \tan\left(\frac{1}{2}\pi-\alpha\right)+o\left(1\right),\end{aligned} \tag{4.1.77}$$

as $t\to 0^+$.

(c) The free surface $\eta\left(\tilde{x},t\right)$ is given by,

$$\eta\left(\tilde{x},t\right) = -\frac{1}{2}t^2+t^{\gamma}\left(-A_0\left(\alpha\right)\cos\alpha\right)^{\frac{1}{2}\gamma}\widehat{\xi}\left(\frac{\tilde{x}}{\kappa\left(\alpha\right)}\right)+o\left(t^{\gamma}\right), \tag{4.1.78}$$

as $t\to 0^+$ for $\tilde{x}\geqslant\tilde{x}_p\left(t\right)$ (see (3.1.3), (4.1.3), and (4.1.71)). It follows from (4.1.78) that $\eta\left(\tilde{x},t\right)$ is monotone increasing in $\tilde{x}\geqslant\tilde{x}_p\left(t\right)$ for all $\alpha\in\left(\frac{1}{4}\pi,\frac{1}{2}\pi\right)$.

(d) The fluid velocity field at the contact point $\mathbf{q}\left(\tilde{x}_p\left(t\right),\tilde{y}_p\left(t\right),t\right)$ is given by,

$$\begin{aligned}\mathbf{q}\left(\tilde{x}_p\left(t\right),\tilde{y}_p\left(t\right),t\right) &= \nabla\phi\left(\tilde{x}_p\left(t\right),\tilde{y}_p\left(t\right),t\right),\\ &= -t\mathbf{j}+t^{\gamma-1}\left(-A_0\left(\alpha\right)\cos\alpha\right)^{\frac{1}{2}\gamma}\Big(\widehat{\psi}_{\tilde{x}}\left(\hat{x}_0\left(\alpha\right),-\hat{x}_0\left(\alpha\right)\tan\alpha\right)\mathbf{i}\\ &\quad+\widehat{\psi}_{\tilde{y}}\left(\hat{x}_0\left(\alpha\right),-\hat{x}_0\left(\alpha\right)\tan\alpha\right)\mathbf{j}\Big)+o\left(t^{\gamma-1}\right),\end{aligned} \tag{4.1.79}$$

as $t\to 0^+$ (see (3.1.4), (4.1.4), (4.1.69), (4.1.70), and (4.1.72)).

4.2 Discussion

At this stage we have completed the asymptotic structure to $[IBVP]$ as $t\to 0^+$ for each pair $(\alpha,\mu)\in\left(0,\frac{1}{2}\pi\right)\times\mathbb{R}$, where $\mu=1+\sigma\tan\alpha$. We began in an *outer asymptotic region* in which $(\overline{x},y)=O\left(1\right)$ as $t\to 0^+$. As discussed in Chapter 2 the leading order terms in the outer region asymptotic expansions for ϕ and η satisfy the required regularity *except* in a neighbourhood of the initial location of the intersection point of the free surface

and the plate, at $(\overline{x}, y) = (0, 0) \in \overline{\mathcal{D}}(0)$. In order to capture the full regularity in the neighbourhood of the intersection point of the plate and the free surface we introduced an *inner asymptotic region* in which $(\overline{x}, y) = O(t^2)$ as $t \to 0^+$. The structure of the solution to $[IBVP]$ in the inner asymptotic region is as follows:

(a) $\underline{(\alpha, \mu) \in \left(0, \frac{1}{2}\pi\right) \times (0, \infty)}$

In the inner asymptotic region we have solved $[PBVP]^+$ numerically for each pair $(\alpha, \mu) \in \left(0, \frac{1}{2}\pi\right) \times (0, \infty)$. As discussed in Section 3.7.1 we have drawn the following conclusions concerning the free surface, fluid velocity field, and dynamic pressure field in the inner asymptotic region:

(i) The contact point is located at

$$(\overline{x}, y) = \frac{1}{2} t^2 (\mu - 1)(-\cot\alpha, 1) + O\left(t^{\frac{\pi}{\alpha}}\right), \tag{4.2.1}$$

as $t \to 0^+$.

(ii) The free surface slope at the contact point is given by,

$$\eta_{\overline{x}}\left(\overline{X}_p(t), t\right) = t^{\frac{\pi}{\alpha}-2} \frac{\pi}{\alpha} \left(1 - \frac{\pi^2}{\alpha^2}\right) A_0(\alpha)\, a_0(\alpha)\, (\mu - 1) \cot\alpha \;\cos\alpha\; \mu^{\frac{\pi}{2\alpha}-2} + o\left(t^{\frac{\pi}{\alpha}-2}\right), \tag{4.2.2}$$

as $t \to 0^+$, with $A_0(\alpha)$ given in (2.0.15) and plotted in Figure 2.3, and $a_0(\alpha)$ plotted in Figure 3.13. We see that the slope of the free surface is positive for those pairs $(\alpha, \mu) \in \left(0, \frac{1}{2}\pi\right) \times (0, 1)$, and negative when $(\alpha, \mu) \in \left(0, \frac{1}{2}\pi\right) \times (1, \infty)$.

(iii) The free surface $\eta\left(\overline{X}, t\right)$ is given by

$$\eta\left(\overline{X}, t\right) = \frac{1}{2} t^2 (\mu - 1) + t^{\frac{\pi}{\alpha}} A_0(\alpha)\, (\mu - 1)\, \mu^{\frac{\pi}{2\alpha}-1} \cos\alpha\; \xi_\alpha^+\left(\frac{\overline{X}}{\mu}\right) + o\left(t^{\frac{\pi}{\alpha}}\right), \tag{4.2.3}$$

as $t \to 0^+$ for $\overline{X} \geqslant \overline{X}_p(t)$, with

$$\overline{X}_p(t) = t^{\frac{\pi}{\alpha}-2}\left(1+\frac{\pi}{\alpha}\right) A_0(\alpha)\, a_0(\alpha)\,(\mu-1)\cot\alpha\cos\alpha\ \mu^{\frac{\pi}{2\alpha}-1} + o\left(t^{\frac{\pi}{\alpha}-2}\right). \tag{4.2.4}$$

Numerical solution of $[PBVP]^+$, after which we obtain ξ_α^+, indicates that $\eta\left(\overline{X},t\right)$ is monotone increasing in $\overline{X} \geqslant \overline{X}_p(t)$ when $(\alpha,\mu) \in \left(0,\frac{1}{2}\pi\right)\times(0,1)$, and is monotone decreasing in $\overline{X} \geqslant \overline{X}_p(t)$ when $(\alpha,\mu) \in \left(0,\frac{1}{2}\pi\right)\times(1,\infty)$.

(iv) The fluid velocity field at the contact point $\mathbf{q}\left(\overline{X}_p(t),\overline{Y}_p(t),t\right)$ is given by

$$\begin{aligned}\mathbf{q}\left(\overline{X}_p(t),\overline{Y}_p(t),t\right) = {} & t(\mu-1)\,\mathbf{j} \\ & + t^{\frac{\pi}{\alpha}-1}\frac{\pi}{\alpha}\left(1+\frac{\pi}{\alpha}\right) A_0(\alpha)\, a_0(\alpha)\,(\mu \\ & -1)\cos\alpha\ \mu^{\frac{\pi}{2\alpha}-1}(\cot\alpha\ \mathbf{i}\ -\mathbf{j}) + o\left(t^{\frac{\pi}{\alpha}-1}\right),\end{aligned} \tag{4.2.5}$$

as $t \to 0^+$ in the inner asymptotic region.

When $\mu > 1$ the acceleration of the inclined plate, to leading order in the inner asymptotic region, induces a positive constant dynamic pressure gradient of $t^2(\mu-1)\,\mathbf{j}$, which drives a jet close to the intersection point of the free surface and the plate, and directed up the plate, of height $\frac{1}{2}t^2(\mu-1)$. When $0 < \mu < 1$, to leading order in the inner asymptotic region, the acceleration of the inclined plate induces a constant negative dynamic pressure gradient of $t^2(\mu-1)\,\mathbf{j}$, which causes the free surface, close to the intersection point of the free surface and the plate, to collapse down the plate to a height of $\frac{1}{2}t^2(\mu-1)$.

(b) $\underline{(\alpha,\mu) \in \left\{\left(0,\frac{1}{2}\pi\right) \setminus \{\alpha_n^* : n = 1,2,\dots\}\right\} \times (-\infty,0)}$

In the inner asymptotic region we have solved $[PBVP]^-$ numerically for each pair $(\alpha,\mu) \in \left\{\left(0,\frac{1}{2}\pi\right) \setminus \{\alpha_n^* : n = 1,2,\dots\}\right\} \times (-\infty,0)$. Pairs of near resonances occur in a small neighbourhood of $\alpha = \alpha_n^*$ $(n = 1,2,\dots)$. Away from the near resonance pairs, we draw the following conclusions regarding the free surface, fluid velocity field, and dynamic pressure field in the inner asymptotic region, namely:

(i) The contact point is located at

$$(\overline{x}, y) = \frac{1}{2}t^2\,(\mu - 1)\,(-\cot\alpha, 1) + O\left(t^{\frac{\pi}{\alpha}}\right), \tag{4.2.6}$$

as $t \to 0^+$.

(ii) The free surface slope at the contact point is given by,

$$\eta_{\overline{x}}\left(\overline{X}_p(t), t\right) = t^{\frac{\pi}{\alpha}-2}\frac{\pi}{\alpha}\left(1 - \frac{\pi^2}{\alpha^2}\right) A_0(\alpha)\, a_0(\alpha)\,(\mu - 1)\cot\alpha\ \cos\alpha\ \mu^{\frac{\pi}{2\alpha}-2} + o\left(t^{\frac{\pi}{\alpha}-2}\right), \tag{4.2.7}$$

as $t \to 0^+$, with $A_0(\alpha)$ given in (2.0.15) and plotted in Figure 2.3, and $a_0(\alpha)$ plotted in Figure 3.28. The slope of the free surface at the contact point is *positive* for those pairs $(\alpha,\mu) \in \left(\alpha_{2n}^*, \alpha_{2n-1}^*\right) \times (-\infty,0)$ $(n = 1,2,\dots)$, and *negative* when $(\alpha,\mu) \in \left(\alpha_{2n+1}^*, \alpha_{2n}^*\right) \times (-\infty,0)$ $(n = 1,2,\dots)$ and $(\alpha,\mu) \in \left(\alpha_1^*, \frac{1}{2}\pi\right) \times (-\infty,0)$.

(iii) The free surface $\eta\left(\overline{X},t\right)$ is given by

$$\eta\left(\overline{X},t\right)=t^{2}\frac{1}{2}\left(\mu-1\right)+t^{\frac{\pi}{\alpha}}A_{0}\left(\alpha\right)\left(\mu-1\right)\cos\alpha\left(-\mu\right)^{\frac{\pi}{2\alpha}-1}\xi_{\alpha}^{-}\left(\frac{\overline{X}}{(-\mu)}\right)+o\left(t^{\frac{\pi}{\alpha}}\right), \tag{4.2.8}$$

as $t\rightarrow0^{+}$, for $\overline{X}\geqslant\overline{X}_{p}\left(t\right)$, with

$$\overline{X}_{p}\left(t\right)=-t^{\frac{\pi}{\alpha}-2}\left(1+\frac{\pi}{\alpha}\right)A_{0}\left(\alpha\right)a_{0}\left(\alpha\right)\left(\mu-1\right)\cot\alpha\cos\alpha\left(-\mu\right)^{\frac{\pi}{2\alpha}-1}+o\left(t^{\frac{\pi}{\alpha}-2}\right). \tag{4.2.9}$$

Numerical solution of $[PBVP]^{-}$, after which ξ_{α}^{-} is obtained via (3.2.3), shows that η is initially decreasing with a single turning point for those pairs $(\alpha,\mu)\in\left(\alpha_{1}^{*},\frac{1}{2}\pi\right)\times(-\infty,0)$. For those pairs $(\alpha,\mu)\in(\alpha_{c}^{*},\alpha_{1}^{*})\times(-\infty,0)$, η is initially increasing with two turning points. For those pairs $(\alpha,\mu)\in(\alpha_{2}^{*},\alpha_{c}^{*}]\times(-\infty,0)$, η is monotone increasing. For those pairs $(\alpha,\mu)\in\left(\alpha_{2n+1}^{*},\alpha_{2n}^{*}\right)\times(-\infty,0)$ $(n=1,2,\dots)$ η is initially decreasing with $(2n-1)$ turning points. Finally, for those pairs $(\alpha,\mu)\in\left(\alpha_{2n}^{*},\alpha_{2n-1}^{*}\right)\times(-\infty,0)$ $(n=1,2,\dots)$ η is initially increasing with $(2n-2)$ turning points.

(iv) The fluid velocity field at the contact point $\mathbf{q}\left(\overline{X}_{p}\left(t\right),\overline{Y}_{p}\left(t\right),t\right)$ is given by

$$\mathbf{q}\left(\overline{X}_{p}\left(t\right),\overline{Y}_{p}\left(t\right),t\right)=t\left(\mu-1\right)\mathbf{j}+t^{\frac{\pi}{\alpha}-1}\frac{\pi}{\alpha}\left(1+\frac{\pi}{\alpha}\right)A_{0}\left(\alpha\right)a_{0}\left(\alpha\right)\left(\mu-1\right)\cos\alpha\left(-\mu\right)^{\frac{\pi}{2\alpha}-1}\left(\cot\alpha\ \mathbf{i}\ -\mathbf{j}\right)+o\left(t^{\frac{\pi}{\alpha}-1}\right), \tag{4.2.10}$$

as $t\rightarrow0^{+}$ in the inner asymptotic region.

Finally, for pairs $(\alpha,\mu)\in\left\{\left(0,\frac{1}{2}\pi\right)\setminus\left\{\alpha_{n}^{*}:n=1,2,\dots\right\}\right\}\times(-\infty,0)$, we see that, to leading order in the inner asymptotic region, the acceleration of the inclined plate induces a constant negative dynamic pressure gradient of $t^{2}\left(\mu-1\right)\mathbf{j}$, which, close

to the intersection point of the free surface and the plate, causes the free surface to collapse to a height of $\frac{1}{2}t^2(\mu-1)$.

(c) $\underline{(\alpha,\mu)\in\{\alpha_n^*:n=1,2,\dots\}\times(-\infty,0)}$

Here, in the inner asymptotic region, $[PBVP]^-$ has a stationary point at the intersection point of the free surface and the inclined accelerating plate. Each angle $\alpha=\alpha_n^*$ $(n=1,2,\dots)$ separates the two near resonances in each near resonance pair. At these near resonance pairs, we draw the following conclusions regarding the free surface, fluid velocity field, and dynamic pressure field in the inner asymptotic region, namely:

(i) The contact point is located at

$$(\overline{x},y)=\frac{1}{2}t^2(\mu-1)(-\cot\alpha_n^*,1)+o\left(t^{\frac{\pi}{\alpha_n^*}}\right), \tag{4.2.11}$$

as $t\to 0^+$.

(ii) The free surface slope at the contact point is given by,

$$\eta_{\overline{x}}\left(\overline{X}_p(t),t\right)=o\left(t^{\frac{\pi}{\alpha_n^*}-2}\right), \tag{4.2.12}$$

as $t\to 0^+$.

(iii) The free surface $\eta\left(\overline{X},t\right)$ is given by

$$\eta\left(\overline{X},t\right)=t^2\frac{1}{2}(\mu-1)+t^{\frac{\pi}{\alpha_n^*}}A_0(\alpha_n^*)(\mu-1)\cos\alpha_n^*(-\mu)^{\frac{\pi}{2\alpha_n^*}-1}\xi_{\alpha_n^*}^-\left(\frac{\overline{X}}{(-\mu)}\right)+o\left(t^{\frac{\pi}{\alpha_n^*}}\right), \tag{4.2.13}$$

as $t\to 0^+$ for $\overline{X}\geqslant\overline{X}_p(t)$, with $\overline{X}_p(t)=o\left(t^{\frac{\pi}{\alpha_n^*}-2}\right)$, and $A_0(\alpha_n^*)$ given in (2.0.15) and plotted in Figure 2.3.

(iv) The fluid velocity field at the contact point $\mathbf{q}\left(\overline{X}_p(t), \overline{Y}_p(t), t\right)$ is given by

$$\mathbf{q}\left(\overline{X}_p(t), \overline{Y}_p(t), t\right) = t(\mu - 1)\mathbf{j} + o\left(t^{\frac{\pi}{\alpha_n^*}-1}\right), \tag{4.2.14}$$

as $t \to 0^+$.

Finally, to leading order in the inner asymptotic region, we have that the acceleration of the inclined plate induces a constant negative dynamic pressure gradient of $t^2(\mu - 1)\mathbf{j}$, which causes the free surface, close to the intersection point of the free surface and the plate, to collapse to a height of $\frac{1}{2}t^2(\mu - 1)$.

(d) $\underline{(\alpha, \mu) \in \left(\frac{1}{4}\pi, \frac{1}{2}\pi\right) \times \{0\}}$

In this degenerate case, the solution to the boundary value problem (3.1.29) - (3.1.34) in the inner asymptotic region which has least singular behaviour at the contact point $\left(\overline{X}, \overline{Y}\right) = (0, 0)$ is simply given by the far-field forms. This requires the introduction of an *inner-inner asymptotic region*, in which $\left(\overline{X}, \overline{Y}\right) = o\left(t^{\Gamma}\right)$, with $\Gamma = \frac{\left(\frac{\pi}{\alpha}-2\right)}{2\left(1-\frac{\pi}{4\alpha}\right)}$ as $t \to 0^+$, in order to capture the full regularity at the contact point.

From Section 4.1 we are able to draw the following conclusions regarding the free surface, fluid velocity field, and dynamic pressure field in the inner-inner asymptotic region, namely:

(i) The contact point is located at

$$\begin{aligned}(\overline{x}, y) = &-\frac{1}{2}t^2(-\cot\alpha, 1) \\ &- t^{\gamma}\left(-A_0(\alpha)\cos\alpha\right)^{\frac{1}{2}\gamma}\tan\alpha\ \hat{x}_0(\alpha)(-\cot\alpha, 1) + o\left(t^{\gamma}\right),\end{aligned} \tag{4.2.15}$$

as $t \to 0^+$, with $\gamma = \Gamma + 2 = \frac{1}{1-\frac{\pi}{4\alpha}}$, $A_0(\alpha)$ given in (2.0.15) and plotted in Figure 2.3, and $\hat{x}_0(\alpha)$ plotted in Figure 4.7a.

(ii) The free surface slope at the contact point is given by

$$\eta_{\overline{x}}\left(\tilde{x}_p\left(t\right),t\right)=\tan\left(\frac{1}{2}\pi-\alpha\right)+o\left(1\right), \tag{4.2.16}$$

as $t\to 0^+$.

(iii) The free surface $\eta\left(\tilde{x},t\right)$ is given by

$$\eta\left(\tilde{x},t\right)=-\frac{1}{2}t^2+t^{\gamma}\left(-A_0\left(\alpha\right)\cos\alpha\right)^{\frac{1}{2}\gamma}\widehat{\xi}\left(\frac{\tilde{x}}{\kappa\left(\alpha\right)}\right)+o\left(t^{\gamma}\right), \tag{4.2.17}$$

as $t\to 0^+$ in $\tilde{x}\geqslant\tilde{x}_p\left(t\right)$, where $\tilde{x}_p\left(t\right)=\kappa\hat{x}_o\left(\alpha\right)+o\left(1\right)$, with $\kappa\left(\alpha\right)=\left(-A_0\left(\alpha\right)\cos\alpha\right)^{\frac{1}{2}\gamma}$ plotted in Figure 4.3.

(iv) The fluid velocity field at the contact point $\mathbf{q}\left(\tilde{x}_p\left(t\right),\tilde{y}_p\left(t\right),t\right)$ is given by

$$\begin{aligned}\mathbf{q}\left(\tilde{x}_p\left(t\right),\tilde{y}_p\left(t\right),t\right)=-t\mathbf{j}+t^{\gamma-1}\left(-A_0\left(\alpha\right)\cos\alpha\right)^{\frac{1}{2}\gamma}\Big(&\widehat{\psi}_{\tilde{x}}\left(\hat{x}_0\left(\alpha\right),-\hat{x}_0\left(\alpha\right)\tan\alpha\right)\mathbf{i}\\&+\widehat{\psi}_{\tilde{y}}\left(\hat{x}_0\left(\alpha\right),-\hat{x}_0\left(\alpha\right)\tan\alpha\right)\mathbf{j}\Big)+o\left(t^{\gamma-1}\right),\end{aligned} \tag{4.2.18}$$

as $t\to 0^+$.

Finally, we see that the acceleration of the inclined plate induces a constant negative dynamic pressure gradient of $-t^{\gamma}\mathbf{j}$, which causes the free surface, close to the intersection point of the free surface and the plate, to collapse to a height of $-\frac{1}{2}t^2$.

(e) $\underline{(\alpha,\mu)\in\left(0,\frac{1}{4}\pi\right]\times\{0\}}$

In this degenerate case, the solution to the boundary value problem (3.1.29) - (3.1.34) in the inner asymptotic region is simply given by the far-field forms, which remain uniform up to the contact point of the free surface and the inclined accelerating plate. Here, we draw the following conclusions concerning the free surface, fluid velocity field, and the dynamic pressure field in the inner asymptotic region:

(i) The contact point is located at

$$(\overline{x}, y) = -\frac{1}{2}t^2\left(-\cot\alpha, 1\right) + o\left(t^{\frac{\pi}{\alpha}}\right), \tag{4.2.19}$$

as $t \to 0^+$.

(ii) The free surface slope at the contact point is given by

$$\eta_{\overline{x}}\left(\overline{X}_p(t), t\right) = \begin{cases} o\left(t^{\frac{\pi}{\alpha}-2}\right), & 0 < \alpha < \frac{1}{4}\pi, \\ -\frac{A_0\left(\frac{1}{4}\pi\right)}{\sqrt{2}}t^2 + o\left(t^2\right), & \alpha = \frac{1}{4}\pi, \end{cases} \tag{4.2.20}$$

as $t \to 0^+$, with $A_0(\alpha)$ given in (2.0.15) and plotted in Figure 2.3.

(iii) The free surface $\eta\left(\overline{X}, t\right)$ is given by

$$\eta\left(\overline{X}, t\right) = -\frac{1}{2}t^2 - t^{\frac{\pi}{\alpha}}A_0(\alpha)\cos\alpha\ \frac{\pi}{4\alpha}\overline{X}^{\frac{\pi}{2\alpha}-1} + o\left(t^{\frac{\pi}{\alpha}}\right), \tag{4.2.21}$$

as $t \to 0^+$ for $\overline{X} \geqslant \overline{X}_p(t)$, with $\overline{X}_p(t) = o\left(t^{\frac{\pi}{\alpha}-2}\right)$.

(iv) The fluid velocity field at the contact point $\mathbf{q}\left(\overline{X}_p(t), \overline{Y}_p(t), t\right)$ is given by

$$\mathbf{q}\left(\overline{X}_p(t), \overline{Y}_p(t), t\right) = -t\mathbf{j} + o\left(t^{\frac{\pi}{\alpha}-1}\right), \tag{4.2.22}$$

as $t \to 0^+$.

Finally, we see that the acceleration of the inclined plate induces a constant negative dynamic pressure gradient of $-t^2\mathbf{j}$, which causes the free surface, close to the intersection point of the free surface and the plate, to collapse to a height of $-\frac{1}{2}t^2$.

The delicate structure in the inner region, *particularly when* $\mu \leqslant 0$, leads us to ask the following two related questions:

(I) Is the problem $[IBVP]$ well-posed with respect to perturbations in initial data in the inner asymptotic region?

and, when the answer to question $[I]$ is positive,

(II) Is the problem $[IBVP]$ stable with respect to perturbations in initial data in the inner asymptotic region?

We consider these two questions in detail in the next Chapter.

Chapter 5

Well-Posedness and Stability of Problem $[IBVP]$

To analyse the well-posedness and stability of the problem $[IBVP]$ with respect to perturbations in initial data in the innermost asymptotic region, we introduce a perturbation to the trivial initial data in $[IBVP]$ in the following form, adjusting the initial conditions in $[IBVP]$ to

$$\phi(\overline{x}, y, 0) = 0, \qquad \overline{x} > 0, \ -\overline{x}\tan\alpha < y < \eta(\overline{x}, 0), \tag{5.0.1}$$

$$\eta(\overline{x}, 0) = \delta\eta_0\left(\frac{\overline{x}}{\delta^r}\right), \qquad \overline{x} > 0, \tag{5.0.2}$$

with $0 < \delta \ll 1$ and

$$\eta_0(\lambda) = \begin{cases} \overline{\eta}_0(\lambda), & 0 \leqslant \lambda \leqslant 1, \\ 0, & \lambda > 1, \end{cases} \tag{5.0.3}$$

where $\overline{\eta}_0(1)$, $\overline{\eta}_0'(1) = 0$, and $\overline{\eta}_0$ continuous with continuous derivatives. We wish to consider the interaction of the initial perturbation in the free surface with the structure of $[IBVP]$ in the innermost region as $t \to 0^+$, and $r > 0$ will be chosen to achieve this. The problem $[IBVP]$ will be referred to as well-posed when the solution to the perturbed prob-

lem approaches the solution to $[IBVP]$ as $\delta \to 0$, uniformly on $\mathcal{S}_T = \bigcup_{t\in[0,T]} \overline{\mathcal{D}}(t) \times \{t\}$, for each $T > 0$. In addition, when $[IBVP]$ is well-posed, we refer to $[IBVP]$ as stable when the solution to the perturbed problem approaches the solution to $[IBVP]$ as $t \to \infty$, uniformly in $\overline{\mathcal{D}}(t)$; otherwise $[IBVP]$ is said to be unstable.

5.1 The Case $\left((\alpha,\mu) \in \left(0, \frac{1}{2}\pi\right) \times \mathbb{R}\right) \setminus \left(\left(\frac{1}{4}\pi, \frac{1}{2}\pi\right) \times \{0\}\right)$

Following an examination of (3.1.1) along with (3.1.3), (3.1.5), and (3.1.23), we require $t^{\frac{\pi}{\alpha}} \sim \delta$ and $t^2 \sim \delta^r$, which, as $\delta \to 0$, requires

$$t = O\left(\delta^{\frac{\alpha}{\pi}}\right), \tag{5.1.1}$$

with

$$r = \frac{2\alpha}{\pi}. \tag{5.1.2}$$

In what follows, we will refer to the initially perturbed modification of $[IBVP]$ (equations (1.2.17) - (1.2.26)) as $[IBVP]'$, and we will address $[IBVP]'$ as $\delta \to 0$ with $t = O\left(\delta^{\frac{\alpha}{\pi}}\right)$. Thus we write

$$t = \delta^{\frac{\alpha}{\pi}}\tau, \tag{5.1.3}$$

with $\tau = O(1)$ as $\delta \to 0$. We can now write $[IBVP]'$ in terms of $\overline{x}$, y, ϕ, η, τ and δ, which becomes,

$$\nabla^2\phi = 0, \qquad (\overline{x}, y) \in \mathcal{D}(\tau),\ \tau > 0; \tag{5.1.4}$$

$$\nabla\phi \cdot \hat{\mathbf{n}} = \delta^{\frac{\alpha}{\pi}}\tau(\mu - 1)\cos\alpha, \qquad y = -\overline{x}\tan\alpha,\ \overline{x}_p(\tau) < \overline{x} < \overline{x}_b,\ \tau > 0; \tag{5.1.5}$$

$$\phi_y = 0, \qquad y = -1,\ \overline{x} > \overline{x}_b,\ \tau > 0; \tag{5.1.6}$$

$$\eta_\tau + \left[\delta^{\frac{\alpha}{\pi}}\phi_{\overline{x}} - \delta^{\frac{2\alpha}{\pi}}\tau(\mu - 1)\cot\alpha\right]\eta_{\overline{x}} - \delta^{\frac{\alpha}{\pi}}\phi_y = 0,$$
$$y = \eta(\overline{x}, \tau),\ \overline{x} > \overline{x}_p(\tau),\ \tau > 0; \tag{5.1.7}$$

$$\phi_\tau - \delta^{\frac{2\alpha}{\pi}} \tau \left(\mu - 1\right) \cot\alpha \; \phi_{\overline{x}} + \delta^{\frac{\alpha}{\pi}} \frac{1}{2} \left|\nabla\phi\right|^2 + \delta^{\frac{\alpha}{\pi}} \eta = 0,$$

$$y = \eta\left(\overline{x}, \tau\right), \; \overline{x} > \overline{x}_p\left(\tau\right), \; \tau > 0; \tag{5.1.8}$$

$$\eta + \overline{x}_p\left(\tau\right) \tan\alpha = 0, \qquad \overline{x} = \overline{x}_p\left(\tau\right), \; \tau > 0; \tag{5.1.9}$$

$$\eta \to 0, \qquad \text{as} \quad \overline{x} \to \infty, \; \tau > 0; \tag{5.1.10}$$

$$\left|\nabla\phi\right| \to 0, \qquad \text{as} \quad \overline{x} \to \infty, \text{ uniformly for } -1 \leqslant y \leqslant \eta\left(\overline{x}, \tau\right), \; \tau > 0; \tag{5.1.11}$$

$$\phi\left(\overline{x}, y, 0\right) = 0, \qquad \left(\overline{x}, y\right) \in \overline{\mathcal{D}}\left(0\right); \tag{5.1.12}$$

$$\eta\left(\overline{x}, 0\right) = \delta\eta_0\left(\delta^{-\frac{2\alpha}{\pi}} \overline{x}\right), \qquad \overline{x} \geqslant 0; \tag{5.1.13}$$

with $\eta_0 : \mathbb{R} \to \mathbb{R}$ as given by (5.0.3).

The structure of the solution to $[IBVP]$ as $t \to 0^+$ indicates that there will be two asymptotic regions in the solution to $[IBVP]'$ as $\delta \to 0$ with $\tau = O\left(1\right)$. In the outer asymptotic region we have $\left(\overline{x}, y\right) \in \overline{\mathcal{D}}\left(\tau\right) = O\left(1\right)$ as $\delta \to 0$ with $\tau = O\left(1\right)$, and we consider this first.

5.1.1 Outer Asymptotic Region

In this section we begin the asymptotic development of the solution to $[IBVP]'$, as $\delta \to 0$ with $\tau = O\left(1\right)$, in an *outer asymptotic region* in which $\left(\overline{x}, y\right) \in \overline{\mathcal{D}}\left(\tau\right) \backslash \mathcal{N}\left(\tau\right)$ as $\delta \to 0$, with $\mathcal{N}\left(\tau\right)$ being a $O\left(\nu\left(\delta\right)\right)$ neighbourhood of $\left(\overline{x}, y\right) = \left(0, 0\right)$, such that $\nu\left(\delta\right) = o\left(1\right)$ as $\delta \to 0$. Here the gauge function $\nu\left(\delta\right)$ will be determined in the course of the analysis. The initial conditions (5.1.12) and (5.1.13) require that ϕ, $\eta = o\left(1\right)$ as $\delta \to 0$ in the outer asymptotic region. In particular, the plate boundary condition (5.1.5) and kinematic boundary condition (5.1.7) require that $\phi = O\left(\delta^{\frac{\alpha}{\pi}}\right)$ and $\eta = O\left(\delta^{\frac{2\alpha}{\pi}}\right)$ as $\delta \to 0$ in the outer asymptotic region. A definition sketch of the outer asymptotic region is shown in Figure 5.1.

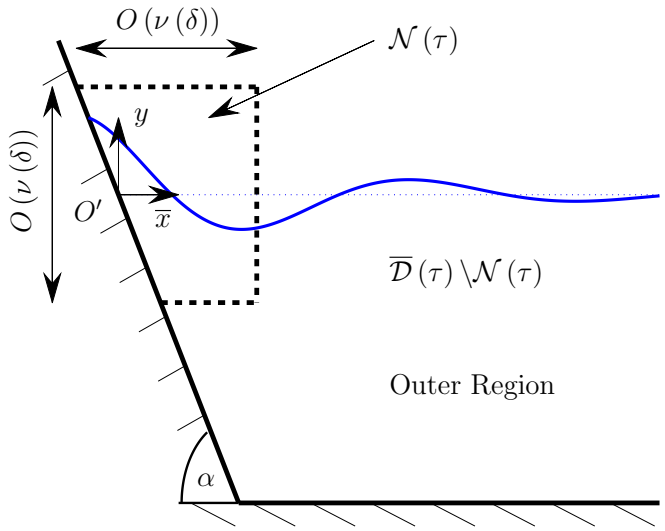

Figure 5.1: Definition sketch of the outer asymptotic region for the case $(\alpha, \mu) \in \left(0, \frac{1}{2}\pi\right) \times \mathbb{R}\backslash\left(\frac{1}{4}\pi, \frac{1}{2}\pi\right) \times \{0\}$

We now introduce the outer region asymptotic expansions in the form,

$$\phi(\overline{x}, y, \tau) = \delta^{\frac{\alpha}{\pi}} (\mu - 1) \cos\alpha \, \widehat{\phi}(\overline{x}, y, \tau) + O\left(\delta^{\frac{2\alpha}{\pi}}\right), \tag{5.1.14}$$

$$\eta(\overline{x}, \tau) = \delta^{\frac{2\alpha}{\pi}} \widehat{\eta}(\overline{x}, \tau) + O\left(\delta^{\frac{3\alpha}{\pi}}\right), \tag{5.1.15}$$

as $\delta \to 0$ in the outer asymptotic region, with the factor $(\mu - 1)\cos\alpha$ in (5.1.14) included for algebraic convenience at a later stage. Substituting expansions (5.1.14) and (5.1.15) into $[IBVP]'$ (with the exception of condition (5.1.9) since the application point $(\overline{x}, y) = (\overline{x}_p(\tau), y_p(\tau))$ lies outside the outer asymptotic region), we obtain the leading order problem in the outer asymptotic region for $\widehat{\phi}$, namely

$$\nabla^2 \widehat{\phi} = 0, \quad (\overline{x}, y) \in \mathcal{D}(0), \ \tau > 0; \tag{5.1.16}$$

$$\nabla \widehat{\phi} \cdot \hat{\mathbf{n}} = \tau, \quad y = -\overline{x}\tan\alpha, \ 0 < \overline{x} < \cot\alpha, \ \tau > 0; \tag{5.1.17}$$

$$\widehat{\phi}_y = 0, \quad y = -1, \ \overline{x} > 0, \ \tau > 0; \tag{5.1.18}$$

$$\widehat{\phi}_\tau = 0, \quad y = 0,\ \overline{x} > 0,\ \tau > 0; \tag{5.1.19}$$

$$\left|\nabla\widehat{\phi}\right| \to 0 \quad \text{as } \overline{x} \to \infty, \text{ uniformly for } -1 \leqslant y \leqslant 0,\ \tau > 0; \tag{5.1.20}$$

$$\widehat{\phi}\,(\overline{x}, y, 0) = 0, \quad (\overline{x}, y) \in \overline{\mathcal{D}}\,(0)\,; \tag{5.1.21}$$

with $\widehat{\eta}$ given, via (5.1.7), (5.1.13), and (5.1.15), by

$$\widehat{\eta}_\tau\,(\overline{x}, \tau) = \frac{1}{2}\,(\mu - 1)\cos\alpha\ \widehat{\phi}_y\,(\overline{x}, \tau)\,, \qquad \overline{x} \geqslant 0,\ \tau > 0; \tag{5.1.22}$$

$$\widehat{\eta}\,(\overline{x}, 0) = 0, \qquad \overline{x} \geqslant 0. \tag{5.1.23}$$

We next introduce $\overline{\phi}\,(\overline{x}, y)$ and $\overline{\eta}\,(\overline{x})$ by writing

$$\widehat{\phi}\,(\overline{x}, y, \tau) = \tau\overline{\phi}\,(\overline{x}, y)\,, \tag{5.1.24}$$

$$\widehat{\eta}\,(\overline{x}, \tau) = \tau^2\overline{\eta}\,(\overline{x})\,. \tag{5.1.25}$$

The resulting problem for $\overline{\phi}$ and $\overline{\eta}$, obtained after substituting (5.1.24) and (5.1.25) into (5.1.16) - (5.1.21) is the same as $[OBVP]$, which was solved and discussed in Chapter 2. We thus have that $\overline{\phi}$ and $\overline{\eta}$ are given, for some real constants A_n, B_n and C_n $(n = 0, 1, 2, \dots)$, by

$$\overline{\phi}\,(r, \theta) = \frac{r\sin\theta}{\cos\alpha} + \sum_{n=0}^{\infty} A_n r^{\left(n+\frac{1}{2}\right)\frac{\pi}{\alpha}} \sin\left(\left(n + \frac{1}{2}\right)\frac{\pi}{\alpha}\theta\right), \tag{5.1.26}$$

for $0 \leqslant r < \text{cosec}\ \alpha$, $-\alpha \leqslant \theta \leqslant 0$, where $\overline{x} = r\cos\theta$ and $y = r\sin\theta$, whilst

$$\overline{\phi}\,(\rho, \psi) = \frac{\rho\cos\psi}{\sin\alpha} + \sum_{n=0}^{\infty} B_n \rho^{n\pi/(\pi-\alpha)} \cos\left(\frac{n\pi\psi}{\pi - \alpha}\right), \tag{5.1.27}$$

for $0 \leqslant \rho < 1$, $0 \leqslant \psi \leqslant \pi - \alpha$, where $\overline{x} - \cot\alpha = \rho\cos\psi$, and $y + 1 = \rho\sin\psi$, and finally

$$\overline{\phi}\,(\overline{x}, y) = \sum_{n=0}^{\infty} C_n e^{-\left(n+\frac{1}{2}\right)\pi\overline{x}} \sin\left(\left(n + \frac{1}{2}\right)\pi y\right), \tag{5.1.28}$$

for $\overline{x} > \cot\alpha$, $-1 \leqslant y \leqslant 0$, after which

$$\overline{\eta}\,(\overline{x}) = \frac{1}{2}(\mu - 1) + \frac{1}{2}(\mu - 1)\cos\alpha \sum_{n=0}^{\infty} \left(n + \frac{1}{2}\right)\frac{\pi}{\alpha} A_n \overline{x}^{\left(n+\frac{1}{2}\right)\frac{\pi}{\alpha} - 1}, \tag{5.1.29}$$

for $0 \leqslant \overline{x} < \operatorname{cosec}\alpha$, and

$$\overline{\eta}\,(\overline{x}) = \frac{1}{2}(\mu - 1)\cos\alpha \sum_{n=0}^{\infty} \left(n + \frac{1}{2}\right)\pi C_n e^{-\left(n+\frac{1}{2}\right)\pi\overline{x}}, \tag{5.1.30}$$

for $\overline{x} \geqslant \operatorname{cosec}\alpha$. It follows from (5.1.26) and (5.1.29) that, as $(\overline{x}, y) \to (0, 0)$, we have

$$\overline{\phi}\,(r, \theta) = \frac{r\sin\theta}{\cos\alpha} + A_0(\alpha)\, r^{\frac{\pi}{2\alpha}} \sin\frac{\pi\theta}{2\alpha} + O\left(r^{\frac{3\pi}{2\alpha}}\right),$$
$$\text{as} \quad r \to 0^+, \text{ with } -\alpha \leqslant \theta \leqslant 0; \tag{5.1.31}$$
$$\overline{\eta}\,(\overline{x}) = \frac{1}{2}(\mu - 1) + A_0(\alpha)\frac{\pi}{4\alpha}(\mu - 1)\cos\alpha\; \overline{x}^{\frac{\pi}{2\alpha} - 1} + O\left(\overline{x}^{\frac{3\pi}{2\alpha} - 1}\right),$$
$$\text{as} \quad \overline{x} \to 0^+, \tag{5.1.32}$$

where r and θ are polar coordinates given by $\overline{x} = r\cos\theta$, $y = r\sin\theta$, and $A_0(\alpha)$ as given in (2.0.15) and displayed in Figure 2.3.

As before, (5.1.32) reveals a weak singularity in $\overline{\eta}'(\overline{x})$ as $\overline{x} \to 0^+$. This singular behaviour as $\overline{x} \to 0^+$ is compounded in higher-order terms in the outer region asymptotic expansion for η in (5.1.15), and also, as $r \to 0$, in the outer region asymptotic expansion for ϕ in (5.1.14), and so the regularity conditions (1.2.30) and (1.2.31) fail to be satisfied by the outer region asymptotic expansions (5.1.14) and (5.1.15) in a neighbourhood of the initial point of intersection of the plate and free surface, where $(\overline{x}, y) = o(1)$ as $\delta \to 0$.

Therefore, in order to capture the full regularity in the neighbourhood of the intersection point of the plate and the free surface, we introduce an *inner asymptotic region*, in which $(\overline{x}, y) = o(1)$ as $\delta \to 0$. The structure of the inner asymptotic region is now considered in detail in the next section.

5.1.2 Inner Asymptotic Region

In this section we introduce the inner asymptotic region associated with $[IBVP]'$ when $(\overline{x}, y) = o(1)$ as $\delta \to 0$. Specifically, following Section 5.1.1 we write $(\overline{x}, y) = O(\nu(\delta))$ with $\nu(\delta) = o(1)$ as $\delta \to 0$. It then follows from (5.1.15), (5.1.25) and (5.1.32) that $\eta = O\left(\delta^{\frac{2\alpha}{\pi}}\right)$ as $\delta \to 0$ in the inner asymptotic region, and so, to capture the free surface in the inner asymptotic region, we must take $\nu(\delta) = O\left(\delta^{\frac{2\alpha}{\pi}}\right)$ as $\delta \to 0$; therefore, without loss of generality, we set $\nu(\delta) = \delta^{\frac{2\alpha}{\pi}}$. An examination of (5.1.14), (5.1.24) and (5.1.31) then requires that $\phi = O\left(\delta^{\frac{3\alpha}{\pi}}\right)$ as $\delta \to 0$ in the inner asymptotic region. Finally, the intersection point of the free surface and the plate must be captured in the inner asymptotic region, and so, $\overline{x}_p(\tau) = O\left(\delta^{\frac{2\alpha}{\pi}}\right)$ as $\delta \to 0$. A sketch of the location of the inner asymptotic region is illustrated in Figure 5.2.

Formally we introduce scaled inner region coordinates (X, Y) by

$$\overline{x} = \delta^{\frac{2\alpha}{\pi}} X, \qquad y = \delta^{\frac{2\alpha}{\pi}} Y, \tag{5.1.33}$$

with $(X, Y) = O(1)$ as $\delta \to 0$ in the inner asymptotic region. The location of the plate in the inner asymptotic region is given by $Y = -X \tan\alpha$, whilst the plate and free surface intersection point is denoted by $(X, Y) = (X_p(\tau), Y_p(\tau))$, with,

$$\overline{x}_p(\tau) = \delta^{\frac{2\alpha}{\pi}} X_p(\tau), \qquad y_p(\tau) = \delta^{\frac{2\alpha}{\pi}} Y_p(\tau), \tag{5.1.34}$$

and $(X_p(\tau), Y_p(\tau)) = O(1)$ as $\delta \to 0$ in the inner asymptotic region. We now write the

free surface and velocity potential in the inner asymptotic region as

$$\eta\left(X,\tau\right)=\delta^{\frac{2\alpha}{\pi}}\eta_I\left(X,\tau\right),\qquad X\geqslant X_p\left(\tau\right),\ \tau\geqslant 0; \tag{5.1.35}$$

$$\phi\left(X,Y,\tau\right)=\delta^{\frac{3\alpha}{\pi}}\phi_I\left(X,Y,\tau\right),\qquad X\geqslant X_p\left(\tau\right),\ -X\tan\alpha\leqslant Y\leqslant\eta_I\left(X,\tau\right),\ \tau\geqslant 0; \tag{5.1.36}$$

with $\eta_I\left(X,\tau\right),\phi_I\left(X,Y,\tau\right)=O\left(1\right)$ as $\delta\to 0$. The inner region asymptotic expansions are then introduced as,

$$\eta_I\left(X,\tau\right)=\tilde{\eta}_0\left(X,\tau\right)+\delta^{1-\frac{2\alpha}{\pi}}\tilde{\eta}_1\left(X,\tau\right)+o\left(\delta^{1-\frac{2\alpha}{\pi}}\right), \tag{5.1.37}$$

$$\phi_I\left(X,Y,\tau\right)=\tilde{\phi}_0\left(X,Y,\tau\right)+\delta^{1-\frac{2\alpha}{\pi}}\tilde{\phi}_1\left(X,Y,\tau\right)+o\left(\delta^{1-\frac{2\alpha}{\pi}}\right), \tag{5.1.38}$$

as $\delta\to 0$ with $\left(X,Y\right)=O\left(1\right)$ in the inner asymptotic region. Finally, it follows from (5.1.33), (5.1.34), (5.1.35) and (5.1.37) that we expand $X_p\left(\tau\right)$ in the form

$$X_p\left(\tau\right)=X_0\left(\tau\right)+\delta^{1-\frac{2\alpha}{\pi}}X_1\left(\tau\right)+o\left(\delta^{1-\frac{2\alpha}{\pi}}\right), \tag{5.1.39}$$

as $\delta\to 0$, with

$$Y_p\left(\tau\right)=-X_p\left(\tau\right)\tan\alpha. \tag{5.1.40}$$

The free surface in the inner asymptotic region is located at

$$Y=\eta_I\left(X,\tau\right),\quad X>X_p\left(\tau\right),\ \tau\geqslant 0, \tag{5.1.41}$$

whilst the spatio-temporal domain in the inner asymptotic region is

$$\mathcal{D}_I\left(\tau\right)=\left\{\left(X,Y\right):X>X_p\left(\tau\right),-X\tan\alpha<Y<\eta_I\left(X,\tau\right)\right\}, \tag{5.1.42}$$

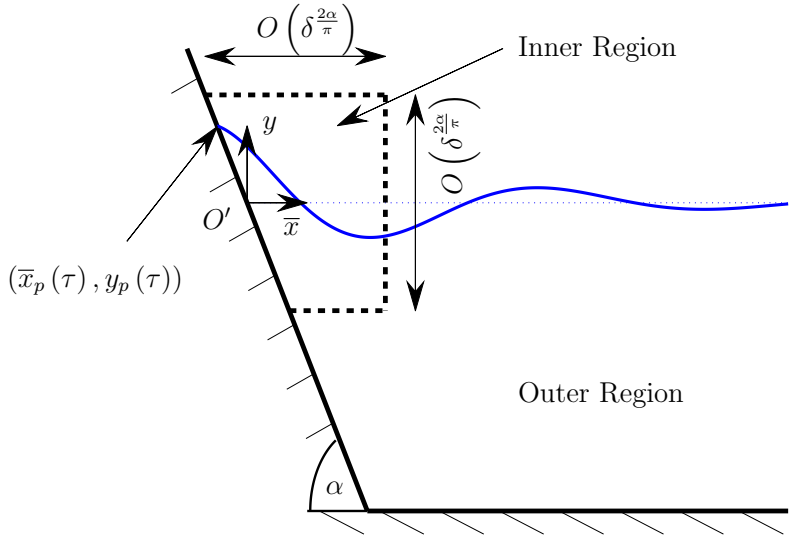

Figure 5.2: A sketch of the location of the inner asymptotic region for the case $(\alpha, \mu) \in \left(0, \frac{1}{2}\pi\right) \times \mathbb{R} \backslash \left(\frac{1}{4}\pi, \frac{1}{2}\pi\right) \times \{0\}$

for $\tau \geqslant 0$, with closure $\overline{\mathcal{D}}_I(\tau)$. A sketch of the inner asymptotic region geometry is given in Figure 5.3.

We now write $[IBVP]'$ in terms of the inner asymptotic region coordinates (X, Y), and τ, and the inner asymptotic region variables ϕ_I, η_I, and X_p, to obtain,

$$\overline{\nabla}^2 \phi_I = 0, \qquad (X, Y) \in \mathcal{D}_I(\tau), \ \tau > 0; \tag{5.1.43}$$

$$\widehat{\nabla}\phi_I \cdot \hat{\mathbf{n}} = \tau(\mu - 1)\cos\alpha, \qquad X > X_p(\tau), \ Y = -X\tan\alpha, \ \tau > 0; \tag{5.1.44}$$

$$\eta_{I,\tau} + [\phi_{I,X} - \tau(\mu - 1)\cot\alpha]\,\eta_{I,X} - \phi_{I,Y} = 0,$$
$$X > X_p(\tau), \ Y = \eta_I(X, \tau), \ \tau > 0; \tag{5.1.45}$$

$$\phi_{I,\tau} - \tau(\mu - 1)\cot\alpha\ \phi_{I,X} + \frac{1}{2}\left|\widehat{\nabla}\phi_I\right|^2 + \eta = 0,$$
$$X > X_p(\tau), \ Y = \eta_I(X, \tau), \ \tau > 0; \tag{5.1.46}$$

$$\eta_I(X_p(\tau), \tau) = -X_p(\tau)\tan\alpha, \qquad \tau > 0; \tag{5.1.47}$$

$$\phi_I(X, Y, 0) = 0, \qquad X \geqslant X_0(0), \ -X\tan\alpha \leqslant \overline{Y} \leqslant \eta_I(X, 0); \tag{5.1.48}$$

$$\eta_I(X, 0) = \delta^{1-\frac{2\alpha}{\pi}}\eta_0(X), \qquad X \geqslant X_0(0); \tag{5.1.49}$$

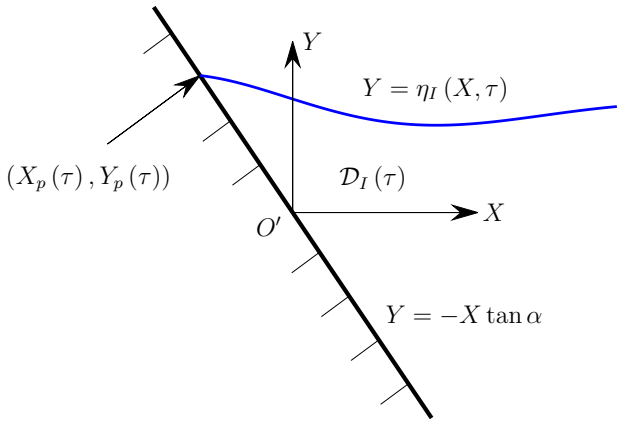

Figure 5.3: The inner asymptotic region geometry as $\delta \to 0$ for the case $(\alpha,\mu) \in \left(0, \frac{1}{2}\pi\right) \times \mathbb{R}\backslash\left(\frac{1}{4}\pi, \frac{1}{2}\pi\right) \times \{0\}$

with $\widehat{\nabla} = (\partial/\partial X, \partial/\partial Y)$. On substituting from (5.1.37) - (5.1.39) into (5.1.43) - (5.1.49) we obtain, at leading order, the following nonlinear harmonic evolution free boundary problem for $\tilde{\phi}_0(X,Y,\tau)$, $\tilde{\eta}_0(X,\tau)$, and $X_0(\tau)$, namely

$$\widehat{\nabla}^2\tilde{\phi}_0 = 0, \qquad X > X_0(\tau),\ -X\tan\alpha < Y < \tilde{\eta}_0(X,\tau),\ \tau > 0; \quad (5.1.50)$$

$$\widehat{\nabla}\phi_0 \cdot \hat{\mathbf{n}} = \tau(\mu-1)\cos\alpha, \qquad X > X_0(\tau),\ Y = -X\tan\alpha,\ \tau > 0; \quad (5.1.51)$$

$$\tilde{\eta}_{0,\tau} + \left[\tilde{\phi}_{0,X} - \tau(\mu-1)\cot\alpha\right]\tilde{\eta}_{0,X} - \tilde{\phi}_{0,Y} = 0,$$

$$X > X_0(\tau),\ Y = \tilde{\eta}_0(X,\tau),\ \tau > 0; \quad (5.1.52)$$

$$\tilde{\phi}_{0,\tau} - \tau(\mu-1)\cot\alpha\ \tilde{\phi}_{0,X} + \frac{1}{2}\left|\widehat{\nabla}\tilde{\phi}_0\right|^2 + \tilde{\eta}_0 = 0,$$

$$X > X_0(\tau),\ Y = \tilde{\eta}_0(X,\tau),\ \tau > 0; \quad (5.1.53)$$

$$\tilde{\phi}_0(X,Y,0) = 0, \qquad X \geqslant 0,\ -X\tan\alpha \leqslant Y \leqslant 0; \quad (5.1.54)$$

$$\tilde{\eta}_0(X,0) = 0, \qquad X \geqslant 0; \quad (5.1.55)$$

$$\tilde{\eta}_0(X_0(\tau),\tau) = -X_0(\tau)\tan\alpha, \qquad \tau > 0. \quad (5.1.56)$$

The problem (5.1.50) - (5.1.56) must be completed by asymptotic matching conditions between the inner asymptotic region and outer asymptotic region. Following Van Dyke's Matching Principle (see, for example, [28]), we obtain

$$\tilde{\phi}_0(R,\theta,\tau) \sim \tau(\mu-1) R\sin\theta \quad \text{as} \quad R\to\infty,\ -\alpha<\theta<0,\ \tau>0; \tag{5.1.57}$$

$$\tilde{\eta}_0(X,\tau) \sim \frac{1}{2}\tau^2(\mu-1) \qquad \text{as} \quad X\to\infty,\ \tau>0, \tag{5.1.58}$$

where R and θ are polar coordinates given by $X = R\cos\theta$, $Y = R\sin\theta$. Although the problem (5.1.50) - (5.1.56) is nonlinear, the simple nature of the matching conditions mean that it is readily established that the exact solution to the leading order problem is given by

$$\tilde{\eta}_0(X,\tau) = \frac{1}{2}\tau^2(\mu-1), \qquad X\geqslant X_0(\tau),\ \tau\geqslant 0, \tag{5.1.59}$$

$$\tilde{\phi}_0(X,Y,\tau) = \tau(\mu-1)Y + \frac{1}{6}\tau^3(1-\mu)(2\mu-1),$$
$$X\geqslant X_0(\tau),\ -X\tan\alpha\leqslant Y\leqslant\frac{1}{2}\tau^2(\mu-1),\ \tau\geqslant 0, \tag{5.1.60}$$

with

$$X_0(\tau) = -\frac{1}{2}\tau^2(\mu-1)\cot\alpha, \qquad \tau\geqslant 0. \tag{5.1.61}$$

This is represented in the inner asymptotic region in Figure 5.4a. We now formulate the problem at $O\left(\delta^{1-\frac{2\alpha}{\pi}}\right)$, where it is convenient to introduce the coordinates $\left(\overline{X},\overline{Y}\right)$, according to

$$X = -\frac{1}{2}\tau^2(\mu-1)\cot\alpha + \overline{X}, \qquad Y = \frac{1}{2}\tau^2(\mu-1) + \overline{Y}, \tag{5.1.62}$$

as shown in Figure 5.4b. We obtain the following linear, harmonic evolution problem for

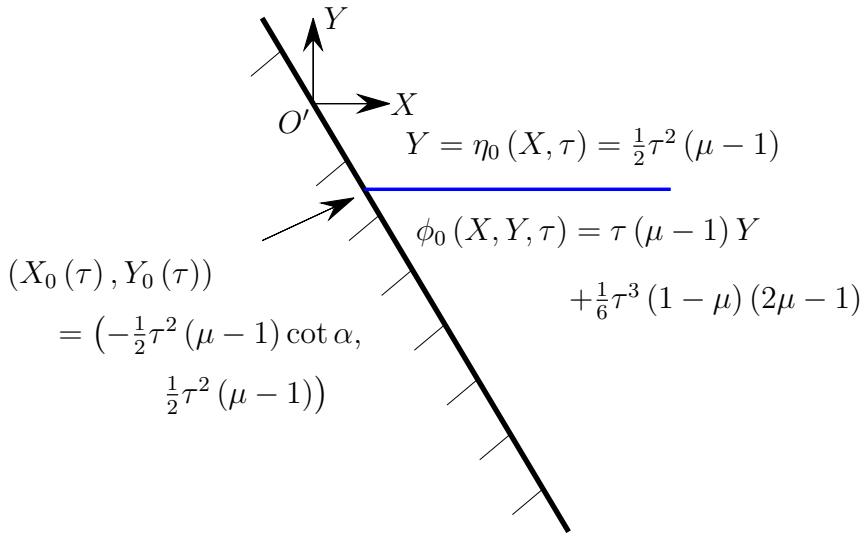

(a) Solution of $[IBVP]'$ at leading order in the inner asymptotic region

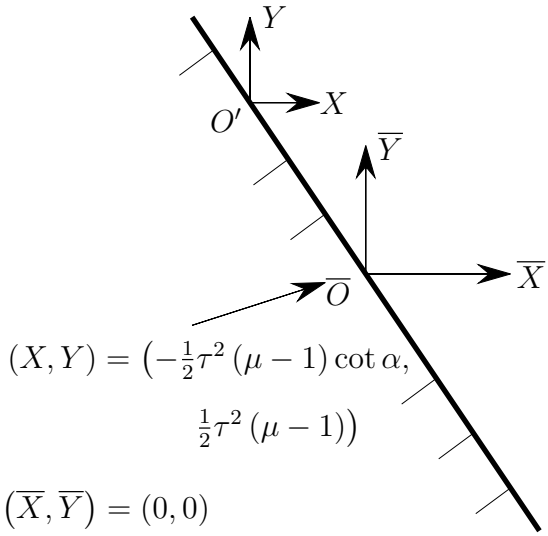

(b) $\left(\overline{X},\overline{Y}\right)$ coordinate system in the inner asymptotic region

Figure 5.4: Sketches in the inner asymptotic region for $\tau > 0$, as $\delta \to 0$, for the case $(\alpha,\mu) \in \left(0,\frac{1}{2}\pi\right) \times \mathbb{R} \backslash \left(\frac{1}{4}\pi,\frac{1}{2}\pi\right) \times \{0\}$

$\tilde{\phi}_1\left(\overline{X},\overline{Y},\tau\right)$, $\tilde{\eta}_1\left(\overline{X},\tau\right)$ and $X_1(\tau)$, namely,

$$\overline{\nabla}^2\tilde{\phi}_1 = 0, \qquad \overline{X} > 0,\ -\overline{X}\tan\alpha < \overline{Y} < 0,\ \tau > 0; \tag{5.1.63}$$

$$\overline{\nabla}\tilde{\phi}_1 \cdot \hat{\mathbf{n}} = 0, \qquad \overline{X} > 0,\ \overline{Y} = -\overline{X}\tan\alpha,\ \tau > 0; \tag{5.1.64}$$

$$\tilde{\eta}_{1,\tau} - \tilde{\phi}_{1,\overline{Y}} = 0, \qquad \overline{X} > 0,\ \overline{Y} = 0,\ \tau > 0; \tag{5.1.65}$$

$$\tilde{\phi}_{1,\tau} + \mu\tilde{\eta}_1 = 0, \qquad \overline{X} > 0,\ \overline{Y} = 0,\ \tau > 0; \tag{5.1.66}$$

$$\tilde{\phi}_1\left(\overline{R},\theta,\tau\right) = -\tau A_0(\alpha)(\mu-1)\cos\alpha\ \overline{R}^{\frac{\pi}{2\alpha}}\cos\frac{\pi}{2\alpha}(\theta+\alpha) + o\left(\overline{R}^{\frac{\pi}{2\alpha}}\right),$$
$$\text{as} \quad \overline{R}\to\infty,\ -\alpha < \theta < 0,\ \tau > 0; \tag{5.1.67}$$

$$\tilde{\eta}_1\left(\overline{X},\tau\right) = \tau^2 A_0(\alpha)\frac{\pi}{4\alpha}(\mu-1)\cos\alpha\ \overline{X}^{\frac{\pi}{2\alpha}-1} + o\left(\overline{X}^{\frac{\pi}{2\alpha}-1}\right),$$
$$\text{as} \quad \overline{X}\to\infty,\ \tau > 0; \tag{5.1.68}$$

$$\tilde{\phi}_1\left(\overline{X},\overline{Y},0\right) = 0, \qquad \overline{X} \geqslant 0,\ -X\tan\alpha \leqslant \overline{Y} \leqslant 0; \tag{5.1.69}$$

$$\tilde{\eta}_1\left(\overline{X},0\right) = \eta_0\left(\overline{X}\right), \qquad \overline{X} \geqslant 0. \tag{5.1.70}$$

Here $\overline{\nabla} = \left(\partial/\partial\overline{X}, \partial/\partial\overline{Y}\right)$, (5.1.67) and (5.1.68) are the matching conditions with the outer asymptotic region, and we have introduced polar coordinates $\left(\overline{R},\theta\right)$, given by $\overline{X} = \overline{R}\cos\theta$, $\overline{Y} = \overline{R}\sin\theta$. Finally we have

$$X_1(\tau) = -\tilde{\eta}_1(0,\tau)\cot\alpha, \qquad \tau > 0. \tag{5.1.71}$$

It is now convenient to write

$$\tilde{\eta}_1\left(\overline{X},\tau\right) = \tilde{\eta}_1\left(\overline{X},\tau\right)\Big|_0 + \xi\left(\overline{X},\tau\right), \tag{5.1.72}$$

$$\tilde{\phi}_1\left(\overline{X},\overline{Y},\tau\right) = \tilde{\phi}_1\left(\overline{X},\overline{Y},\tau\right)\Big|_0 + \psi\left(\overline{X},\overline{Y},\tau\right), \tag{5.1.73}$$

where $\tilde{\eta}_1\Big|_0$ and $\tilde{\phi}_1\Big|_0$ are the solution to (5.1.63) - (5.1.68) in the case of zero initial data, as discussed in Chapter 3. Rewriting the problem (5.1.63) - (5.1.70) in terms of ξ and ψ,

we obtain

$$\overline{\nabla}^2\psi = 0, \qquad \overline{X} > 0,\ -\overline{X}\tan\alpha < \overline{Y} < 0,\ \tau > 0; \tag{5.1.74}$$

$$\overline{\nabla}\psi \cdot \hat{\mathbf{n}} = 0, \qquad \overline{X} > 0,\ \overline{Y} = -\overline{X}\tan\alpha,\ \tau > 0; \tag{5.1.75}$$

$$\xi_\tau - \psi_{\overline{Y}} = 0, \qquad \overline{X} > 0,\ \overline{Y} = 0,\ \tau > 0; \tag{5.1.76}$$

$$\psi_\tau + \mu\xi = 0, \qquad \overline{X} > 0,\ \overline{Y} = 0,\ \tau > 0; \tag{5.1.77}$$

$$\psi\left(\overline{R}, \theta, \tau\right) \to 0 \qquad \text{as} \quad \overline{R} \to \infty,\ -\alpha < \theta < 0,\ \tau > 0; \tag{5.1.78}$$

$$\xi\left(\overline{X}, \tau\right) \to 0 \qquad \text{as} \quad \overline{X} \to \infty,\ \tau > 0; \tag{5.1.79}$$

$$\psi\left(\overline{X}, \overline{Y}, 0\right) = 0, \qquad \overline{X} \geqslant 0,\ -\overline{X}\tan\alpha \leqslant \overline{Y} \leqslant 0; \tag{5.1.80}$$

$$\xi\left(\overline{X}, 0\right) = \eta_0\left(\overline{X}\right), \qquad \overline{X} \geqslant 0. \tag{5.1.81}$$

We begin our investigation of the problem (5.1.74) - (5.1.81) in the case $(\alpha, \mu) \in \left(0, \frac{1}{2}\pi\right) \times (\mathbb{R}\backslash\{0\})$. We seek solutions of the form

$$\psi\left(\overline{X}, \overline{Y}, \tau\right) = e^{-\lambda\tau}\overline{\psi}\left(\overline{X}, \overline{Y}\right), \tag{5.1.82}$$

$$\xi\left(\overline{X}, \tau\right) = e^{-\lambda\tau}\overline{\xi}\left(\overline{X}\right), \tag{5.1.83}$$

with $\lambda \in \mathbb{C}$, which leads to the linear harmonic boundary value problem for $\overline{\psi}$, given by

$$\overline{\nabla}^2\overline{\psi} = 0, \qquad \overline{X} > 0,\ -\overline{X}\tan\alpha < \overline{Y} < 0; \tag{5.1.84}$$

$$\overline{\nabla}\overline{\psi} \cdot \hat{\mathbf{n}} = 0, \qquad \overline{X} > 0,\ \overline{Y} = -\overline{X}\tan\alpha; \tag{5.1.85}$$

$$\overline{\psi}_{\overline{Y}} - k\overline{\psi} = 0, \qquad \overline{X} > 0,\ \overline{Y} = 0; \tag{5.1.86}$$

$$\overline{\psi},\ \overline{\nabla}\overline{\psi} \text{ bounded as } \overline{R} \to \infty, \text{ uniformly for } -\alpha < \theta < 0; \tag{5.1.87}$$

with $k = -\lambda^2/\mu$ (for $\mu \neq 0$), after which we obtain $\overline{\xi}$ from

$$\overline{\xi}\left(\overline{X}\right) = \frac{\lambda}{\mu}\overline{\psi}\left(\overline{X}, 0\right), \qquad \overline{X} \geqslant 0. \tag{5.1.88}$$

Here, according to the regularity conditions (1.2.30) and (1.2.31), we require that solutions to (5.1.84) - (5.1.87), $\overline{\psi} : \overline{\mathcal{G}}_\infty \to \mathbb{C}$, have regularity

$$\overline{\psi} \in C^1\left(\overline{\mathcal{G}}_\infty\right) \cap C^2\left(\mathcal{G}_\infty\right), \tag{5.1.89}$$

with

$$\mathcal{G}_\infty = \left\{\left(\overline{X}, \overline{Y}\right) : -\overline{X}\tan\alpha < \overline{Y} < 0,\ \overline{X} > 0\right\}. \tag{5.1.90}$$

The linear harmonic problem (5.1.84) - (5.1.87) is a spectral problem with spectral parameter $k \in \mathbb{C}$, which we refer to as $[SP\,(k)]$. It is clear that $[SP\,(k)]$ has the trivial solution for each $k \in \mathbb{C}$. Further, let $\overline{\psi}_k : \mathcal{G}_\infty \to \mathbb{C}$ be a nontrivial solution to $[SP\,(k)]$, then it is straight forward to establish the following:

(i) $\underline{k \in \mathbb{R}^+}$

$$\begin{aligned}\overline{\psi}_k\left(\overline{R}, \theta\right) = &\left(c_k e^{ik\overline{R}\cos\theta} + d_k e^{-ik\overline{R}\cos\theta}\right) e^{k\overline{R}\sin\theta} \\ &+ a_k \frac{1}{\overline{R}^{\frac{\pi}{2\alpha}}} \cos\frac{\pi}{2\alpha}\left(\theta + \alpha\right) + O\left(\frac{1}{\overline{R}^{\frac{\pi}{2\alpha}+1}}\right),\end{aligned} \tag{5.1.91}$$

as $\overline{R} \to \infty$ uniformly for $-\alpha \leqslant \theta \leqslant 0$. Here, c_k, d_k, $a_k \in \mathbb{C}$ are non-zero constants.

(ii) $\underline{\text{k} = 0}$

$$\overline{\psi}_0\left(\overline{R}, \theta\right) = a_0 + b_0 \frac{1}{\overline{R}^{\frac{\pi}{\alpha}}} \cos\frac{\pi}{\alpha}\theta + O\left(\frac{1}{\overline{R}^{2\frac{\pi}{\alpha}}}\right), \tag{5.1.92}$$

as $\overline{R} \to \infty$ uniformly for $-\alpha \leqslant \theta \leqslant 0$. Here a_0, $b_0 \in \mathbb{C}$ are non-zero constants.

(iii) $\underline{k \in \mathbb{C} \backslash \left(\mathbb{R}^{+} \cup \{0\}\right)}$

$$\overline{\psi}_k\left(\overline{R}, \theta\right) = a_k \frac{1}{\overline{R}^{\frac{\pi}{2\alpha}}} \cos \frac{\pi}{2\alpha}\left(\theta + \alpha\right) + O\left(\frac{1}{\overline{R}^{\frac{\pi}{2\alpha}+1}}\right), \tag{5.1.93}$$

as $\overline{R} \to \infty$ uniformly for $-\alpha \leqslant \theta \leqslant 0$. Here, $a_k \in \mathbb{C}$ is a non-zero constant.

Our object now is to classify the spectrum of $[SP\left(k\right)]$. We define the spectrum of $[SP\left(k\right)]$ to be $\mathbf{S}$, where

$$\mathbf{S} = \left\{k \in \mathbb{C} : [SP\left(k\right)] \text{ has a non-trivial solution}\right\}. \tag{5.1.94}$$

The set of eigenvalues of $[SP\left(k\right)]$ is $\mathbf{S}^d$, where

$$\mathbf{S}^d = \left\{k \in \mathbb{C} : \exists \text{ a non-trivial solution to } [SP\left(k\right)] \text{ with } \overline{\psi} \to 0 \text{ as } \overline{R} \to \infty\right\}, \tag{5.1.95}$$

and the continuous spectrum of $[SP\left(k\right)]$ is $\mathbf{S}^c$, where

$$\mathbf{S}^c = \left\{k \in \mathbb{C} : \exists \text{ a non-trivial solution to } [SP\left(k\right)] \text{ with } \overline{\psi} \nrightarrow 0 \text{ as } \overline{R} \to \infty\right\}, \tag{5.1.96}$$

with the limits as $\overline{R} \to \infty$ considered as uniform for $-\alpha \leqslant \theta \leqslant 0$. We observe that

$$\mathbf{S} = \mathbf{S}^c \cup \mathbf{S}^d. \tag{5.1.97}$$

Following Needham [25], together with the use of (5.1.91) - (5.1.93) above we can establish that,[1]

$$\mathbf{S}^c = \mathbb{R}^{+}, \qquad \mathbf{S}^d = \varnothing, \tag{5.1.98}$$

[1]See Appendix A.5 for the details of the classification of the spectrum of $[SP\left(k\right)]$

and so

$$\mathbf{S}_k = \mathbb{R}^+. \tag{5.1.99}$$

We now introduce $\mathbf{S}_\lambda \subseteq \mathbb{C}$, where

$$\mathbf{S}_\lambda = \left\{\lambda \in \mathbb{C} : \lambda^2 = -\mu k,\ k \in \mathbf{S}\right\}. \tag{5.1.100}$$

Following (5.1.99), *for* $\mu > 0$, we have,

$$\mathbf{S}_\lambda = \mathbf{S}_\lambda^+ = \left\{\lambda \in \mathbb{C} : \lambda = \pm i\sqrt{\mu}k^{\frac{1}{2}},\ k \in \mathbb{R}^+\right\}, \tag{5.1.101}$$

whilst, *for* $\mu < 0$, we have

$$\mathbf{S}_\lambda = \mathbf{S}_\lambda^- = \left\{\lambda \in \mathbb{C} : \lambda = \pm\sqrt{(-\mu)}k^{\frac{1}{2}},\ k \in \mathbb{R}^+\right\} = \mathbb{R}. \tag{5.1.102}$$

Now, the linear evolution problem (5.1.74) - (5.1.81) is:

(a) Well-posed and stable when $\mathrm{Re}\,(\lambda) \geqslant 0$ for all $\lambda \in \mathbf{S}_\lambda$.

(b) Well-posed and unstable when there exists $M \in \mathbb{R}$ such that $\mathrm{Re}\,(\lambda) \geqslant M$ for all $\lambda \in \mathbf{S}_\lambda$, and there exists $\lambda^* \in \mathbf{S}_\lambda$ such that $\mathrm{Re}\,(\lambda^*) < 0$.

(c) Ill-posed when there exists a sequence $\{\lambda_n\}_{n\in\mathbb{N}}$, with $\lambda_n \in \mathbf{S}_\lambda$ for all $n \in \mathbb{N}$, such that $\mathrm{Re}\,(\lambda_n) \to -\infty$ as $n \to \infty$.

It now follows directly from (5.1.101) and (5.1.102) that the linear evolution problem (5.1.74) - (5.1.81) is

(I) Well-posed and stable when $\mu > 0$.

(II) Ill-posed when $\mu < 0$.

We conclude that $[IBVP]$ is well-posed and stable when $(\alpha,\mu)\in\left(0,\frac{1}{2}\pi\right)\times\mathbb{R}^{+}$, whilst $[IBVP]$ is ill-posed when $(\alpha,\mu)\in\left(0,\frac{1}{2}\pi\right)\times\mathbb{R}^{-}$.

We next consider the problem (5.1.74) - (5.1.81) in the case $(\alpha,\mu)\in\left(0,\frac{1}{4}\pi\right]\times\{0\}$, where we obtain, from (5.1.74) - (5.1.81), the linear harmonic evolution problem for ψ given by

$$\overline{\nabla}^{2}\psi=0, \qquad \overline{X}>0,-\overline{X}\tan\alpha<\overline{Y}<0,\ \tau>0; \tag{5.1.103}$$

$$\overline{\nabla}\psi\cdot\hat{\mathbf{n}}=0, \qquad \overline{X}>0,\ \overline{Y}=-\overline{X}\tan\alpha,\ \tau>0; \tag{5.1.104}$$

$$\psi_{\tau}=0, \qquad \overline{X}>0,\ \overline{Y}=0,\ \tau>0; \tag{5.1.105}$$

$$\psi\left(\overline{R},\theta,\tau\right)\rightarrow 0 \qquad \text{as } \overline{R}\rightarrow\infty,\ -\alpha<\theta<0,\ \tau>0; \tag{5.1.106}$$

$$\psi\left(\overline{X},\overline{Y},0\right)=0, \qquad \overline{X}\geqslant 0,\ -\overline{X}\tan\alpha\leqslant\overline{Y}\leqslant 0; \tag{5.1.107}$$

after which we obtain ξ from

$$\xi_{\tau}=\psi_{\overline{Y}}\left(\overline{X},0,\tau\right), \qquad \overline{X}>0,\ \tau>0, \tag{5.1.108}$$

$$\xi\left(\overline{X},0\right)=\eta_{0}\left(\overline{X}\right), \qquad \overline{X}\geqslant 0. \tag{5.1.109}$$

It is straightforward to show that the only solution to the problem (5.1.103) - (5.1.109) is given by the initial conditions,

$$\psi\left(\overline{X},\overline{Y},\tau\right)=0, \qquad \overline{X}\geqslant 0,\ -\overline{X}\tan\alpha\leqslant\overline{Y}\leqslant 0,\ \tau\geqslant 0, \tag{5.1.110}$$

$$\xi\left(\overline{X},\tau\right)=\eta_{0}\left(\overline{X}\right), \qquad \overline{X}\geqslant 0,\ \tau\geqslant 0, \tag{5.1.111}$$

and thus the linear evolution problem (5.1.74) - (5.1.81) is well-posed and stable for all pairs $(\alpha,\mu)\in\left(0,\frac{1}{4}\pi\right]\times\{0\}$. We conclude that $[IBVP]$ is well-posed and stable when $(\alpha,\mu)\in\left(0,\frac{1}{4}\pi\right]\times\{0\}$.

We now consider the well-posedness and stability of $[IBVP]$ for those pairs $(\alpha, \mu) \in \left(\frac{1}{4}\pi, \frac{1}{2}\pi\right) \times \mathcal{G}(\delta)$, with $\mathcal{G}(\delta)$ being a $o(1)$ neighbourhood of $\mu = 0$ as $\delta \to 0$.

5.2 The Case: $(\alpha, \mu) \in \left(\frac{1}{4}\pi, \frac{1}{2}\pi\right) \times \mathcal{G}(\delta)$

In this section we investigate the well-posedness and stability of the problem $[IBVP]$ with respect to perturbations in initial data for those pairs $(\alpha, \mu) \in \left(\frac{1}{4}\pi, \frac{1}{2}\pi\right) \times \mathcal{G}(\delta)$, with $\mathcal{G}(\delta)$ being a $o(1)$ neighbourhood of $\mu = 0$ as $\delta \to 0$. We write

$$\mu = \nu(\delta)\,\overline{\mu}, \tag{5.2.1}$$

where $\overline{\mu} = O(1)$ and $\nu(\delta) = o(1)$ as $\delta \to 0$. Here the gauge function $\nu(\delta)$ will be determined in the course of the analysis.

Following an examination of (4.1.1) and (4.1.3), we require $t^\gamma \sim \delta$ and $t^\gamma \sim \delta^r$, which, as $\delta \to 0$, requires

$$t = O\left(\delta^{1/\gamma}\right), \tag{5.2.2}$$

where $\gamma = \frac{1}{1-\frac{\pi}{4\alpha}}$, with

$$r = 1. \tag{5.2.3}$$

In what follows, we will refer to the initially perturbed modification of $[IBVP]$ as $[IBVP]''$, and we will address $[IBVP]''$ as $\delta \to 0$ with $t = O\left(\delta^{1/\gamma}\right)$. Thus we write

$$t = \delta^{1/\gamma}\tau, \tag{5.2.4}$$

with $\tau = O(1)$ as $\delta \to 0$. We can now write $[IBVP]''$ in terms of $\overline{x}$, y, ϕ, η, τ and δ,

which becomes,

$$\nabla^2\phi = 0, \qquad (\overline{x}, y) \in \mathcal{D}(\tau),\ \tau > 0; \tag{5.2.5}$$

$$\nabla\phi \cdot \hat{\mathbf{n}} = \delta^{1/\gamma}\tau\left(\nu(\delta)\,\overline{\mu} - 1\right)\cos\alpha, \qquad y = -\overline{x}\tan\alpha,\ \overline{x}_p(\tau) < \overline{x} < \overline{x}_b,\ \tau > 0; \tag{5.2.6}$$

$$\phi_y = 0, \qquad y = -1,\ \overline{x} > \overline{x}_b,\ \tau > 0; \tag{5.2.7}$$

$$\eta_\tau + \left[\delta^{1/\gamma}\phi_{\overline{x}} - \delta^{2/\gamma}\tau\left(\nu(\delta)\,\overline{\mu} - 1\right)\cot\alpha\right]\eta_{\overline{x}} - \delta^{1/\gamma}\phi_y = 0,$$
$$y = \eta(\overline{x}, \tau),\ \overline{x} > \overline{x}_p(\tau),\ \tau > 0; \tag{5.2.8}$$

$$\phi_\tau - \delta^{2/\gamma}\tau\left(\nu(\delta)\,\overline{\mu} - 1\right)\cot\alpha\ \phi_{\overline{x}} + \delta^{1/\gamma}\frac{1}{2}\left|\nabla\phi\right|^2 + \delta^{1/\gamma}\eta = 0,$$
$$y = \eta(\overline{x}, \tau),\ \overline{x} > \overline{x}_p(\tau),\ \tau > 0; \tag{5.2.9}$$

$$\eta + \overline{x}_p(\tau)\tan\alpha = 0, \qquad \overline{x} = \overline{x}_p(\tau),\ \tau > 0; \tag{5.2.10}$$

$$\eta \to 0, \qquad \text{as} \quad \overline{x} \to \infty,\ \tau > 0; \tag{5.2.11}$$

$$|\nabla\phi| \to 0, \qquad \text{as} \quad \overline{x} \to \infty, \text{ uniformly for } -1 \leqslant y \leqslant \eta(\overline{x}, \tau),\ \tau > 0; \tag{5.2.12}$$

$$\phi(\overline{x}, y, 0) = 0, \qquad (\overline{x}, y) \in \overline{\mathcal{D}}(0); \tag{5.2.13}$$

$$\eta(\overline{x}, 0) = \delta\eta_0\left(\delta^{-1}\overline{x}\right), \qquad \overline{x} \geqslant 0; \tag{5.2.14}$$

with $\eta_0 : \mathbb{R} \to \mathbb{R}$ as given by (5.0.3).

The structure of the solution to $[IBVP]$ as $t \to 0^+$ indicates that there will be three asymptotic regions in the solution to $[IBVP]''$ as $\delta \to 0$ with $\tau = O(1)$. In the outer asymptotic region we have $(\overline{x}, y) \in \overline{\mathcal{D}}(\tau) = O(1)$ as $\delta \to 0$ with $\tau = O(1)$, and we consider this first.

5.2.1 Outer Asymptotic Region

In this section we begin the asymptotic development of the solution to $[IBVP]''$, as $\delta \to 0$ with $\tau = O(1)$, in an *outer asymptotic region* in which $(\overline{x}, y) \in \overline{\mathcal{D}}(\tau) \setminus \mathcal{N}(\tau)$ as $\delta \to 0$, with $\mathcal{N}(\tau)$ being a $O(\overline{\nu}(\delta))$ neighbourhood of $(\overline{x}, y) = (0, 0)$, such that $\overline{\nu}(\delta) = o(1)$ as

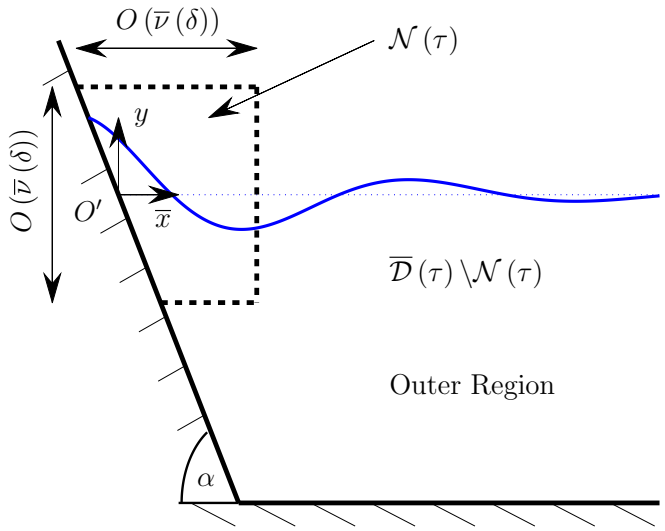

Figure 5.5: Definition sketch of the outer asymptotic region for the case $(\alpha, \mu) \in \left(\frac{1}{4}\pi, \frac{1}{2}\pi\right) \times \mathcal{G}(\mu)$

$\delta \to 0$. Here the gauge function $\overline{\nu}(\delta)$ will be determined in the course of the analysis. The initial conditions (5.2.13) and (5.2.14) require that $\phi, \eta = o(1)$ as $\delta \to 0$ in the outer asymptotic region. In particular, the plate boundary condition (5.2.6) and kinematic boundary condition (5.2.8) require that $\phi = O\left(\delta^{1/\gamma}\right)$ and $\eta = O\left(\delta^{2/\gamma}\right)$ as $\delta \to 0$ in the outer asymptotic region. A definition sketch of the outer asymptotic region is shown in Figure 5.5.

We now introduce the outer region asymptotic expansions in the form,

$$\phi(\overline{x}, y, \tau) = -\delta^{1/\gamma} \cos\alpha \, \widehat{\phi}(\overline{x}, y, \tau) + O\left(\delta^{2/\gamma}\right), \tag{5.2.15}$$

$$\eta(\overline{x}, \tau) = \delta^{2/\gamma} \widehat{\eta}(\overline{x}, \tau) + O\left(\delta^{3/\gamma}\right), \tag{5.2.16}$$

as $\delta \to 0$ in the outer asymptotic region, with the factor $-\cos\alpha$ in (5.2.15) included for algebraic convenience at a later stage. Substituting expansions (5.2.15) and (5.2.16) into $[IBVP]''$ (with the exception of condition (5.2.10) since the application point $(\overline{x}, y) =$

$(\overline{x}_p(\tau), y_p(\tau))$ lies outside the outer asymptotic region), we obtain the leading order problem in the outer asymptotic region for $\widehat{\phi}$, namely

$$\nabla^2\widehat{\phi} = 0, \quad (\overline{x}, y) \in \mathcal{D}(0), \ \tau > 0; \tag{5.2.17}$$

$$\nabla\widehat{\phi}\cdot\hat{\mathbf{n}} = \tau, \quad y = -\overline{x}\tan\alpha, \ 0 < \overline{x} < \cot\alpha, \ \tau > 0; \tag{5.2.18}$$

$$\widehat{\phi}_y = 0, \quad y = -1, \ \overline{x} > 0, \ \tau > 0; \tag{5.2.19}$$

$$\widehat{\phi}_\tau = 0, \quad y = 0, \ \overline{x} > 0, \ \tau > 0; \tag{5.2.20}$$

$$\left|\nabla\widehat{\phi}\right| \to 0 \quad \text{as } \overline{x} \to \infty, \text{ uniformly for } -1 \leqslant y \leqslant 0, \ \tau > 0; \tag{5.2.21}$$

$$\widehat{\phi}(\overline{x}, y, 0) = 0, \quad (\overline{x}, y) \in \overline{\mathcal{D}}(0). \tag{5.2.22}$$

with $\widehat{\eta}$ given, via (5.2.8), (5.2.14), and (5.2.16), by

$$\widehat{\eta}_\tau(\overline{x}, \tau) = -\frac{1}{2}\cos\alpha\ \widehat{\phi}_y(\overline{x}, \tau), \qquad \overline{x} \geqslant 0, \ \tau > 0; \tag{5.2.23}$$

$$\widehat{\eta}(\overline{x}, 0) = 0, \qquad \overline{x} \geqslant 0. \tag{5.2.24}$$

Notice that the problem (5.2.17) - (5.2.24) is the same as (5.1.16) - (5.1.23) when $\mu = 0$, which was studied in Section 5.1.1. Following Section 5.1.1, we introduce $\overline{\phi}(\overline{x}, y)$ and $\overline{\eta}(\overline{x})$ by writing

$$\widehat{\phi}(\overline{x}, y, \tau) = \tau\overline{\phi}(\overline{x}, y), \tag{5.2.25}$$

$$\widehat{\eta}(\overline{x}, \tau) = \tau^2\overline{\eta}(\overline{x}). \tag{5.2.26}$$

The resulting problem for $\overline{\phi}$ and $\overline{\eta}$, obtained after substituting (5.2.25) and (5.2.26) into (5.2.17) - (5.2.22) is the same as $[OBVP]$, which was solved and discussed in Chapter 2. We thus have that $\overline{\phi}$ and $\overline{\eta}$ are given, for some real constants A_n, B_n and C_n

$(n = 0, 1, 2, \dots)$, by

$$\overline{\phi}\,(r,\theta) = \frac{r\sin\theta}{\cos\alpha} + \sum_{n=0}^{\infty} A_n r^{\left(n+\frac{1}{2}\right)\frac{\pi}{\alpha}} \sin\left(\left(n+\frac{1}{2}\right)\frac{\pi}{\alpha}\theta\right), \tag{5.2.27}$$

for $0 \leqslant r < \operatorname{cosec}\alpha$, $-\alpha \leqslant \theta \leqslant 0$, where $\overline{x} = r\cos\theta$ and $y = r\sin\theta$, whilst

$$\overline{\phi}\,(\rho,\psi) = \frac{\rho\cos\psi}{\sin\alpha} + \sum_{n=0}^{\infty} B_n \rho^{n\pi/(\pi-\alpha)} \cos\left(\frac{n\pi\psi}{\pi-\alpha}\right), \tag{5.2.28}$$

for $0 \leqslant \rho < 1$, $0 \leqslant \psi \leqslant \pi - \alpha$, where $\overline{x} - \cot\alpha = \rho\cos\psi$, and $y + 1 = \rho\sin\psi$, and finally

$$\overline{\phi}\,(\overline{x}, y) = \sum_{n=0}^{\infty} C_n e^{-\left(n+\frac{1}{2}\right)\pi\overline{x}} \sin\left(\left(n+\frac{1}{2}\right)\pi y\right), \tag{5.2.29}$$

for $\overline{x} > \cot\alpha$, $-1 \leqslant y \leqslant 0$, after which

$$\overline{\eta}\,(\overline{x}) = -\frac{1}{2} - \frac{1}{2}\cos\alpha \sum_{n=0}^{\infty} \left(n+\frac{1}{2}\right)\frac{\pi}{\alpha} A_n \overline{x}^{\left(n+\frac{1}{2}\right)\frac{\pi}{\alpha}-1}, \tag{5.2.30}$$

for $0 \leqslant \overline{x} < \operatorname{cosec}\alpha$, and

$$\overline{\eta}\,(\overline{x}) = -\frac{1}{2}\cos\alpha \sum_{n=0}^{\infty} \left(n+\frac{1}{2}\right)\pi C_n e^{-\left(n+\frac{1}{2}\right)\pi\overline{x}}, \tag{5.2.31}$$

for $\overline{x} \geqslant \operatorname{cosec}\alpha$. It follows from (5.2.27) and (5.2.30) that, as $(\overline{x}, y) \to (0,0)$, we have

$$\overline{\phi}\,(r,\theta) = \frac{r\sin\theta}{\cos\alpha} + A_0(\alpha)\, r^{\frac{\pi}{2\alpha}} \sin\frac{\pi\theta}{2\alpha} + O\left(r^{\frac{3\pi}{2\alpha}}\right),$$
$$\text{as} \quad r \to 0^+, \ \text{with} \ -\alpha \leqslant \theta \leqslant 0; \tag{5.2.32}$$

$$\overline{\eta}\,(\overline{x}) = -\frac{1}{2} - A_0(\alpha)\,\frac{\pi}{4\alpha}\cos\alpha\ \overline{x}^{\frac{\pi}{2\alpha}-1} + O\left(\overline{x}^{\frac{3\pi}{2\alpha}-1}\right), \qquad \text{as} \quad \overline{x} \to 0^+; \tag{5.2.33}$$

where r and θ are polar coordinates given by $\overline{x} = r\cos\theta$, $y = r\sin\theta$, and $A_0(\alpha)$ as given in (2.0.15) and displayed in Figure 2.3.

As before, (5.2.33) reveals a weak singularity in $\overline{\eta}'(\overline{x})$ as $\overline{x} \to 0^+$. This singular behaviour as $\overline{x} \to 0^+$ is compounded in higher-order terms in the outer region asymptotic expansion for η in (5.2.16), and also, as $r \to 0$, in the outer region asymptotic expansion for ϕ in (5.2.15), and so the regularity conditions (1.2.30) and (1.2.31) fail to be satisfied by the outer region asymptotic expansions (5.2.15) and (5.2.16) in a neighbourhood of the initial point of intersection of the plate and free surface, where $(\overline{x}, y) = o(1)$ as $\delta \to 0$. Therefore, in order to capture the full regularity in the neighbourhood of the intersection point of the plate and the free surface, we introduce an *inner asymptotic region*, in which $(\overline{x}, y) = o(1)$ as $\delta \to 0$. The structure of the inner asymptotic region is now considered in detail in the next section.

5.2.2 Inner Asymptotic Region

In this section we introduce the inner asymptotic region associated with $[IBVP]''$ when $(\overline{x}, y) = o(1)$ as $\delta \to 0$. Specifically, following Section 5.2.1 we write $(\overline{x}, y) = O(\overline{\nu}(\delta))$ with $\overline{\nu}(\delta) = o(1)$ as $\delta \to 0$. It then follows from (5.2.16), (5.2.26) and (5.2.33) that $\eta = O\left(\delta^{2/\gamma}\right)$ as $\delta \to 0$ in the inner asymptotic region, and so, to capture the free surface in the inner asymptotic region, we must take $\overline{\nu}(\delta) = O\left(\delta^{2/\gamma}\right)$ as $\delta \to 0$; therefore, without loss of generality, we set $\overline{\nu}(\delta) = \delta^{2/\gamma}$. An examination of (5.2.15), (5.2.25) and (5.2.32) then requires that $\phi = O\left(\delta^{3/\gamma}\right)$ as $\delta \to 0$ in the inner asymptotic region. Finally, the intersection point of the free surface and the plate must be captured in the inner asymptotic region, and so, $\overline{x}_p(\tau) = O\left(\delta^{2/\gamma}\right)$ as $\delta \to 0$. A sketch of the location of the inner asymptotic region is illustrated in Figure 5.6.

Formally we introduce scaled inner region coordinates (X, Y) by

$$\overline{x} = \delta^{2/\gamma} X, \qquad y = \delta^{2/\gamma} Y, \tag{5.2.34}$$

with $(X, Y) = O(1)$ as $\delta \to 0$ in the inner asymptotic region. The location of the plate in

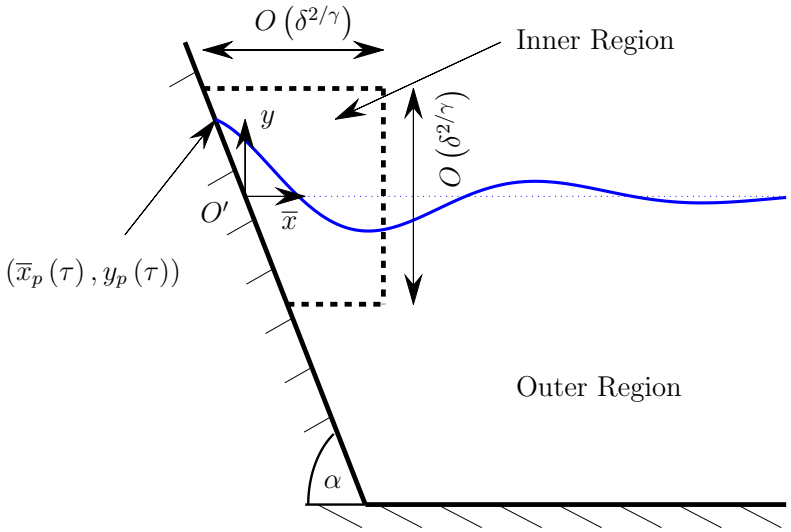

Figure 5.6: A sketch of the location of the inner asymptotic region for the case $(\alpha, \mu) \in \left(\frac{1}{4}\pi, \frac{1}{2}\pi\right) \times \mathcal{G}\left(\delta\right)$

the inner asymptotic region is given by $Y = -X\tan\alpha$, whilst the plate and free surface intersection point is denoted by $(X, Y) = \left(X_p\left(\tau\right), Y_p\left(\tau\right)\right)$, with,

$$\overline{x}_p\left(\tau\right) = \delta^{2/\gamma} X_p\left(\tau\right), \qquad y_p\left(\tau\right) = \delta^{2/\gamma} Y_p\left(\tau\right), \tag{5.2.35}$$

and $\left(X_p\left(\tau\right), Y_p\left(\tau\right)\right) = O\left(1\right)$ as $\delta \to 0$ in the inner asymptotic region. We now write the free surface and velocity potential in the inner asymptotic region as

$$\eta\left(X, \tau\right) = \delta^{2/\gamma}\eta_I\left(X, \tau\right), \qquad X \geqslant X_p\left(\tau\right),\ \tau \geqslant 0; \tag{5.2.36}$$

$$\phi\left(X, Y, \tau\right) = \delta^{3/\gamma}\phi_I\left(X, Y, \tau\right), \qquad X \geqslant X_p\left(\tau\right),\ -X\tan\alpha \leqslant Y \leqslant \eta_I\left(X, \tau\right),\ \tau \geqslant 0; \tag{5.2.37}$$

with $\eta_I\left(X, \tau\right), \phi_I\left(X, Y, \tau\right) = O\left(1\right)$ as $\delta \to 0$. The inner region asymptotic expansions are

then introduced as,

$$\eta_I(X,\tau) = \tilde{\eta}_0(X,\tau) + \delta^{\left(\frac{\pi}{\alpha}-2\right)/\gamma}\tilde{\eta}_1(X,\tau) + o\left(\delta^{\left(\frac{\pi}{\alpha}-2\right)/\gamma}\right), \tag{5.2.38}$$

$$\phi_I(X,Y,\tau) = \tilde{\phi}_0(X,Y,\tau) + \delta^{\left(\frac{\pi}{\alpha}-2\right)/\gamma}\tilde{\phi}_1(X,Y,\tau) + o\left(\delta^{\left(\frac{\pi}{\alpha}-2\right)/\gamma}\right), \tag{5.2.39}$$

as $\delta \to 0$ with $(X,Y) = O(1)$ in the inner asymptotic region. Finally, it follows from (5.2.34), (5.2.35), (5.2.36) and (5.2.38) that we expand $X_p(\tau)$ in the form

$$X_p(\tau) = X_0(\tau) + \delta^{\left(\frac{\pi}{\alpha}-2\right)/\gamma}X_1(\tau) + o\left(\delta^{\left(\frac{\pi}{\alpha}-2\right)/\gamma}\right), \tag{5.2.40}$$

as $\delta \to 0$, with

$$Y_p(\tau) = -X_p(\tau)\tan\alpha. \tag{5.2.41}$$

The free surface in the inner asymptotic region is located at

$$Y = \eta_I(X,\tau), \quad X > X_p(\tau),\ \tau \geqslant 0, \tag{5.2.42}$$

whilst the spatio-temporal domain in the inner asymptotic region is

$$\mathcal{D}_I(\tau) = \{(X,Y) : X > X_p(\tau), -X\tan\alpha < Y < \eta_I(X,\tau)\}, \tag{5.2.43}$$

for $\tau \geqslant 0$, with closure $\overline{\mathcal{D}}_I(\tau)$. A sketch of the inner asymptotic region geometry is given in Figure 5.7.

We now write $[IBVP]''$ in terms of the inner asymptotic region coordinates (X,Y), and τ, and the inner asymptotic region variables ϕ_I, η_I, and X_p, to obtain,

$$\widehat{\nabla}^2\phi_I = 0, \qquad (X,Y) \in \mathcal{D}_I(\tau),\ \tau > 0; \tag{5.2.44}$$

$$\widehat{\nabla}\phi_I \cdot \hat{\mathbf{n}} = -\tau\cos\alpha + \nu(\delta)\tau\overline{\mu}\cos\alpha, \qquad X > X_p(\tau),\ Y = -X\tan\alpha,\ \tau > 0; \tag{5.2.45}$$

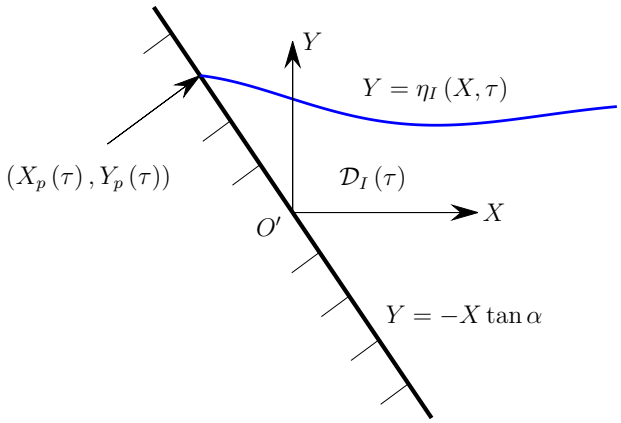

Figure 5.7: The inner asymptotic region geometry as $\delta \to 0$ for the case $(\alpha,\mu) \in \left(\frac{1}{4}\pi, \frac{1}{2}\pi\right) \times \mathcal{G}(\delta)$

$$\eta_{I,\tau} + \left[\phi_{I,X} + \tau\cot\alpha\right]\eta_{I,X} - \phi_{I,Y} - \nu(\delta)\,\tau\overline{\mu}\cot\alpha\;\eta_{I,X} = 0,$$
$$X > X_p(\tau),\; Y = \eta_I(X,\tau),\; \tau > 0; \quad (5.2.46)$$

$$\phi_{I,\tau} + \tau\cot\alpha\;\phi_{I,X} + \frac{1}{2}\left|\widehat{\nabla}\phi_I\right|^2 + \eta - \nu(\delta)\,\tau\overline{\mu}\cot\alpha\;\phi_{I,X} = 0,$$
$$X > X_p(\tau),\; Y = \eta_I(X,\tau),\; \tau > 0; \quad (5.2.47)$$

$$\eta_I(X_p(\tau),\tau) = -X_p(\tau)\tan\alpha, \qquad \tau > 0; \quad (5.2.48)$$

$$\phi_I(X,Y,0) = 0, \qquad (X,Y) \in \mathcal{D}_I(0); \quad (5.2.49)$$

$$\eta_I(X,0) = \delta^{1-2/\gamma}\eta_0\left(\delta^{2/\gamma-1}X\right), \qquad X \geqslant X_0(0); \quad (5.2.50)$$

with $\widehat{\nabla} = (\partial/\partial X, \partial/\partial Y)$. On substituting from (5.2.38) - (5.2.40) into (5.2.44) - (5.2.50) we obtain, at leading order, the following nonlinear harmonic evolution free boundary problem for $\tilde{\phi}_0(X,Y,\tau)$, $\tilde{\eta}_0(X,\tau)$, and $X_0(\tau)$, namely

$$\widehat{\nabla}^2\tilde{\phi}_0 = 0, \qquad X > X_0(\tau),\; -X\tan\alpha < Y < \tilde{\eta}_0(X,\tau),\; \tau > 0; \quad (5.2.51)$$

$$\widehat{\nabla}\phi_0 \cdot \hat{\mathbf{n}} = -\tau\cos\alpha, \qquad X > X_0(\tau),\; Y = -X\tan\alpha,\; \tau > 0; \quad (5.2.52)$$

$$\tilde{\eta}_{0,\tau} + \left[\tilde{\phi}_{0,X} + \tau\cot\alpha\right]\tilde{\eta}_{0,X} - \tilde{\phi}_{0,Y} = 0, \qquad X > X_0(\tau),\ Y = \tilde{\eta}_0(X,\tau),\ \tau > 0; \quad (5.2.53)$$

$$\tilde{\phi}_{0,\tau} + \tau\cot\alpha\ \tilde{\phi}_{0,X} + \frac{1}{2}\left|\widehat{\nabla}\tilde{\phi}_0\right|^2 + \tilde{\eta}_0 = 0, \qquad X > X_0(\tau),\ Y = \tilde{\eta}_0(X,\tau),\ \tau > 0; \quad (5.2.54)$$

$$\tilde{\phi}_0(X,Y,0) = 0, \qquad X \geqslant 0,\ -X\tan\alpha \leqslant Y \leqslant 0; \quad (5.2.55)$$

$$\tilde{\eta}_0(X,0) = 0, \qquad X \geqslant 0; \quad (5.2.56)$$

$$\tilde{\eta}_0(X_0(\tau),\tau) = -X_0(\tau)\tan\alpha, \qquad \tau > 0. \quad (5.2.57)$$

The problem (5.2.51) - (5.2.57) must be completed by asymptotic matching conditions between the inner asymptotic region and outer asymptotic region. Following Van Dyke's Matching Principle (see, for example, [28]), we obtain

$$\tilde{\phi}_0(R,\theta,\tau) \sim -\tau R\sin\theta \quad \text{as} \quad R\to\infty,\ -\alpha < \theta < 0,\ \tau > 0; \quad (5.2.58)$$

$$\tilde{\eta}_0(X,\tau) \sim -\frac{1}{2}\tau^2 \quad \text{as} \quad X\to\infty,\ \tau > 0; \quad (5.2.59)$$

where R and θ are polar coordinates given by $X = R\cos\theta$, $Y = R\sin\theta$. Although the problem (5.2.51) - (5.2.57) is nonlinear, the simple nature of the matching conditions mean that it is readily established that the exact solution to the leading order problem is given by

$$\tilde{\eta}_0(X,\tau) = -\frac{1}{2}\tau^2, \qquad X \geqslant X_0(\tau),\ \tau \geqslant 0, \quad (5.2.60)$$

$$\tilde{\phi}_0(X,Y,\tau) = -\tau Y - \frac{1}{6}\tau^3, \qquad X \geqslant X_0(\tau),\ -X\tan\alpha \leqslant Y \leqslant -\frac{1}{2}\tau^2,\ \tau \geqslant 0, \quad (5.2.61)$$

with

$$X_0(\tau) = \frac{1}{2}\tau^2\cot\alpha, \qquad \tau \geqslant 0. \quad (5.2.62)$$

This is represented in the inner asymptotic region in Figure 5.8a. We now formulate the problem at $O\left(\delta^{1-\frac{2\alpha}{\pi}}\right)$, where it is convenient to introduce the coordinates $\left(\overline{X},\overline{Y}\right)$,

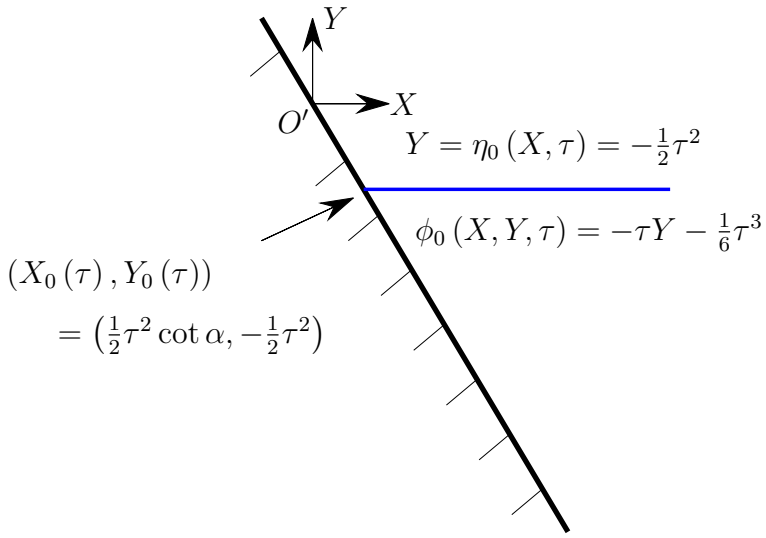

(a) Solution of $[IBVP]''$ at leading order in the inner asymptotic region

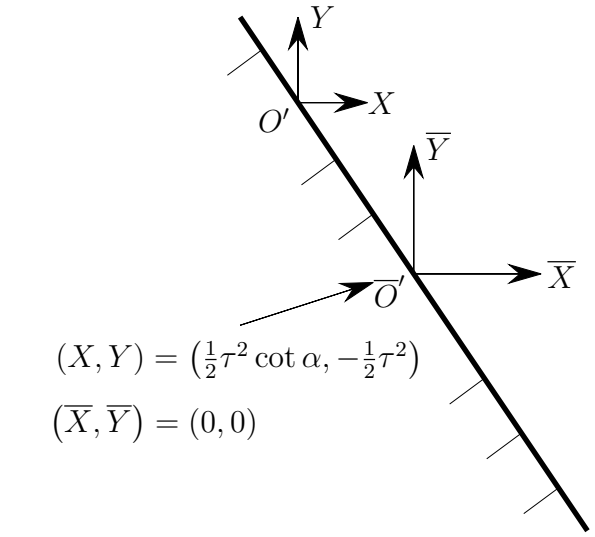

(b) $\left(\overline{X},\overline{Y}\right)$ coordinate system in the inner asymptotic region

Figure 5.8: Sketches in the inner asymptotic region for $\tau > 0$, as $\delta \to 0$, for the case $(\alpha,\mu) \in \left(\frac{1}{4}\pi, \frac{1}{2}\pi\right) \times \mathcal{G}(\delta)$

according to

$$X = \frac{1}{2}\tau^2 \cot\alpha + \overline{X}, \qquad Y = -\frac{1}{2}\tau^2 + \overline{Y}, \tag{5.2.63}$$

as shown in Figure 5.8b. We obtain the following linear, harmonic evolution problem for $\tilde{\phi}_1\left(\overline{X}, \overline{Y}, \tau\right)$, $\tilde{\eta}_1\left(\overline{X}, \tau\right)$ and $X_1(\tau)$, namely,

$$\overline{\nabla}^2 \tilde{\phi}_1 = 0, \qquad \overline{X} > 0,\ -\overline{X}\tan\alpha < \overline{Y} < 0,\ \tau > 0; \tag{5.2.64}$$

$$\overline{\nabla}\tilde{\phi}_1 \cdot \hat{\mathbf{n}} = 0, \qquad \overline{X} > 0,\ \overline{Y} = -\overline{X}\tan\alpha,\ \tau > 0; \tag{5.2.65}$$

$$\tilde{\eta}_{1,\tau} - \tilde{\phi}_{1,\overline{Y}} = 0, \qquad \overline{X} > 0,\ \overline{Y} = 0,\ \tau > 0; \tag{5.2.66}$$

$$\tilde{\phi}_{1,\tau} = 0, \qquad \overline{X} > 0,\ \overline{Y} = 0,\ \tau > 0; \tag{5.2.67}$$

$$\tilde{\phi}_1\left(\overline{R}, \theta, \tau\right) = \tau A_0(\alpha)\cos\alpha\ \overline{R}^{\frac{\pi}{2\alpha}} \cos\frac{\pi}{2\alpha}(\theta + \alpha) + o\left(\overline{R}^{\frac{\pi}{2\alpha}}\right)$$

$$\text{as} \quad \overline{R} \to \infty,\ -\alpha < \theta < 0,\ \tau > 0; \tag{5.2.68}$$

$$\tilde{\eta}_1\left(\overline{X}, \tau\right) = -\tau^2 A_0(\alpha)\frac{\pi}{4\alpha}\cos\alpha\ \overline{X}^{\frac{\pi}{2\alpha}-1} + o\left(\overline{X}^{\frac{\pi}{2\alpha}-1}\right) \quad \text{as} \quad \overline{X} \to \infty,\ \tau > 0; \tag{5.2.69}$$

$$\tilde{\phi}_1\left(\overline{X}, \overline{Y}, 0\right) = 0, \qquad \overline{X} \geqslant 0,\ -X\tan\alpha \leqslant \overline{Y} \leqslant 0; \tag{5.2.70}$$

$$\tilde{\eta}_1\left(\overline{X}, 0\right) = 0, \qquad \overline{X} \geqslant 0. \tag{5.2.71}$$

Here $\overline{\nabla} = \left(\partial/\partial\overline{X}, \partial/\partial\overline{Y}\right)$, (5.2.68) and (5.2.69) are the matching conditions with the outer asymptotic region, and we have introduced polar coordinates $\left(\overline{R}, \theta\right)$, given by $\overline{X} = \overline{R}\cos\theta$, $\overline{Y} = \overline{R}\sin\theta$. Finally we have

$$X_1(\tau) = -\tilde{\eta}_1(0, \tau)\cot\alpha, \qquad \tau > 0. \tag{5.2.72}$$

It is straightforward to show that, in this degenerate case, the solution to the problem (5.2.64) - (5.2.71) with least singular behaviour at $\left(\overline{X}, \overline{Y}\right) = (0, 0)$ is simply given by the

far-field forms, that is

$$\tilde{\phi}_1\left(\overline{R},\theta,\tau\right) = \tau A_0\left(\alpha\right)\cos\alpha\ \overline{R}^{\frac{\pi}{2\alpha}}\cos\frac{\pi}{2\alpha}\left(\theta+\alpha\right),$$

$$\overline{R}>0,\ -\alpha<\theta<0,\ \tau>0; \tag{5.2.73}$$

$$\tilde{\eta}_1\left(\overline{X},\tau\right) = -\tau^2 A_0\left(\alpha\right)\frac{\pi}{4\alpha}\cos\alpha\ \overline{X}^{\frac{\pi}{2\alpha}-1}, \qquad \overline{X}>0,\ \tau>0. \tag{5.2.74}$$

We see from (5.2.73) and (5.2.74) that a weak nonuniformity in derivatives $\left(\eta_{I,\overline{X}},\overline{\nabla}\phi_I\right)$ persists close to the contact point and, in particular, when $\overline{X},\ \overline{Y} = O\left(\delta^{\frac{\pi}{2\alpha}-1}\right)$. This requires the introduction of an *inner-inner asymptotic region*, in which $\overline{X},\ \overline{Y} = O\left(\delta^{\frac{\pi}{2\alpha}-1}\right)$ as $\delta\to 0$. The structure of the inner-inner asymptotic region is now considered in detail in the next section.

5.2.3 Inner-Inner Asymptotic Region

In this section we introduce the inner-inner asymptotic region associated with $[IBVP]''$ when $\left(\overline{X},\overline{Y}\right) = o\left(1\right)$ as $\delta\to 0$, with $\alpha\in\left(\frac{1}{4}\pi,\frac{1}{2}\pi\right)$. Specifically, following Section 5.2.2, we write $\left(\overline{X},\overline{Y}\right) = O\left(\Delta\left(\delta\right)\right)$ with $\Delta\left(\delta\right) = o\left(1\right)$ as $\delta\to 0$ in the inner-inner asymptotic region. It then follows from (5.2.38), together with (5.2.60) and (5.2.74) that $\overline{Y}_I = \frac{1}{2}\tau^2+\eta_I = O\left(\delta^{\left(\frac{\pi}{\alpha}-2\right)/\gamma}\Delta\left(\delta\right)^{\frac{\pi}{2\alpha}-1}\right)$ as $\delta\to 0$ in the inner-inner asymptotic region. The free-surface must be captured in the inner-inner asymptotic region. This requires

$$\Delta\left(\delta\right) = O\left(\delta^{\frac{\pi}{2\alpha}-1}\right), \tag{5.2.75}$$

as $\delta\to 0$. A sketch of the location of the inner-inner asymptotic region is illustrated in Figure 5.9.

Formally, we introduce scaled inner-inner asymptotic region coordinates $(\tilde{x},\tilde{y})$ by

$$\overline{X} = \delta^{\frac{\pi}{2\alpha}-1}\tilde{x}, \qquad \overline{Y} = \delta^{\frac{\pi}{2\alpha}-1}\tilde{y}, \tag{5.2.76}$$

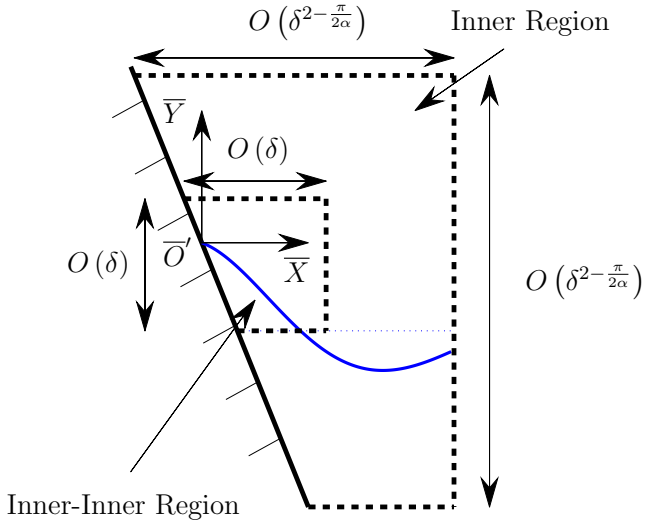

Figure 5.9: A sketch of the location of the inner-inner asymptotic region for the case $(\alpha, \mu) \in \left(\frac{1}{4}\pi, \frac{1}{2}\pi\right) \times \mathcal{G}(\delta)$

with $(\tilde{x}, \tilde{y}) = O(1)$ as $\delta \to 0$ in the inner-inner asymptotic region. The location of the plate in the inner-inner asymptotic region is given by $\tilde{y} = -\tilde{x}\tan\alpha$, whilst the intersection point of the plate and the fluid free surface is denoted by $(\tilde{x}, \tilde{y}) = (\tilde{x}_p(\tau), \tilde{y}_p(\tau))$, with,

$$\overline{X}_p(\tau) = \delta^{\frac{\pi}{2\alpha}-1}\tilde{x}_p(\tau), \qquad \overline{Y}_p(\tau) = \delta^{\frac{\pi}{2\alpha}-1}\tilde{y}_p(\tau), \tag{5.2.77}$$

for $\tau > 0$, with $(\tilde{x}_p(\tau), \tilde{y}_p(\tau)) = O(1)$ as $\delta \to 0$ in the inner-inner asymptotic region. An examination of (5.2.38) and (5.2.39), together with (5.2.60), (5.2.61), (5.2.73), and (5.2.74) reveals that $\eta_I = -\frac{1}{2}\tau^2 + O\left(\delta^{\frac{\pi}{2\alpha}-1}\right)$ and $\phi_i = \frac{1}{3}\tau^3 - \delta^{\frac{\pi}{2\alpha}-1}\tau\tilde{y} + O\left(\delta^{\frac{\pi}{\alpha}-2}\right)$ as $\delta \to 0$ in the inner-inner asymptotic region. We now write the free surface and velocity potential in the inner-inner asymptotic region as

$$\eta_I(\tilde{x}, \tau) = -\frac{1}{2}\tau^2 + \delta^{\frac{\pi}{2\alpha}-1}\eta_{II}(\tilde{x}, \tau), \qquad \tilde{x} > \tilde{x}_p(\tau),\ \tau \geqslant 0; \tag{5.2.78}$$

$$\phi_I(\tilde{x}, \tilde{y}, \tau) = \frac{1}{3}\tau^3 - \delta^{\frac{\pi}{2\alpha}-1}\tau\tilde{y} + \delta^{\frac{\pi}{\alpha}-2}\phi_{II}(\tilde{x}, \tilde{y}, \tau), \qquad (\tilde{x}, \tilde{y}) \in \mathcal{D}_{II}(\tau),\ \tau \geqslant 0; \tag{5.2.79}$$

with $\eta_{II}(\tilde{x},\tau)$, $\phi_{II}(\tilde{x},\tilde{y},\tau) = O(1)$ as $\delta \to 0$. The inner-inner region asymptotic expansions are then introduced as,

$$\eta_{II}(\tilde{x},\tau) = \widehat{\eta}_0(\tilde{x},\tau) + o(1), \tag{5.2.80}$$

$$\phi_{II}(\tilde{x},\tilde{y},\tau) = \widehat{\phi}_0(\tilde{x},\tilde{y},\tau) + o(1), \tag{5.2.81}$$

as $\delta \to 0$, with $(\tilde{x},\tilde{y}) = O(1)$ in the inner-inner asymptotic region. Finally it follows from (5.2.77) - (5.2.78), and (5.2.80) that we expand $\tilde{x}_p(\tau)$ in the form

$$\tilde{x}_p(\tau) = \tilde{x}_0(\tau) + o(1), \tag{5.2.82}$$

as $\delta \to 0$, with

$$\tilde{y}_p(\tau) = -\tilde{x}_p(\tau)\tan\alpha. \tag{5.2.83}$$

The free surface in the inner-inner asymptotic region is located at

$$\tilde{y} = \eta_{II}(\tilde{x},\tau), \qquad \tilde{x} > \tilde{x}_p(\tau),\ \tau \geqslant 0, \tag{5.2.84}$$

whilst the spatio-temporal domain in the inner-inner asymptotic region is

$$\mathcal{D}_{II}(\tau) = \left\{(\tilde{x},\tilde{y}) : \tilde{x} > \tilde{x}_p(\tau),\ -\tilde{x}\tan\alpha < \tilde{y} < \eta_{II}(\tilde{x},\tau)\right\}, \tag{5.2.85}$$

for $\tau \geqslant 0$, with closure $\overline{\mathcal{D}}_{II}(\tau)$. A sketch of the inner-inner asymptotic region geometry is given in Figure 5.10.

An examination of the plate boundary condition (5.2.6) along with (5.2.76) and (5.2.79) then requires that $\nu(\delta) = O\left(\delta^{\frac{\pi}{2\alpha}-1}\right)$ (from which it follows that $\mathcal{G}(\nu) = O\left(\delta^{\frac{\pi}{2\alpha}-1}\right)$),

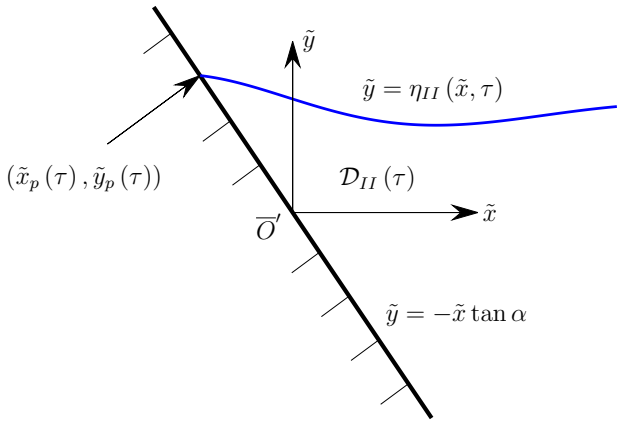

Figure 5.10: The inner-inner asymptotic region geometry as $\delta \to 0$ for the case $(\alpha, \mu) \in \left(\frac{1}{4}\pi, \frac{1}{2}\pi\right) \times \mathcal{G}(\delta)$

and so, without loss of generality, we choose

$$\nu(\delta) = \delta^{\frac{\pi}{2\alpha}-1}. \tag{5.2.86}$$

We are now able to write $[IBVP]''$ in terms of the inner-inner asymptotic region coordinates $(\tilde{x}, \tilde{y})$, and τ, and the inner-inner asymptotic region variables ϕ_{II}, η_{II} and $\tilde{x}_p$, to obtain,

$$\widetilde{\nabla}^2 \phi_{II} = 0, \qquad (\tilde{x}, \tilde{y}) \in \mathcal{D}_{II}(\tau),\ \tau > 0; \tag{5.2.87}$$

$$\widetilde{\nabla}\phi_{II} \cdot \hat{\mathbf{n}} = \tau\overline{\mu}\cos\alpha, \qquad \tilde{x} > \tilde{x}_p(\tau),\ \tilde{y} = -\tilde{x}\tan\alpha,\ \tau > 0; \tag{5.2.88}$$

$$\eta_{II,\tau} + \phi_{II,\tilde{x}}\eta_{II,\tilde{x}} - \tau\overline{\mu}\cot\alpha\ \eta_{II,\tilde{x}} - \phi_{II,\tilde{y}} = 0,\ \tilde{x} > \tilde{x}_p(\tau),\ \tilde{y} = \eta_{II}(\tilde{x}, \tau),\ \tau > 0; \tag{5.2.89}$$

$$\phi_{II,\tau} - \tau\overline{\mu}\cot\alpha\ \phi_{II,\tilde{x}} + \frac{1}{2}\left|\widetilde{\nabla}\phi_{II}\right|^2 = 0, \qquad \tilde{x} > \tilde{x}_p(\tau),\ \tilde{y} = \eta_{II}(\tilde{x}, \tau),\ \tau > 0; \tag{5.2.90}$$

$$\eta_{II}(\tilde{x}_p(\tau), \tau) = -\tilde{x}_p(\tau)\tan\alpha, \qquad \tau > 0; \tag{5.2.91}$$

$$\phi_{II}\left(\tilde{x},\tilde{y},0\right)=0, \qquad \left(\tilde{x},\tilde{y}\right)\in\mathcal{D}_{II}\left(0\right); \quad (5.2.92)$$

$$\eta_{II}\left(\tilde{x},0\right)=\eta_0\left(\tilde{x}\right), \qquad \tilde{x}>\tilde{x}_p\left(0\right); \quad (5.2.93)$$

with $\widetilde{\nabla}=\left(\partial/\partial\tilde{x},\partial/\partial\tilde{y}\right)$. On substituting from (5.2.80) - (5.2.82) into (5.2.87) - (5.2.93) we obtain, at leading order, the following nonlinear harmonic evolution free boundary problem for $\widehat{\phi}_0\left(\tilde{x},\tilde{y},\tau\right)$, $\widehat{\eta}_0\left(\tilde{x},\tau\right)$ and $\tilde{x}_0\left(\tau\right)$, namely

$$\widetilde{\nabla}^2\widehat{\phi}_0=0, \qquad \tilde{x}>\tilde{x}_0\left(\tau\right),\ -\tilde{x}\tan\alpha<\tilde{y}<\widehat{\eta}_0\left(\tilde{x},\tau\right),\ \tau>0; \quad (5.2.94)$$

$$\widetilde{\nabla}\widehat{\phi}_0\cdot\hat{\mathbf{n}}=\tau\overline{\mu}\cos\alpha, \qquad \tilde{x}>\tilde{x}_0\left(\tau\right),\ \tilde{y}=-\tilde{x}\tan\alpha,\ \tau>0; \quad (5.2.95)$$

$$\widehat{\eta}_{0,\tau}+\widehat{\phi}_{0,\tilde{x}}\widehat{\eta}_{0,\tilde{x}}-\tau\overline{\mu}\cot\alpha\ \widehat{\eta}_{0,\tilde{x}}-\widehat{\phi}_{0,\tilde{y}}=0, \qquad \tilde{x}>\tilde{x}_0\left(\tau\right),\ \tilde{y}=\widehat{\eta}_0\left(\tilde{x},\tau\right),\ \tau>0; \quad (5.2.96)$$

$$\widehat{\phi}_{0,\tau}-\tau\overline{\mu}\cot\alpha\ \widehat{\phi}_{0,\tilde{x}}+\frac{1}{2}\left|\widetilde{\nabla}\widehat{\phi}_0\right|^2=0, \qquad \tilde{x}>\tilde{x}_0\left(\tau\right),\ \tilde{y}=\widehat{\eta}_0\left(\tilde{x},\tau\right),\ \tau>0; \quad (5.2.97)$$

$$\widehat{\eta}_0\left(\tilde{x}_0\left(\tau\right),\tau\right)=-\tilde{x}_0\left(\tau\right)\tan\alpha, \qquad \tau>0; \quad (5.2.98)$$

$$\widehat{\phi}_0\left(\tilde{x},\tilde{y},0\right)=0, \qquad \tilde{x}>\tilde{x}_0\left(0\right),\ -\tilde{x}\tan\alpha<\tilde{y}<\widehat{\eta}_0\left(\tilde{x},0\right); \quad (5.2.99)$$

$$\widehat{\eta}_0\left(\tilde{x},0\right)=\eta_0\left(\tilde{x}\right), \qquad \tilde{x}>\tilde{x}_0\left(0\right). \quad (5.2.100)$$

The problem (5.2.94) - (5.2.100) must be completed by asymptotic matching conditions between the inner-inner asymptotic region and the inner asymptotic region. Following Van Dyke's Matching Principle (see, for example, [28]), we obtain,

$$\widehat{\phi}_0\left(\tilde{r},\theta,\tau\right)=\tau A_0\left(\alpha\right)\cos\alpha\ \tilde{r}^{\frac{\pi}{2\alpha}}\cos\frac{\pi}{2\alpha}\left(\theta+\alpha\right)+o\left(\tilde{r}^{\frac{\pi}{2\alpha}}\right)$$
$$\text{as} \quad \tilde{r}\to\infty,\ -\alpha<\theta<0,\ \tau>0; \quad (5.2.101)$$

$$\widehat{\eta}_0\left(\tilde{x},\tau\right)=-\tau^2A_0\left(\alpha\right)\frac{\pi}{4\alpha}\cos\alpha\ \tilde{x}^{\frac{\pi}{2\alpha}-1}+o\left(\tilde{x}^{\frac{\pi}{2\alpha}-1}\right) \qquad \text{as} \qquad \tilde{x}\to\infty,\ \tau>0; \quad (5.2.102)$$

where $\tilde{r}$ and θ are polar coordinates given by $\tilde{x}=\tilde{r}\cos\theta$, $\tilde{y}=\tilde{r}\sin\theta$. Finally we have

$$\tilde{x}_0\left(\tau\right)=-\widehat{\eta}_0\left(\tilde{x}_0\left(\tau\right),\tau\right)\cot\alpha, \qquad \tau>0. \quad (5.2.103)$$

It is now convenient to introduce the variables ψ and ξ, according to

$$\widehat{\phi}_0(\tilde{x},\tilde{y},\tau) = \psi(\hat{x},\hat{y},\tau) + \overline{\mu}\tau\tilde{y} - \frac{1}{3}\overline{\mu}^2\tau^3, \tag{5.2.104}$$

$$\widehat{\eta}_0(\tilde{x},\tau) = \xi(\tilde{x},\tau) + \frac{1}{2}\overline{\mu}\tau^2, \tag{5.2.105}$$

with the forms of (5.2.104) and (5.2.105) chosen for algebraic convenience at a later stage. We now write the problem (5.2.94) - (5.2.102) in terms of ψ and ξ as

$$\widetilde{\nabla}^2\psi = 0, \qquad \tilde{x} > \tilde{x}_0(\tau),\ -\tilde{x}\tan\alpha < \tilde{y} < \xi(\tilde{x},\tau) + \frac{1}{2}\overline{\mu}\tau^2,\ \tau > 0; \tag{5.2.106}$$

$$\widetilde{\nabla}\psi\cdot\hat{\mathbf{n}} = 0, \qquad \tilde{x} > \tilde{x}_0(\tau),\ \tilde{y} = -\tilde{x}\tan\alpha,\ \tau > 0; \tag{5.2.107}$$

$$\xi_\tau + \psi_{\tilde{x}}\xi_{\tilde{x}} - \tau\overline{\mu}\cot\alpha\ \xi_{\tilde{x}} - \psi_{\tilde{y}} = 0, \qquad \tilde{x} > \tilde{x}_0(\tau),\ \tilde{y} = \xi(\tilde{x},\tau) + \frac{1}{2}\overline{\mu}\tau^2,\ \tau > 0; \tag{5.2.108}$$

$$\psi_\tau - \tau\overline{\mu}\cot\alpha\ \widehat{\psi}_{\tilde{x}} + \frac{1}{2}\left|\widetilde{\nabla}\psi\right|^2 = 0, \qquad \tilde{x} > \tilde{x}_0(\tau),\ \tilde{y} = \xi(\tilde{x},\tau) + \frac{1}{2}\overline{\mu}\tau^2,\ \tau > 0; \tag{5.2.109}$$

$$\xi(\tilde{x}_0(\tau),\tau) = -\tilde{x}_0(\tau)\tan\alpha - \frac{1}{2}\overline{\mu}\tau^2, \qquad \tau > 0; \tag{5.2.110}$$

$$\psi(\tilde{x},\tilde{y},0) = 0, \qquad \tilde{x} > \tilde{x}_0(0),\ -\tilde{x}\tan\alpha < \tilde{y} < \xi(\tilde{x},0); \tag{5.2.111}$$

$$\xi(\tilde{x},0) = \eta_0(\tilde{x}), \qquad \tilde{x} > \tilde{x}_0(0); \tag{5.2.112}$$

$$\psi(\tilde{r},\theta,\tau) = \tau A_0(\alpha)\cos\alpha\ \tilde{r}^{\frac{\pi}{2\alpha}}\cos\frac{\pi}{2\alpha}(\theta+\alpha) + o\left(\tilde{r}^{\frac{\pi}{2\alpha}}\right)$$
$$\text{as} \quad \tilde{r}\to\infty,\ -\alpha < \theta < 0,\ \tau > 0; \tag{5.2.113}$$

$$\xi(\tilde{x},\tau) = -\tau^2 A_0(\alpha)\frac{\pi}{4\alpha}\cos\alpha\ \tilde{x}^{\frac{\pi}{2\alpha}-1} + o\left(\tilde{x}^{\frac{\pi}{2\alpha}-1}\right) \qquad \text{as } \tilde{x}\to\infty,\ \tau > 0. \tag{5.2.114}$$

Finally we introduce the coordinates $(\hat{x},\hat{y})$, according to

$$\hat{x} = \tilde{x} + \frac{1}{2}\overline{\mu}\tau^2\cot\alpha, \qquad \hat{y} = \tilde{y} - \frac{1}{2}\overline{\mu}\tau^2. \tag{5.2.115}$$

We obtain the following nonlinear harmonic evolution free boundary problem for $\psi(\hat{x},\hat{y},\tau)$,

$\xi(\hat{x},\tau)$ and $\hat{x}_0(\tau)$, namely

$$\widehat{\nabla}^2\psi = 0, \qquad \hat{x} > \hat{x}_0(\tau),\ -\hat{x}\tan\alpha < \hat{y} < \xi(\hat{x},\tau),\ \tau > 0; \tag{5.2.116}$$

$$\widehat{\nabla}\psi\cdot\hat{\mathbf{n}} = 0, \qquad \hat{x} > \hat{x}_0(\tau),\ \hat{y} = -\hat{x}\tan\alpha,\ \tau > 0; \tag{5.2.117}$$

$$\xi_\tau + \psi_{\hat{x}}\xi_{\hat{x}} - \psi_{\hat{y}} = 0, \qquad \hat{x} > \hat{x}_0(\tau),\ \hat{y} = \xi(\hat{x},\tau),\ \tau > 0; \tag{5.2.118}$$

$$\psi_\tau + \frac{1}{2}\left|\widehat{\nabla}\psi\right|^2 + \overline{\mu}\xi = 0, \qquad \hat{x} > \hat{x}_0(\tau),\ \hat{y} = \xi(\hat{x},\tau),\ \tau > 0; \tag{5.2.119}$$

$$\xi(\hat{x}_0(\tau),\tau) = -\hat{x}_0(\tau)\tan\alpha, \qquad \tau > 0; \tag{5.2.120}$$

$$\psi(\hat{x},\hat{y},0) = 0, \qquad \hat{x} > \hat{x}_0(0),\ -\hat{x}\tan\alpha < \hat{y} < \xi(\hat{x},0); \tag{5.2.121}$$

$$\xi(\hat{x},0) = \eta_0(\hat{x}), \qquad \hat{x} > \hat{x}_0(0); \tag{5.2.122}$$

$$\psi(\hat{r},\theta,\tau) = \tau A_0(\alpha)\cos\alpha\ \hat{r}^{\frac{\pi}{2\alpha}}\cos\frac{\pi}{2\alpha}(\theta+\alpha) + o\left(\hat{r}^{\frac{\pi}{2\alpha}}\right)$$
$$\text{as} \quad \hat{r}\to\infty,\ -\alpha < \theta < 0,\ \tau > 0; \tag{5.2.123}$$

$$\xi(\hat{x},\tau) = -\tau^2 A_0(\alpha)\frac{\pi}{4\alpha}\cos\alpha\ \hat{x}^{\frac{\pi}{2\alpha}-1} + o\left(\hat{x}^{\frac{\pi}{2\alpha}-1}\right) \qquad \text{as} \quad \hat{x}\to\infty,\ \tau > 0; \tag{5.2.124}$$

where $\hat{r}$, and θ are polar coordinates given by $\hat{x} = \hat{r}\cos\theta$ and $\hat{y} = \hat{r}\sin\theta$, and $\widehat{\nabla} = (\partial/\partial\hat{x},\ \partial/\partial\hat{y})$[2], with

$$\hat{x}_0(\tau) = \tilde{x}_0(\tau) + \frac{1}{2}\overline{\mu}\tau^2\cot\alpha. \tag{5.2.125}$$

The initial boundary value evolution problem (5.2.116) - (5.2.124), henceforth referred to as $[EBVP]$, can now be solved numerically using a boundary integral method, which follows the approach discussed in Chapter 4, with implicit time-stepping to evolve the solution in time.

In solving $[EBVP]$ numerically we must specify the initial free surface profile. For the

[2]Notation not to be confused with that used in Chapter 3.

following results we have chosen $\xi(\hat{x},0)$ to be given by

$$\xi(\hat{x},0)=\eta_0(\hat{x})=\begin{cases}0.02\left(1-\cos 2\pi\hat{x}\right), & 0\leqslant\hat{x}\leqslant 1,\\ 0, & \hat{x}>1.\end{cases} \tag{5.2.126}$$

Numerical solutions of $[EBVP]$ are plotted in Figures 5.11 - 5.14. In Figure 5.11 we present the comparison between the free surface $\xi(\hat{x},\tau)$ calculated with zero initial data (shown in each plot as a dotted red line) and the free surface $\xi(\hat{x},\tau)$ calculated with the initial free surface profile given in (5.2.126) (shown in each plot as a solid blue line) for the case $\alpha=1.4$, with $\overline{\mu}=1$. It is clear to see, as predicted by the theory presented in Section 5.1.2, that, when initially perturbed, the free surface $\xi(\hat{x},\tau)$ collapses to the self-similar solution, indicating that the problem $[EBVP]$ is well-posed and stable in this case. This behaviour is typical of all pairs $(\alpha,\overline{\mu})$ tested in the range $(\alpha,\overline{\mu})\in\left(\frac{1}{4}\pi,\frac{1}{2}\pi\right)\times\mathbb{R}^{+}$, and of all initial free surface profiles $\eta_0(\hat{x})$ tested. As we decrease $\overline{\mu}$ and choose values with $\overline{\mu}<0$ we are unable to obtain numerically any converged solutions to $[EBVP]$. This indicates that the problem $[EBVP]$ is ill-posed, which is in agreement with the the theory presented in Section 5.1.2. In Figure 5.12 we present the comparison between the free surface $\xi(\hat{x},\tau)$ calculated with zero initial data (shown in each plot as a dotted red line) and the free surface $\xi(\hat{x},\tau)$ calculated with the initial free surface profile given in (5.2.126) (shown in each plot as a solid blue line) for the case $\alpha=1.4$, with $\overline{\mu}=0$. Here we see that the continuation of the numerical solution when $\overline{\mu}=0$ indicates that the case $\overline{\mu}=0$ separates the regions where the problem $[EBVP]$ is well-posed ($\overline{\mu}>0$) and ill-posed ($\overline{\mu}<0$). Finally, Figures (5.13) and (5.14) demonstrate the good agreement of the numerical solution with the far-field asymptotic form in $[EBVP]$ (5.2.124).

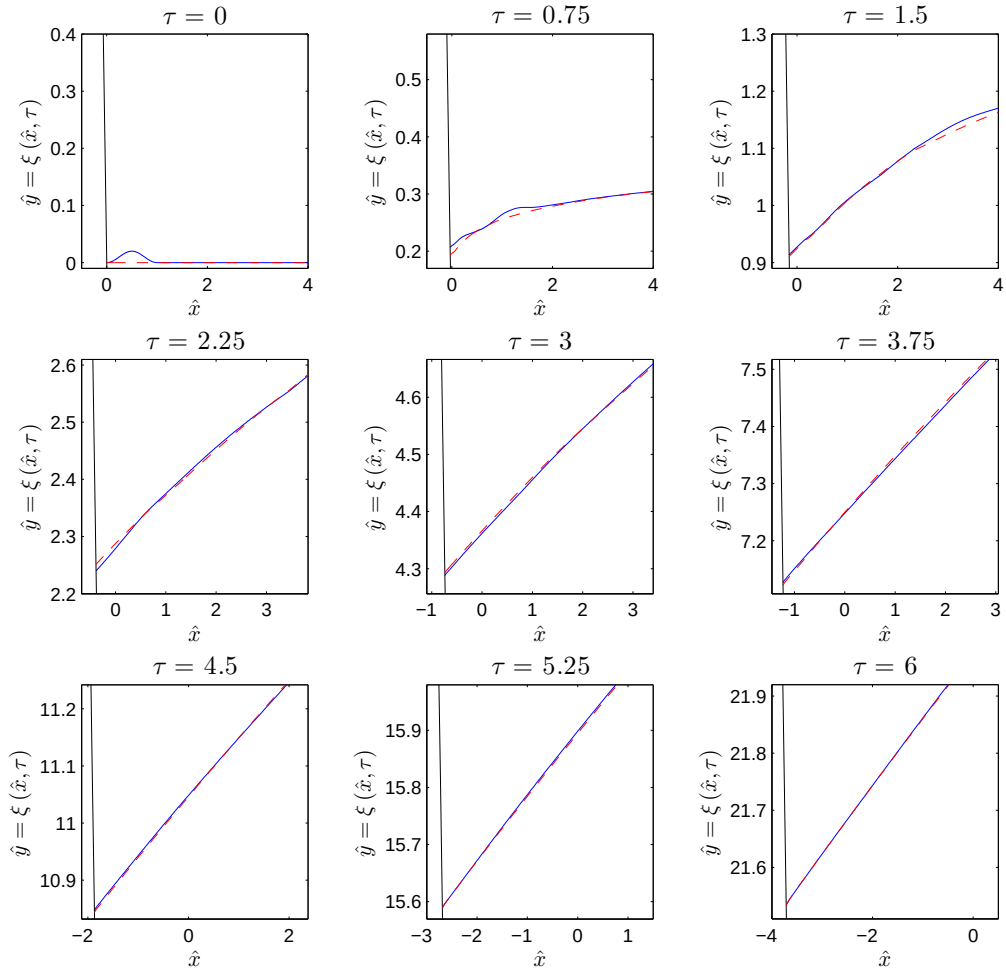

Figure 5.11: Graph of the evolution of $\xi(\hat{x}, \tau)$ against $\hat{x}$ for the numerical solution of $[EBVP]$, for increasing values of τ with $\overline{\mu} = 1$ and $\alpha = 1.4$. In each plot a black line shows the location of the plate, a dotted red line shows the solution for the case of zero initial data, and a blue line shows the solution when the initial data is as given in (5.2.126)

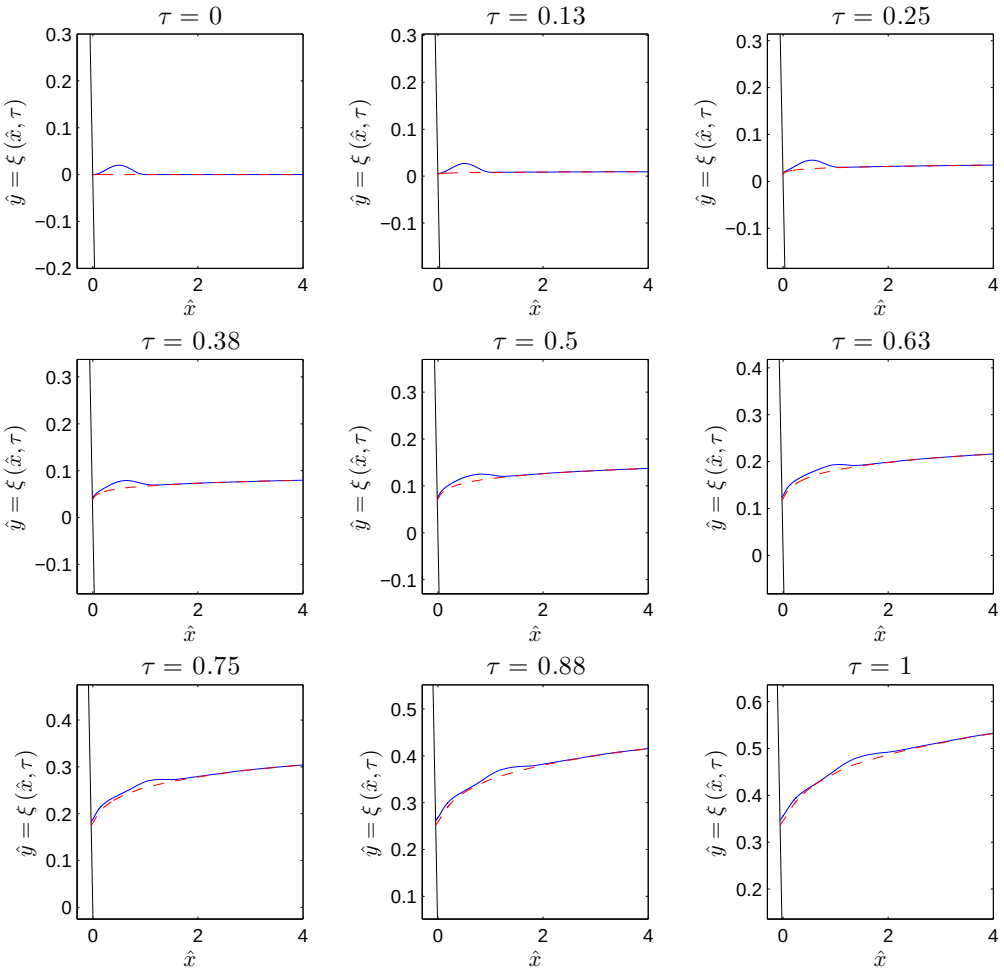

Figure 5.12: Graph of the evolution of $\xi(\hat{x}, \tau)$ against $\hat{x}$ for the numerical solution of $[EBVP]$, for increasing values of τ with $\overline{\mu} = 0$ and $\alpha = 1.4$. In each plot a black line shows the location of the plate, a dotted red line shows the solution for the case of zero initial data, and a blue line shows the solution when the initial data is as given in (5.2.126)

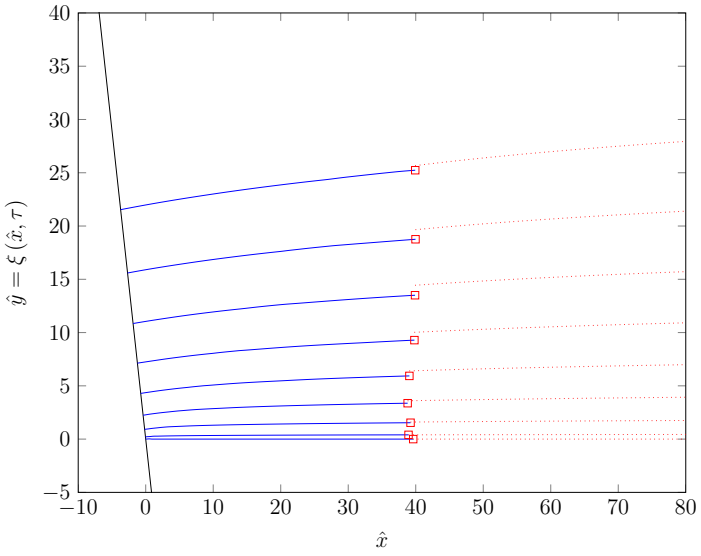

Figure 5.13: Graph of the evolution of $\xi(\hat{x}, \tau)$ against $\hat{x}$, showing agreement with the far-field asymptotic form (5.2.124) for the numerical solution of $[EBVP]$, with $\overline{\mu} = 1$, $\alpha = 1.4$, and increasing values of τ as given in Figure 5.11. In each plot a black line shows the location of the plate, and blue lines show the solution when the initial data is as given in (5.2.126)

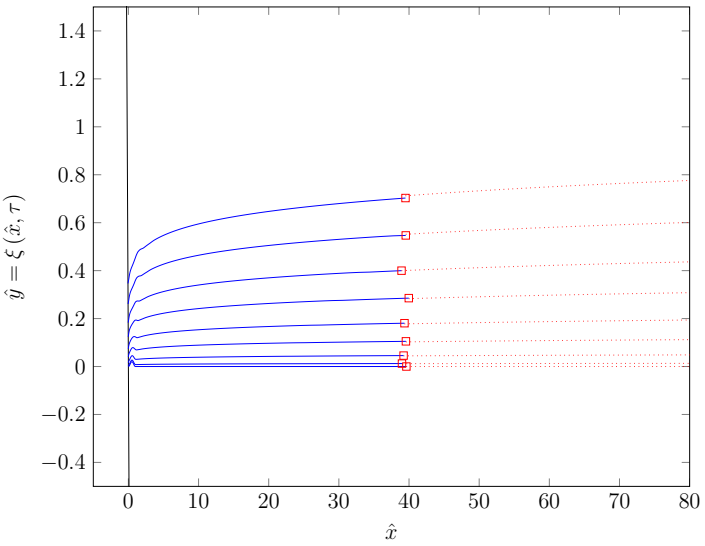

Figure 5.14: Graph of the evolution of $\xi(\hat{x}, \tau)$ against $\hat{x}$, showing agreement with the far-field asymptotic form (5.2.124) for the numerical solution of $[EBVP]$, with $\overline{\mu} = 0$, $\alpha = 1.4$, and increasing values of τ as given in Figure 5.12. In each plot a black line shows the location of the plate, and blue lines show the solution when the initial data is as given in (5.2.126)

5.3 Discussion

We have now completed the analysis of the well-posedness and stability of the problem $[IBVP]$ with respect to perturbations in initial data in the innermost asymptotic region as $t \to 0$, for each pair $(\alpha, \mu) \in \left(0, \frac{1}{2}\pi\right) \times \mathbb{R}$, where $\mu = 1 + \sigma \tan\alpha$. We introduced a perturbation to the trivial initial data in $[IBVP]$ of the form

$$\phi(\overline{x}, y, 0) = 0, \qquad \overline{x} > 0, \ -\overline{x}\tan\alpha < y < \eta(\overline{x}, 0), \tag{5.3.1}$$

$$\eta(\overline{x}, 0) = \delta\eta_0\left(\frac{\overline{x}}{\delta r}\right), \qquad \overline{x} > 0, \tag{5.3.2}$$

with $0 < \delta \ll 1$ and

$$\eta_0(\lambda) = \begin{cases} \overline{\eta}_0(\lambda), & 0 \leqslant \lambda \leqslant 1, \\ 0, & \lambda > 0, \end{cases} \tag{5.3.3}$$

where $\overline{\eta}_0(1)$, $\overline{\eta}_0'(1) = 0$ and $\overline{\eta}_0$ continuous with continuous derivatives. We have not as yet included the effects of surface tension in our model. We believe that, for those cases where $[IBVP]$ is ill-posed with respect to perturbations in initial data in the innermost asymptotic region, the inclusion of weak surface tension terms in our model will result in the governing initial boundary value problem becoming well-posed and unstable with respect to perturbations in initial data in the innermost asymptotic region.

We have drawn the following conclusions regarding the well-posedness and stability of the problem $[IBVP]$ with respect to perturbations in initial data in the innermost region:

(a) $\underline{(\alpha, \mu) \in \left(0, \frac{1}{2}\pi\right) \times \mathbb{R}^+}$

Here, the initial boundary value problem $[IBVP]$ is well-posed and stable with respect to perturbations in initial data in the inner asymptotic region as $t \to 0^+$. We anticipate that the inclusion in our model of the effect of weak surface tension will

not qualitatively change the structure of the solution in this case.

(b) $\underline{(\alpha, \mu) \in \left(0, \frac{1}{2}\pi\right) \times \mathbb{R}^-}$

Here, the initial boundary value problem $[IBVP]$ is ill-posed with respect to perturbations in initial data in the inner asymptotic region as $t \to 0^+$. We anticipate that the inclusion of weak surface tension in our model will result in the governing initial value problem $[IBVP]$ becoming well-posed but unstable with respect to perturbations in initial data in the inner asymptotic region.

(c) $\underline{(\alpha, \mu) \in \left(0, \frac{1}{4}\pi\right] \times \{0\}}$

Here, the initial boundary value problem $[IBVP]$ is well-posed and stable with respect to perturbations in initial data in the inner asymptotic region as $t \to 0^+$. We anticipate that the inclusion in our model of the effect of weak surface tension will not qualitatively change the structure of the solution in this case.

(d) $\underline{(\alpha, \mu) \in \left(\frac{1}{4}\pi, \frac{1}{2}\pi\right) \times (\mathcal{G}(\delta) \cap \mathbb{R}^+)}$

Here, the initial boundary value problem $[IBVP]$ is well-posed and stable with respect to perturbations in initial data in the inner-inner asymptotic region as $t \to 0^+$. We anticipate that the inclusion in our model of the effect of weak surface tension will not qualitatively change the structure of the solution in this case.

(e) $\underline{(\alpha, \mu) \in \left(\frac{1}{4}\pi, \frac{1}{2}\pi\right) \times (\mathcal{G}(\delta) \cap \mathbb{R}^-)}$

Here, the initial boundary value problem $[IBVP]$ is ill-posed with respect to perturbations in initial data in the inner-inner asymptotic region as $t \to 0^+$. We anticipate that the inclusion of weak surface tension in our model will result in the governing initial value problem $[IBVP]$ becoming well-posed but unstable with respect to perturbations in initial data in the inner-inner asymptotic region.

Chapter 6

Conclusions

In this thesis we have studied the problem of a rigid plate, inclined at an angle $\alpha \in \left(0, \frac{1}{2}\pi\right)$ to the horizontal, accelerating uniformly from rest, into or away from a semi-infinite expanse of inviscid, incompressible fluid, via the method of matched asymptotic expansions.

We began in an *outer asymptotic region* in which $(\overline{x}, y) = O(1)$ as $t \to 0^+$. Here, we have established that the leading order terms in the outer region asymptotic expansions for the velocity potential ϕ (2.0.1), and the free surface elevation η (2.0.2), satisfy the required regularity (1.2.30) and (1.2.31), *except* in a neighbourhood of the initial location of the intersection point of the free surface and the plate, at $(\overline{x}, y) = (0, 0)$. This motivated the introduction of an *inner asymptotic region*, in which $(\overline{x}, y) = o(1)$ as $t \to 0^+$, in order to capture the full regularity in this neighbourhood.

The results for the solution of the governing initial boundary value problem ($[IBVP]$), as $t \to 0^+$ in the inner asymptotic region, fall into four distinct cases depending upon α and $\mu = 1 + \sigma \tan \alpha$ (with σ being the dimensionless acceleration of the inclined plate).

1. $\underline{(\alpha, \mu) \in \left(0, \frac{1}{2}\pi\right) \times (0, \infty)}$

   Here, we have solved $[PBVP]^+$ numerically for each $\alpha \in \left(0, \frac{1}{2}\pi\right)$. We establish that, when $\mu > 1$, the free surface in the inner asymptotic region is monotone decreasing.

For $0 < \mu < 1$, the free surface in the inner asymptotic region is monotone increasing.

2. $(\alpha, \mu) \in \left\{\left(0, \frac{1}{2}\pi\right) \setminus \{\alpha_n^* : n = 1, 2, \dots\}\right\} \times (-\infty, 0)$

   Here, we have solved $[PBVP]^-$ numerically for each $\alpha \in \left(0, \frac{1}{2}\pi\right) \setminus \{\alpha_n^* : n = 1, 2, \dots\}$. Pairs of near resonances occur in a small neighbourhood of $\alpha = \alpha_n^*$ $(n = 1, 2, \dots)$. Away from the near resonance pairs, for those $\alpha \in \left(\alpha_1^*, \frac{1}{2}\pi\right)$, the free surface has one turning point and is initially decreasing. For angles $\alpha \in (\alpha_c^*, \alpha_1^*)$ the free surface has two turning points and is initially increasing. For angles $\alpha \in (\alpha_2^*, \alpha_c^*]$ the free surface is monotone increasing. For angles $\left(\alpha_{2n+1}^*, \alpha_{2n}^*\right)$ $(n = 1, 2, \dots)$, the free surface has $(2n - 1)$ turning points and is initially decreasing. For angles $\left(\alpha_{2n}^*, \alpha_{2n-1}^*\right)$ $(n = 2, 3, \dots)$, the free surface has $(2n - 2)$ turning points and is initially increasing.

3. $(\alpha, \mu) \in \{\alpha_n^* : n = 1, 2, \dots\} \times (-\infty, 0)$

   Here, $[PBVP]^-$ has a stationary point at the intersection point of the free surface and the inclined plate. Each angle $\alpha = \alpha_n^*$ $(n = 1, 2, \dots)$ separates the two near resonances in each near resonance pair.

4. $(\alpha, \mu) \in \left(0, \frac{1}{4}\pi\right) \times \{0\}$

   In this degenerate case, the solution to the boundary value problem (3.1.29) - (3.1.34) in the inner asymptotic region is simply given by the far-field forms (3.2.19) and (3.2.22), which remain uniform up to the intersection point of the free surface and the inclined accelerating plate.

5. $(\alpha, \mu) \in \left(\frac{1}{4}\pi, \frac{1}{2}\pi\right) \times \{0\}$

   In this degenerate case, the solution to the boundary value problem (3.1.29) - (3.1.34) in the inner asymptotic region which has least singular behaviour at the contact point is simply given by the far-field forms (3.2.19) and (3.2.22). This required the introduction of an *inner-inner asymptotic region*, in which $\left(\overline{X}, \overline{Y}\right) = o\left(t^{\Gamma}\right)$, with $\Gamma = \frac{\left(\frac{\pi}{\alpha} - 2\right)}{2\left(1 - \frac{\pi}{4\alpha}\right)}$ as $t \to 0^+$, in order to capture the full regularity at the contact point.

Here,we have solved $[RBVP]$ numerically for each $\alpha \in \left(\frac{1}{4}\pi, \frac{1}{2}\pi\right)$. We establish that the free surface in the inner-inner asymptotic region is monotone increasing, and meets the plate with a constant angle of $\frac{1}{2}\pi$ for all $\alpha \in \left(\frac{1}{4}\pi, \frac{1}{2}\pi\right)$.

We have also analysed the well-posedness and stability of the problem $[IBVP]$ with respect to perturbations in initial data in the innermost asymptotic region. We have drawn the following conclusions:

1. $(\alpha, \mu) \in \left(0, \frac{1}{2}\pi\right) \times \mathbb{R}^+$

   Here, the initial boundary value problem $[IBVP]$ is well-posed and stable with respect to perturbations in initial data in the inner asymptotic region as $t \to 0^+$. We anticipate that the inclusion in our model of the effect of weak surface tension will not qualitatively change the structure of the solution in this case.

2. $(\alpha, \mu) \in \left(0, \frac{1}{2}\pi\right) \times \mathbb{R}^-$

   Here, the initial boundary value problem $[IBVP]$ is ill-posed with respect to perturbations in initial data in the inner asymptotic region as $t \to 0^+$. We anticipate that the inclusion of weak surface tension in our model will result in the governing initial value problem $[IBVP]$ becoming well-posed but unstable with respect to perturbations in initial data in the inner asymptotic region.

3. $(\alpha, \mu) \in \left(0, \frac{1}{4}\pi\right] \times \{0\}$

   Here, the initial boundary value problem $[IBVP]$ is well-posed and stable with respect to perturbations in initial data in the inner asymptotic region as $t \to 0^+$. We anticipate that the inclusion in our model of the effect of weak surface tension will not qualitatively change the structure of the solution in this case.

4. $(\alpha, \mu) \in \left(\frac{1}{4}\pi, \frac{1}{2}\pi\right) \times (\mathcal{G}(\delta) \cap \mathbb{R}^+)$

   Here, the initial boundary value problem $[IBVP]$ is well-posed and stable with respect to perturbations in initial data in the inner-inner asymptotic region as $t \to 0^+$. We anticipate that the inclusion in our model of the effect of weak surface tension will not qualitatively change the structure of the solution in this case.

5. $(\alpha, \mu) \in \left(\frac{1}{4}\pi, \frac{1}{2}\pi\right) \times (\mathcal{G}(\delta) \cap \mathbb{R}^-)$

   Here, the initial boundary value problem $[IBVP]$ is ill-posed with respect to perturbations in initial data in the inner-inner asymptotic region as $t \to 0^+$. We anticipate that the inclusion of weak surface tension in our model will result in the governing initial value problem $[IBVP]$ becoming well-posed but unstable with respect to perturbations in initial data in the inner-inner asymptotic region.

The asymptotic solution to $[IBVP]$ as $t \to 0^+$ for those pairs $(\alpha, \mu) \in \left(0, \frac{1}{2}\pi\right) \times \mathbb{R}$ is now complete.

6.1 Future Work

The work presented in this thesis has posed a number of questions which remain unanswered. Regarding the physical problem, that $[IBVP]$ is ill-posed with respect to perturbations in initial data in the innermost asymptotic region for the case $\mu < 0$ suggests that we should include the effects of surface tension in our model. We anticipate that the introduction of surface tension should result in a well-posed problem in the innermost asymptotic region, but that $[IBVP]$ will be unstable with respect to perturbations in initial data.

In terms of the plate inclination angle α, we have not yet considered the cases $\alpha = \frac{1}{2}\pi$ (the extension of the work done by King and Needham [14]), or $\alpha \in \left(\frac{1}{2}\pi, \pi\right)$ (the extension of the work done by Needham et al [24]). These remain to be investigated.

We believe that an interesting topic of future work concerns the case of an inclined vibrating plate accelerating uniformly from rest away from a semi-infinite expanse of inviscid incompressible fluid. With the vibration of the plate chosen such that we see several periods of oscillation in the inner asymptotic region, we believe that some interesting results could be achieved. Here, the inclusion of surface tension terms will be essential in ensuring the existence of structure in the solution of the free surface. This problem more closely models that of a ship accelerating from rest in a body of water, with vibrations in the hull generated by its engine.

Appendices

A.1 Derivation of Problems in the Inner Asymptotic Region

This appendix details the derivation of problems in the inner asymptotic region. We have introduced in Section 3.1 the scaled coordinates

$$\overline{x} = t^2 X, \qquad y = t^2 Y, \tag{A.1.1}$$

along with the scaled variables

$$\eta\left(X,t\right) = t^2 \eta_I\left(X,t\right), \quad X \geqslant X_p\left(t\right),\ t \geqslant 0; \tag{A.1.2}$$

$$\phi\left(X,Y,t\right) = t^3 \phi_I\left(X,Y,t\right), \quad \left(X,Y\right) \in \overline{\mathcal{D}}_I\left(t\right),\ t \geqslant 0; \tag{A.1.3}$$

$$\overline{x}_p\left(t\right) = t^2 X_p\left(t\right), \quad t \geqslant 0; \tag{A.1.4}$$

and the asymptotic expansions

$$\eta_I\left(X,t\right) = \eta_0\left(X\right) + t^{\frac{\pi}{\alpha}-2}\overline{\eta}\left(X\right) + o\left(t^{\frac{\pi}{\alpha}-2}\right), \tag{A.1.5}$$

$$\phi_I\left(X,Y,t\right) = \phi_0\left(X,Y\right) + t^{\frac{\pi}{\alpha}-2}\overline{\phi}\left(X,Y\right) + o\left(t^{\frac{\pi}{\alpha}-2}\right), \tag{A.1.6}$$

$$X_p\left(t\right) = X_0 + t^{\frac{\pi}{\alpha}-2} X_1 + o\left(t^{\frac{\pi}{\alpha}-2}\right), \tag{A.1.7}$$

as $t \to 0^+$ in the inner asymptotic region. To begin we substitute (A.1.1) - (A.1.7) into the Laplace equation (1.2.17), to give

$$O\left(1\right): \qquad \overline{\nabla}^2 \phi_0 = 0, \quad X > X_0, -X\tan\alpha < Y < \eta_0\left(X\right); \tag{A.1.8}$$

$$O\left(t^{\frac{\pi}{\alpha}-2}\right): \qquad \overline{\nabla}^2 \overline{\phi} = 0, \quad X > X_0, -X\tan\alpha < Y < \eta_0\left(X\right). \tag{A.1.9}$$

where $\overline{\nabla} = \left(\frac{\partial}{\partial X}, \frac{\partial}{\partial Y}\right)$. Similarly, along the plate we obtain,

$$O\left(1\right): \qquad \overline{\nabla}\phi_0 \cdot \hat{\mathbf{n}} = \sigma\sin\alpha, \quad X > X_0, Y = -X\tan\alpha; \tag{A.1.10}$$

$$O\left(t^{\frac{\pi}{\alpha}-2}\right): \qquad \overline{\nabla}\overline{\phi} \cdot \hat{\mathbf{n}} = 0, \quad X > X_0, Y = -X\tan\alpha. \tag{A.1.11}$$

On substitution of (A.1.1) - (A.1.7) into the kinematic boundary condition (1.2.20) we arrive at

$$\begin{aligned} 2t\left(\eta_0+t^{\frac{\pi}{\alpha}-2}\overline{\eta}\right)+\left(\frac{\pi}{\alpha}-2\right)t^{\frac{\pi}{\alpha}-1}\overline{\eta}-2Xt\left(\eta_{0X}+t^{\frac{\pi}{\alpha}-2}\overline{\eta}_X\right) \\ +t\left(\phi_{0X}+t^{\frac{\pi}{\alpha}-2}\left(\phi_{0XY}\overline{\eta}+\overline{\phi}_X\right)-\sigma\right)\left(\eta_{0X}+t^{\frac{\pi}{\alpha}-2}\overline{\eta}_X\right) \\ -t\left(\phi_{0Y}+t^{\frac{\pi}{\alpha}-2}\left(\phi_{0YY}\overline{\eta}+\overline{\phi}_Y\right)\right)+o\left(t^{\frac{\pi}{\alpha}-1}\right)=0, \\ \text{on } Y=\eta_0(X),\ X>X_0,\ t>0. \end{aligned} \tag{A.1.12}$$

Collecting terms in (A.1.12) we arrive at,

$$O(t):\quad 2\eta_0-(2X+\sigma-\phi_{0X})\eta_{0X}-\phi_{0Y}=0 \quad \text{on} \quad Y=\eta_0(X),\ X>X_0. \tag{A.1.13}$$

$$\begin{aligned} O\left(t^{\frac{\pi}{\alpha}-1}\right):\quad &\left(\frac{\pi}{\alpha}+\eta_{0X}\phi_{0XY}-\phi_{0YY}\right)\overline{\eta}+(\phi_{0X}-2X)\overline{\eta}_X \\ &+\eta_{0X}\overline{\phi}_X-\overline{\phi}_Y=0 \quad \text{on} \quad Y=\eta_0(X),\ X>X_0. \end{aligned} \tag{A.1.14}$$

Next, substitution of (A.1.1) - (A.1.4) into the dynamic boundary condition (1.2.21) gives,

$$\begin{aligned} 3t^2\phi_I+t^3\phi_{It}-2t^2X\phi_{IX}-2t^2\eta_I\phi_{IY}-\sigma t^2\phi_{IX}+\frac{1}{2}t^2\left(\phi_{IX}^2+\phi_{IY}^2\right)+t^2\eta_I=0, \\ \text{on} \quad Y=\eta_I(X,t),\ X>X_p(t),\ t>0. \end{aligned} \tag{A.1.15}$$

Now we substitute from (A.1.5) - (A.1.7) into (A.1.15) to obtain

$$\begin{aligned} &3t^2\left(\phi_0+t^{\frac{\pi}{\alpha}-2}\left(\phi_{0Y}\overline{\eta}+\overline{\phi}\right)\right)+\left(\frac{\pi}{\alpha}-2\right)t^{\frac{\pi}{\alpha}}\overline{\phi} \\ &-2t^2\left(X+\frac{1}{2}\sigma\right)\left(\phi_{0X}+t^{\frac{\pi}{\alpha}-2}\left(\phi_{0XY}\overline{\eta}+\overline{\phi}_X\right)\right) \\ &-2t^2\left(\eta_0+t^{\frac{\pi}{\alpha}-2}\overline{\eta}\right)\left(\phi_{0Y}+t^{\frac{\pi}{\alpha}-2}\left(\phi_{0YY}\overline{\eta}+\overline{\phi}_Y\right)\right) \\ &+\frac{1}{2}t^2\left(\phi_{0X}^2+2t^{\frac{\pi}{\alpha}-2}\left(\phi_{0XY}\overline{\eta}+\overline{\phi}_X\right)+\phi_{0Y}^2+2t^{\frac{\pi}{\alpha}-2}\left(\phi_{0YY}\overline{\eta}+\overline{\phi}_Y\right)\right) \\ &+t^2\left(\eta_0+t^{\frac{\pi}{\alpha}-2}\overline{\eta}\right)+o\left(t^{\frac{\pi}{\alpha}}\right)=0 \quad \text{on} \quad Y=\eta_0(X),\ X>X_0,\ t>0. \end{aligned} \tag{A.1.16}$$

Collecting terms in (A.1.16) gives,

$$\begin{aligned} O\left(t^2\right):\qquad &3\phi_0-2\left(X+\frac{1}{2}\sigma\right)\phi_{0X}-2\eta_0\phi_{0Y}+\frac{1}{2}\left|\overline{\nabla}\phi_0\right|^2+\eta_0=0, \\ &\text{on} \quad Y=\eta_0(X),\ X>X_0. \end{aligned} \tag{A.1.17}$$

$$O\left(t^{\frac{\pi}{\alpha}}\right): \qquad \left(1+\frac{\pi}{\alpha}\right)\overline{\phi}+\left(\phi_{0X}-2\left(X+\frac{1}{2}\sigma\right)\right)\overline{\phi}_X+\left(\phi_{0Y}-2\eta_0\right)\overline{\phi}_Y$$
$$+\left(\phi_{0Y}-2\left(X+\frac{1}{2}\sigma\right)\phi_{0XY}-2\eta_0\phi_{0YY}+\phi_{0X}\phi_{0XY}\right.$$
$$\left.+\phi_{0Y}\phi_{0YY}+1\right)\overline{\eta}=0 \quad \text{on} \quad Y=\eta_0(X),\ X>X_0. \tag{A.1.18}$$

Finally, we substitute from (A.1.1), (A.1.2), (A.1.4), (A.1.5) and (A.1.7) into the contact point boundary condition (1.2.22). We arrive at,

$$\eta_0+t^{\frac{\pi}{\alpha}-2}\left(\eta_{0X}X_1+\overline{\eta}\right)+\tan\alpha\left(X_0+t^{\frac{\pi}{\alpha}-2}X_1\right)+o\left(t^{\frac{\pi}{\alpha}-2}\right)=0,$$
$$\text{when} \quad X=X_0,\ t>0. \tag{A.1.19}$$

Collecting terms in (A.1.19) gives,

$$O(1): \qquad \eta_0+X_0\tan\alpha=0 \quad \text{at} \quad X=X_0. \tag{A.1.20}$$
$$O\left(t^{\frac{\pi}{\alpha}-2}\right): \qquad \overline{\eta}+\left(\eta_{0X}+\tan\alpha\right)X_1=0 \quad \text{at} \quad X=X_0. \tag{A.1.21}$$

Collecting together (A.1.8), (A.1.10), (A.1.13), (A.1.17) and (A.1.20) we arrive at the harmonic free boundary problem (3.1.16) - (3.1.20) for ϕ_0 and η_0. Similarly collecting together (A.1.9), (A.1.11), (A.1.14), (A.1.18) and (A.1.21), and using (3.1.23) - (3.1.25) for η_0, ϕ_0 and X_0, together with the scaling (3.1.27) and (3.1.28) we arrive at the linear harmonic boundary value problem (3.1.29) - (3.1.32) and (3.1.35) for $\hat{\phi}$, $\hat{\eta}$ and X_1.

A.2 Scaling of the Boundary Value Problem (3.1.29) - (3.1.35) to Obtain $[BVP]^{\pm}$

This appendix contains the derivation of scalings (3.1.36), which reduce the boundary value problem (3.1.29) - (3.1.35) to $[BVP]^{\pm}$. When $\mu \neq 0$ we write

$$\hat{\phi}=|\mu|^n\psi, \qquad \overline{R}=|\mu|^m\widehat{R}, \qquad \overline{X}=|\mu|^m\widehat{X},$$
$$\overline{Y}=|\mu|^m\widehat{Y}, \qquad \hat{\eta}=|\mu|^l\xi, \tag{A.2.1}$$

where $\mu=1+\sigma\tan\alpha$ and l,m,n are to be chosen. The Laplace equation (3.1.29) and the plate boundary condition (3.1.30) are invariant under the scaling (A.2.1). The kinematic boundary condition (3.1.31) remains invariant under the scaling (A.2.1) provided we take

$$l+m-n=0. \tag{A.2.2}$$

To remove μ from the dynamic boundary condition (3.1.32), we must take

$$l-n=-1. \tag{A.2.3}$$

Finally, the far-field conditions (3.1.33) and (3.1.34) remain invariant under the scaling (A.2.1) provided we take

$$\frac{\pi}{2\alpha}m - n = 0, \tag{A.2.4}$$

$$l - \left(\frac{\pi}{2\alpha} - 1\right) m = 0. \tag{A.2.5}$$

We have four linear algebraic equations (A.2.2), (A.2.3), (A.2.4) and (A.2.5) which must be satisfied by l, m and n. In echelon form, the system of linear algebraic equations becomes,

$$\begin{pmatrix} 1 & 1 & -1 \\ 0 & 1 & 0 \\ 0 & 0 & 1 \\ 0 & 0 & 0 \end{pmatrix} \begin{pmatrix} l \\ m \\ n \end{pmatrix} = \begin{pmatrix} 0 \\ 1 \\ \frac{\pi}{2\alpha} \\ 0 \end{pmatrix}, \tag{A.2.6}$$

which has the unique solution,

$$l = \frac{\pi}{2\alpha} - 1, \quad m = 1, \quad n = \frac{\pi}{2\alpha}. \tag{A.2.7}$$

With the above choices for l, m and n, the scaling (A.2.1) reduces the boundary value problem (3.1.29) - (3.1.35) to $[BVP]^{\pm}$.

A.3 The Near-Field Boundary Condition for the Numerical Solution of $[PBVP]^{\pm}$

This appendix contains the formulation of a suitable regularity condition representing (3.2.1), required for numerical solution of $[PBVP]^{\pm}$. We numerically implement the regularity condition (3.2.1) on $[PBVP]^{\pm}$ as $\widehat{R} \to 0$ by requiring, via (3.2.11), that,

$$\psi_\theta + \widehat{R}\tan(\theta + \alpha)\psi_{\widehat{R}} = O\left(\widehat{R}^2\right), \tag{A.3.1}$$

as $\widehat{R} \to 0$, uniformly for $-\alpha \leqslant \theta \leqslant 0$. Numerical implementation of (A.3.1) is achieved by requiring

$$\psi_\theta + \widehat{R}\tan(\theta + \alpha)\psi_{\widehat{R}} = 0, \tag{A.3.2}$$

at $\widehat{R} = \varepsilon$, $-\alpha \leqslant \theta \leqslant 0$, with $\varepsilon > 0$ chosen to be sufficiently small. Thereafter the near-field constant a_0 for $[PBVP]^{\pm}$, respectively, can be approximated using the finite difference scheme discussed in §3.3.

A.4 Finite Difference Approximations

This appendix details the discretisation of $[PBVP]^{\pm}$, and thus the formulation of the decoupled large sparse system of linear algebraic equations outlined in §3.3.

A.4.1 The Laplace Equation

Using (3.3.5) we discretise the Laplace equation and apply associated discretised conditions at the boundaries. In the wedge we discretise Laplace's equation to give

$$\frac{2}{\delta}\left(\frac{\psi_{i+1,j}-\psi_{i,j}}{\Delta\widehat{R}_l}-\frac{\psi_{i,j}-\psi_{i-1,j}}{\Delta\widehat{R}_k}\right)+\frac{1}{\widehat{R}_i}\left(\frac{\psi_{i+1,j}-\psi_{i-1,j}}{\delta}\right)$$
$$+\frac{1}{\widehat{R}_i^2}\left(\frac{\psi_{i,j-1}-2\psi_{i,j}+\psi_{i,j+1}}{\Delta\theta^2}\right)=0, \tag{A.4.1}$$

which rearranges to

$$c_i^w\psi_{i-1,j}+c_i^o\psi_{i,j}+c_i^e\psi_{i+1,j}+c_i^n\psi_{i,j-1}+c_i^s\psi_{i,j+1}=0, \tag{A.4.2}$$

for $i=1,2,\ldots,N,N+1$ $j=1,2,\ldots,J,J+1$ where $c_i^n,c_i^s,c_i^e,c_i^w,c_i^o$ are the coefficients of the five-point stencil given by

$$c_i^w=\widehat{R}_i^2\delta^*\left(\frac{2}{\delta\Delta\widehat{R}_k}-\frac{1}{\delta\widehat{R}_i}\right), \tag{A.4.3}$$

$$c_i^o=-2\widehat{R}_i^2\delta^*\left(\frac{1}{\Delta\theta^2\widehat{R}_i^2}+\frac{1}{\delta^*}\right), \tag{A.4.4}$$

$$c_i^e=\widehat{R}_i^2\delta^*\left(\frac{2}{\delta\Delta\widehat{R}_l}+\frac{1}{\delta\widehat{R}_i}\right), \tag{A.4.5}$$

$$c_i^n=c_i^s=\frac{\delta^*}{\Delta\theta^2}, \tag{A.4.6}$$

with $\delta^*=\Delta\widehat{R}_k\Delta\widehat{R}_l$. We note that at the boundaries, where $i=1,N+1$, $j=1,J+1$, we must discretise and apply the boundary conditions (3.2.5), (3.2.6), (3.2.25) and (A.3.2).

A.4.2 Plate Boundary Condition

For discretised points on the plate we apply the Neumann boundary condition (3.1.38) to generate an equation for $\psi_{i,J+2}$ in terms of interior points, given by

$$\psi_{i,J+2}=\psi_{i,J},\quad i=1,2,\ldots,N+1, \tag{A.4.7}$$

which reduces (A.4.2), when $j=J+1$, to

$$c_i^w\psi_{i-1,J+1}+c_i^o\psi_{i,J+1}+c_i^e\psi_{i+1,J+1}+\left(c_i^n+c_i^s\right)\psi_{i,J}=0, \tag{A.4.8}$$

for $i=2,3,\ldots,N-1$.

A.4.3 Free Surface Boundary Condition

Discretisation of (3.2.4) gives

$$\frac{\pi}{\alpha}\left(1+\frac{\pi}{\alpha}\right)\psi_{i,1}+2\widehat{R}_i\left(1-2\frac{\pi}{\alpha}\right)\left(\frac{\psi_{i+1,1}-\psi_{i-1,1}}{\delta}\right)+ 4\widehat{R}_i^2\frac{2}{\delta}\left(\frac{\psi_{i+1,1}-\psi_{i,1}}{\Delta\widehat{R}_l}-\frac{\psi_{i,1}-\psi_{i-1,1}}{\Delta\widehat{R}_k}\right)\pm\frac{1}{\widehat{R}_i}\left(\frac{\psi_{i,0}-\psi_{i,2}}{2\Delta\theta}\right)=0, \tag{A.4.9}$$

which rearranges to,

$$\left(c_i^w+c_i^nc_i^{fw}\right)\psi_{i-1,1}+\left(c_i^o+c_i^nc_i^{fo}\right)\psi_{i,1} + \left(c_i^e+c_i^nc_i^{fe}\right)\psi_{i+1,1}+\left(c_i^s+c_i^n\right)\psi_{i,2}=0, \tag{A.4.10}$$

for $i=2,3,\ldots,N-1$, with

$$c_i^{fw}=\mp2\widehat{R}_i\Delta\theta\left[\frac{8\widehat{R}_i^2}{\delta\Delta\widehat{R}_k}-2\widehat{R}_i\frac{1}{\delta}\left(1-2\frac{\pi}{\alpha}\right)\right], \tag{A.4.11}$$

$$c_i^{fo}=\mp2\widehat{R}_i\Delta\theta\left[\frac{\pi}{\alpha}\left(1+\frac{\pi}{\alpha}\right)-\frac{2}{\delta}\left(\frac{4\widehat{R}_i^2}{\Delta\widehat{R}_l}+\frac{4\widehat{R}_i^2}{\Delta\widehat{R}_k}\right)\right], \tag{A.4.12}$$

$$c_i^{fe}=\mp2\widehat{R}_i\Delta\theta\left[\frac{8\widehat{R}_i^2}{\delta\Delta\widehat{R}_l}+2\widehat{R}_i\frac{1}{\delta}\left(1-2\frac{\pi}{\alpha}\right)\right]. \tag{A.4.13}$$

A.4.4 Far-field Boundary Condition

At $\widehat{R}=\widehat{R}_\infty$ we apply the far-field boundary condition (3.2.25), giving

$$\psi_{N+1,j}=-\widehat{R}_\infty^{\frac{\pi}{2\alpha}}\cos\frac{\pi}{2\alpha}\left(\theta_j+\alpha\right)\mp\frac{12\alpha\sin\alpha}{\pi}\widehat{R}_\infty^{\frac{\pi}{2\alpha}-1}\cos\left(\frac{\pi}{2\alpha}-1\right)\left(\theta_j+\alpha\right) + \frac{3\left(2\alpha-\pi\right)}{20\alpha}\widehat{R}_\infty^{\frac{\pi}{2\alpha}-2}\cos\left(\frac{\pi}{2\alpha}-2\right)\left(\theta_j+\alpha\right), \tag{A.4.14}$$

which rearranges to

$$c_N^w\psi_{N-1,j}+c_N^o\psi_{N,j}+c_N^n\psi_{N,j-1}+c_N^s\psi_{N,j+1}=-c_N^e\psi_{N+1,j}, \tag{A.4.15}$$

for $j=2,3,\ldots,J$. At the intersection $(i,j)=(N,1)$ we combine (A.4.2), (A.4.10) and (A.4.15) to give

$$\left(c_N^w+c_N^nc_N^{fw}\right)\psi_{N-1,1}+\left(c_N^o+c_N^nc_N^{fo}\right)\psi_{N,1} + \left(c_N^s+c_N^n\right)\psi_{N,2}=-\left(c_N^e+c_N^nc_N^{fe}\right)\psi_{N+1,1}. \tag{A.4.16}$$

Similarly, at the intersection point $(i,j) = (N, J+1)$ we combine (A.4.2), (A.4.8) and (A.4.15), giving

$$c_N^w \psi_{N-1,J+1} + c_N^o \psi_{N,J+1} + \left(c_N^n + c_N^s\right) \psi_{N,J} = -c_N^e \psi_{N+1,J+1}. \tag{A.4.17}$$

A.4.5 Near-Field Boundary Condition

We apply condition (A.3.2), in discretised form, to (A.4.2), which gives

$$\begin{aligned} c_1^o \psi_{1,j} + \left(c_1^e + c_1^w\right) \psi_{2,j} + \left(c_1^n + \frac{\delta}{2\Delta\theta \widehat{R}_1 \tan\left(\theta_j + \alpha\right)} c_1^w \right) \psi_{1,j-1} \\ + \left(c_1^s - \frac{\delta}{2\Delta\theta \widehat{R}_1 \tan\left(\theta_j + \alpha\right)} c_1^w \right) \psi_{1,j+1} = 0, \end{aligned} \tag{A.4.18}$$

for $j = 2, 3, \ldots, J$. Combining (A.4.2), (A.4.8) and (A.4.18) we get, at the intersection point $(i,j) = (1, J+1)$,

$$c_1^o \psi_{1,J+1} + \left(c_1^e + c_1^w\right) \psi_{2,J+1} + \left(c_1^n + c_1^s\right) \psi_{1,J} = 0, \tag{A.4.19}$$

and, at the intersection point $(i,j) = (1,1)$, we combine (A.4.2), (A.4.10) and (A.4.18) to obtain,

$$\begin{aligned} \left[c_1^0 + \frac{1}{1 - \frac{\delta}{2\Delta\theta \widehat{R}_1 \tan\alpha} c_1^{fw}} c_1^{fo} \right] \psi_{1,1} \\ + \left[c_1^e + c_1^w + \frac{1}{\left(1 - \frac{\delta}{2\Delta\theta \widehat{R}_1 \tan\alpha} c_1^{fw}\right)} \left(c_1^{fe} + c_1^{fw} \right) \right] \psi_{2,1} \\ + \left[c_1^n + c_1^s \right] \psi_{1,2} = 0. \end{aligned} \tag{A.4.20}$$

Thus, via (A.4.2), (A.4.8), (A.4.10), (A.4.15), (A.4.16), (A.4.17), (A.4.18), (A.4.19) and (A.4.20), we arrive at the large, sparse linear algebraic system (3.3.8).

A.5 Classification of the Spectrum of $[SP(k)]$

This appendix details the classification of the spectrum of $[SP(k)]$. In Section 5.1.2 we define the spectral problem $[SP(k)]$ to be given by

$$\overline{\nabla}^2 \overline{\psi} = 0, \qquad \overline{X} > 0,\ -\overline{X} \tan\alpha < \overline{Y} < 0; \tag{A.5.1}$$

$$\overline{\nabla} \overline{\psi} \cdot \hat{\mathbf{n}} = 0, \qquad \overline{X} > 0,\ \overline{Y} = -\overline{X} \tan\alpha; \tag{A.5.2}$$

$$\overline{\psi}_{\overline{Y}} - k\overline{\psi} = 0, \qquad \overline{X} > 0,\ \overline{Y} = 0; \tag{A.5.3}$$

$$\overline{\psi},\ \overline{\nabla}\overline{\psi} \text{ bounded as } \overline{R} \to \infty, \text{ uniformly for } -\alpha < \theta < 0; \tag{A.5.4}$$

with $k = -\lambda^2/\mu$ (for $\mu \neq 0$), and we require that solutions to $[SP(k)]$, $\overline{\psi} : \overline{\mathcal{G}}_\infty \to \mathbb{C}$, have regularity given by (5.1.89). We define the spectrum of $[SP(k)]$ to be given by

$$\mathbf{S} = \{k \in \mathbb{C} : [SP(k)] \text{ has a non-trivial solution}\}. \tag{A.5.5}$$

The set of eigenvalues of $[SP(k)]$ is $\mathbf{S}^d$, where

$$\mathbf{S}^d = \left\{k \in \mathbb{C} : \exists \text{ a non-trivial solution to } [SP(k)] \text{ with } \overline{\psi} \to 0 \text{ as } \overline{R} \to \infty\right\}, \tag{A.5.6}$$

and the continuous spectrum of $[SP(k)]$ is $\mathbf{S}^c$, where

$$\mathbf{S}^c = \left\{k \in \mathbb{C} : \exists \text{ a non-trivial solution to } [SP(k)] \text{ with } \overline{\psi} \nrightarrow 0 \text{ as } \overline{R} \to \infty\right\}, \tag{A.5.7}$$

with the limits as $\overline{R} \to \infty$ considered as uniform for $-\alpha \leqslant \theta \leqslant 0$. Finally, we observe that

$$\mathbf{S} = \mathbf{S}^c \cup \mathbf{S}^d. \tag{A.5.8}$$

We now determine $\mathbf{S}_k$. Following Needham [25], we obtain the following results.

Theorem 1

$$\mathbf{S} \subseteq \{k \in \mathbb{C} : \mathrm{Re}(k) > 0\} \cup \{0\} = R_+. \tag{A.5.9}$$

Proof. The proof requires that, for each $k \in \mathbb{C}\backslash R_+$, we establish that $[SP(k)]$ has only the trivial solution. Let $k \in \mathbb{C}\backslash R_+$, and let $\overline{\psi} : \overline{\mathcal{G}}_\infty \to \mathbb{C}$ be a solution to $[SP(k)]$. Green's theorem (see, for example, [12]), along with the regularity (5.1.89), and (A.5.1), gives that

$$\iint\limits_{\overline{\mathcal{G}}_{R^*}} \left\{\nabla\overline{\psi}^* \cdot \nabla\overline{\psi}\right\} \overline{R}\, \mathrm{d}\overline{R}\, \mathrm{d}\theta = \int\limits_{\partial\mathcal{G}} \left\{\overline{\psi}^* \left(\nabla\overline{\psi} \cdot \hat{\mathbf{n}}\right)\right\} \mathrm{d}S, \tag{A.5.10}$$

where $\overline{\mathcal{G}}_{R^*} = \overline{\mathcal{G}}_\infty \backslash (R^*, \infty) \times [-\alpha, 0]$, and $\partial\mathcal{G} = \left\{\left(\overline{R}, \theta\right) : 0 \leqslant \overline{R} \leqslant R^*,\ \theta = 0\right\}$ $\cup\left\{\left(\overline{R}, \theta\right) : \overline{R} = R^*,\ -\alpha < \theta < 0\right\} \cup \left\{\left(\overline{R}, \theta\right) : 0 \leqslant \overline{R} \leqslant R^*,\ \theta = -\alpha\right\}$. It follows from (A.5.10) and (A.5.2) that

$$\iint\limits_{\overline{\mathcal{G}}_{R^*}} \left(\left|\overline{\psi}_{\overline{R}}\right|^2 + \left|\frac{1}{\overline{R}}\overline{\psi}_\theta\right|^2\right) \overline{R}\, \mathrm{d}\overline{R}\, \mathrm{d}\theta = \int\limits_{-\alpha}^{0} \left(\overline{R}\overline{\psi}^*\overline{\psi}_{\overline{R}}\right)_{\overline{R}=R^*} \mathrm{d}\theta + \int\limits_{0}^{R^*} \left(\overline{\psi}^* \frac{1}{\overline{R}}\overline{\psi}_\theta\right)_{\theta=0} \mathrm{d}\overline{R}, \tag{A.5.11}$$

which becomes, using (A.5.3),

$$\iint\limits_{\overline{\mathcal{G}}_{R^*}} \left(\left|\overline{\psi}_{\overline{R}}\right|^2 + \left|\frac{1}{\overline{R}}\overline{\psi}_\theta\right|^2\right) \overline{R}\, \mathrm{d}\overline{R}\, \mathrm{d}\theta - k \int\limits_{0}^{R^*} \left(\left|\overline{\psi}\right|^2\right)_{\theta=0} \mathrm{d}\overline{R} = \int\limits_{-\alpha}^{0} \left(\overline{R}\overline{\psi}^*\overline{\psi}_{\overline{R}}\right)_{\overline{R}=R^*} \mathrm{d}\theta, \tag{A.5.12}$$

for each $R^* > 0$. We now introduce u and v, where

$$u\left(\overline{R},\theta\right) = \mathrm{Re}\left[\overline{\psi}\left(\overline{R},\theta\right)\right], \qquad v\left(\overline{R},\theta\right) = \mathrm{Im}\left[\overline{\psi}\left(\overline{R},\theta\right)\right], \tag{A.5.13}$$

after which we obtain from (A.5.12)

$$\begin{aligned}\iint\limits_{\overline{\mathcal{G}}^*_{R^*}} \left(\left|\overline{\psi}_{\overline{R}}\right|^2 + \left|\frac{1}{\overline{R}}\overline{\psi}_\theta\right|^2\right) \overline{R}\,\mathrm{d}\overline{R}\,\mathrm{d}\theta - k\int\limits_0^{R^*}\left(\left|\overline{\psi}\right|^2\right)_{\theta=0}\mathrm{d}\overline{R} \\ = \frac{1}{2}R^*\frac{d}{dR^*}\left\{\int\limits_{-\alpha}^{0}\left(\left|\overline{\psi}\right|^2_{\overline{R}=R^*}\mathrm{d}\theta\right)\right\} + iR^*\int\limits_{-\alpha}^{0}\left(uv_{\overline{R}} - u_{\overline{R}}v\right)_{\overline{R}=R^*}\mathrm{d}\theta. \end{aligned}\tag{A.5.14}$$

Taking the real part of (A.5.14) gives

$$\begin{aligned}\iint\limits_{\overline{\mathcal{G}}_{R^*}} \left(\left|\overline{\psi}_{\overline{R}}\right|^2 + \left|\frac{1}{\overline{R}}\overline{\psi}_\theta\right|^2\right) \overline{R}\,\mathrm{d}\overline{R}\,\mathrm{d}\theta - \mathrm{Re}\left(k\right)\int\limits_0^{R^*}\left(\left|\overline{\psi}\right|^2\right)_{\theta=0}\mathrm{d}\overline{R} \\ = \frac{1}{2}R^*\frac{d}{dR^*}\left\{\int\limits_{-\alpha}^{0}\left(\left|\overline{\psi}\right|^2_{\overline{R}=R^*}\right)\mathrm{d}\theta\right\}, \end{aligned}\tag{A.5.15}$$

for each $R^* > 0$. Using (5.1.93) we can now write the right-hand side of (A.5.15), in the limit $R^* \to \infty$, as

$$\begin{aligned}&\frac{1}{2}R^*\frac{d}{dR^*}\left\{\int\limits_{-\alpha}^{0}\left(\left|\overline{\psi}\right|^2_{\overline{R}=R^*}\mathrm{d}\theta\right)\right\} \\ &\qquad = \frac{1}{2}R^*\frac{d}{dR^*}\left\{\int\limits_{-\alpha}^{0}\left(\left|a_k\right|^2\frac{1}{R^{*\frac{\pi}{\alpha}}}\cos^2\frac{\pi}{2\alpha}\left(\theta+\alpha\right) + O\left(\frac{1}{R^{*\frac{\pi}{\alpha}+1}}\right)\right)\mathrm{d}\theta\right\}, \\ &\qquad = -\frac{\pi}{4}\left|a_k\right|^2\frac{1}{R^{*\frac{\pi}{\alpha}}} + O\left(\frac{1}{R^{*\frac{\pi}{\alpha}+1}}\right), \end{aligned}\tag{A.5.16}$$

which is bounded as $R^* \to \infty$. Since $\mathrm{Re}\left(k\right) \leqslant 0$, is then follows from (A.5.15) that

$$\iint\limits_{\overline{\mathcal{G}}_{R^*}} \left(\left|\overline{\psi}_{\overline{R}}\right|^2 + \left|\frac{1}{\overline{R}}\overline{\psi}_\theta\right|^2\right) \overline{R}\,\mathrm{d}\overline{R}\,\mathrm{d}\theta \leqslant \frac{1}{2}R^*\frac{d}{dR^*}\left\{\int\limits_{-\alpha}^{0}\left(\left|\overline{\psi}\right|^2_{\overline{R}=R^*}\mathrm{d}\theta\right)\right\}, \tag{A.5.17}$$

and so the left-hand side of (A.5.17) is bounded and non-decreasing as $R^* \to \infty$, and thus

has a finite non-negative limit as $R^* \to \infty$, so that

$$\lim_{R^*\to\infty} \iint\limits_{\overline{\mathcal{G}}_{R^*}} \left(\left|\overline{\psi}_{\overline{R}}\right|^2 + \left|\frac{1}{\overline{R}}\overline{\psi}_{\theta}\right|^2 \right) \overline{R}\, \mathrm{d}\overline{R}\, \mathrm{d}\theta = \beta, \tag{A.5.18}$$

for some $\beta \geqslant 0$. However, it now follows from (A.5.17), (A.5.18) and (A.5.16) that $\beta \leqslant 0$, and so we conclude that $\beta = 0$. We then have from (A.5.18) that

$$\lim_{R^*\to\infty} \iint\limits_{\overline{\mathcal{G}}_{R^*}} \left(\left|\overline{\psi}_{\overline{R}}\right|^2 + \left|\frac{1}{\overline{R}}\overline{\psi}_{\theta}\right|^2 \right) \overline{R}\, \mathrm{d}\overline{R}\, \mathrm{d}\theta = 0, \tag{A.5.19}$$

for all $R^* > 0$. The condition (A.5.19) (along with regularity (5.1.89)) then requires that $\overline{\psi}\left(\overline{R},\theta\right) = C$ for all $\left(\overline{R},\theta\right) \in [0,\infty) \times [-\alpha, 0]$, for some constant $C \in \mathbb{C}$. However, since $k \neq 0$, we have from (A.5.3) that $C = 0$, so that $\overline{\psi}\left(\overline{R},\theta\right) = 0$ for all $\left(\overline{R},\theta\right) \in [0,\infty) \times [-\alpha, 0]$, which is the trivial solution, and the proof is complete. ■

Theorem 2

$$\mathbf{S} \subset \mathbb{R}^+ \cup \{0\}. \tag{A.5.20}$$

Proof. Let $k \in R_+ \backslash (\mathbb{R}^+ \cup \{0\})$,and $\overline{\psi} : \overline{\mathcal{G}}_\infty \to \mathbb{C}$ be a solution to $[SP(k)]$. We must show that $\overline{\psi}$ is the trivial solution. We have from (5.1.93) that

$$\overline{\psi}_k\left(\overline{R},\theta\right) = a_k \frac{1}{\overline{R}^{\frac{\pi}{2\alpha}}} \cos\frac{\pi}{2\alpha}\left(\theta+\alpha\right) + O\left(\frac{1}{\overline{R}^{\frac{\pi}{2\alpha}+1}}\right), \tag{A.5.21}$$

as $\overline{R} \to \infty$, uniformly for $-\alpha \leqslant \theta \leqslant 0$. We also have from (A.5.14), that

$$\mathrm{Im}\,(k) \int\limits_0^{R^*} \left(\left|\overline{\psi}\right|^2\right)_{\theta=0} \mathrm{d}\overline{R} + R^* \int\limits_{-\alpha}^{0} (\overline{uv}_{\overline{R}} - \overline{u}_{\overline{R}}\overline{v})_{\overline{R}=R^*}\, \mathrm{d}\theta = 0, \tag{A.5.22}$$

$$\iint\limits_{\overline{\mathcal{G}}_{R^*}} \left(\left|\overline{\psi}_{\overline{R}}\right|^2 + \left|\frac{1}{\overline{R}}\overline{\psi}_{\theta}\right|^2 \right) \overline{R}\mathrm{d}\overline{R}\mathrm{d}\theta - \mathrm{Re}\,(k) \int\limits_0^{R^*} \left(\left|\overline{\psi}\right|^2\right)_{\theta=0} \mathrm{d}\overline{R}$$

$$= \frac{1}{2} R^* \frac{d}{dR^*} \left\{ \int\limits_{-\alpha}^{0} \left(\left|\overline{\psi}\right|^2\right)_{\overline{R}=R^*} \mathrm{d}\theta \right\}. \tag{A.5.23}$$

Now, via (A.5.21) we have that,

$$\lim_{R^*\to\infty} R^* \int_{-\alpha}^{0} (\overline{uv_{\overline{R}}} - \overline{u}_{\overline{R}}\overline{v})_{\overline{R}=R^*}\, \mathrm{d}\theta = 0. \tag{A.5.24}$$

It then follows from (A.5.22), since $\mathrm{Im}\,(k) \neq 0$, that,

$$\lim_{R^*\to\infty} \int_{0}^{R^*} \left(\left|\overline{\psi}\right|^2\right)_{\theta=0} \mathrm{d}\overline{R} = 0, \tag{A.5.25}$$

and so,

$$\int_{0}^{R^*} \left(\left|\overline{\psi}\right|^2\right)_{\theta=0} \mathrm{d}\overline{R} = 0, \tag{A.5.26}$$

for all $R^* > 0$. Next, considering (A.5.23), (A.5.26), and (A.5.16), we have that

$$\lim_{R^*\to\infty} \iint_{\overline{\mathcal{G}}_{R^*}} \left(\left|\overline{\psi}_{\overline{R}}\right|^2 + \left|\frac{1}{\overline{R}}\overline{\psi}_{\theta}\right|^2\right) \overline{R} d\overline{R} d\theta = 0. \tag{A.5.27}$$

It then immediately follows that $\overline{\psi}\left(\overline{R},\theta\right) = 0$, for all $\left(\overline{R},\theta\right) \in [0,\infty) \times [-\alpha, 0]$, which is the trivial solution, and the proof is complete. ■

In fact $\mathbf{S} = \mathbb{R}^+ \cup \{0\}$. Clearly, $0 \in \mathbf{S}$, since when $k = 0$, $\overline{\psi}\left(\overline{R},\theta\right) = 1$ for all $\left(\overline{R},\theta\right) \in [0,\infty) \times [-\alpha, 0]$, solves $[SP\,(0)]$. Moreover John [11] has established that $k \in \mathbf{S}$ for all $k \in \mathbb{R}^+$, and in addition that, $\mathbf{S}^c = \mathbb{R}^+ \cup (0)$ whilst $\mathbf{S}^d = \varnothing$.

List of References

[1] D.J. Acheson. *Elementary Fluid Dynamics*. Oxford Applied Mathematics and Computing Science Series. Oxford University Press on Demand, 1990.

[2] G.K. Batchelor. *An Introduction to Fluid Dynamics*. Cambridge Mathematical Library. Cambridge University Press, 2000.

[3] L. Campbell and W. Garnett. *The Life of James Clerk Maxwell: With a Selection from His Correspondence and Occasional Writings and a Sketch of His Contributions to Science*. Cambridge Library Collection - Physical Sciences. Cambridge University Press, 2010.

[4] P.G. Drazin. *Introduction to Hydrodynamic Stability*. Cambridge Texts in Applied Mathematics. Cambridge University Press, 2002.

[5] T.A. Driscoll and L.N. Trefethen. *Schwarz-Christoffel Mapping*. Cambridge Monographs on Applied and Computational Mathematics. Cambridge University Press, 2002.

[6] M. Greenhow. Wedge entry into initially calm water. *Applied Ocean Research*, 9(4):214–223, 1987.

[7] M. Greenhow and W. Lin. Nonlinear-free surface effects: Experiments and theory. Technical report, DTIC Document, 1983.

[8] D.B. Haidvogel and A. Beckmann. *Numerical Ocean Circulation Modeling*. Series on Environmental Science and Management. Imperial College Press, 1999.

[9] S. D. Howison, J. R. Ockendon, and S. K. Wilson. Incompressible water-entry problems at small deadrise angles. *Journal of Fluid Mechanics*, 222:215–230, 1 1991.

[10] A. Iafrati and A.A. Korobkin. Starting flow generated by the impulsive start of a floating wedge. *Journal of Engineering Mathematics*, 51(2):99–126, 2005.

[11] Fritz John. Waves in the presence of an inclined barrier. *Communications on Pure and Applied Mathematics*, 1(2):149–200, 1948.

[12] W. Kaplan. *Advanced Calculus*. Addison-Wesley higher mathematics. Addison-Wesley, 2002.

[13] J. Kevorkian. *Partial Differential Equations: Analytical Solution Techniques*. Texts in Applied Mathematics. Springer, 2010.

[14] A. C. King and D. J. Needham. The initial development of a jet caused by fluid, body and free-surface interaction. Part 1. A uniformly accelerating plate. *Journal of Fluid Mechanics*, 268:89–101, 5 1994.

[15] A.C. King, J. Billingham, and S.R. Otto. *Differential Equations: Linear, Nonlinear, Ordinary, Partial*. Cambridge University Press, 2003.

[16] B. Kirby. *Micro- and Nanoscale Fluid Mechanics: Transport in Microfluidic Devices*. Cambridge University Press, 2013.

[17] P.K. Kundu, I.M. Cohen, and D.R. Dowling. *Fluid Mechanics*. Elsevier Science, 2011.

[18] M. C. Lai. A note on finite difference discretizations for poisson equation on a disk. *Numerical Methods for Partial Differential Equations*, 17(3):199–203, 2001.

[19] J.A. Leach and D.J. Needham. *Matched Asymptotic Expansions in Reaction-Diffusion Theory*. Springer Monographs in Mathematics. SPRINGER VERLAG GMBH, 2004.

[20] H. Lewy. *Developments at the confluence of analytic boundary conditions*, volume 1. University of California Press, 1950.

[21] MATLAB. *version 7.10.0 (R2010a)*. The MathWorks Inc., Natick, Massachusetts, 2010.

[22] V. Mazya and T.O. Shaposhnikova. *Jacques Hadamard: A Universal Mathematician*. History of mathematics. American Mathematical Society, 1999.

[23] D. J. Needham, J. Billingham, and A. C. King. The initial development of a jet caused by fluid, body and free-surface interaction. Part 2. An impulsively moved plate. *Journal of Fluid Mechanics*, 578:67–84, 4 2007.

[24] D. J. Needham, P. G. Chamberlain, and J. Billingham. The initial development of a jet caused by fluid, body and free surface interaction. Part 3. An inclined accelerating plate. *The Quarterly Journal of Mechanics and Applied Mathematics*, 61(4):581–614, 2008.

[25] D.J. Needham. The initial development of a jet caused by fluid, body and free surface interaction. Part 4. The large-time structure. *IMA Journal of Applied Mathematics*, 77(4):451–472, 2012.

[26] J.N. Newman. *Marine Hydrodynamics*. Wei Cheng Cultural Enteroprise Company, 1977.

[27] K.F. Riley, M.P. Hobson, and S.J. Bence. *Mathematical Methods for Physics and Engineering*. Cambridge University Press, 2006.

[28] M. Van Dyke. *Perturbation Methods in Fluid Mechanics*. Number v. 8 in Applied mathematics and mechanics. Academic Press, 1964.

[29] S. A. Yang and A. T. Chwang. Nonlinear viscous waves produced by an impulsively moving plate. Technical report, IIHR Report No. 332, Iose Institute of Hydraulic Research, The University of Iowa, 1989.

[30] S. A. Yang and A. T. Chwang. An experimental study of nonlinear waves produced by an accelerating plate. *Physics of Fluids A: Fluid Dynamics*, 4(11):2456–2465, 1992.